Feasibility Study: Alternatives to Prevent Settlements and Bumps at Bridge Approach

FINAL REPORT

Seunghee Kim, Ph.D., P.E.

Jongwan Eun, Ph.D., P.E.

Yusuf Alhowaidi, Graduate Research Assistant

Daniel Robertson, Graduate Research Assistant

Department of Civil and Environmental Engineering

University of Nebraska-Lincoln

Sponsored By

Nebraska Department of Transportation and U.S. Department of Transportation Federal Highway Administration

May 2021

NEBRASKA
Good Life. Great Journey.
DEPARTMENT OF TRANSPORTATION

UNIVERSITY OF Nebraska Lincoln

Technical Report Documentation Page

1. Report No. M106	**2. Government Accession No.**	**3. Recipient's Catalog No.**
4. Title and Subtitle Feasibility Study: Alternatives to Prevent Settlements and Bumps at Bridge Approach		**5. Report Date** May 2021 **6. Performing Organization Code**
7. Author(s) Seunghee Kim, Jongwan Eun, Yusuf Alhowaidi, and Daniel Robertson		**8. Performing Organization Report No.** If applicable, enter any/all unique numbers assigned to the performing organization.
9. Performing Organization Name and Address Board of Regents, University of Nebraska-Lincoln		**10. Work Unit No.** **11. Contract** SPR-P1(20) M106
12. Sponsoring Agency Name and Address Nebraska Department of Transportation Research Section 1400 Hwy 2 Lincoln, NE 68502		**13. Type of Report and Period Covered** Final Report July 2019 – May 2021 **14. Sponsoring Agency Code**

15. Supplementary Notes
If applicable, enter information not included elsewhere, such as translation of (or by), report supersedes, old edition number, alternate title (e.g. project name), or hypertext links to documents or related information.

16. Abstract
This project aims to examine the feasibility of improving the current design practice of the approach slab foundation in Nebraska and the alternative of using geosynthetic reinforcement of soils to prevent the bump issues near the end of bridge approaches via an in-depth numerical simulation study. A large-scale pullout test is also conducted as complementary to provide input parameters for the interaction between the regional soil and selected geosynthetics. Based on the results, it is recommended that the number of grade beam piles could be reduced to 40-50 % of the total number of abutment piles while maintaining the same dimension and length to sufficiently prevent the "bump" issue not only near the interface of the bridge abutment and the approach but also at the interface of the approach and the roadway pavement. In the geosynthetic reinforcement case, 2-3 layers of individual geosynthetic reinforcements at both near the interface of the bridge abutment and the approach and the interface of the approach and the roadway pavement could be recommended to efficiently prevent the bump issue. Unlike individual geosynthetic reinforcement, extended geosynthetic reinforcement is not recommended due to its less efficacy, constructability, and economic reasons. Alternatively, a combination of grade beam piles (current design practice) and 2-3 layers of individual geosynthetic reinforcement near the interface of the approach and the roadway pavement could also be recommended to prevent differential settlements at both areas. Such an approach can also be used for the repair of an existing bridge approach and the roadway pavement. Considering the estimated costs for the installment of grade beam piles and geosynthetics, the alternative design of using geosynthetic reinforcement could be a more cost-effective and economical method compared to the current design practice.

17. Key Words Approach slab, settlements, soils, pile, abutment, geosynthetics, numerical modeling, a large-scale pullout test, cost analysis	**18. Distribution Statement** No restrictions. This document is available through the National Technical Information Service. 5285 Port Royal Road Springfield, VA 22161

19. Security Classification (of this report) Unclassified	**20. Security Classification (of this page)** Unclassified	**21. No. of Pages** 161	**22. Price**

Form DOT F 1700.7 (8-72) Reproduction of completed page authorized

DISCLAIMER

The contents of this report reflect the views of the authors, who are responsible for the facts and the accuracy of the information presented herein. The contents do not necessarily reflect the official views or policies neither of the Nebraska Department of Transportations nor the University of Nebraska-Lincoln. This report does not constitute a standard, specification, or regulation. Trade or manufacturers' names, which may appear in this report, are cited only because they are considered essential to the objectives of the report.

The United States (U.S.) government and the State of Nebraska do not endorse products or manufacturers. This material is based upon work supported by the Federal Highway Administration under SPR-P1(20) M106. Any opinions, findings and conclusions or recommendations expressed in this publication are those of the author(s) and do not necessarily reflect the views of the Federal Highway Administration."

Table of Contents

List of Figures

List Of Tables

1. Introduction

1.1 Background

The ubiquitous bridge approach slab problem, also known as "bump at the end of the bridge," often occurs near the interface of the bridge abutment and the approach, or that of the approach and the roadway pavement. The main cause is a differential settlement between the abutment and the approach (Abu-Hejleh et al., 2008; Figure 1.1). This problem may lead to uncomfortable & dangerous driving conditions, a negative perception in the minds of transportation users, and substantial damages to bridges, which may result in frequent maintenance, an additional budget for the repair, and traffic delay. The "bump" problem has been reported to affect about 25% of entire bridges in the United States (i.e., about 150,000 structures nationwide out of 600,000 bridges; Mishra et al., 2010). Moreover, at least $100 million has been spent every year on necessary repairs with this issue (Lenke, 2006). Based on the number of bridges, it can be roughly estimated that the cost in Nebraska could be around $2-3 million every year.

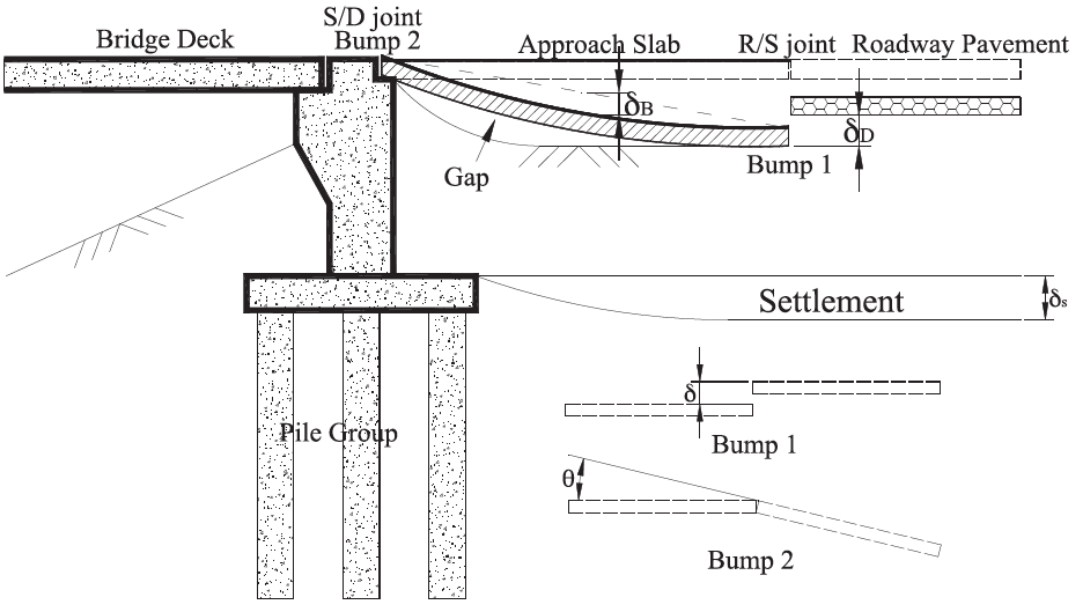

Figure 1.1 A schematic illustration of the "bump at the end of the bridge" problem. The image is from Chen and Abu-Farsakh (2016).

Approach slabs are constructed to join the end of the bridge to the roadway for a smoother transition of vehicles. Many researchers studied the causes of the complex problem of bump formation at the end of the bridge. For example, Wahls (1990), Schaefer and Koch (1992), Stark et al. (1995), Briaud et al. (1997), White et al. (2005), Abu-Hejleh et al. (2006), and White et al.

(2007) related the settlement of bridge approach, which leads eventually to the bump issue as follows:

- Settlement of foundation soils.
- Compression of the embankment fill material.
- Poor drainage.
- Erosion of embankment fill material.
- Abutment type and foundation support.
- Poor construction practice.
- Temperature cycling.

Tadros and Benak (1989) suggested that the consolidation of the foundation soil could mainly contribute to the bump issue in Nebraska. A schematic illustration of the summarized factors contributing to the bump formation at the end of the bridge is shown in Figure 1.2.

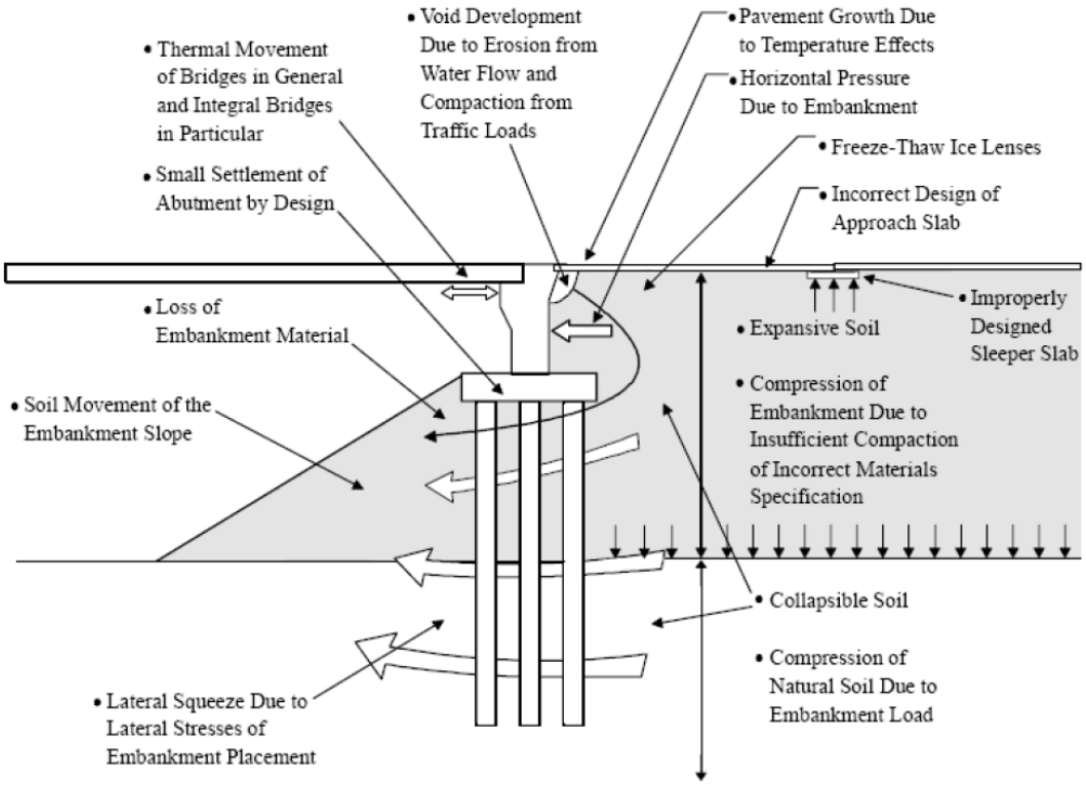

Figure 1.2 A schematic illustration of causes of the "bump at the end of the bridge" problem. The image is from Briaud et al. (1997).

1.2 Problem statement

To minimize the occurrence of the "bump at the end of the bridge" problem due to the differential settlement, the Nebraska Department of Transportation (NDOT) has been applying a grade beam policy to new approach slabs (NDOR Bridge Division, 2016; Figure 1.3). According to the policy in BOPP, grade beams are to be parallel to the abutment and located 20 ft beyond the end of the bridge floor, and be extended to the outside edges of the approach section. The grade beam that typically involves driven piles to meet the required bearing capacity is used to support the approach slab, which is enough to prevent any substantial differential settlements.

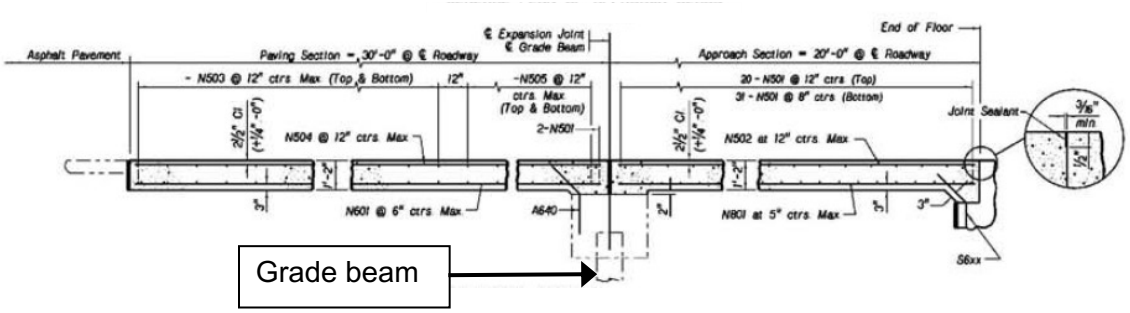

Figure 1.3 Grade beam section from the bridge office policies and procedures (BOPP; NDOR Bridge Division, 2016) of Nebraska.

This method has been very successful, resulting in negligible bridge settlement of the bridge approaches. Indeed, a recent nationwide survey showed that Nebraska retains a lower percentage (0-25%) of bridges that have been experiencing the "bump" issues (Figure 1.4; Yasrobi et al., 2016). Most bridges with the "bump" issues are those that were constructed before the new grade beam policy was at practice. However, the current practice in Nebraska does not provide many details in terms of the design. For example, when grade beam piles are installed, the variation for the length and spacing of the grade beam piles might not be considered. Such a lack of detailed guidelines might lead to an unnecessary increase in the construction cost. In some cases, the current design may result in an overachievement with the pre-assigned length & dimension of the grade beam pile. Moreover, in the current method, considerable settlements were sometimes observed at the interface between the approach slab and the asphalt pavement section where the grade beam is not installed.

Accordingly, there is an important research need to provide more details and make necessary revisions to the current grade beam policy to minimize the settlement and bumps at the bridge approaches with less cost and the same confidence level as before. Besides, there is a research

need to investigate other potential alternatives to prevent such a differential settlement not only at the interface of the bridge abutment and the approach but also at the interface of the approach and the roadway pavement.

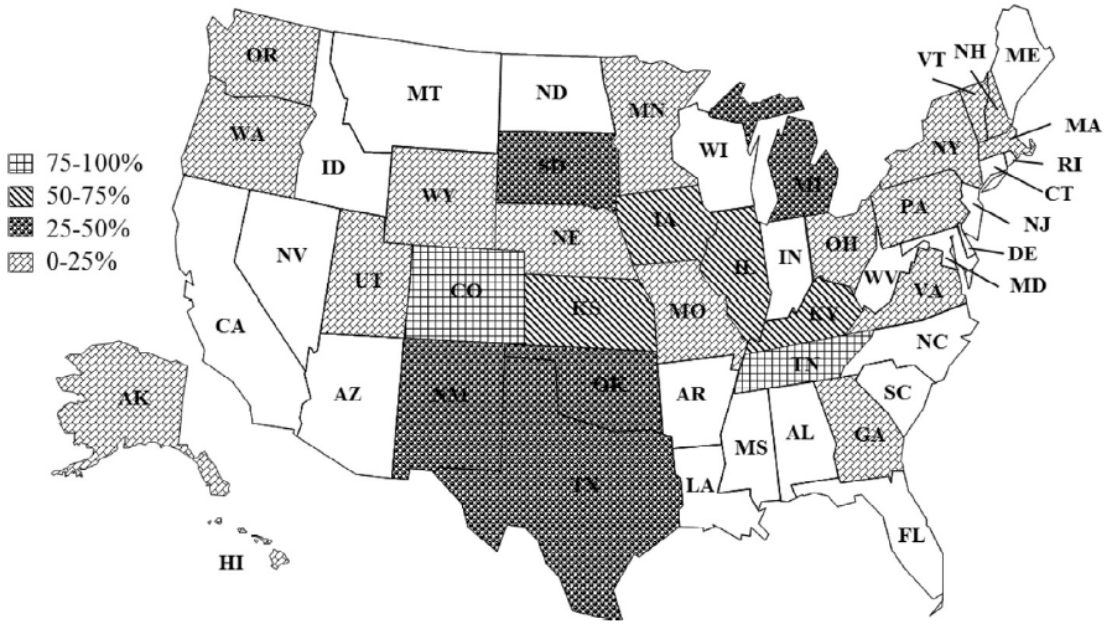

Figure 1.4 Percentage of bridges with approach slab settlement in reporting states. Survey results and image are from Yasrobi et al. (2016).

One of the feasible alternatives to mitigate such "bump at the end of the bridge" and the different settlement of an approach slab is the application of geosynthetic reinforcement (or geosynthetic reinforced soil, GRS) underneath the approach slab. This method needs to achieve backfill compaction at the optimal moisture content, especially for a coarse-grained backfill material (Abu-Hejleh et al., 2006). According to previous researches (Abu-Hejleh et al., 2006; Helwany et al., 2007; Abu-Farsakh et al., 2013; Bai et al., 2013; Chen and Abu-Farsakh, 2016; Eun et al., 2017), the use of geosynthetic reinforced soil resulted in that the monitored movements of the bridge structure were mitigated compared to those anticipated from the design phase or allowed by the performance requirements. In addition, with the use of GRS systems, post-construction movements can be reduced substantially; thus, the bump problem at the bridge transition is minimized. Furthermore, the obvious advantages of this method are cost-effectiveness, being simple and fast to construct, having a good seismic performance, and that the method can tolerate greater deformation without structural failure. Nonetheless, only a handful of state

DOTs, such as LA, CO, WI, TX, NJ, and OK DOT, have implemented it in practice, probably due to the limited familiarity of this method with the contractors. Also, the design practice might be varied depending on the state's soil condition and environment.

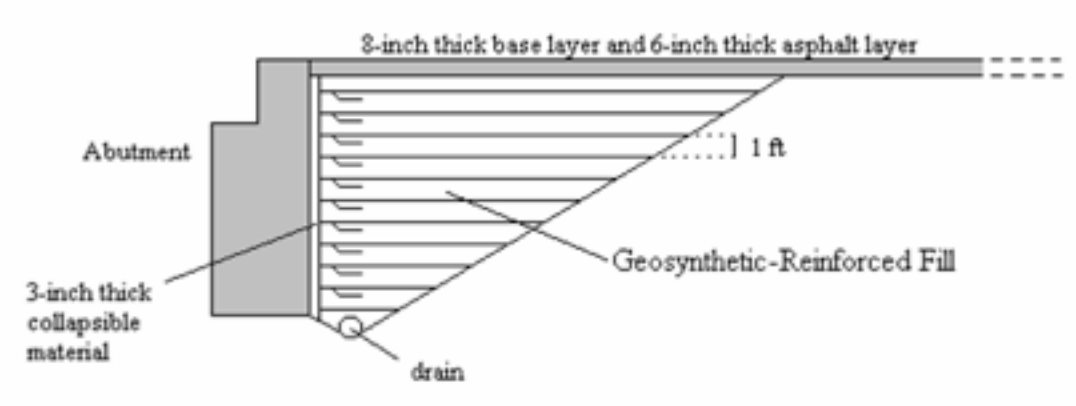

Figure 1.5 A schematic of the geosynthetic reinforced backfill. Image is from Helwany et al. (2007).

1.3 Objective of the study

This project pursues two principal goals: (1) improve the current design practices of the approach slab foundation in Nebraska in terms of pile lengths and spacings, and (2) examine the feasibility of applying geosynthetic reinforcement of soils in Nebraska for preventing the settlement issues at the bridge approaches with less cost. The proposed scope of work consists of five main tasks as follows:

- Task 1. Extensive survey & review of current bridge approaches in Nebraska
- Task 2. Review of cases and solutions in other states in the USA
- Task 3. Detailed analysis on the improvement of current bridge approach design in Nebraska
- Task 4. Detailed analysis on the feasibility of geosynthetic reinforcement of soils
- Task 5. Cost-effectiveness and constructability analysis

Chapter 2 in this report contains the outcomes of Tasks 1 and 2. Chapters 3 and 4 describe the results of Tasks 3 and 4, respectively. The following chapters address discussion regarding Task 5 and final recommendations for the design modification.

2. Literature Review

2.1 Bridge approaches in Nebraska

2.1.1 Old design

Nebraska, similar to many other states, had problematic bump issues caused by differential settlements between the sleeper slab (or grade beam), where the approach slab is placed on one side and on the bridge abutment from the other side.

The previous design in Nebraska (before 1990) consisted of constructing a grade beam (box-shape) directly resting on the soil. The dimensions of the grade beam were 4 ft. in height, and 3 ft. in width, and the approach slab span length was 25 feet. Figure 2.1 shows the previous design of the approach slab and grade beam used in Nebraska.

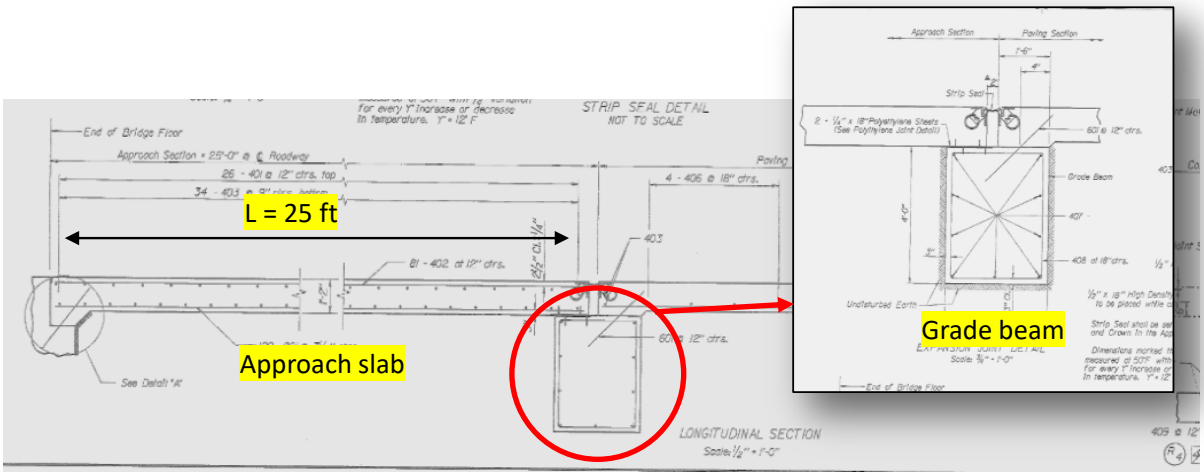

Figure 2.1 Previous grade beam and approach slab design used in Nebraska (prior to 1990).

This design had led to numerous bump issues in many approach slabs in Nebraska. That is, bridges constructed with the old grade beam and approach slab design exhibited severe differential settlement problems, which caused visual bump formation and required maintenance work (discussion with DOT engineers). Figure 2.2 shows an example of the apparent bump that occurred in the approach slab of bridges with the previous design in Nebraska.

2.1.2 Current design

Nebraska DOT modified the design to mitigate such a differential settlement between the grade beam and the bridge abutment. In the new design, the grade beam rests on a group of bearing piles. The Bridge Office Policies and Procedures of Nebraska (BOPP, 2016) provides the following details on the approach slab and grade beam policies.

Figure 2.2 An example of the bump problems encountered near the end of approach slab of bridges built with the old design in Nebraska.

Approach slab policies

- The length of the approach slab is 20 ft. from the end of the bridge floor to the centerline of the grade beam.
- The depth of the approach slab section is 14 in. and is placed over the abutment wings and the grade beam.
- There is a 2-1/8 in gap kept between the bottom of the approach slab and the top of the wing walls to allow for live load deflection. This gap is indicated on the construction plans as 1/8 in. hardboard on top of a 2 in. extruded polystyrene.

A longitudinal view that shows the approach slab details and reinforcement is shown in Figure 2.3.

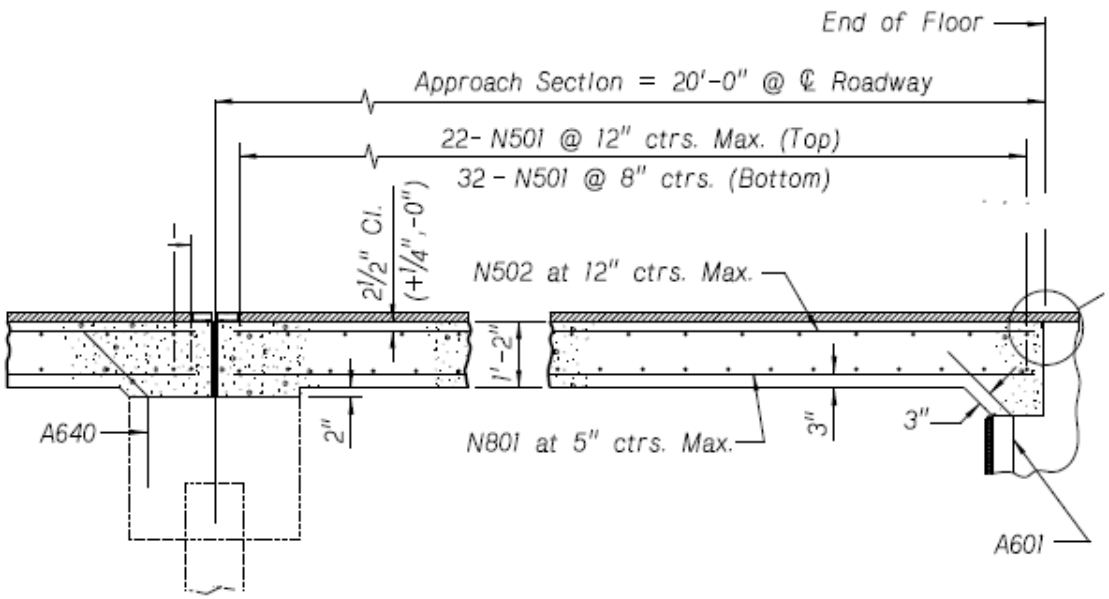

Figure 2.3 A typical section that shows the dimensions and reinforcement of the approach slab in the new design of Nebraska.

Typically, the geometry of the approach slab is determined based on the location of the bridge site. That is, a skewed or non-skewed approach slab depending on the orientation of the approach slab. These two cases, along with a cross section across the grade beam, are presented in Figures 2.4 and 2.5, respectively.

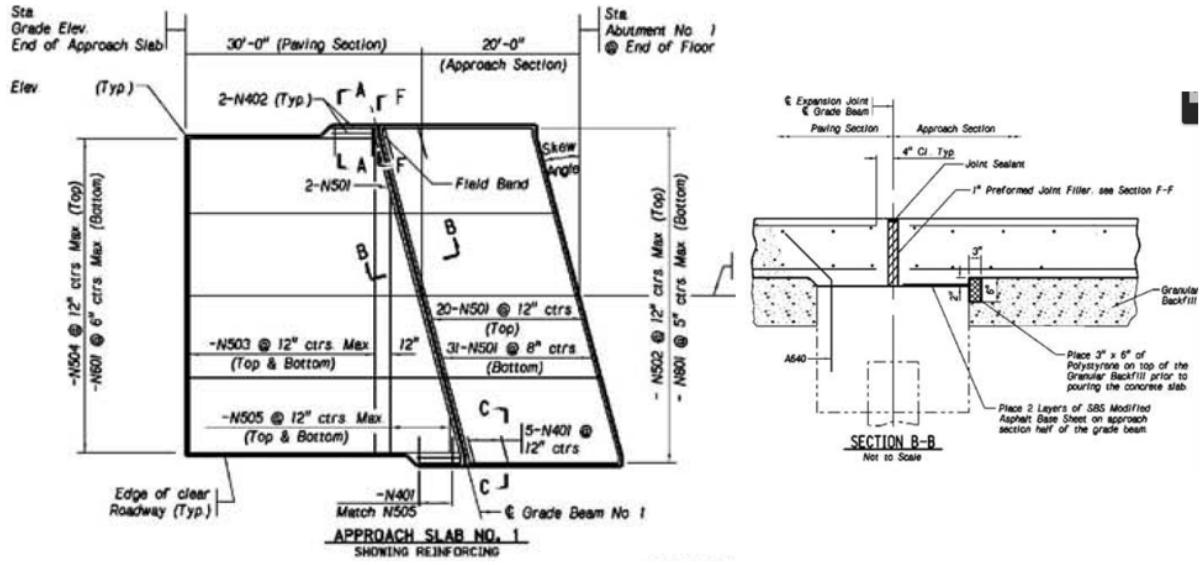

Figure 2.4 Details of the skewed approach slab (left), and the cross-section along with the grade beam (right) in Nebraska.

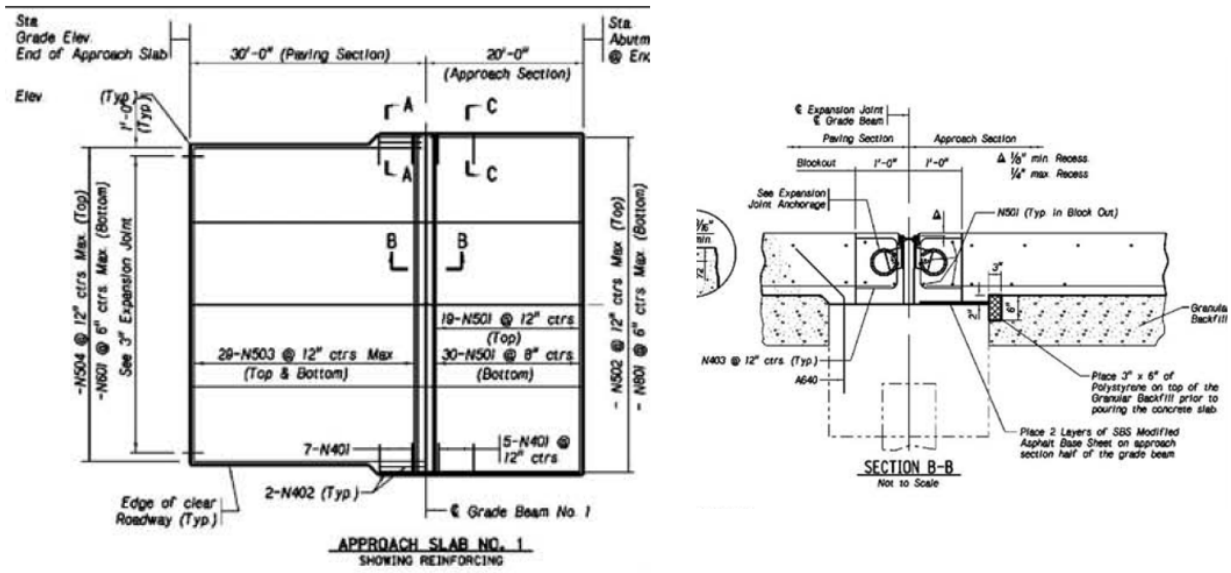

Figure 2.5 Details of the non-skewed approach slab (left), and the cross-section along with the grade beam (right) in Nebraska.

Approach slabs in several different states were compared in terms of the depth and span length in a study by Thiagarajan and Gopalarathnam (2010). Some of these results are illustrated in Figures 2.6 and 2.7.

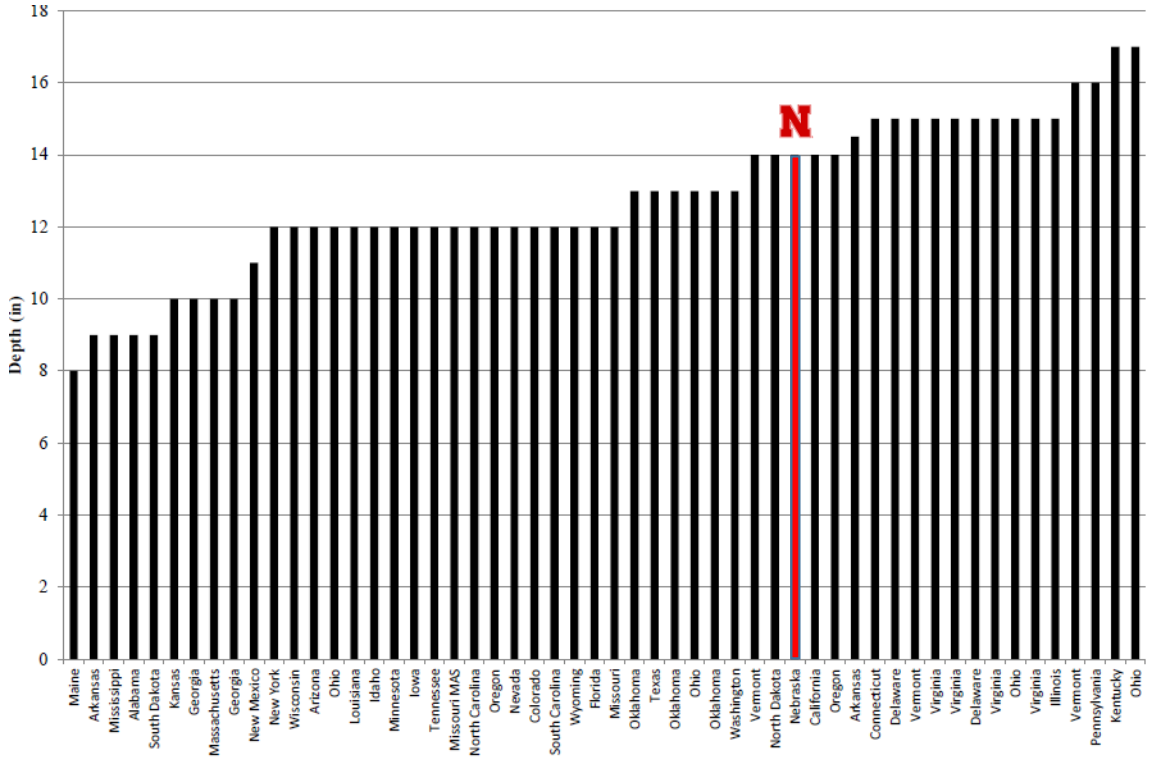

Figure 2.6 A comparison of the depth of approach slabs from various states.

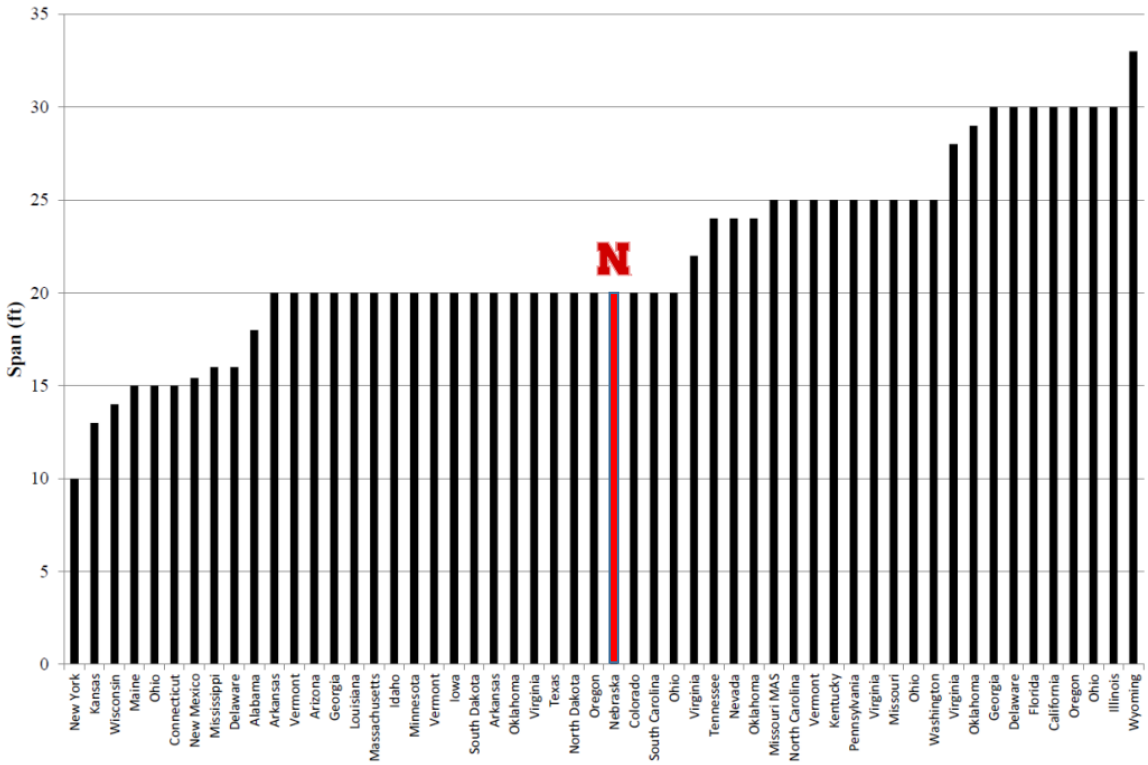

Figure 2.7 A comparison of the span length of approach slabs from various states.

It was observed that about 37% of the state DOTs had been using 20 ft span length for the approach slab (including Nebraska; Thiagarajan and Gopalarathnam, 2010). On the other hand, its depth varies between 8 and 18 inches.

Grade beam policies

It is stated that a grade beam is required unless there is any new approach slab is specified (BOPP, 2016). The box shape of the grade beam in the new design has a length of 2.5 ft. and a width of 3.0 ft. The grade beam is supported by piles. #4 closed-stirrups bars and #7 bars are adopted as the beam reinforcement based on conservative estimates for live load impact and pavement section reaction. Details of a typical grade beam are presented in Figure 2.8.

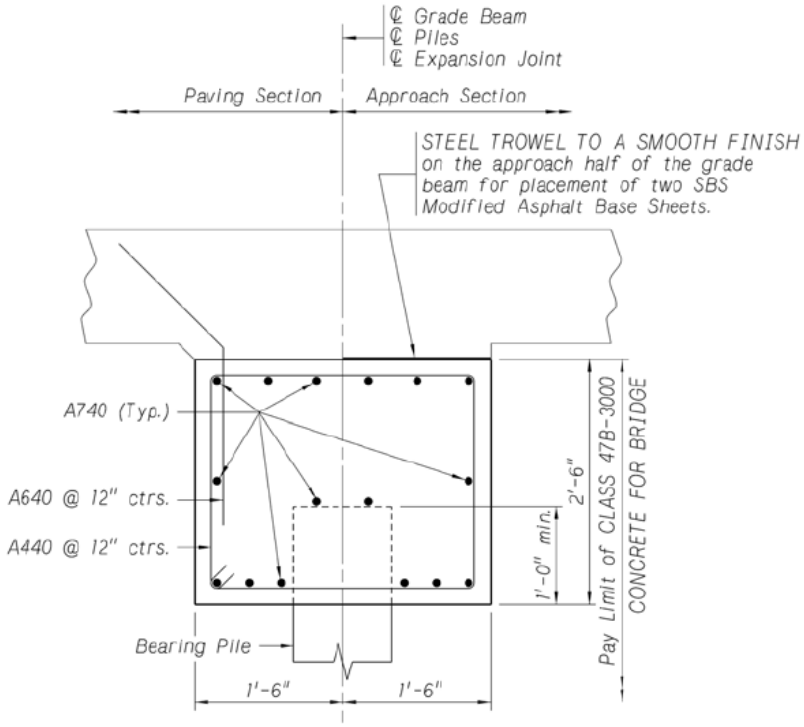

Figure 2.8 A typical section of the grade beam that supports the approach slab in Nebraska.

Nebraska DOT reported that there had been no major bump issue reported in the approach slab with the new design. It is also consistent with the survey conducted by Ng et al. (2015). Nonetheless, minor cracks occurred to several approach slabs, which were resolved by increasing the amount of steel reinforcement.

Survey of current design

A total of representative 50 bridges were surveyed and examined to check the performance of the current design in this project. Although the new approach slab design resulted in overall good performance, some minor observations related to the settlement were found at some bridges, as shown in Figure 2.9.

Figure 2.9 An example of minor problems encountered in the approach slab with the new design in Nebraska.

It is worth noting that there was no specific information on how the number or the length of grade beam piles are to be determined in the current BOPP. The project team compiled the data of current grade beam piles from the surveyed bridges that were built after 1990. Those results are summarized in terms of the ratio of pile length (grade beam-to-abutment pile) and the ratio of pile number (grade beam-to-abutment pile) in Figure 2.10. As shown in Figure 2.10, both the number and length of grade beam piles show a wide variance in the range of 0.4-1.0 of the number and length of abutment piles. Besides, such scattered data in the ratio of grade beam-to-abutment piles imply that each approach slab design was prepared site-specifically without a consistent design policy.

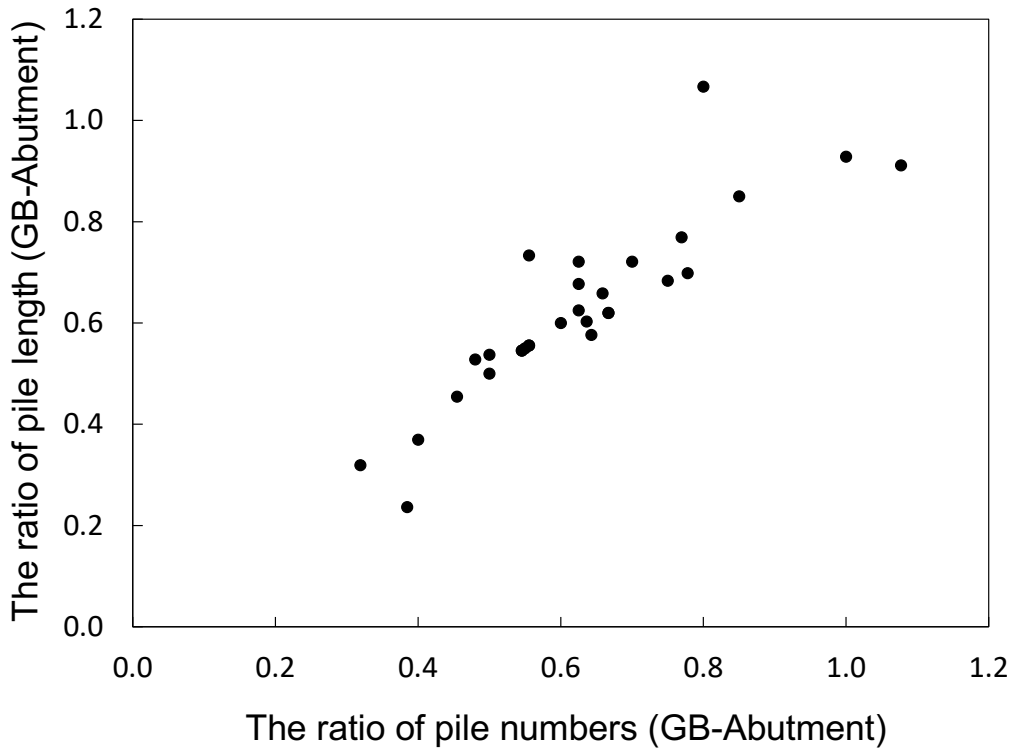

Figure 2.10 A compiled data of surveyed bridges in Nebraska that shows information of grade beam (GB) piles in comparison to the abutment piles.

Other observations from the current design

While surveying the current design to gain a better insight on the performance of the bridge, severe void formation and erosion problems were observed at some bridges, as shown in Figure 2.11. A study by Edgar et al. (1989) suggested that a heavily reinforced approach slab with high flexural rigidity may allow the void propagation due to the settlement. In this regard, a certain countermeasure is needed to address those minor problems.

Figure 2.11 An example of soil erosion problems observed at some of the surveyed bridges in Nebraska that were built with the current design policy.

2.2 Cases and solutions in other States

A review of the approach slab foundation designs and policies in other states was carried out in this study. Salient observations are as follows:

- The width and height of the approach slab foundation vary.
- The approach slab foundation is either of three representative types:
  1. Box-shaped sleeper slab or grade beam (with or without piles).
  2. L-shaped sleeper slab
  3. Inverted T-shaped sleeper slab.
- The settlement issue is inevitable in every state, but its impact is different depending on the design and the site conditions.

Figure 2.12 shows 16 states that are surveyed in this study with the following distribution:

- Mid-West: IA, KS, IN, MO, WI
- South East: MS, FL, NC, LA
- South West: TX, NM, OK
- East: VA, NJ
- West: CO, WY

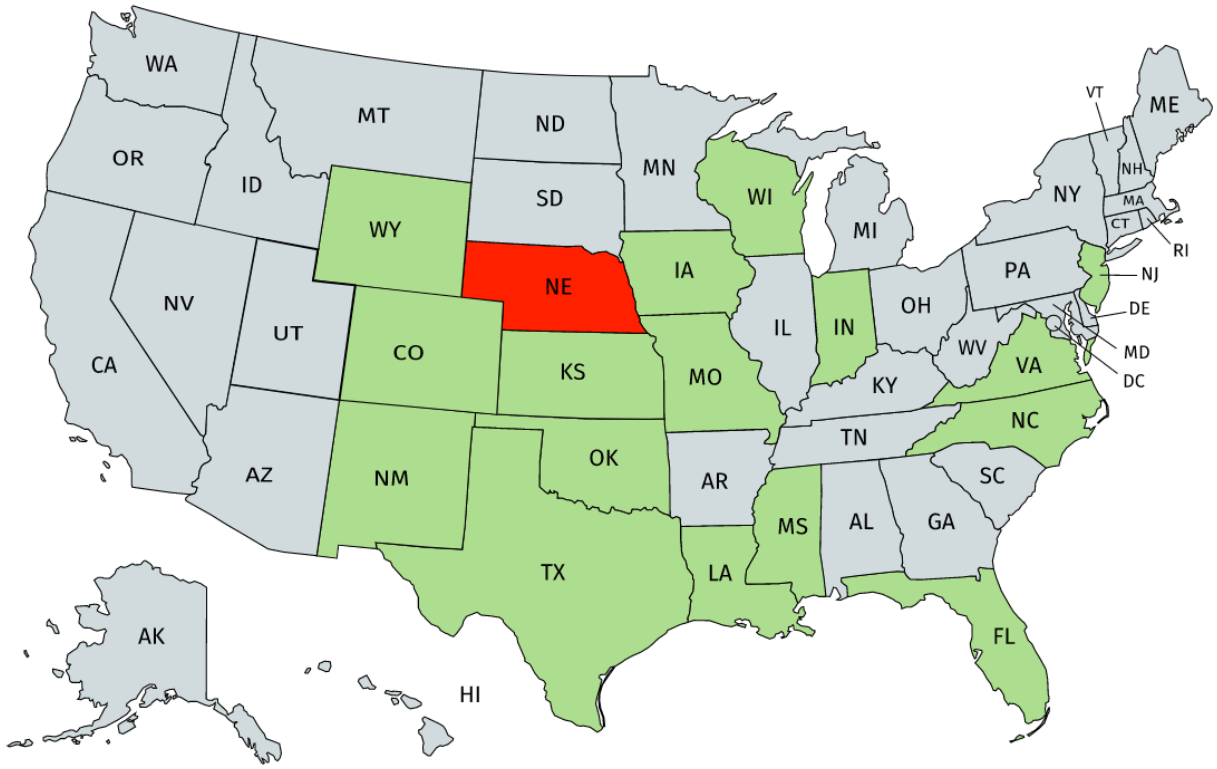

Figure 2.12 States surveyed in this study (highlighted in green).

These states could be grouped according to the type of the approach slab foundation as follows:

- Box-shape (8 states): OK, KS, MS, MO, WI, WY, TX, LA
- L-shape (3 states): IN, NJ, NC
- Inverted T-shape (4 states): IA, CO, VA, NM
- No slab (1 state): FL

A review of each state DOT guidelines, design of the approach slab foundation, and observed issues are presented in the following paragraphs.

Oklahoma

An example of the approach slab foundation is presented in Figure 2.13 based on the drawings obtained from ODOT (Oklahoma Department of Transportation), while Figure 2.14 shows the sleeper slab plan and elevation. The dimension of the grade beam is 2 ft in height and 3 ft in width, supported by bearing piles to mitigate the settlement issues. Overall, such an approach slab foundation design is very similar to that in Nebraska.

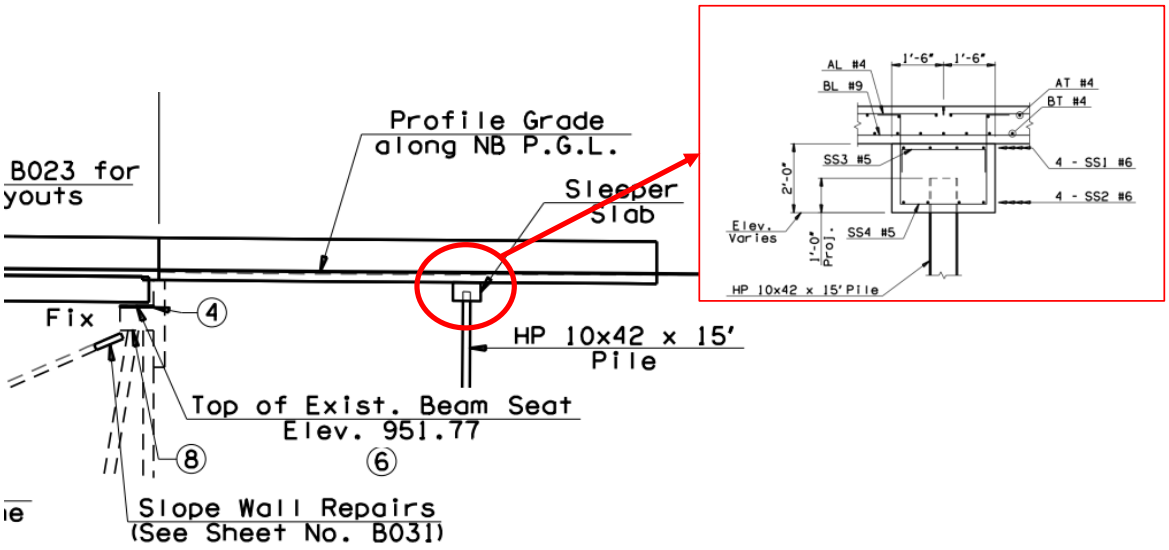

Figure 2.13 An example of the approach slab foundation design in Oklahoma (ODOT, 2019).

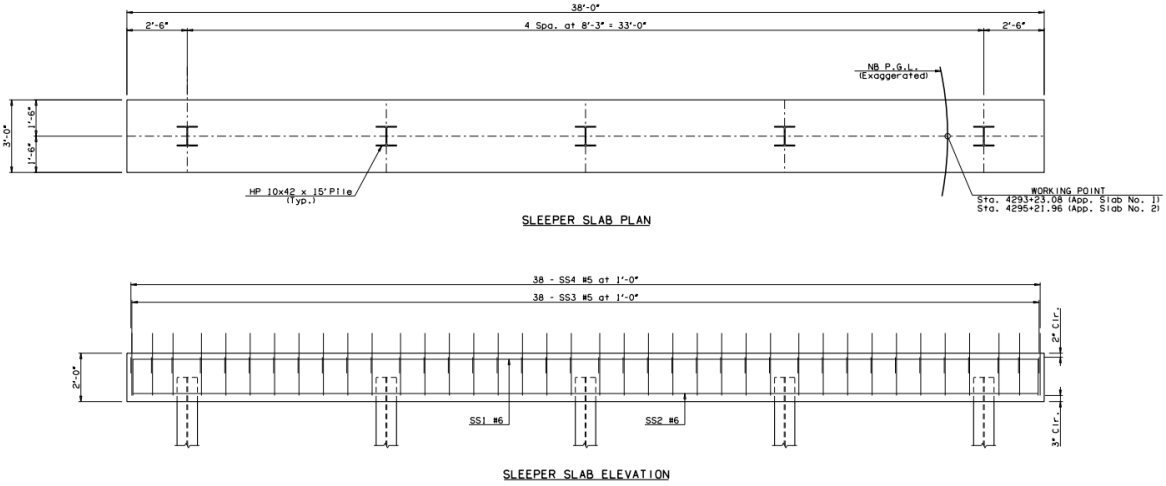

Figure 2.14 An example of the grade beam plan and elevation, along with the bearing piles.

According to the study by Miller et al. (2013), following problems were reported in Oklahoma:

- Substantial void formation under the approach slab

- Excessive settlement of the approach slab
- Large distress under approach slab
- V-shaped deformation under the approach slab

Some examples of such issues are shown in Figure 2.15. Miller et al. (2013) recommended the following solutions to mitigate the settlement issue in the approach slab:

- A better control of the drainage of the embankment under the approach slab, especially where the approach slab meets the bridge and where a potential lateral flow of water is expected to minimize the soil loss.
- Use of piles in the foundation soil under the embankment.
- Deep soil mixing (DSM), which is an economical solution for big projects constructed in compressible soft foundation soils.
- Controlled Modulus Columns (CMC) or Rammed Aggregate Piers (RAP) for the foundation soils.
- Use of lightweight aggregates (LWA) as an embankment material, which will reduce the weight imposed on the foundation soil. One of these LWA proposed to be used is expanded clays and shales (ECS).
- The use of intelligent compaction (IC), where the vibratory rollers is equipped with a system that can control the compaction parameters.

Figure 2.15 Some examples of the differential settlement problems encountered in the approach slabs in Oklahoma (after Miller et al., 2013).

Texas

The approach slab rests on a 5 ft length × 1 ft high box-shaped sleeper slab. Figure 2.16 shows details of the design obtained from TxDOT.

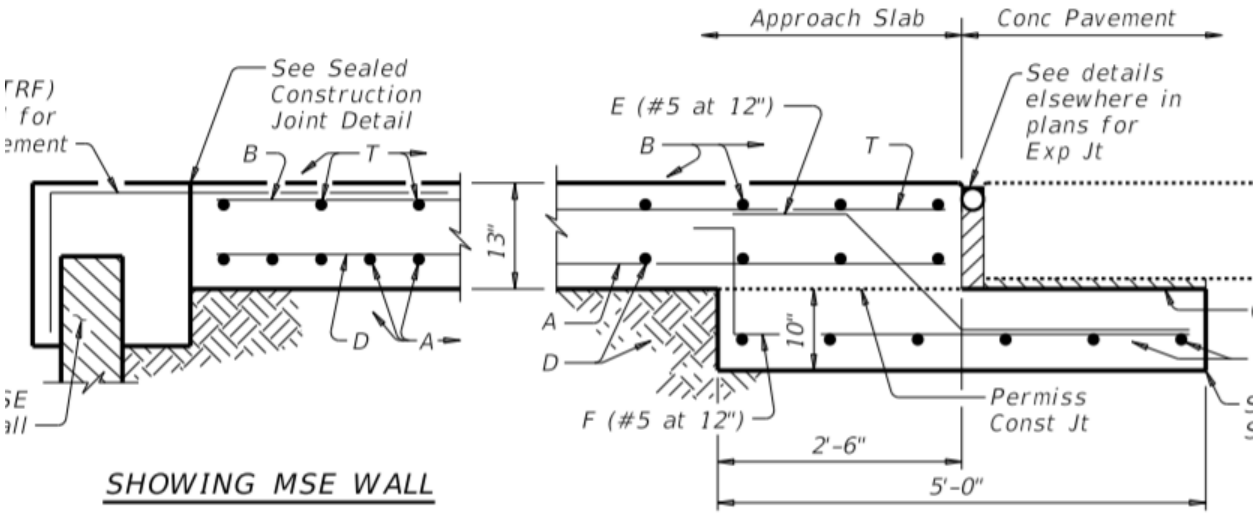

Figure 2.16 Details of the approach slab design in Texas (TxDOT, 2019).

In a study conducted by Briaud et al. (2002), major issues associated with the approach slab settlement were identified as follows:

- Settlement of the natural soil under the embankment.
- Compression of embankment fills.
- Erosion of the embankment due to poor drainage behind the abutment.

Another study conducted by Jayawickrama et al. (2005) stated that the differential settlement at the approach slabs is a very common problem in many bridges in Texas. An example of such a problem associated with the approach slab settlement in Texas is shown in Figure 2.17; the erosion of the backfill material (classified as non-plastic poorly graded sand) and the settlement of the foundation soils caused the approach slab distress and the failure of the modular block. Puppala et al. (2012) provided a flow chart, as shown in Figure 2.18, to mitigate the settlements, and thus, to prevent bump formations on the approach slab in Texas.

Figure 2.17 A modular block failure and erosion in the embankment fill under the approach slab. (after Puppala et al., 2012).

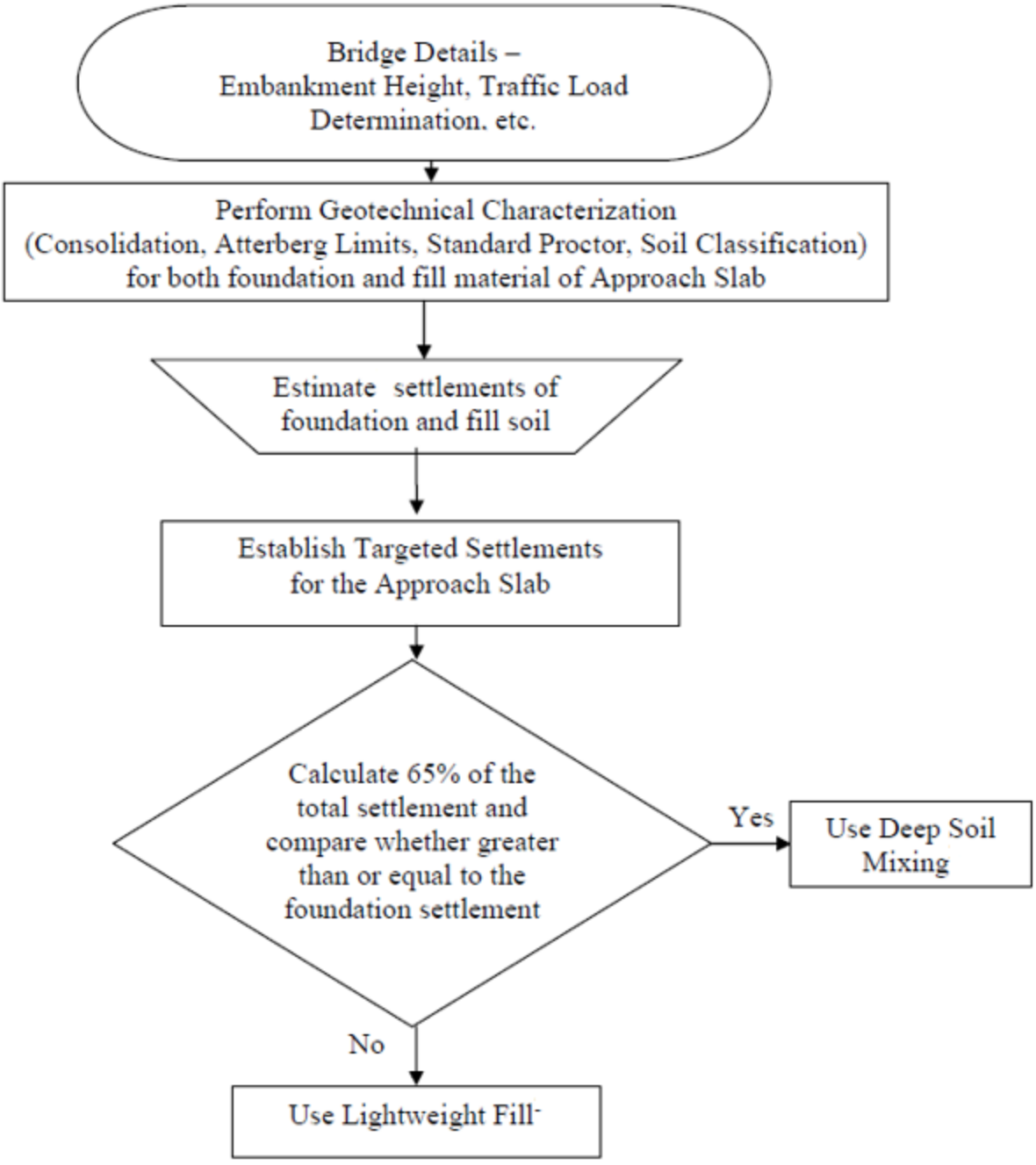

Figure 2.18 A procedure for choosing the best mitigation alternative for the approach slab settlement problems.

Kansas

Details of the approach slab design in Kansas are presented in Figure 2.19. The approach slab foundation is a box shape with a length of 4 ft and a height of 2 ft, which rests directly on compacted soils.

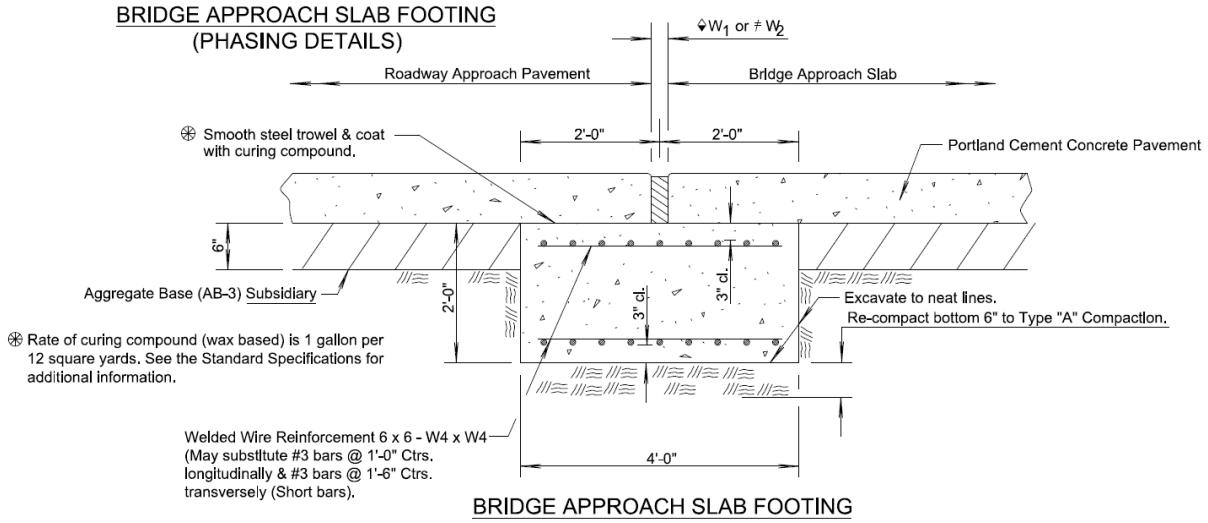

Figure 2.19 Details of the approach slab design in Kansas (2019).

Thiagarajan and Gopalarathnam (2010) reported that the backfill soils beneath the approach slab settled in several sites, which led to a differential settlement in the approach slab itself. It resulted in cracks appearing on the approach slab section. Soil erosion underneath the approach slab was also reported. Figure 2.20 shows an example of problems encountered with the approach slab in Kansas.

Figure 2.20 An example of problems encountered in the approach slabs in Kansas (Thiagarajan and Gopalarathnam, 2010).

In this regard, it was recommended to use 95% of the maximum density of backfill soils based on the standard proctor test and to target the water content of ± 2% of the optimum moisture content (Parsons et al., 2001). A study conducted by Dupont and Allen (2002) indicated that 38 states use compacted granular backfill, while 17 states may use compacted clay soils as well. Ha et al. (2002) found that clay embankments resulted in higher settlement than the embankment constructed from granular materials.

Wyoming

The typical design of the approach slab in Wyoming is shown in Figure 2.21. It represents a box-shaped approach slab with 1 ft of height and 6 ft of width.

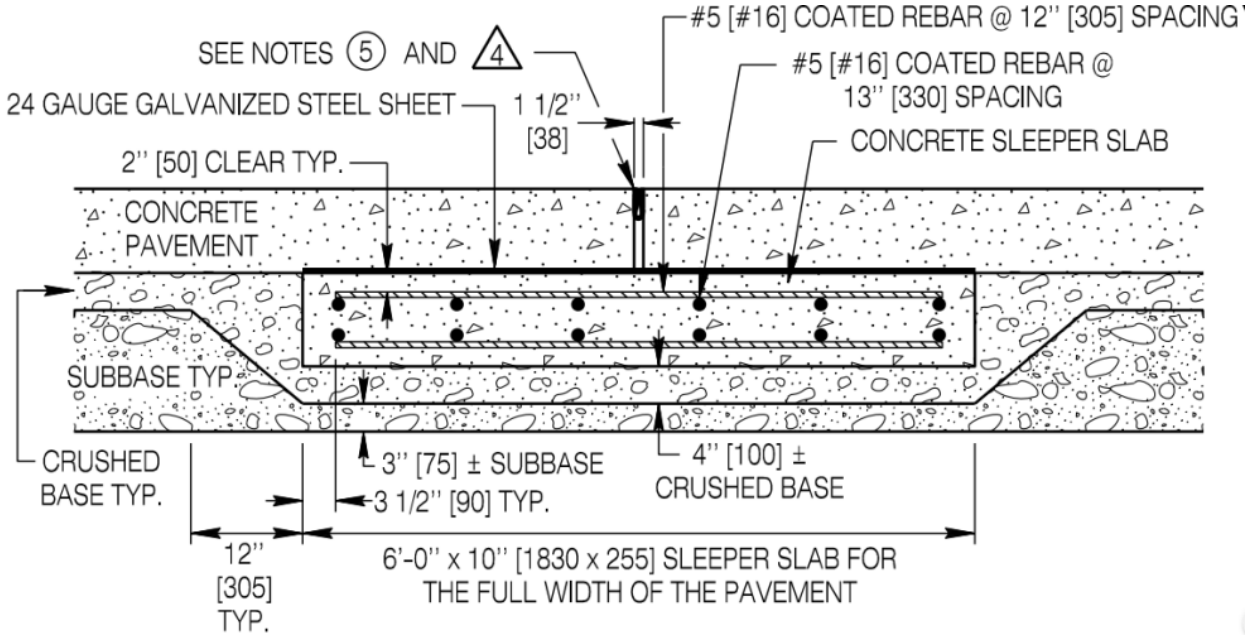

Figure 2.21 Details of the approach slab design in Wyoming (WYDOT, 2018).

In a study by Ng et al. (2015), they reported the formation of voids ranging from 6 in. to 12 in. deep between the base of the approach slab and the backfill, as shown in Figure 2.22. It was reported that the settlement in some cases led to damages in the abutment corbels.

Figure 2.22 An example of problems encountered in the approach slab in Wyoming (Ng et al., 2015).

Yasrobi et al. (2016) confirmed the previous findings and recommended the following:

- Increase or retain the thickness of the approach slab to between 12-16 in. while checking the corbel depth when a thicker approach slab is designed.
- Use a well-graded material as backfill to enhance the drainage. Additionally, the backfill material should be compacted to at least 95 % of the standard proctor density, which agrees with Hopp (1999).

Iowa

The approach slab is designed to be supported on the bridge abutment at one end and on the embankment fill or a sleeper slab (or wider beam) at the other end. Details of the approach slab in Iowa are shown in Figure 2.23.

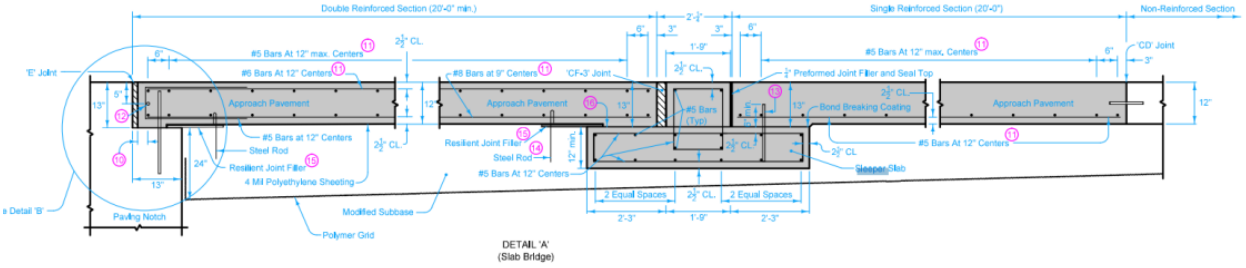

Figure 2.23 Details of the approach slab design in Iowa (2017).

White et al. (2005) surveyed six districts in Iowa and provided a list of encountered problems. Their findings are described in Figure 2.24.

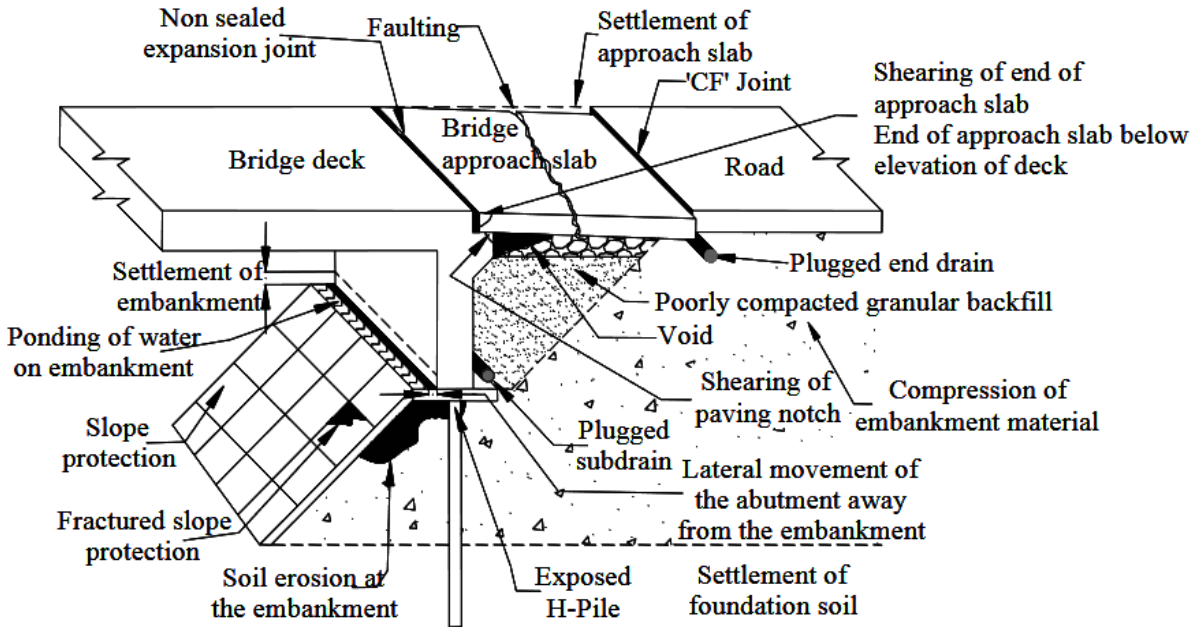

Figure 2.24 A survey of problems encountered in the approach slabs in Iowa (White et al., 2005).

White et al. (2005) also recommended the following to avoid a severe bump issue:

- Use porous backfill and geocomposite drainage system behind the abutment. It will lead to a reduction in the erosion at the abutment and increase the drainage capacity.
- Adjust the granular backfill in that a percentage of passing No. 8 sieve is below 60%; control the moisture content to be in a range of 8% to 12%.
- For bridges with soft foundations, use improvement techniques such as foundation preloading.

Louisiana

A new approach slab system had been introduced in Louisiana in which geosynthetic reinforcements are placed beneath the sleeper slab. Details of this new approach slab design are shown in Figure 2.25 (note: an older design is placed in the red inset rectangle).

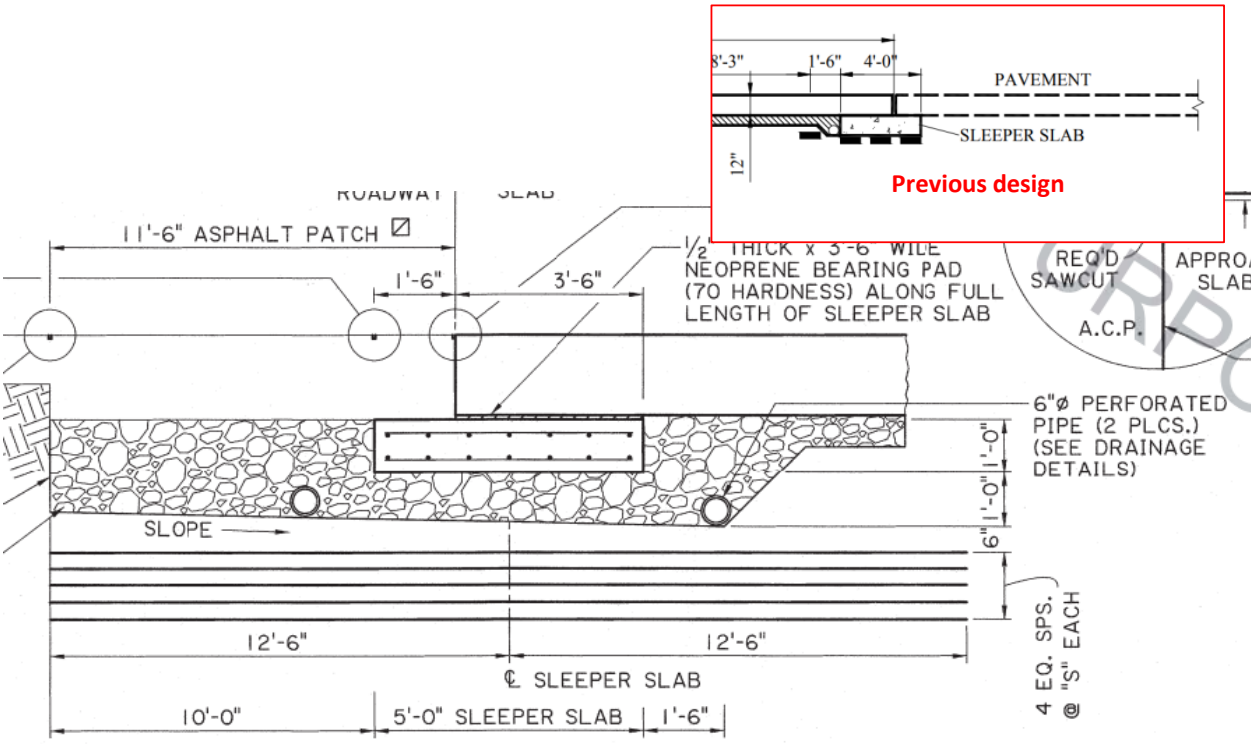

Figure 2.25 Details of the approach slab design in Louisiana (LDOTD, 2017).

Problems encountered with the previous design were reported by Cai et al. (2005). They showed how the differential settlement led to a decrease in the contact area between the approach slab and the embankment soil using a numerical model. It enforced a larger load to be carried by the sleeper slab.

Abu Farsakh and Chen (2014) evaluated the new approach slab design in Louisiana with the geosynthetic reinforcement under the sleeper slab. They monitored two embankments, one constructed with the previous design and the other with the new design that includes 25 ft-five geosynthetic layers equally placed beneath a sleeper slab in a subgrade, as shown in Figure 2.26. Their study results show that the new approach slab design performed well. It was also reported that the new approach slab design showed no loss of contact after the first static load test, but the second load test led to contact loss between the approach slab and the embankment soil.

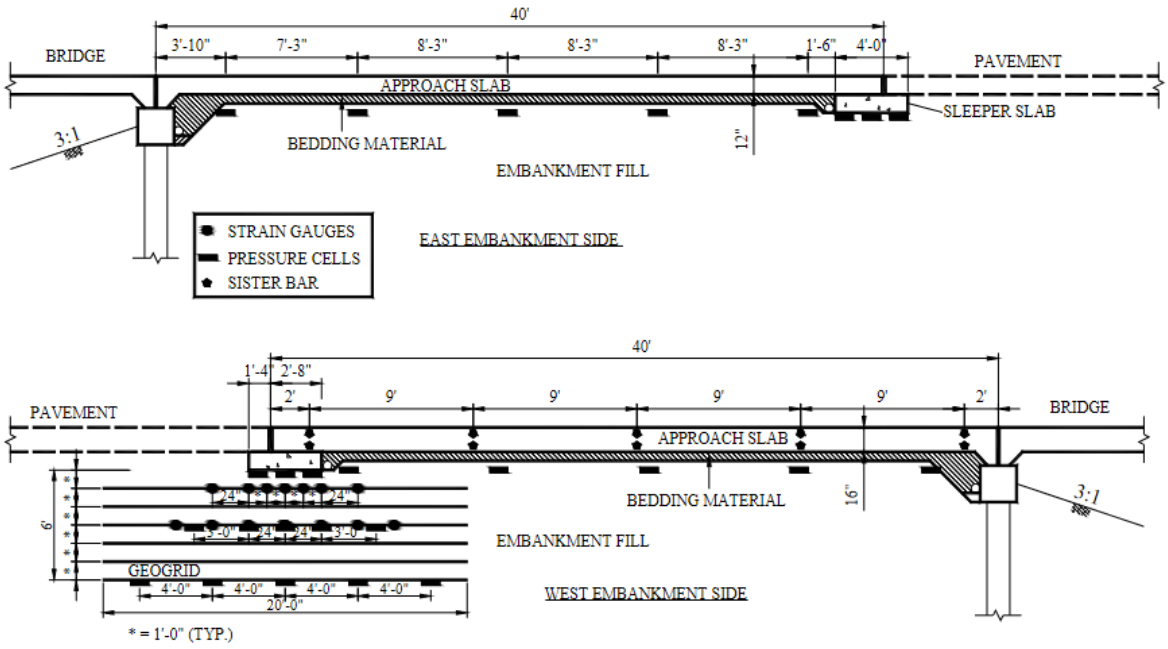

Figure 2.26 The previous and new approach slab design monitored by Abu Farsakh and Chen (2014).

Table 2.1 provides a summary of the approach slab foundation and major problems/issues from those states surveyed in this study.

Table 2.1 Summary of the review on the approach slab foundation design and major issues in many states in the US.

State	Approach slab foundation	Major issues	References
IA	Sleeper slab Inverted T-shape Width: 6.2 ft Height: 2 ft	· Differential settlement of approach slab. · Void formation under approach slab.	IOWA DOT (2017) White et al. (2007) White et al. (2005)
CO	Sleeper slab Inverted T-shape Width: 4 ft Height: 2 ft	· Significant approach slab settlement. · High repair cost.	CDOT (2019) Abu-Hejleh et al. (2006)
TX	Sleeper slab Box-shape Width: 5 ft Height: 1 ft	· Settlement of natural soil under embankment. · Erosion of embankment.	TxDOT (2019) Briaud et al. (2002)
VA	Sleeper slab Inverted T-shape Width: 5.5 ft	· Excessive settlement in the approach slab due to the lack of compaction in the approach fill.	VDOT (2008) Hoppe (1999)

	Height: 2.2 ft	· Settlement in the foundation soil. · High maintenance cost.	
KS	Sleeper slab Box-shape Width: 4 ft Height: 2 ft	· Backfill settlement. · Differential settlement in the approach slab. · Cracking in the approach due to uneven settlements. · Soil erosion underneath the approach slab.	KDOT (2019) Thiagarajan and Gopalartnam (2010)
MS	Sleeper slab Box-shape Width: 6 ft Height: 1 ft	· Frequent problems in settlement of approach slab and potholes were reported. · Pavement distress near bridge end due to insufficient compaction effort of the base and movement of the approach slab.	MDOT (2017) Lu et al. (2018) Thiagarajan and Gopalartnam (2010)
FL	N/A	· Asphalt pavement cracking and rutting. · Embankment settlement. · Settlement of approach slab. · Movement away from the backwall. · Erosion at the edges of approach slab.	FDOT (2016) Lu et al. (2018) Tayabji (2018)
NM	Sleeper slab Inverted T-shape	· Excessive approach slab settlement. · Extreme distress with cracking in the approach slab. · Severe settlements were reported in the approach embankment; it was related to no preconsolidation in foundation soil before the construction.	NMDOT (2012) Lenke (2006) Thiagarajan and Gopalarthnam (2010)
IN	Sleeper slab L-shape Width: 6 ft Height: 2 ft	· Settlement of approach slab. · Cracking on the approach slab.	INDOT (2020) Chee (2018) Lu et al. (2018)
MO	Grade beam Box-shape Width: 3 ft Height: 1.5 ft	· Major cracks on the approach slab. · Soil erosion under the approach slab. · Settlement of approach slab.	MoDOT (2020) Thiagarajan and Gopalarthnam (2010) Luna et al. (2004)
NC	Sleeper slab L-shape Width: 2.65 ft Height: 1.5 ft	· Natural soil settlement beneath the embankment. · Settlement in approach slab. · Joint failure between approach slab and structure.	NCDOT (2006) Wahls (1990) Thiagarajan and Gopalarthnam (2010)
OK	Grade Beam + Pile Grade beam: Box-shape Width: 3 ft Height: 2 ft	· Substantial void formation under the approach slab. · Excessive settlement of the approach slab. · Large distress under approach slab. · V-shaped deformation of the approach slab.	ODOT (2019) Miller et al. (2013)
WI	Sleeper slab Box-shape Width: 5 ft	· Settlement of approach slab. · Void formation beneath the approach slab. · Approach slab cracks at the abutment.	WisDOT (2018) Helwany (2007)

	Height: 1.5 ft		
WY	Sleeper slab Box-shape Width: 6 ft Height: 1 ft	· Voids ranging from 6 to 12 in. between the base of the approach slab and the backfill. · Settlement in some cases led to damages in abutment corbels.	WYDOT (2018) Ng et al. (2014)
NJ	Sleeper slab L-shape Width: 2.5 ft Height: 2 ft	· 50 % of the approach slabs developed cracks. · Settlement in the approach slab.	NJDOT (2005) Chee (2018) Nassif et al. (2007)
LA	Sleeper slab + geosynthetics Sleeper slab: Width: 5 ft Height: 1 ft	Previous design issue: · Differential settlement at the approach slab. · Approach slab embankment settlement. · Contact loss between the approach slab and the embankment.	LDOTD (2017) Abu-Farsakh and Chen (2014) Cai et al. (2005) Bakeer et al. (2005)

3. Study I: Improvement of Current Bridge Approach Design

3.1 Soil conditions and constitutive models

A bridge site in Nebraska shown in Figure 3.1 was chosen for a detailed numerical study I and II in the following chapter. The foundation soil is composed of Peoria loess and silty soils, underlain by glacial till. This bridge was chosen as it represents one of the sites in which the grade beam piles and abutment piles retain the same spacing of 7.2 ft, as shown in Figure 3.2. Given that the first objective of the detailed numerical study is to investigate the effect of pile spacing increase and the pile length reduction under the grade beam, this bridge site can serve as a good starting base model. The detail of the backfill soil design in Nebraska is shown in Figure 3.3, which is also incorporated into the numerical simulation model.

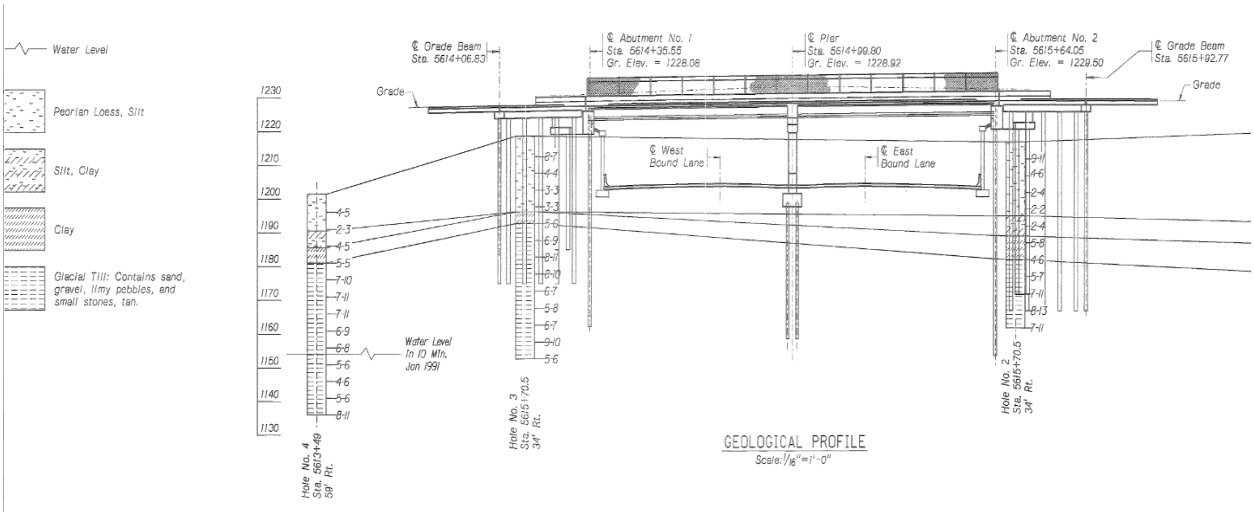

Figure 3.1 The bridge site in Nebraska (structure number S006-36093) that is used for in-depth numerical study.

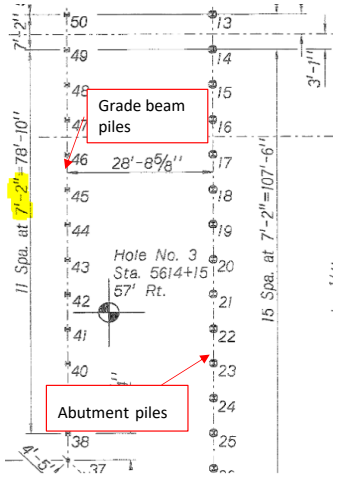

Figure 3.2 Top view – the spacing of abutment piles (right) and grade beam piles (left).

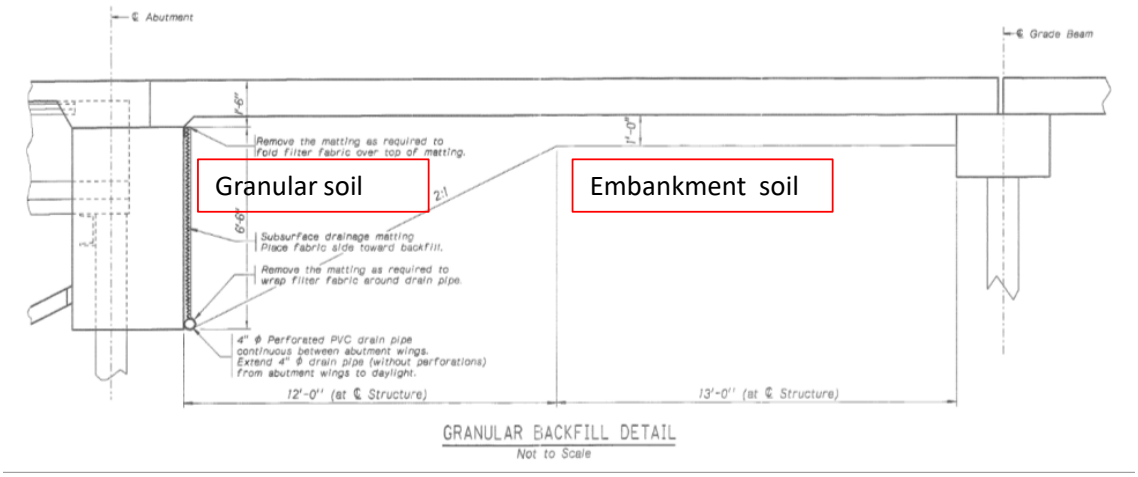

Figure 3.3 An example of the granular backfill design in Nebraska.

A two-dimensional finite different analysis using FLAC (Fast Lagrangian Analysis of Continua) is used to numerically model the bridge (structure number S006-36093), including abutment structure, approach slab, and roadway pavement, in Nebraska. The bridge model (Figure 3.8) is restrained in both horizontal and vertical directions at the bottom. Moreover, a roller is placed on both sides to confine any horizontal movements while allowing vertical deformation. The mesh is established with a ratio to be of a diminutive size on the top of the model to account for the smallest changes in the model and to obtain a higher accuracy than a coarse grid.

The soils were modeled as linearly elastic and perfectly plastic materials with the Mohr-Coulomb failure criterion. The property of soils used in the numerical simulation model in FLAC 2D is summarized in Table 3.1. Note that the property of embankment soil is based on the input supplied by the NDOT engineers.

Concrete parts (abutment, approach slab, and paving section) and the asphalt overlay were simulated as an elastic model. Table 3.2 presents the properties of the concrete and the asphalt overlay used in the numerical simulation. The abutment and grade beam piles were modeled using pile elements in FLAC 2D. The input parameters for the pile elements used in this study are summarized in Table 3.3. The pile elements interact with the soil through shear and normal coupling springs. The material behavior of those shear and normal coupling springs is illustrated in Figures 3.4 and 3.5, respectively, in which F_s and F_n denote the shear and normal forces that develop in those coupling springs, respectively. σ'_c denotes the mean effective confining pressure. The details of geogrid reinforcement used in a further simulation model are discussed in Section 4.2.

Table 3.1 The property of soils used in the numerical study.

Parameter	Soil type			
	Granular soil	Embankment soil	Peoria loess	Foundation soil (Glacial till)
Modulus of elasticity (psi)	4,786 [(1)]	7,251 [(2)]	4,267 [(7)]	10,152 [(5)]
Density (pcf)	110 [(2)]	122 [(2)]	110 [(2)]	120 [(2)]
Poisson's ratio (-)	0.3 [(1)]	0.25	0.25 [(3)]	0.25
Cohesion (psi)	0 [(2)]	0	2.5 [(4)]	3.47[(6)]
Friction angle (°)	30 [(2)]	28 [(2)]	27 [(2)]	29 [(2)]
Dilatancy Angle (°)	6 [(1)]	0	0	0

References: [(1)] Hatami and Bathurst (2001), [(2)] NDOT (1990), [(3)] Lambe and Whitman (1969) [(4)], Song et al (2019), [(5)] Radhakrishna and Klym (1974) [(6)] IOWA DOT (2015). [(7)] Subramanian (2006).

Table 3.2 The property of concrete and paving section parts used in the numerical study.

Parameter	Layer			
	Concrete*	Granular subbase	Subgrade sand	Asphalt
Modulus of elasticity (psi)	3.481×10^6	4,786	7,252	174.1×10^3
Density (pcf)	156	133	124.8	143.5
Poisson's ratio (-)	0.2	0.3	0.25	0.25
Cohesion (psi)	0	0	0	0
Friction angle (°)	0	65	35	0
Reference	(1)	(2)	(3)	(4)

* It represents the concrete layer in the abutment, grade beam, approach slab and paving section.
References: [(1)] Zheng et al. (2014), [(2)] Karpurapu et al. (2014), [(3)] IOWA DOT (2015), and [(4)] Tan et al. (2017)

Table 3.3 The input parameters for the pile element in the numerical study.

Parameter	Value
Pile radius (in)	6
The modulus of elasticity (psi)	2.9×10^7
Shearing friction angle, cs_fric (°)	20
Shearing stiffness, cs_sstiff (psf)	27.2×10^8
Cohesion strength of the shear coupling spring, cs_scoh (lb/ft)	34,000
Normal stiffness, cs_nstiff (psf)	27.2×10^5
Cohesion strength of the normal coupling spring, cs_ncoh (lb/ft)	340
Normal friction angle, cs_nfric (°)	10

References: Owino (2018)

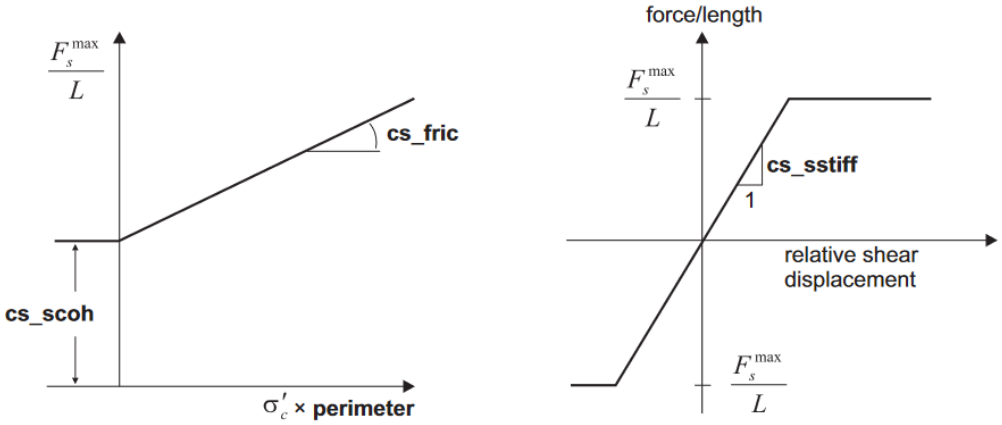

Figure 3.4 The material behavior of the shear coupling spring for pile element (Itasca, 2016).

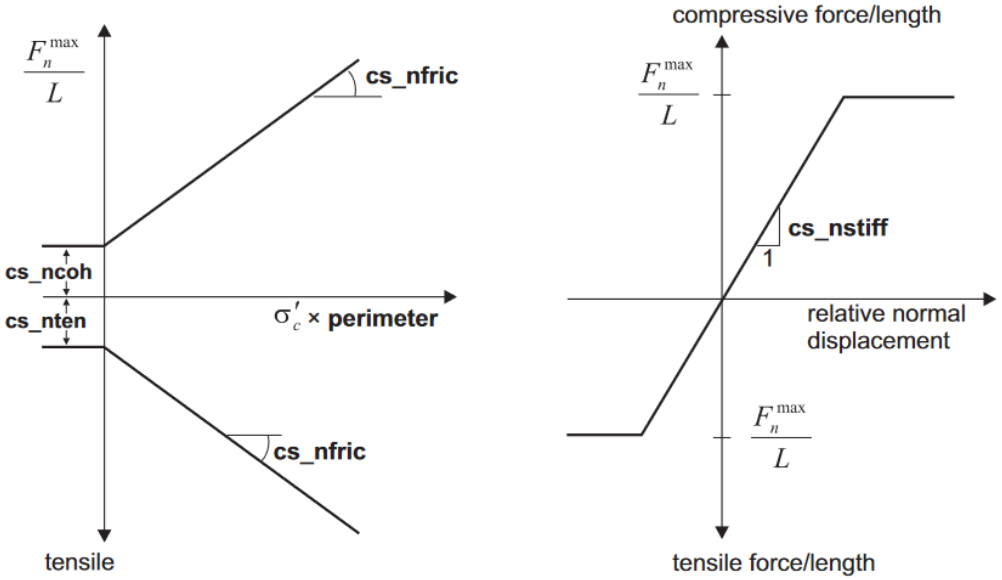

Figure 3.5 The material behavior of the normal coupling spring for pile element (Itasca, 2016)

3.2 Numerical simulation model

3.2.1 Loading condition and validation of soil-pile interaction in the model

A tandem vehicle, rather than the design truck, was chosen to represent the highest load that could be imposed on the approach slab. Note that the distance between loading points is smaller in the tandem load (4 ft), compared to that in the design truck (14 ft). Such a loading condition was shown to belong to the worst loading conditions to evaluate the approach slab performance in Missouri (Thiagarajan and Gopalaratnam, 2010).

Besides, the design lane load of 640 lbs per linear foot is to be included for a span that is longer than 15ft, according to provision 3.4.3.4 of AASHTO-LRFD (2015). In this regard, a combination of the tandem vehicle loading (25 kips) and the design lane loading (uniform 640 lbs/ft) was determined as the final loading condition, as shown in Figure 3.6 (highlighted in red).

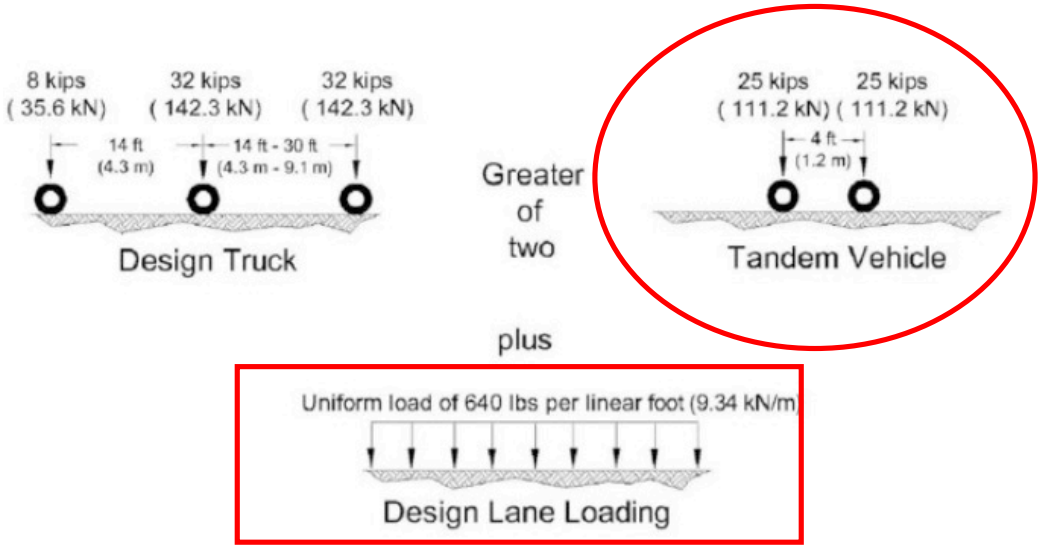

Figure 3.6 The loading condition selected for the numerical study.

In order to validate the soil-pile interaction in the numerical simulation approach by the team, an axisymmetric axially loaded pile was modeled in FLAC, and its results were compared with those from an analytical solution. Readers are referred to Section (1) “Validation of the numerical simulation approach: soil-pile interaction” in the Appendices for the detail.

3.2.2 Simulation model

(1) Investigation of the grade beam pile spacing

A parametric study was conducted to evaluate the effect of increasing the grade beam pile spacing on the differential settlement near the approach slab. The numerical model for this parametric study is shown in Figure 3.7. The spacing of grade beam piles was increased in the range between 150% to 300% (i.e., 67% to 33% decrease in the number of grade beam piles), as presented in Table 3.4. The axial forces and skin frictions along the grade beam and abutment piles due to such an increase are analyzed. The vertical settlement profiles under the abutment (AB) section, grade beam (GB) section, and the pacing section (Figure 3.8) are also investigated. Lastly, the differential settlements between the abutment-grade beam sections and the grade beam-paving sections are compared.

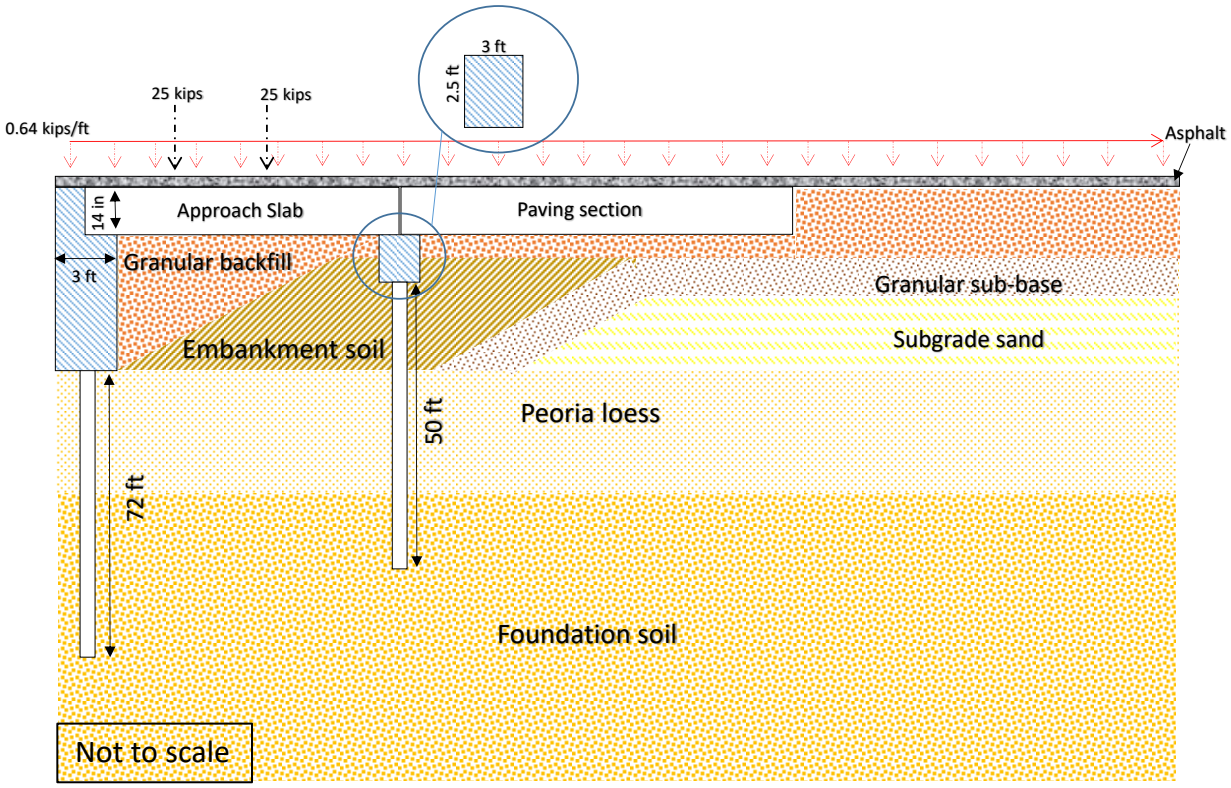

Figure 3.7 The numerical simulation model to investigate the effect of grade beam pile spacing.

Table 3.4 Cases for the investigation of the spacing of grade beam (GB) piles.

Case #	Spacing between GB piles	Increase from the base case (decrease in the pile number)
Base (original design)	7.2 ft	-
I-1-1	10.8 ft	150% (67%)
I-1-2	14 ft	200% (50%)
I-1-3	18 ft	250% (40%)
I-1-4	21 ft	300% (33%)

Note: the length of grade beam piles is the same at 50 ft.

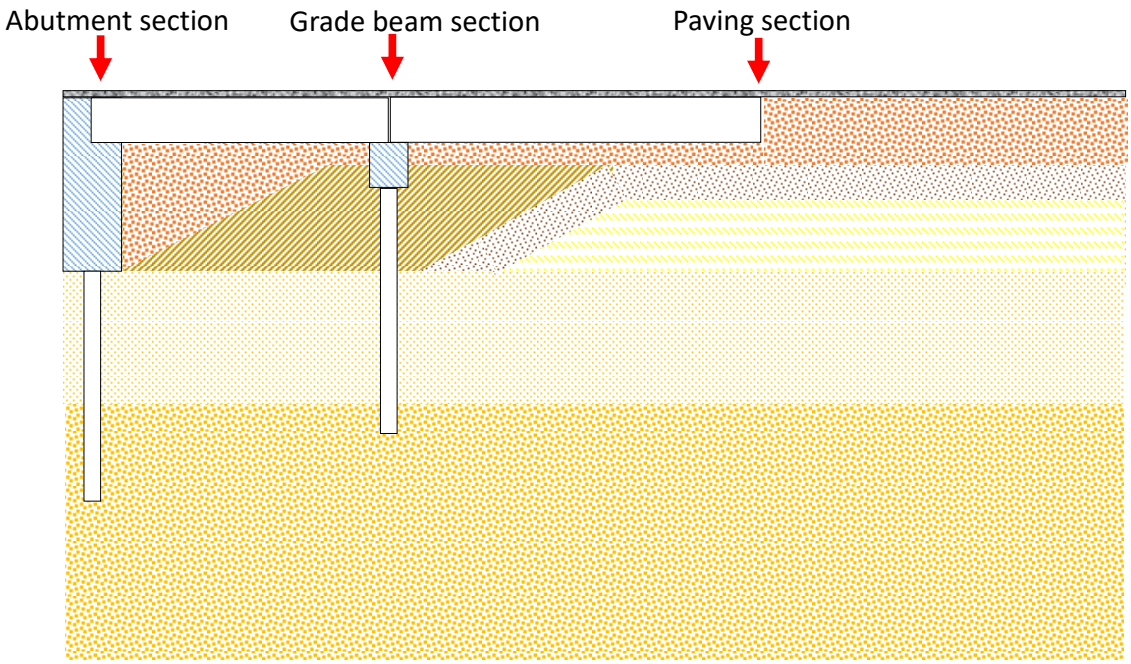

Figure 3.8 A schematic drawing that shows the location of the abutment (AB), grade beam (GB) and paving sections.

(2) Investigation of the grade beam pile length

The effect of reduction in the length of the grade beam piles is investigated in the next parametric study. Two cases, 35% and 70% reduction in length were selected for this study (Table 3.5). The details of the simulation model are shown in Figure 3.9.

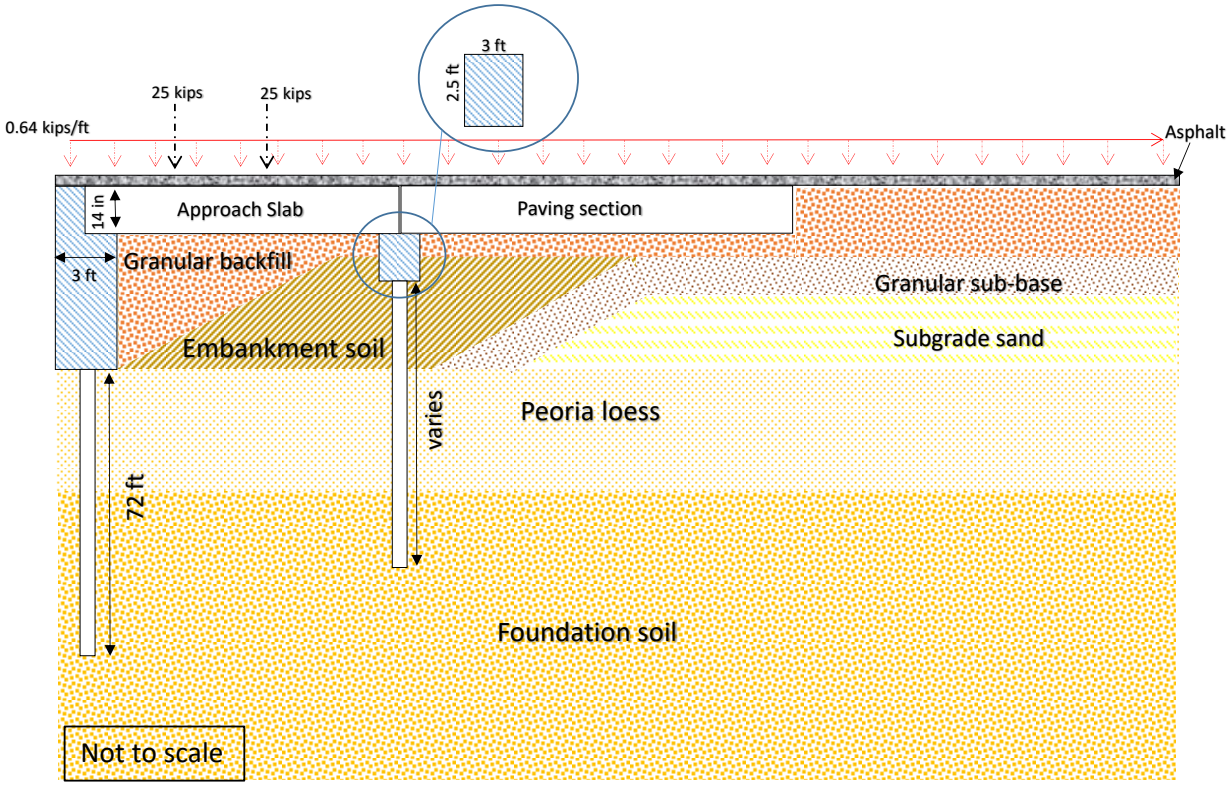

Figure 3.9 The numerical simulation model to investigate the effect of grade beam pile length.

Table 3.5 Cases for the investigation of the length of grade beam (GB) piles.

Case #	Length of GB piles	Decrease from the base case
Base (original design)	50 ft	-
I-2-1	32 ft	~35%
I-2-2	16 ft	~70%

Note: the spacing of grade beam piles is the same at 7.2 ft.

3.3 Results and analyses

(1) Investigation of the grade beam pile spacing

Widening the spacing of grade beam piles (that is, reducing the number of grade beam piles) may result in the increase in the axial load and the mobilized side frictional resistance not only along with the grade beam piles but also the abutment piles. In this regard, we investigated the axial load transmitted to the piles and the mobilized skin frictional resistance along with the piles for all examined cases in Table 3.5. First, those results for the abutment piles are compiled in Figures 3.10 and 3.11, respectively. As shown in those figures, widening the spacing of grade beam piles yields a minor impact on both the axial load transmitted to the abutment piles and the mobilized skin frictional resistance.

It is worth noting that negative skin friction is developed along with the upper portion of the abutment piles. It is known to occur if the settlement of the adjacent soils is large and so creates a down drag force to the pile (example: Wong and Teh (1995), Yao (2012), and Fellenius (2017)). In such a case, a neutral point, about which the skin friction turns from negative to positive, coincides with the depth where the axial load transmitted to the pile is at its maximum value (see Figures 3.10 and 3.11).

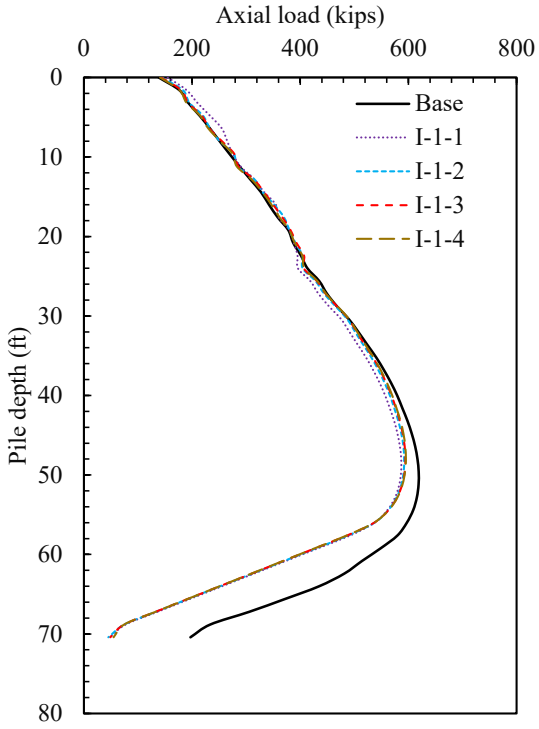

Figure 3.10 The axial load transmitted to the abutment piles for different cases with the grade beam pile spacing (I-1-1 to I-1-4).

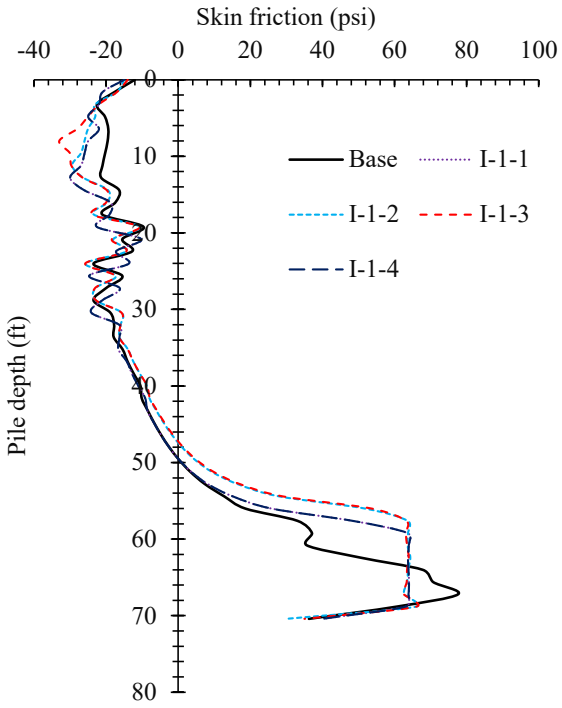

Figure 3.11 The mobilized skin frictional resistance along with the abutment piles for different cases with the grade beam pile spacing (I-1-1 to I-1-4).

In contrast to the abutment piles, widening the spacing of grade beam piles has a noticeable impact on both the axial load and skin frictional resistance mobilized along with the grade beam piles. As expected, a higher axial load is imposed on each grade beam pile as wider pile spacing is considered (Figure 3.12). It is obvious because a fewer number of grade beam piles needs to support the surface loads. Similarly, a higher frictional resistance is mobilized along the grade beam pile shaft as the wider pile spacing is applied due to an increase in the load carried by each pile (Figure 3.13).

Figures 3.14 to 3.16 present the vertical and horizontal stress profiles in the soil in the vicinity of the abutment pile (Figure 3.14), grade beam pile (Figure 3.15), and near the end of the paving section (Figure 3.16), respectively. As shown in those figures, widening the spacing of grade beam piles has a minor impact on both the vertical and horizontal stress profiles developed in the surrounding soils.

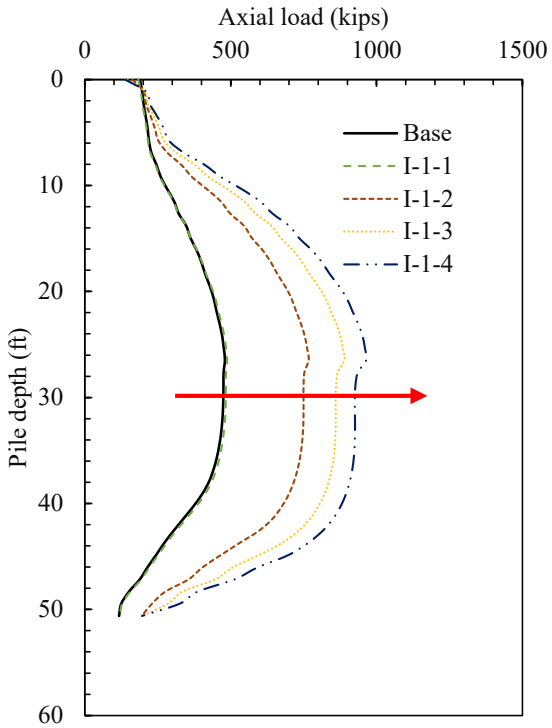

Figure 3.12 The axial load transmitted to the grade beam piles for different cases with the grade beam pile spacing (I-1-1 to I-1-4).

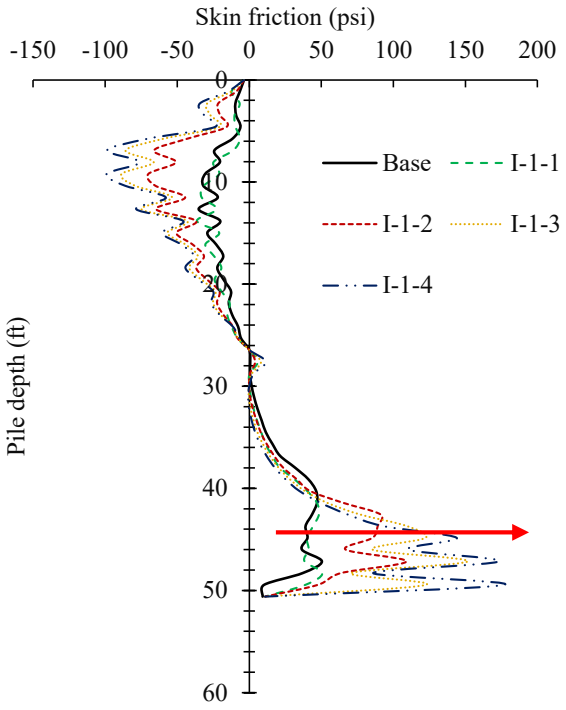

Figure 3.13 The mobilized skin frictional resistance along with the grade piles for different cases with the grade beam pile spacing (I-1-1 to I-1-4).

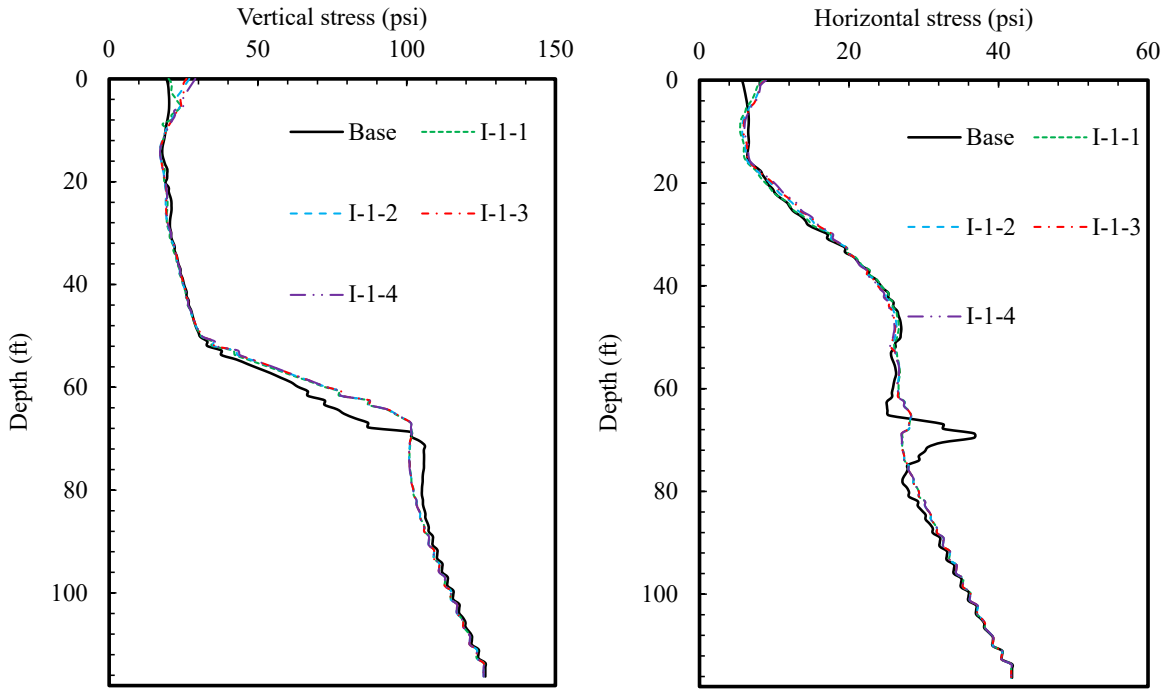

Figure 3.14 The vertical and horizontal stress profiles in the soil in the vicinity of the abutment pile for different cases with the grade beam pile spacing (I-1-1 to I-1-4).

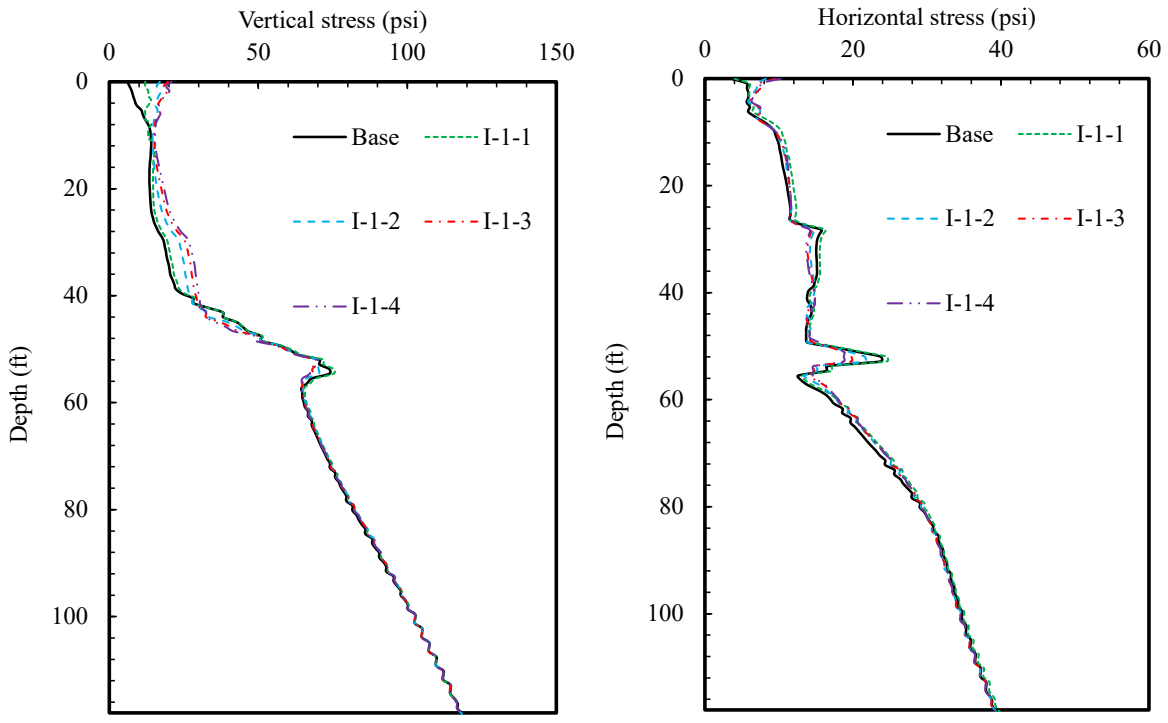

Figure 3.15 The vertical and horizontal stress profiles in the soil in the vicinity of the grade beam pile for different cases with the grade beam pile spacing (I-1-1 to I-1-4).

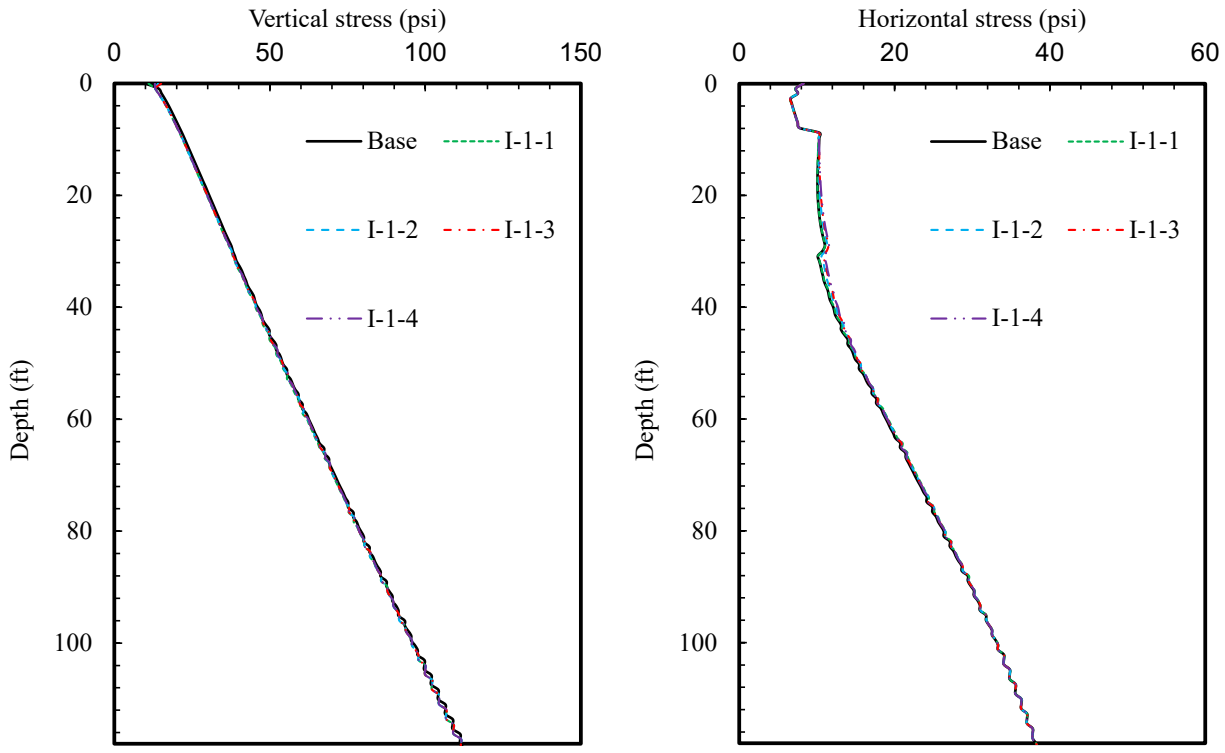

Figure 3.16 The vertical and horizontal stress profiles in the soil near the end of paving section for different cases with the grade beam pile spacing (I-1-1 to I-1-4).

Widening the spacing of grade beam piles results in a minor impact on the vertical settlement profiles across the abutment section, as shown in Figure 3.17. Overall, the vertical settlement profiles for all examined pile spacing cases are acceptable, with the maximum value on the surface being less than a quarter-inch in all the studied cases.

In contrast, increasing the spacing of grade beam piles has a nontrivial consequence on the vertical settlement profiles across the grade beam section, as presented in Figure 3.18. The maximum vertical deformation value on the surface increases as the wider pile spacing is applied. Nevertheless, its maximum deformation is less than 0.4 inches for all studies cases where the spacing was widened up to 300% from the base case. On the other hand, widening the spacing of grade beam piles barely affects the vertical settlement profiles across the paving section (Figure 3.19).

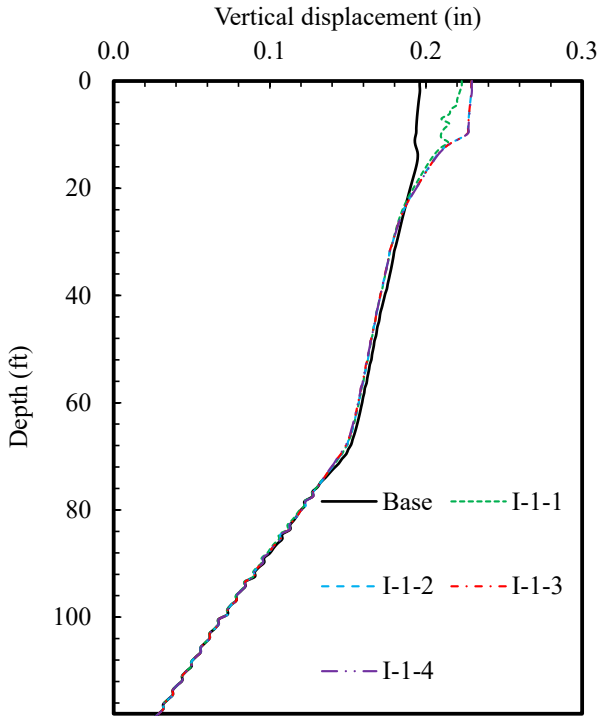

Figure 3.17 The vertical settlement profile across the abutment section for different cases with the grade beam pile spacing (I-1-1 to I-1-4).

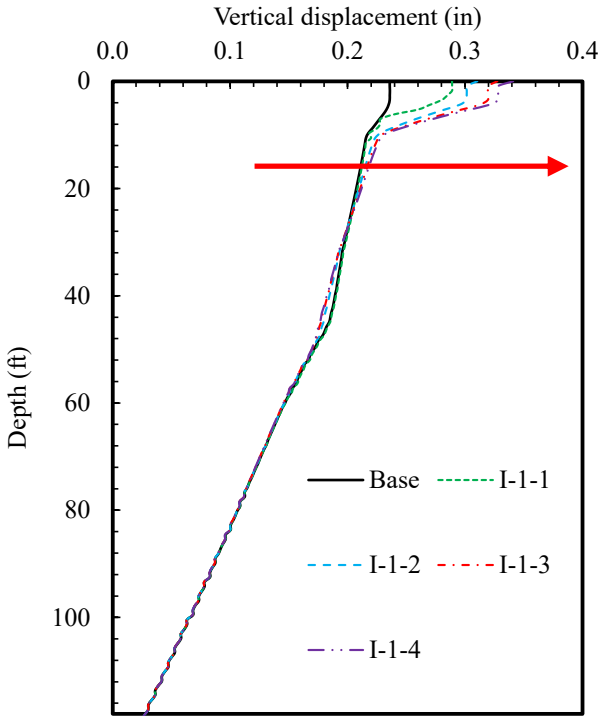

Figure 3.18 The vertical settlement profile across the grade beam section for different cases with the grade beam pile spacing (I-1-1 to I-1-4).

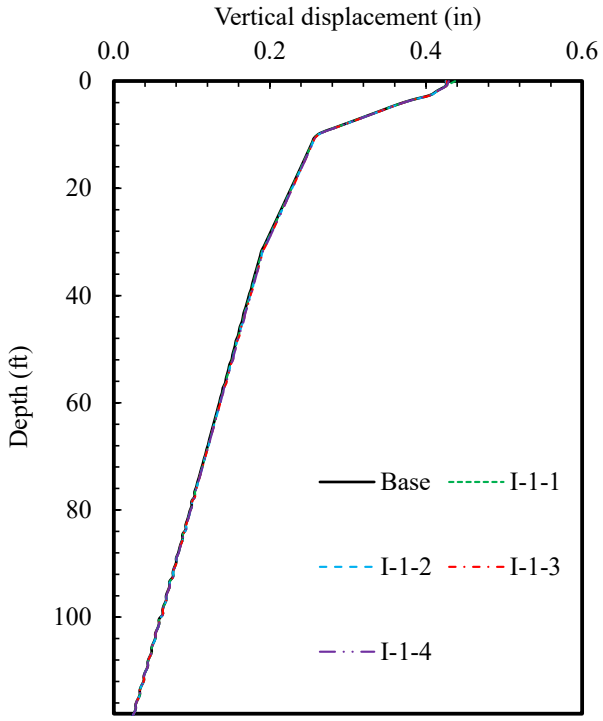

Figure 3.19 The vertical settlement profile across the paving section for different cases with the grade beam pile spacing (I-1-1 to I-1-4).

With those vertical settlements at each section, differential settlements between the abutment and grade beam sections as well as between the grade beam and end of paving sections are examined. First, Figure 3.20 shows the differential settlement between the abutment and grade beam sections. As expected, widening the spacing of grade beam piles results in a slightly increased differential settlement between those two points. Nonetheless, such a differential settlement is less than 0.1 inch for most examined cases (except I-1-4), which can be regarded as tolerable. For reference, the acceptable range of settlements was suggested to be between 0.6 to 2.4 inches for an approach slab which spans a range between 10 to 40 feet (Hoppe, 1999).
Interestingly, widening the spacing of grade beam piles is observed to contribute to alleviating the differential settlement between the grade beam and paving sections, as shown in Figure 3.21. It seems that the differential settlement could be alleviated to around less than 0.1 inches when the grade beam pile spacing is increased to more than 200% of that in the original base case. It occurs because as a smaller number of piles is installed underneath the grade beam, it acts to render the grade beam support less stiff and thus, reduce the settlement difference from that near the paving section. Therefore, widening the spacing of the grade beam pile could help alleviate

the undesirable bump issue near the end of the paving section while maintaining a tolerable level of the differential settlement at the end of the approach slab.

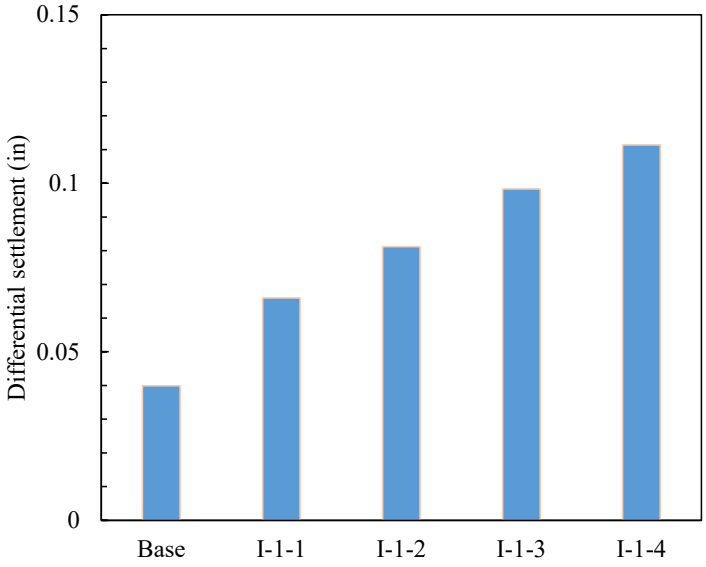

Figure 3.20 Differential settlement between the abutment and grade beam sections for different cases with the grade beam pile spacing (I-1-1 to I-1-4).

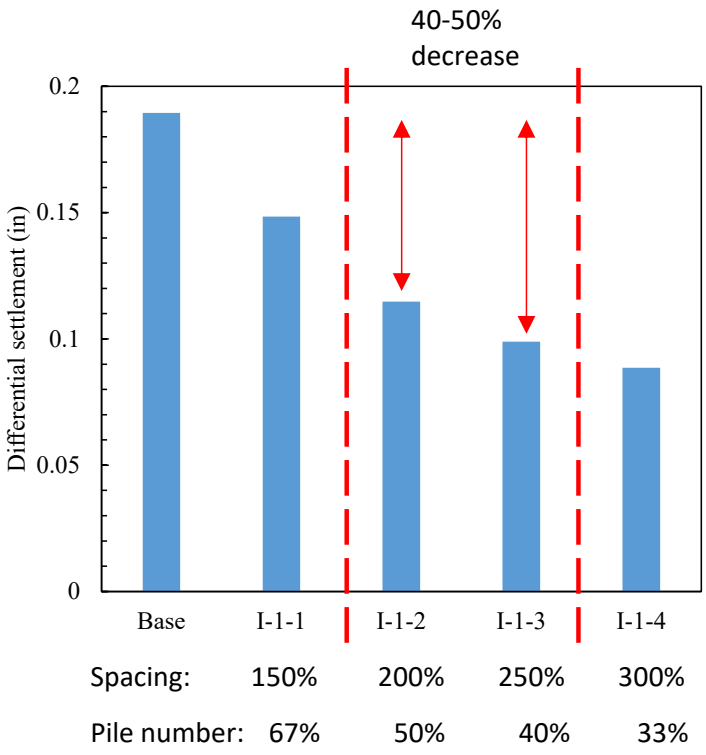

Figure 3.21 Differential settlement between the grade beam and paving sections for different cases with the grade beam pile spacing (I-1-1 to I-1-4).

(2) Investigation of the grade beam pile length

Similar to the investigation of the grade beam pile spacing, shortening the length of grade beam piles has a minor impact on the axial load transmitted to and the frictional resistance mobilized along with the abutment piles. In detail, the axial load slightly increased as the length of grade beam piles is shortened, but its increase was less than 10% even after the length of grade beam piles is reduced by 70% of the base case (Figure 3.22). Shortening the length also yields a minor impact on the skin frictional resistance that is mobilized along with abutment piles (Figure 3.23). In contrast, shortening the length of grade beam piles has a conspicuous impact on the axial load and skin frictional resistance along with the grade beam piles. In detail, the axial load transmitted to the grade beam piles is dramatically decreased when the length is shortened (Figure 3.24), which may have consequences on the mobilized side frictional resistance and settlement of the pile. Figure 3.25 confirms that a larger side frictional resistance is mobilized along with the longer portion of the grade beam pile as the length is shortened. It will lead to an increase in the vertical settlement of the pile.

Figures 3.26 to 3.28 present the vertical and horizontal stress profiles in the soil near the abutment pile (Figure 3.26), grade beam pile (Figure 3.27), and the end of the paving section (Figure 3.28), respectively. As shown in those figures, shortening the length of grade beam piles has a minor impact on both the vertical and horizontal stress profiles developed in the soils near the abutment pile and the end of the paving section. However, significant changes on the stress profiles in the soil are induced near the grade beam pile, which is consistent with the observation in the axial load and skin frictional resistance along with the grade beam piles.

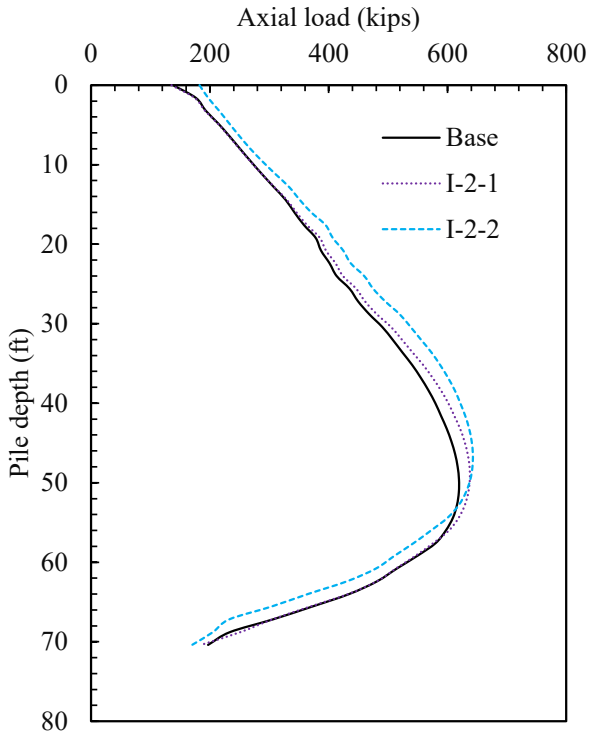

Figure 3.22 The axial load transmitted to the abutment piles for different cases with the grade beam pile length (I-2-1 to I-2-2).

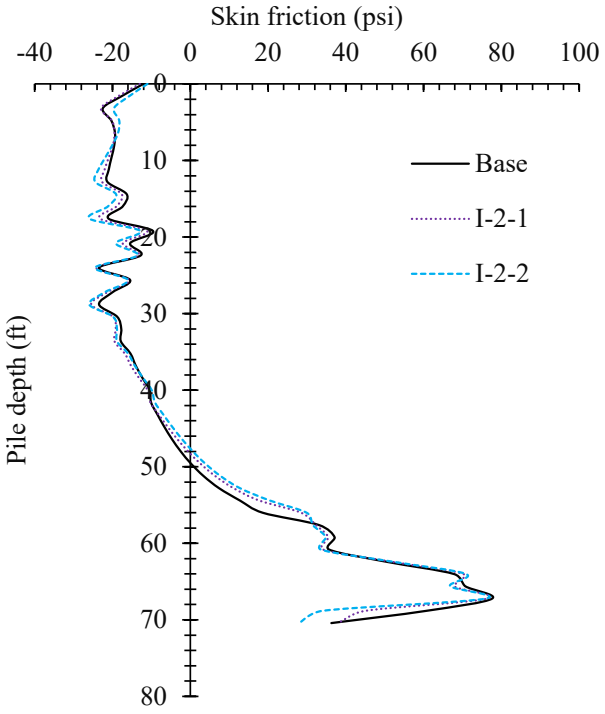

Figure 3.23 The mobilized skin frictional resistance along with the abutment piles for different cases with the grade beam pile length (I-2-1 to I-2-2).

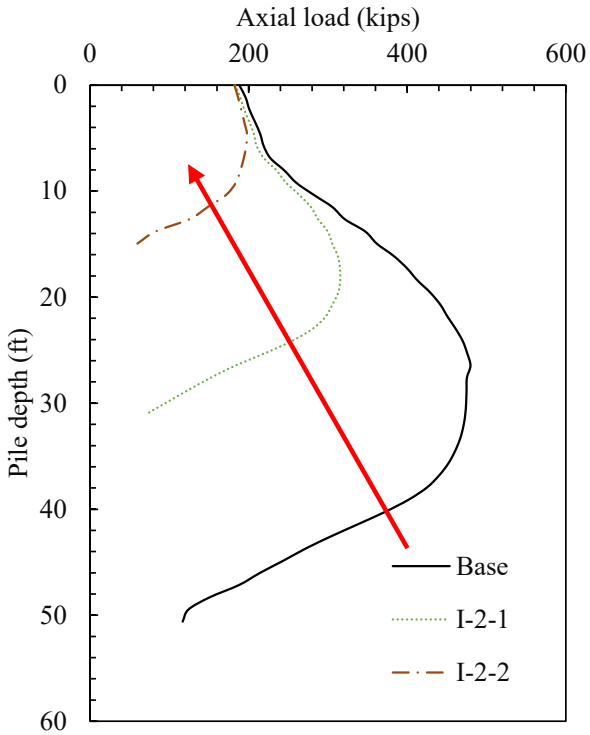

Figure 3.24 The axial load transmitted to the grade beam piles for different cases with the grade beam pile length (I-2-1 to I-2-2).

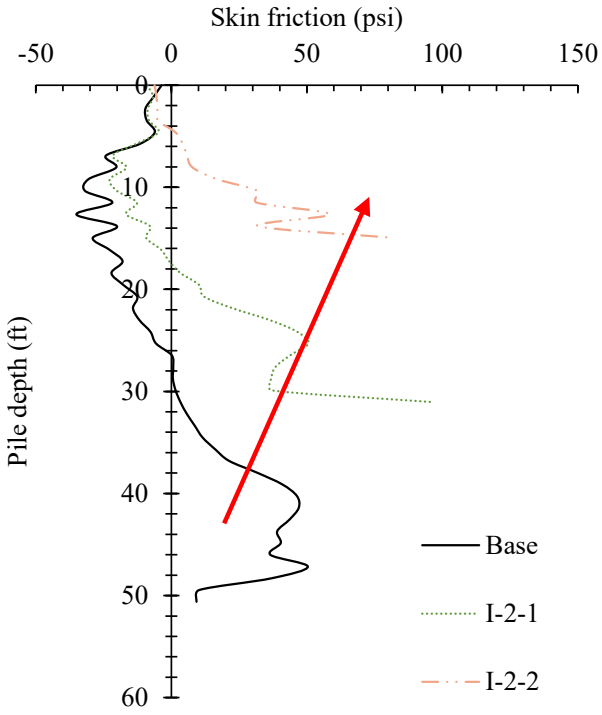

Figure 3.25 The mobilized skin frictional resistance along with the grade beam piles for different cases with the grade beam pile length (I-2-1 to I-2-2).

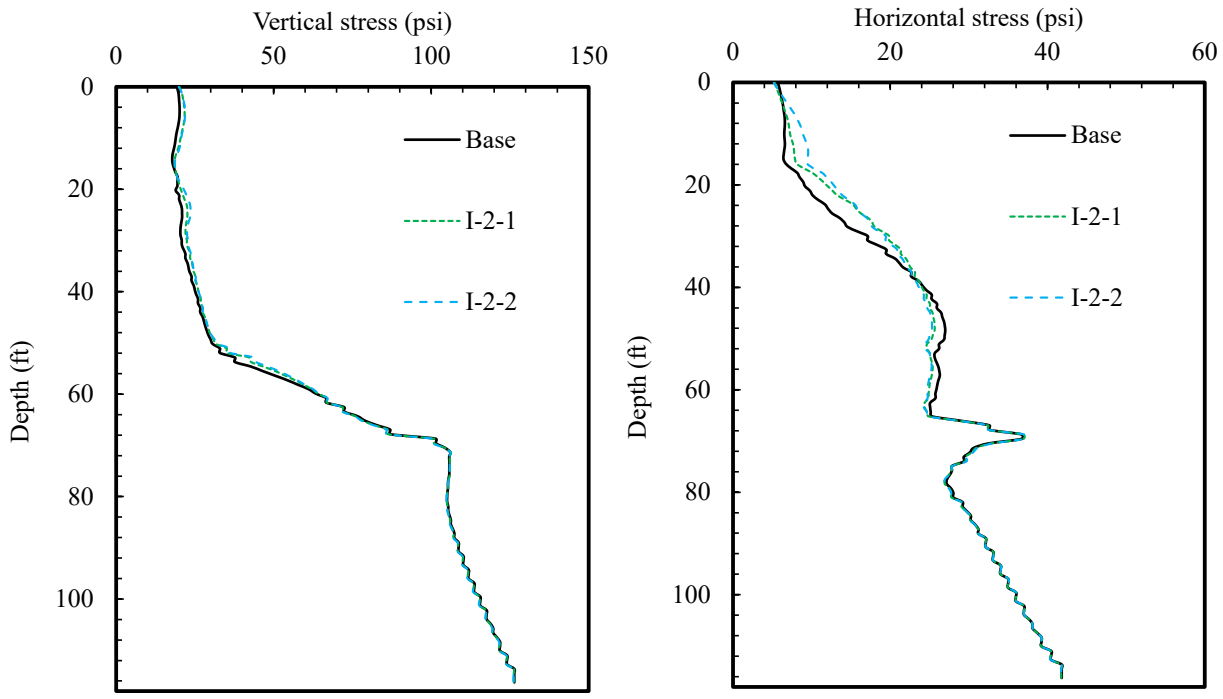

Figure 3.26 The vertical and horizontal stress profiles in the soil in the vicinity of the abutment pile for different cases with the grade beam pile length (I-2-1 to I-2-2).

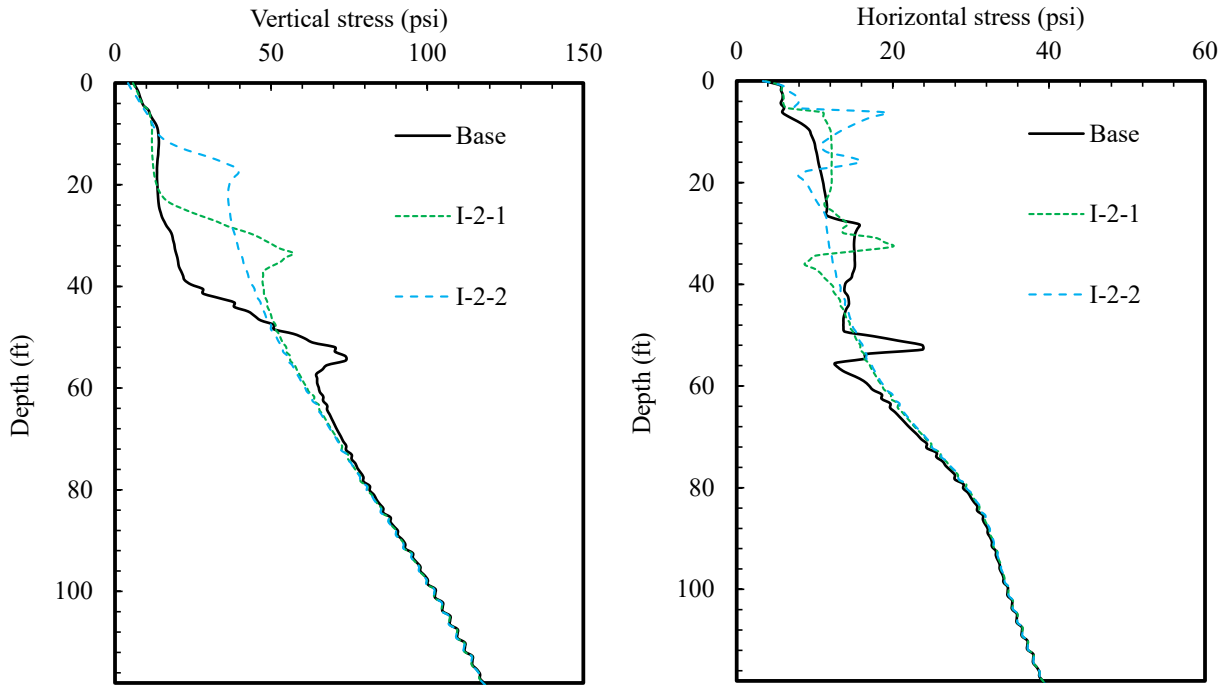

Figure 3.27 The vertical and horizontal stress profiles in the soil in the vicinity of the grade beam pile for different cases with the grade beam pile length (I-2-1 to I-2-2).

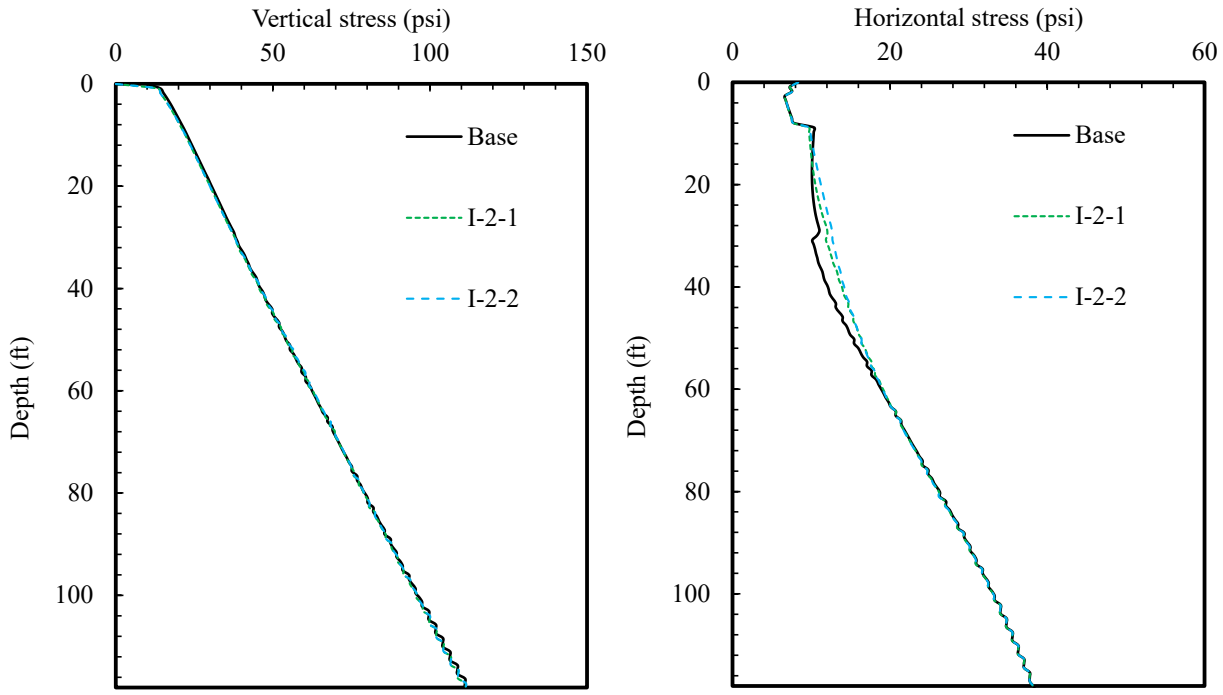

Figure 3.28 The vertical and horizontal stress profiles in the soil near the end of paving section for different cases with the grade beam pile length (I-2-1 to I-2-2).

Shortening the length of grade beam piles has a minor impact on the vertical settlement profiles across the abutment section, as shown in Figure 3.29. Overall, the vertical displacement profiles for all examined pile length cases are acceptable, with the maximum value on the surface being less than a quarter-inch in all the studies cases.

In contrast, shortening the length of grade beam piles could result in an increased vertical settlement along the grade beam section. However, its maximum deformation is less than 0.3 inches for the examined cases as long as the pile spacing is maintained the same (Figure 3.30). On the other hand, shortening the length of grade beam piles barely affects the vertical settlement profiles across the paving section (Figure 3.31).

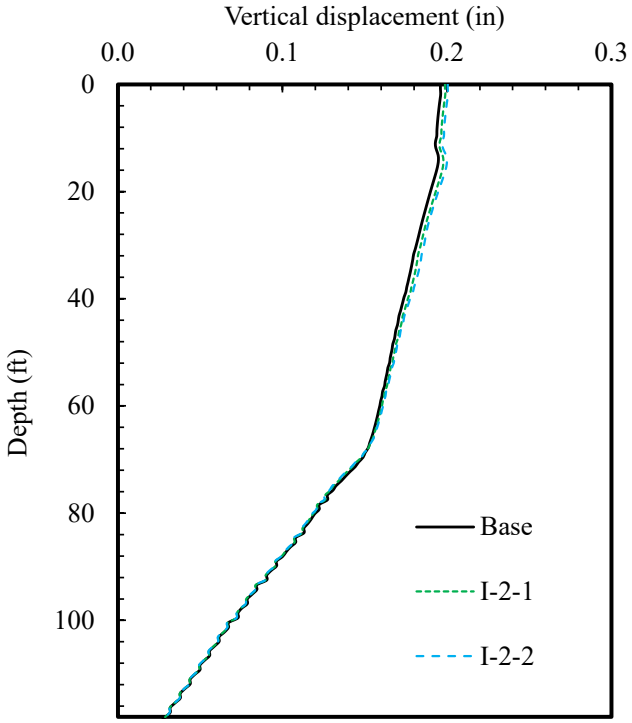

Figure 3.29 The vertical settlement profile across the abutment section for different cases with the grade beam pile length (I-2-1 to I-2-2).

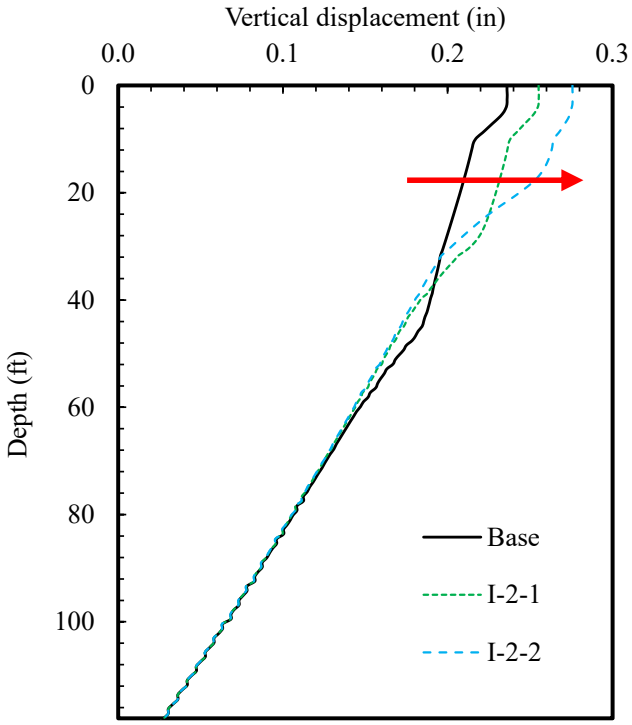

Figure 3.30 The vertical settlement profile across the grade beam section for different cases with the grade beam pile length (I-2-1 to I-2-2).

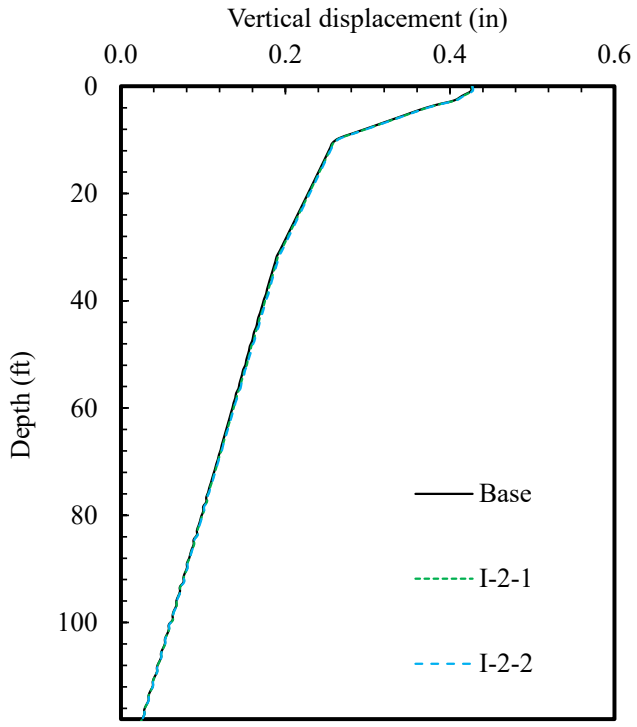

Figure 3.31 The vertical settlement profile across the paving section for different cases with the grade beam pile length (I-2-1 to I-2-2).

With those vertical settlements at each section, differential settlements are examined in a similar way. First, Figure 3.32 shows the differential settlement between the abutment and grade beam sections. As expected, shortening the length of grade beam piles would result in an increased differential settlement between those two points. Even though such a differential settlement is still less than 0.1 inch for all examined cases, it is worth noting that the differential settlement is almost doubled up when the pile length is reduced by 70% of the base case (Figure 3.32). Apparently, shortening the length of grade beam piles is also observed to contribute to alleviating the differential settlement between the grade beam and paving sections to some extent, as shown in Figure 3.33. But its impact is much less prominent compared to the previous analysis in which a wider spacing of grade beam piles is considered. With those observations between the abutment, grade beam, and paving sections, shortening the length of the grade beam piles may not be a recommendable alternative over the widening the spacing of grade beam piles.

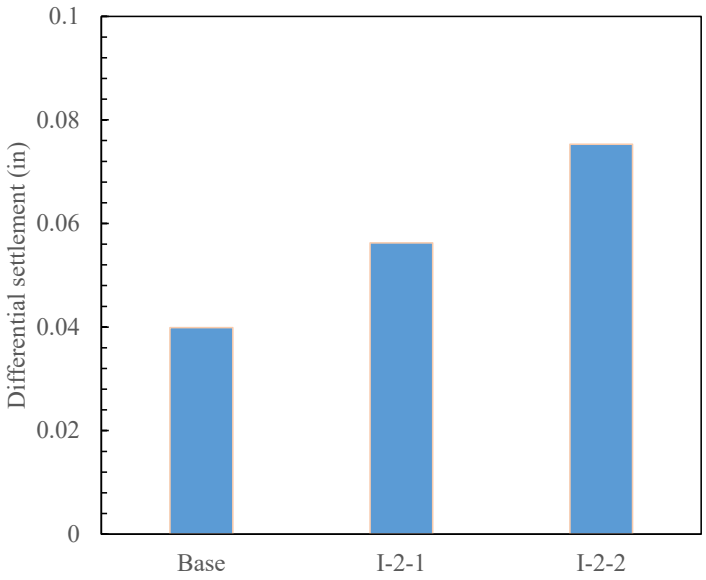

Figure 3.32 Differential settlement between the abutment and grade beam sections for different cases with the grade beam pile length (I-2-1 to I-2-2).

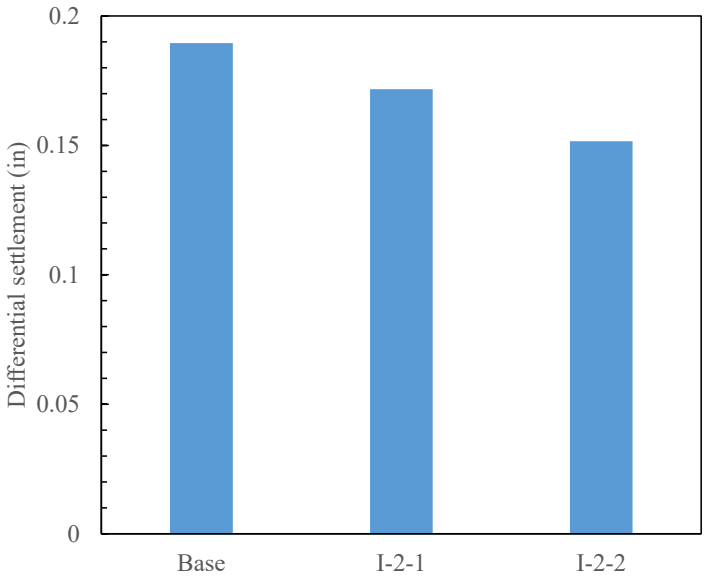

Figure 3.33 Differential settlement between the grade beam and paving sections for different cases with the grade beam pile length (I-2-1 to I-2-2).

4. Study II: Feasibility of Geosynthetics Reinforcement of Soils

4.1 Laboratory test

To evaluate interface properties between soils and geosynthetic, a large-scale geosynthetic pullout test was newly constructed and conducted. For the numerical simulation, the input properties obtained from the pullout test were used to simulate the soil conditions in Nebraska. The testing procedure and the materials used for conducting the test are described in this section.

4.1.1 Properties of the tested materials

The materials used for conducting the large-scale pullout test are described in this section. The soil used was sand reinforced with geogrids (BX1200).

(1) Backfill soils used in this study

The soil was taken from a location south of Omaha, Nebraska, between the towns of South Bend and Louisville, north of the Platte River. There is a plant that holds sand representative of Nebraska backfill soils shown in Figure 4.1. Their grain size distribution is shown in Figure 4.2, and Table 4.1 shows the basic geotechnical properties of the sandy soils. The sand contains hardly any gravel. Fine sand also is minimal; it is mostly medium-grained that is somewhere between poorly to well-graded. This soil works well with geogrids due to the fact that these geosynthetics are for interlocking with soils or aggregates.

Figure 4.1 Acquisition of backfill soils for the pull-out test in this study.

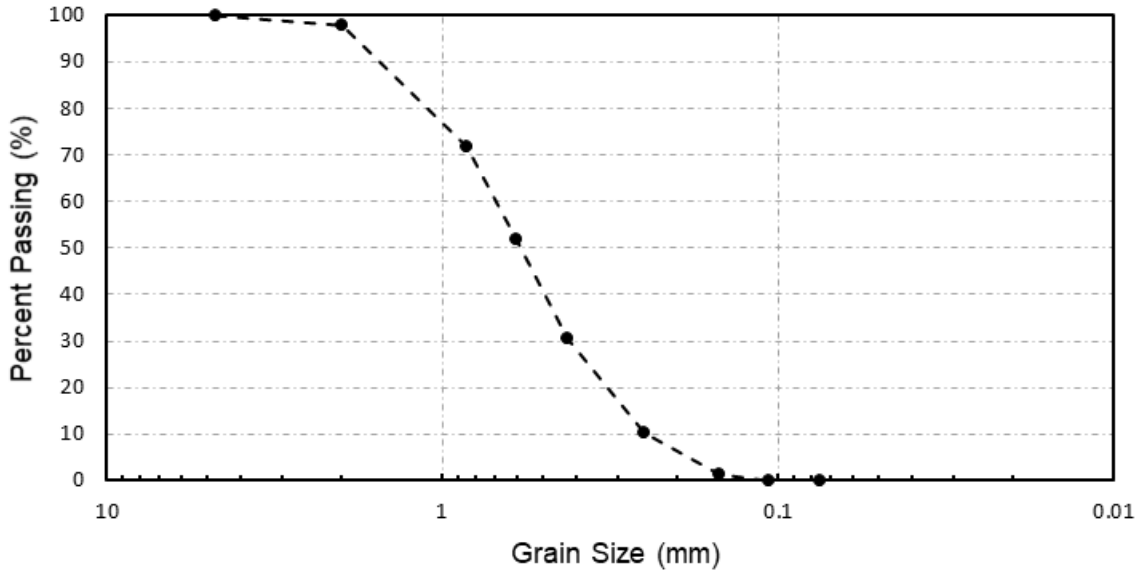

Figure 4.2 A grain size distribution curve of the backfill soil used in this study.

Table 4.1 Properties of the backfill granular soil used in the pullout test.

Property	Value
D_{60}	0.69
D_{30}	0.41
Uniformity coefficient (C_u)	3.14
Coefficient of curvature (C_c)	1.11
AASHTO classification	A-1-b
Relative density (%)	80
Specific gravity (G_s)	2.65
Angle of internal friction (degrees)	30

(2) Geosynthetics

The geosynthetic used in this test was a Biaxial BX1200 geogrid manufactured by the Tensar company. The geogrid was donated to the University of Nebraska-Lincoln geotechnical group. Figure 4.3 shows a sample of the received biaxial geogrid.

Geogrid is a stiff plastic sheet-like material that has punctured holes stretched in both directions, leaving a product that is integrally formed, usually made of polyester or polypropylene. These directions represent either the machine direction or cross-machine direction – simply put, they

indicate which way the material was pulled after the holes were punctured. The holes, whether they are rectangular or triangular, determine the type of geogrid, resulting in biaxial or triaxial material. The lengths of plastic that are molded due to material stretching are known as the ribs. The benefit to geogrid is its apertures, which help with its reinforcement. The soil has friction between individual particles and with the geosynthetic interface as well. This will enhance the behavior of soil beneath the grade beam and paving section to reduce the differential settlement (Ebrahimian (2010) and Zheng and Fox (2017)). Table 4.2 provides further details about these selected geosynthetics. The geogrid used in the study was made of polypropylene.

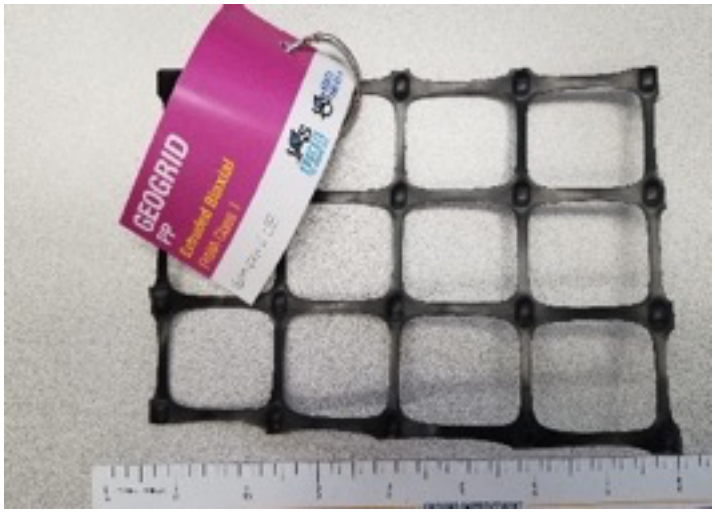

Figure 4.3 The biaxial BX 1200 geogrid used in the pullout test for this project.

Table 4.2 Characteristics of BX1200 geogrid used in this study. (After Tensar Corp.)

Geosynthetic parameters	Values	
Index properties	MD[1]	XMD[2]
Aperture dimensions (in.)	1	1.3
Minimum rib thickness (in.)	0.05	0.05
Tensile strength at 2% strain (lbf/ft)	34.2	620
Tensile strength at 5% strain (lbf/ft)	67.5	1340
Ultimate tensile strength (lbf/ft)	109.2	1970
Structural integrity		
Junction efficiency (%)	93	
Flexural stiffness (ft-lbf)	0.054	
Aperture Stability (N-m/deg)	0.65	

[1] Machine Direction; [2] Cross-Machine Direction

After evaluating several states from across the United States that use geosynthetics for roadway design practices, a general summary was created. The advice listed below pertains to geogrid and geotextiles specifically. Though this summation is accurate, a more complete list of particulars can be found with each states' specifications.

- In accordance with AASHTO M288, geosynthetic rolls shall be elevated off the ground and stored in a waterproof cover to protect against ultraviolet radiation. The ground should be relatively undisturbed. Rolls shall be covered with a suitable wrapping and stored to protect against moisture and natural elements, such as dirt, mud, or debris.
- The geogrid shall be placed longitudinally in the direction of traffic along the ground without any wrinkles or folds. The geogrid may be cut to conform to curves along the roadway if need be. Damaged geogrid should not be used, or, if salvageable, the damaged area must be covered an additional 24-36 inches in all directions. Any construction equipment should not be operated atop the bare geogrid.
- Geogrid shall either overlap or be sewn to an adjacent roll. Overlap shall cover at least 24-36 inches. Make sure the previous roll lies atop the new one. Seams are to be either J-seams or butterfly seams. Threads should use polyester, polypropylene, or Kevlar with durability greater or equal to the material. Compose all geosynthetics of at least 85% by weight polyesters, polyolefins, or polyamides. Geotextiles shall have fibers consisting of polymers, composed of 95% by weight polyesters or polyolefins.

4.1.2 Laboratory tests of the soil-geosynthetics interaction using the pullout box

(1) Pullout box design and specifications

A design of the pullout box was followed by ASTM D6706-01 and fabricated at a Puritan Inc., which is a local manufacturing plant (Omaha, Nebraska). Through the test, the soil-geosynthetic interaction, specifically tailored for small displacement failure, can be evaluated. The pullout box design by the University of Nebraska-Lincoln shown in Figure 4.4 was equipped with several individual wall segments to raise or lower the height of the box to make it capable of measuring the pullout force of multilayered soil. These wall segments were each 0.5-foot-tall and were easily removable due to their bolted connections, as presented in Figure 4.5 that represents the assembled box. The interior of the box was cleaned and spray-painted with a black gloss to minimize friction and to prevent rust, especially once the sample within the box was saturated. The walls connected to a base that was immovable and was welded to one section of steel.

Furthermore, the base sat atop four large caster wheels that were locked to prevent the sliding of the apparatus.

Figure 4.4 A schematic diagram of the large-scale pullout test box design.

Figure 4.5 A photo of the fully assembled large-scale pullout test box by the research team.

The large-scale pullout box was constructed with 5-foot-wide, 6.5-foot-long, and 5-foot-tall (1.5 meter × 2 meter × 1.5 meter) internal dimensions. It was modified in the lab at PKI (Peter Kiewit Institute of UNL) to its new dimensions of a 2.7-foot width, 4.3-foot length, and a 1.0-foot depth to allow for a more desirable set-up for testing one layer of geosynthetic. Two of the wall pieces were bolted down to the bottom of the apparatus, as shown in Figure 4.6, for the new wall lining. These walls were used as the outer boundary of the test, keeping in mind the geosynthetic would only be 1.65 feet (0.5 meters) in width to negate the boundary condition. Due to the boundary condition, undesirable friction where the geosynthetic material rubs against the wall of the apparatus can be minimized under normal stress conditions, which affects the pullout results. Two wooden boards were screwed together with a gap between them and placed in the back of the box. The gap provided the spacing for the linear variable displacement transducer (LVDT) lines to connect to the geosynthetic. The gap was placed at a 0.5-foot height to coincide with the height of the first layer shown in Figure 4.7 for a photo about the rear wooden boards with LVDTs attachments coming through.

Figure 4.6 A modified large-scale pull-out test box for the testing of soil-geosynthetic interactions.

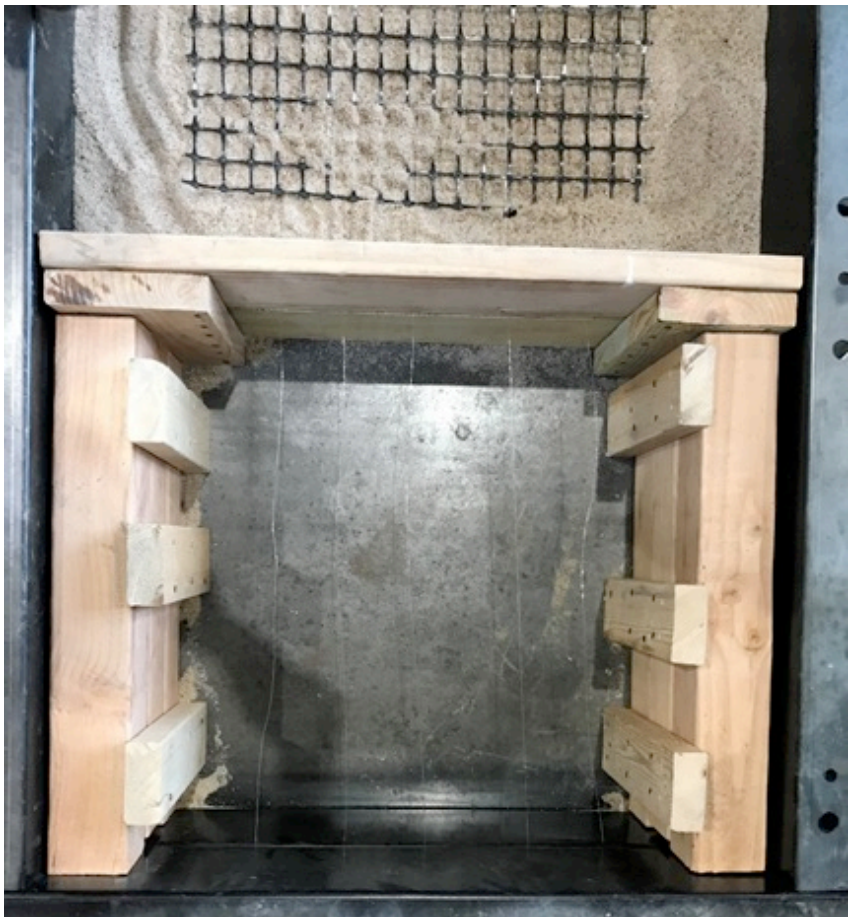

Figure 4.7 A slit in the backwall for the LVDTs' extension cables to pass through.

(2) Soil preparation

The soil was used to represent the backfill material on an abutment for a bridge. It was taken off-site and stored in a 50-gallon drum until it was needed for testing. It was air-dried extensively before it was used, and then water was added to the soil to represent field conditions after it was dried and ready for testing. The air-dried soil had 3% moisture remaining, so 6% water was added to the soil (i.e., total moisture content of 9%) since it was predominantly sand. Once the box was cleaned, the soil was poured into the modified dimensions, one sub-layer at a time. There were two layers – one layer was below the geosynthetic while the other was above it. Each layer needed to be 0.5-foot-tall to match the height of the wall segment. Likewise, each layer was compacted into three sub-layers, where each sub-layer was a third of the 0.5-foot height. Proper weight of soil needed before it was placed into the box to achieve a relative density of 80% for each sub-layer was calculated in advance. A geosynthetic pullout test usually requires medium to high relative density because the maximum pullout force is measured between the medium and high density of

soils (Roodi 2016, Part et al. 2017, ASTM 6706). Please note that the density for the pullout test is different from the actual condition. Then, each sub-layer was compacted by dropping 8 inches × 8 inches square steel tamper from the same height with the same force. The sub-layer was deemed adequate after the soil had reached 80% compaction of its relative density, and observation of the soil height was confirmed.

(3) Linear variable displacement transducers

Five linear variable displacement transducers (LVDTs), also known as telltales, were attached to the back of the box to measure the geosynthetic-soil interface interaction and displacements. They were screwed into a wooden platform that extended from the back of the apparatus, as shown in Figure 4.8. There was an opening in the rear wooden wall where the lines could run through to the tested material. Certain points along the geogrid were chosen to tie the lines to monitor the elongation and movement of the geosynthetic at the different locations. Figure 4.9 demonstrates these positioned places presented as red points. An inextensible cable (i.e., tensioned fishing line) was used to tie the LVDTs to the geosynthetic. The cable was a good material to use due to its low strain and thin circumference, keeping the recorded deformation values accurate. Besides, it minimizes friction with the soil.

Figure 4.8 LVDTs (telltales) attached to the rear portion of the test box.

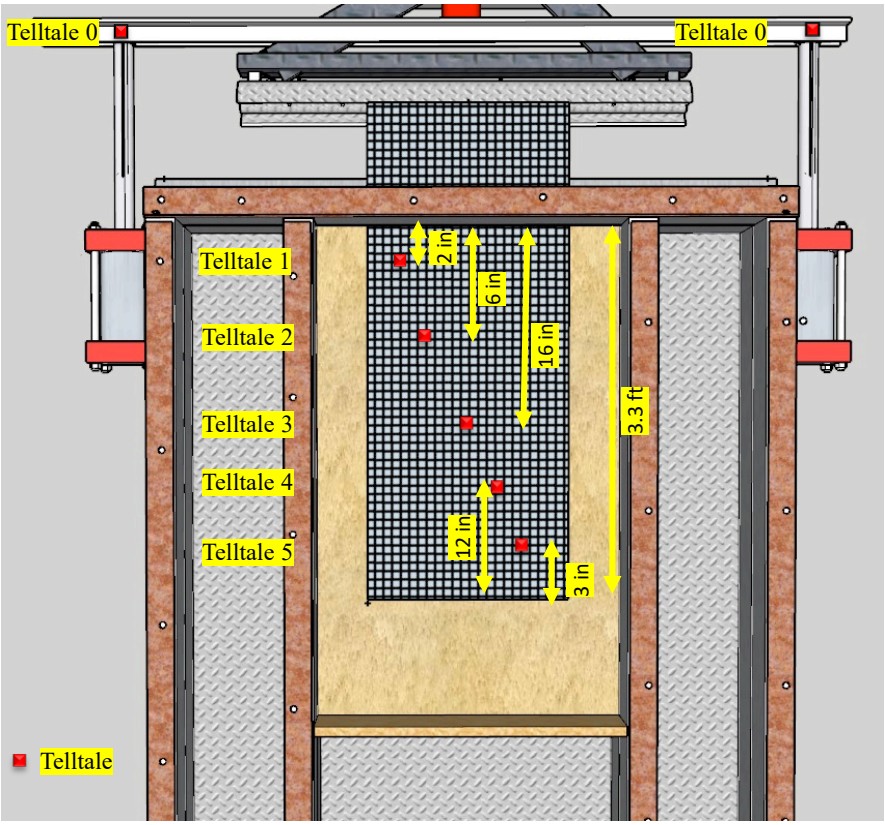

Figure 4.9 The locations of LVDTs (Telltales) placed across the tested soil-geosynthetics.

In addition to the five LVDTs that were attached to the back of the box, there were two on top of the hydraulic pistons attached to the frontal clamp to measure actual displacement, one for each piston. Blocks of wood were secured on both the hydraulic piston and the cross-bar. An LVDT was screwed into the block on top of the hydraulic piston. A screw stuck out of the block atop the cross-bar. A tensioned fishing line was used to connect the LVDT to the screw in a straight line. The start of the test represented a zero displacement for the LVDTs, but it was made sure that the hydraulic arms had an equal length to begin the test in order to eliminate any distortion in the front grip. During the test, the displacements from two arms were continuously monitored to check to apply the equivalent pullout shift.

(4) Pneumatic pistons

Once the soil had been laid properly and compacted, it was covered with a wooden plate, which allowed for uniform load upon the soil beneath it once applied from the pneumatic pistons on the top. Gupta (2009) instead tried using airbags to create this normal pressure but found they were

prone to recurring leakage. Roodi (2016) updated the process and performed a pullout test with pyramidal wooden structures beneath the air cylinders. It proved no difference in uniform loading. Therefore, the idea was not pursued in this study. A piece of stiff styrofoam was laid above the wooden plate to provide an upright cushion for the air cylinders. These cylinders had a non-uniform base that did not allow them to lay flat on the wood. As such, the styrofoam was gradually chipped away so there would be a space for the hump to rest comfortably and keep the cylinder erect.

There were six cylinders, as shown in Figure 4.10, atop the apparatus, all connected by tubing and all being supplied by an air hose adjacent to the box on the wall. Additionally, an air pressure regulator was used to control the rate of the applied pressure and to ensure it remains constant during the entire test.

These cylinders created the vertical pressure to represent the same pressure that soil undergoes in the field at various depths. These cylinders used a manufactured ceiling (the reaction plate) on the box as a counterforce to help displace the load into the soil. The reaction plate was very stiff, and thus, its deformation is negligible. Nonetheless, a steel rod was placed in both holes of the reaction plates to help stiffen the ceiling, as shown in Figure 4.11.

Figure 4.10 The pneumatic pistons used to apply the vertical pressure to the soil.

Figure 4.11 A rigid steel rod that runs through the reaction plate to minimize any differential deformation of the plate.

(5) Pump and hoses

A 10,000 psi hydraulic pump was used to carry the oil through 3,000 psi capacity hoses that had male quick-release couplings at their ends. These could be inserted into female release couplings attached to the hydraulic pistons on the box. A hydraulic piston had an inlet on the front and another inlet on the rear, where the rear inlet allowed the expansion of the hydraulic arm and the front inlet retracted it. When the hose was inserted into the rear inlet, the oil fed through the needle valve, past the pressure gauge, and filled the piston (this arrangement was true for both the front and the rear of the hydraulic piston even though the rear inlet is not pictured). The pressure gauge, needle valve, and female coupling were attached together using appropriate hardware. The pieces were lubricated with a PTFE thread sealing compound to prevent any oil leaks. The lubrication was known as the “toothpaste” due to its consistency.

The pump had two main hose lines, as shown in Figure 4.12. These hose lines had male quick-release couplings at their ends. Both main hose lines lead to their own female coupling (that made two female couplings, one for each main hose line as shown in Figure 4.12b and 4.12c that bisected the flow evenly into either the rear of the hydraulic piston to extend the arm or the front

of the hydraulic piston to release the arm. The set of hoses that lead to the rear of both hydraulic pistons had a needle valve and pressure gauge attached after the female coupling from the pump, as shown in Figure 4.12b, to account for the initial pressure.

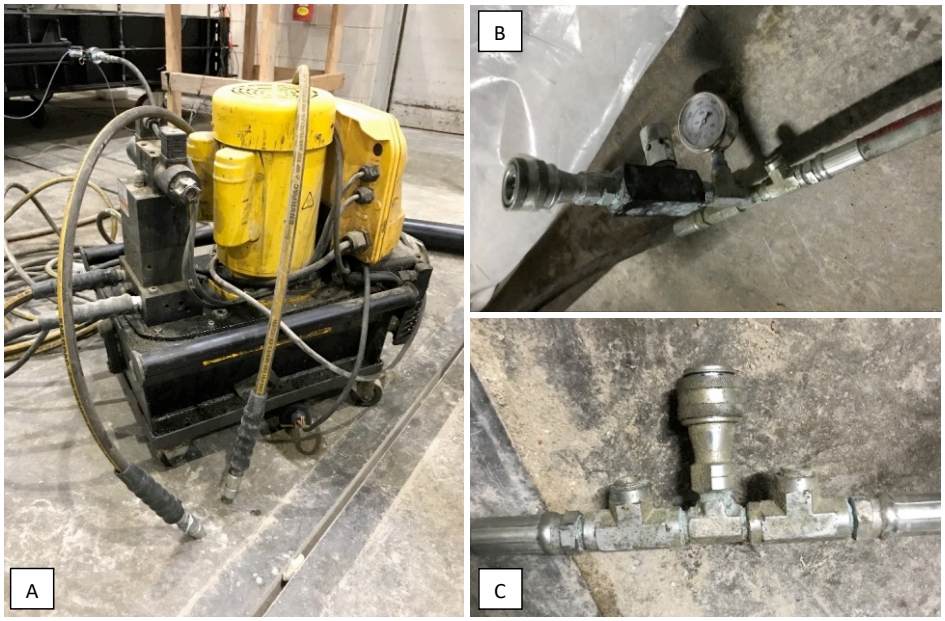

Figure 4.12 (A): the hydraulic pump used in this test, and (B) and (C): the quick disconnectors used to attach the pump to the hydraulic pistons.

(6) Hydraulic pistons

Two hydraulic pistons were attached to the side of the outer walls in the horizontal direction to apply the pullout force. These pistons were able to withstand 2,500 psi of pressure and were connected to the lower two segments of the steel wall. The hydraulic pistons were connected to a front cross-bar, which allowed them to move together and conjointly pull the geosynthetic out from the machine. The hydraulic arms started at the same length, about 25 inches so that the pullout would be even between both hydraulic pistons, considering that their rates were also the same. The desired rate for the hydraulic pistons was 0.04 in/min (1 mm/min), which was quite slow. This being the case, it was assumed that the geosynthetic would also be pulled out at this rate.

The front of the box had a cross-bar and a roller clamp to secure the geosynthetic specimen. They were supported by hydraulic pumps and three individual caster wheels. Since these wheels were connected by nuts and washers along a rod that went through the roller clamp, the height of the roller clamp could be slightly raised or lowered to align the geosynthetic. In this way, it was ensured the geosynthetic would be pulled out at exactly a parallel surface to the slot in the front

of the box. Therefore, as the geosynthetic hooked around the roller clamp, it was in line with the rest of itself and caused no downward off-degree error.

With the geosynthetic wrapped around the underside of the roller clamp, the top of the clamp had a flat steel bar that bolted down to hold the geosynthetic in place. Additionally, the geosynthetic was bolted to the underside with another steel bar. These connections were important to hold the specimen properly and not allow for any slippage. A load cell was attached on the front of the crossbar, having a 30,000 lbs capacity, which displayed the force generated. These pistons were important, and special care should be taken not to build up pressure to avoid any burst.

(7) Procedure of the pullout tests

The test begins by compacting the backfill soils to their desired density (relative density = 80%). The first layer of soil is 0.5 feet thick, having been compacted into three sublayers. This thickness complies with the minimum thickness specified by the ASTM D6706 standard. The geosynthetic is laid out on top of this layer. It covers an area of 5.45 square feet (1.65 foot × 3.3 foot) in the box and extends through a slot in the front wall section, which is then properly attached to the clamp and held there for the remainder of the test. Additionally, the LVDTs from the back of the box are tied to the geosynthetic. The second layer of soil is compacted on top of the geosynthetic, in the same manner for the first layer. Figure 4.13 shows an example of the soil preparation for testing.

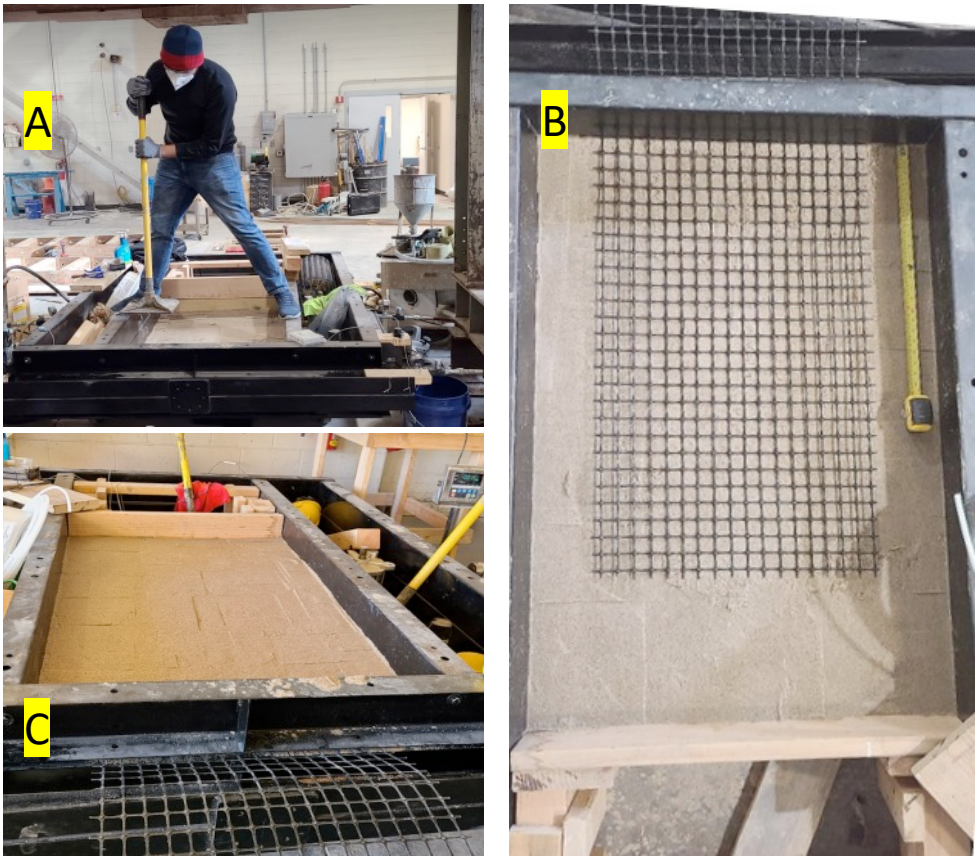

Figure 4.13 An example of test preparations. (A): compaction of the bottom soil layer, (B): placement of the geogrid reinforcement, and (C) compaction of the topsoil layer.

(8) Instrumentation

The geosynthetic is compressed between both layers of soils. The material passes through a slot in the front of the apparatus and wraps around a roller grip where it is bolted in place, ready to be properly pulled. Many previous studies have determined that there is lateral earth pressure developed at the front wall, which causes an increase in pullout resistance (Palmeira, 1987; Palmeira and Milligan, 1989; Raju, 1995; Sugimoto et al. 2001). Alternatives have been suggested to minimize this effect, such as using sleeves to keep the pullout load away from the front wall (Christopher et al. 1986). The testing slot in the front wall was deemed big enough that it did not encroach upon any additional earth lateral pressure. Two hydraulic pistons were mounted to the side of the box attached to the cross-bar at the front of the apparatus. These pistons provided the pullout force. The force was measured with a 30,000 lbs load cell which was bolted to the cross-bar, and recorded the power it recognizes from the roller clamp while the geosynthetic was in tension. As stated, LVDTs were tied to strategic points along the

geosynthetic, accounting for different embedment lengths in the backfill to provide a better understanding of how the geosynthetic interacts with the soil under loading and pullout conditions. They record the final displacement of the geosynthetic. For the data acquisition system, a data logger from Keysight DAQ970A with a 20-channel multiplexer was used to read data from the load cell and the LVDTs. Benchvue software was provided to obtain the data. Figure 4.14 shows the data acquisition system used.

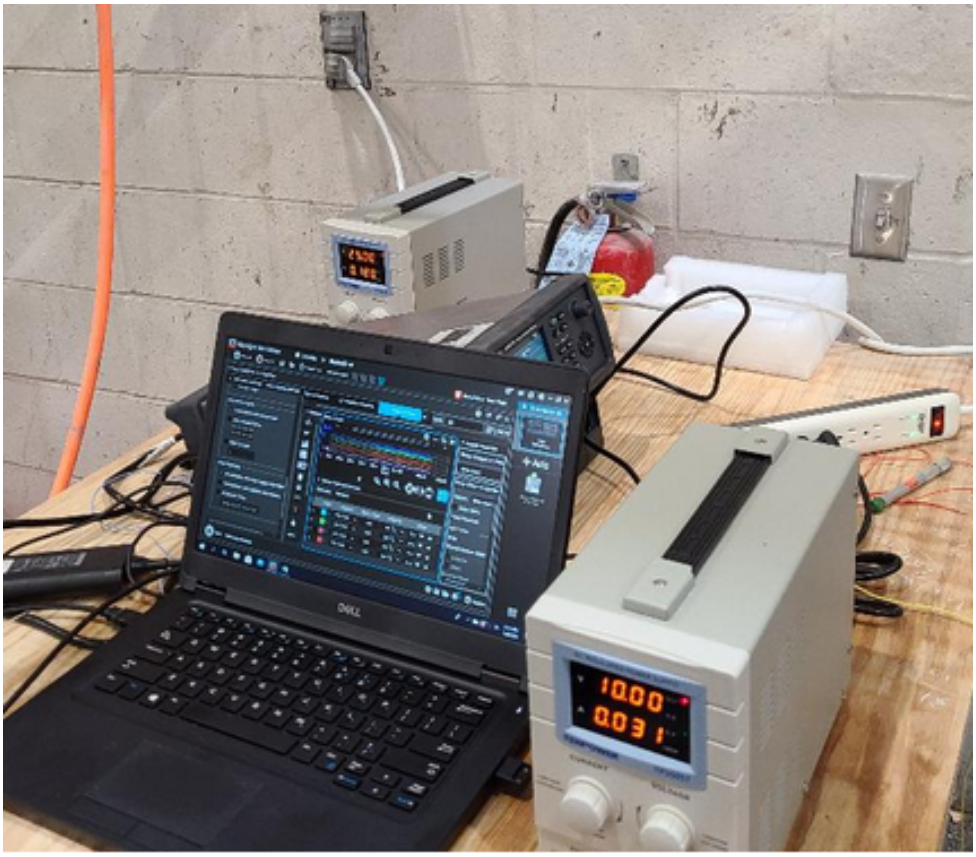

Figure 4.14 The data acquisition system used to automatically obtain the monitoring data during the pullout tests.

(9) Vertical stress application

After securing the test materials in the box and proper instrumentational set-up, a wooden box was laid upon the second layer of soil, followed by the styrofoam. Six air cylinders were positioned on the styrofoam and provided the vertical pressure. The cylinders were subjected to three different air pressures, such as 1.45 psi, 3.60 psi, and 5.50 psi (10 kPa, 25 kPa, and 38 kPa), which can reflect deeper soil depths.

(10) Testing

After the vertical pressure was stabilized, the geosynthetic was pulled out at a constant rate of 0.04 in/min (1 mm/minute). Testing was stopped when there was no increase in force while the displacement continued to increase. For reference, one geogrid was ruptured during one pullout test due to the distortion of the roller grip in the front, as shown in Figure 4.15.

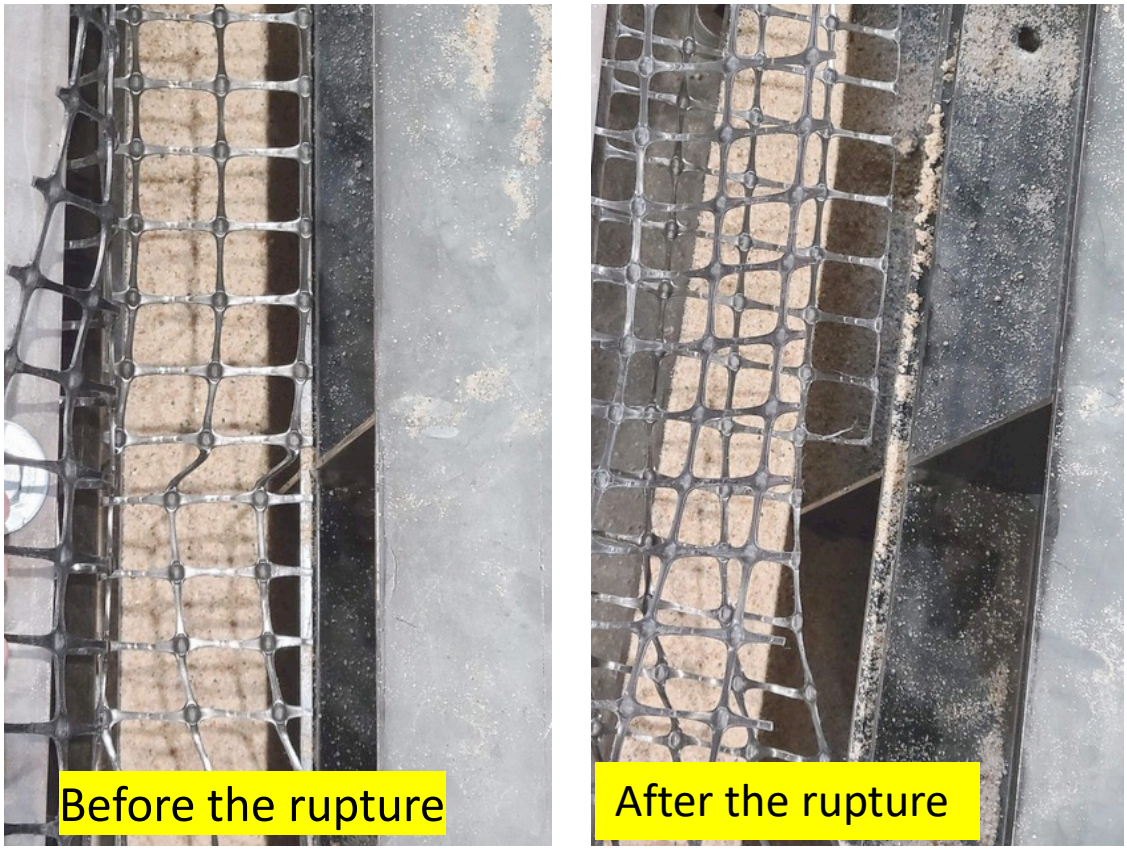

Figure 4.15 An example of the observed failure at the geogrid grip during pullout tests in this study.

The complete testing setup is shown in Figure 4.16, which provides information about each part before proceeding with the test.

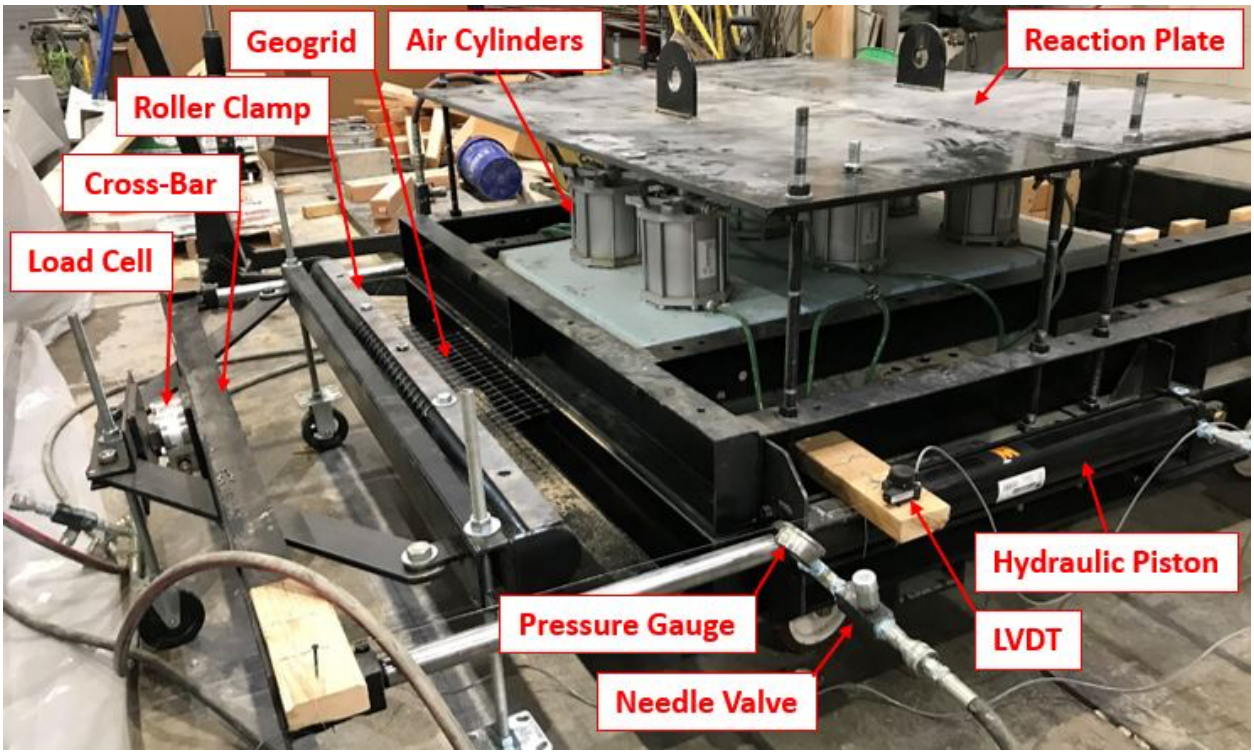

Figure 4.16 A photo of the completed testing setup of the large-scale pullout tests.

4.1.3 Results and discussion

Telltales are position transducers installed across the geogrid specimen to measure the internal displacement along the confined portion of the geogrid while it is being pulled out from the backfill soil. It indicates the gradual mobilization with the pullout force (Bakeer et al. 1998, Eun et al. 2017, Roodi et al. 2018, Ghaaowd and McCartney 2020).

As mentioned earlier, seven linear variable differential transformers were attached to the box, 2 LVDTs were attached to the clamp portion (denoted as telltale 0) to measure the pullout speed and check the consistency of the piston movement at the required rate. Telltales #1 to #5 were attached internally to the pulled sample internally, and their distances across the geogrid sample are shown in Figure 4.17 (same as Figure 4.9).

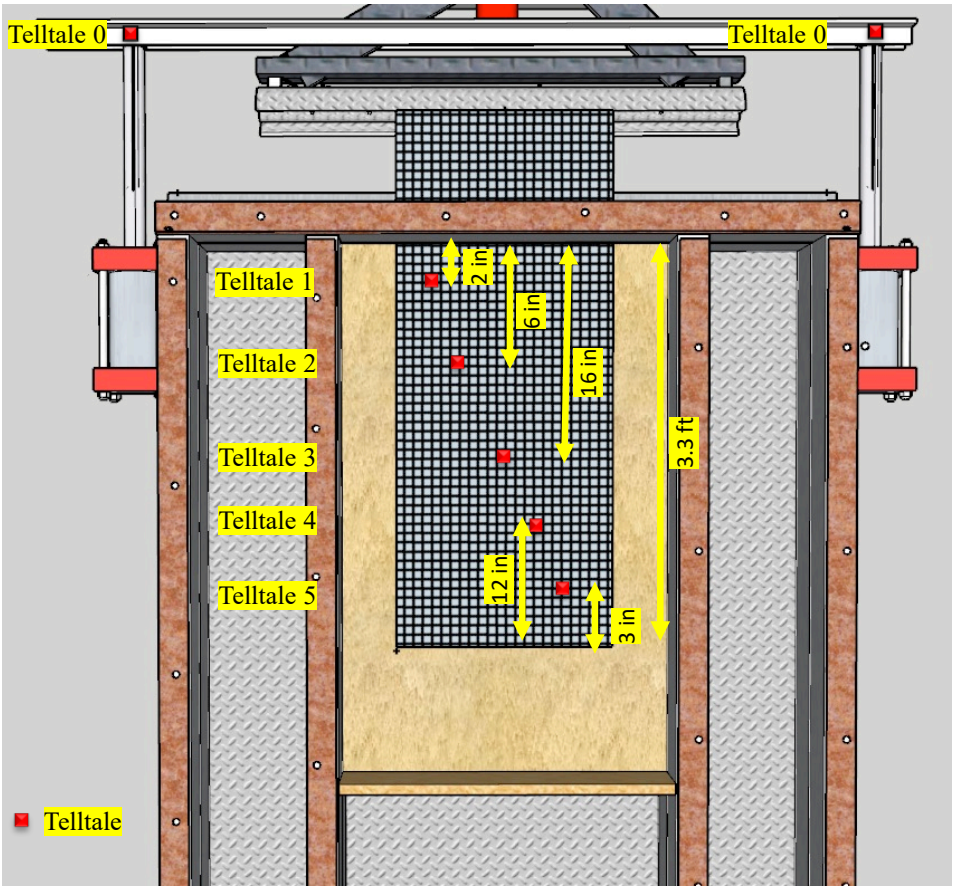

Figure 4.17 A top view of the pullout test box that shows the attached telltales and their locations.

The normal pressure from the pneumatic pistons on top of the tested materials was applied and was kept for 20 minutes to ensure a uniform pressure distribution across the soils. Three tests were conducted under each normal pressure of 1.45 psi, 3.6 psi, and 5.5 psi, respectively. The test was also repeated twice in the beginning under 1.45 psi of vertical pressure to check the repeatability of the results. Figure 4.18 shows the frontal displacement of the geogrid with the resulted pullout force. The two tests show a good agreement in the results, thus demonstrate good repeatability of the tests.

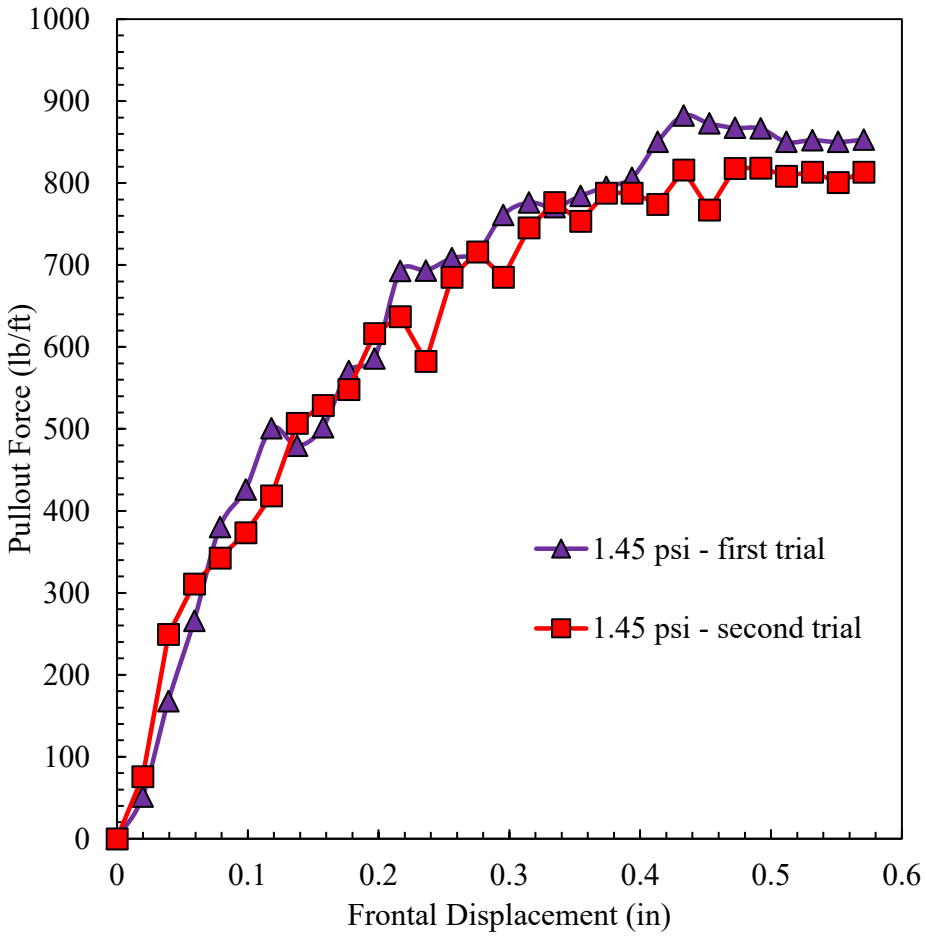

Figure 4.18 Repeatability check of the pullout tests under the same vertical pressure of 1.45 psi.

Besides, the results of the internal displacements in the geogrid measured by the telltales are shown in Figure 4.19. Note that the displacements are initiated differently depending on the location of several LVDTs. That is, the displacement and pullout force at the telltale placed at the front of the box occurs first, and then the order to generate the forces follows by the telltale placement. This phenomenon is because of the elastic deformation of the geosynthetics and the pullout force transfer along to the interface of soil-geosynthetic. The maximum pullout forces were approximately 800 lb/ft for the 3.6 psi of vertical pressure.

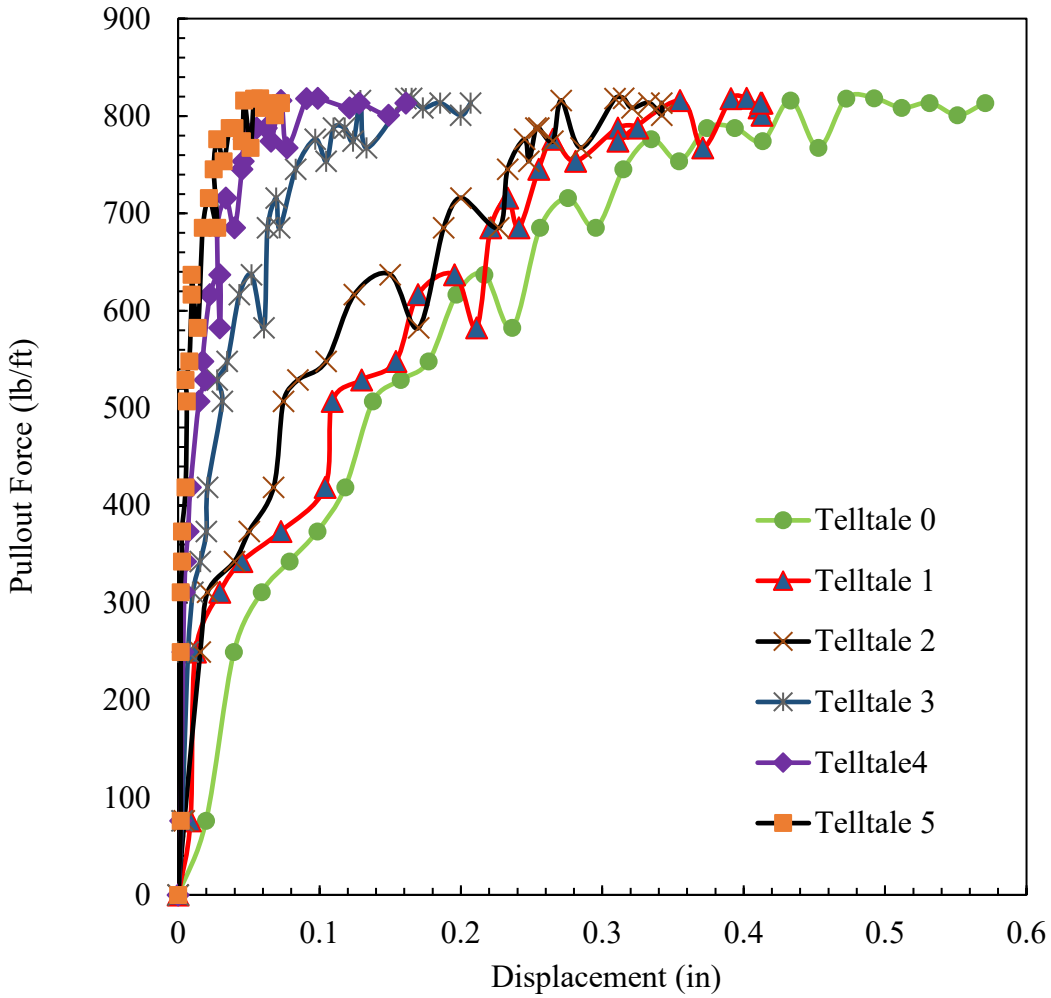

Figure 4.19 An example of pullout test results: pullout forces and telltale displacements across the tested geogrid. The applied vertical pressure is 1.45 psi.

The test was then continued with the other vertical pressure of 3.6 psi and 5.5 psi. Their results are shown in Figures 4.20 and 4.21, respectively. It should be noted that telltale 0 denotes the frontal displacement in all tests. For 3.6 psi and 5.5 psi of vertical pressure, the maximum pullout forces were approximately 1600 lb/ft and 2000 lb/ft, respectively. The pullout force generally increases as higher vertical pressure is applied, even though its increment is not linear.

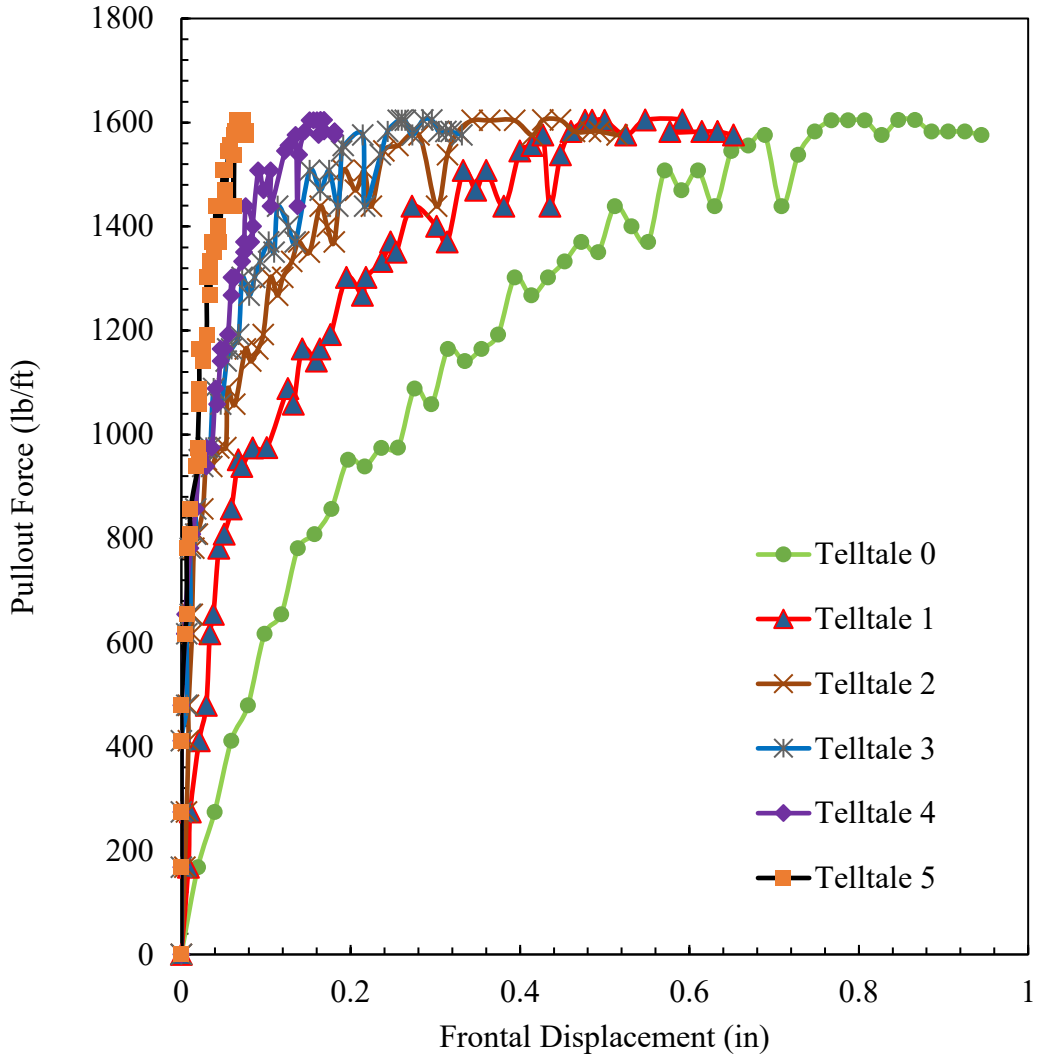

Figure 4.20 An example of pullout test results: pullout force and telltale displacements across the tested geogrid. The applied vertical pressure is 3.6 psi.

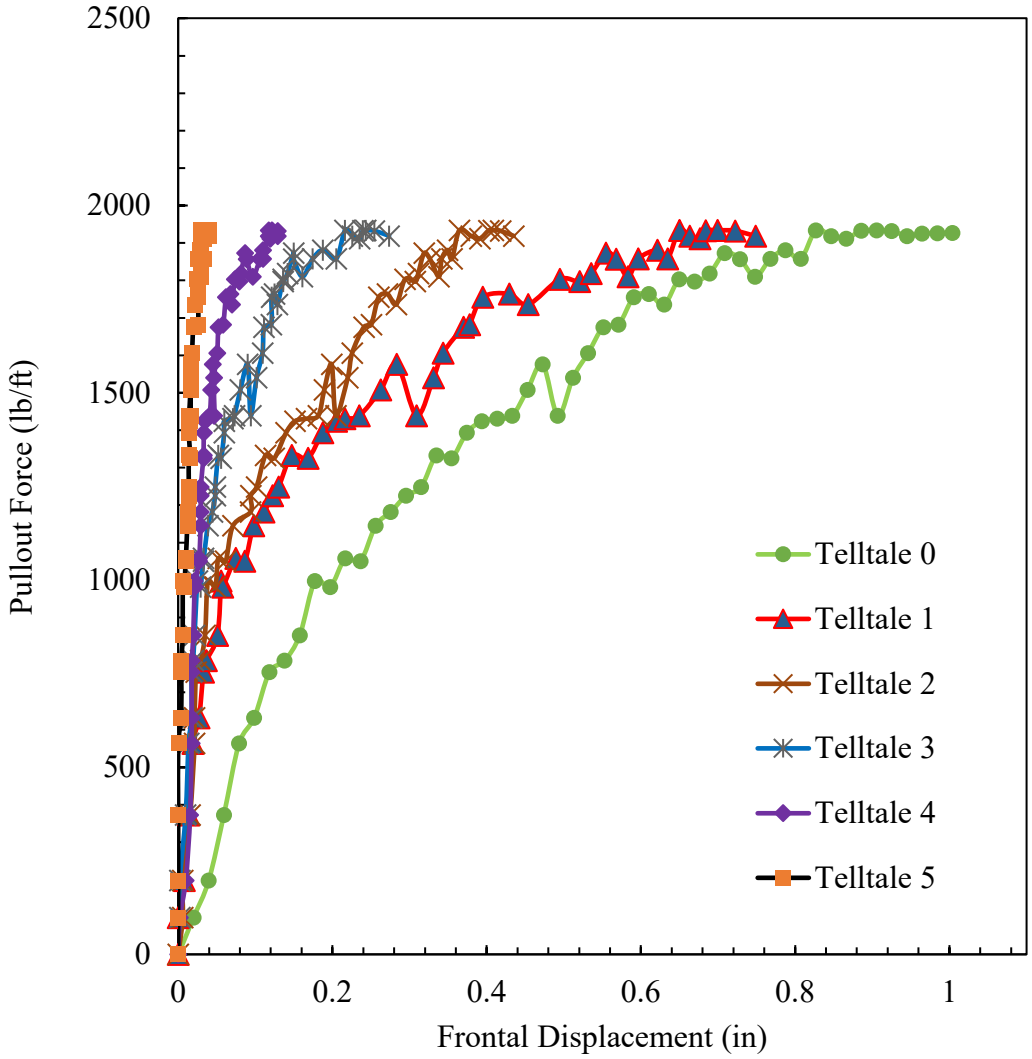

Figure 4.21 An example of pullout test results: pullout force and telltale displacements across the tested geogrid. The applied vertical pressure is 5.5 psi.

From the obtained results, the pullout force increased at higher rates at the beginning of the test and then decreased until there was no further change in the pullout force at the end. It indicates that the interface between the geogrid and soil has yielded. The gradual mobilization of the pullout force across the specimens is captured with the internally attached telltales (1 through 5). From the presented data, the telltales closest to the source of the pullout were triggered first and the last telltales to be triggered were the one which is deeply embedded in the soil. Care must be taken, however, given that that telltale 4 and 5 were triggered at the same time although they were placed at different distances. This issue could be attributed to attachment malfunction of the

telltale wires or the presence of waves in the geogrid due to compaction. The same behavior was reported by Roodi et al. (2018).

Koerner (2005) defined the efficiency factor of the soil-geosynthetic interaction as *tan* δ/*tan* φ, where δ represents the interface friction angle of the soil-geosynthetics and φ denotes the internal angle of soil friction. However, other researchers, such as Ingold (1983), Ochai et al. (1996), Wang and Richwien (2002), and Prashanth et al. (2016), expressed the results of the pullout tests with the friction coefficient (f^*). The friction coefficient is expressed with the maximum pullout resistance force (P_{max}), or the maximum shear resistance (τ_{max}), that the interface withstands under the applied normal stress (σ_n) as follows:

$$f^* = \tan\delta = \frac{P_{max}}{2 \times b \times l \times \sigma_n}$$

$$f^* = tan\ \delta = \frac{\tau_{max}}{\sigma_n}$$

where b and l are the width and length of the confined geosynthetics tested (1.6 ft × 3.3 ft in this study). Table 4.3 presents the maximum pullout forces, the maximum shear resistances of the interface, and the corresponding friction coefficients from the pullout tests of this study. The summarized results show how the pullout force could be sensitive to the normal pressure change. It also can be observed how the pullout friction coefficient could be reduced as the normal stress on the specimen increases, which could be related to the nonlinear behavior of the pullout force with increased normal pressure (Prashanth et al., 2016).

Table 4.3 A summary of the pullout test results.

Normal stress, σ_n (psi)	Maximum pullout force, P_{max} (lbf/ft)	Maximum shear resistance, τ_{max} (psi)	Friction coefficient (f^*)
1.45	818.47	0.861	0.59
3.6	1604.8	1.688	0.47
5.5	1933.7	2.034	0.37

4.2 Numerical simulation

The numerical simulation of the part of the bridge system for the abutment-approach slab-grade beam-paving section, including soil layers reinforced with geosynthetic, was conducted to evaluate the response of the system reinforced with geosynthetics and the effect of the reinforcement on the approach slab and other sections. For the comparison, the base case of the current system, including a grade beam with piles, was also simulated. The FLAC 2D simulation package was used for the numerical simulation. Input parameters of the soils and concrete structures identical with the previous case for the current practice, including a grade beam with piles, were used for the simulation. The properties for the geosynthetic reinforcement were used from the values calibrated from the pullout tests and literature. The shear behavior of the grout annulus between the geogrid-grout interface and soil-grout interface during the relative movement is provided by the grout shear stiffness (Kbond), as shown in Figure 4.22. The cable element in FLAC has been shown to provide a good representation of geosynthetic materials in the literature (e.g., Holtz and Lee (1998), Vulova and Leshchinsky (2003), Ebrahimian (2010), and Zheng and Fox (2017)). The properties of the geosynthetics materials used in the numerical simulation are summarized in Table 4.4.

Those geosynthetics were modeled using the cable element feature, and the interface between soils and geosynthetics was simulated by the governing equation based on Column's friction law. The friction at the interface can be addressed by the bond stiffness and bond friction angle in the model. The properties used for the geosynthetic reinforcement were also presented in Table 4.4.

Table 4.4 The property of cable elements used in the numerical study to model the geosynthetic material.

Parameters	Values from literature	Values based on the pullout test
Cross sectional area (ft^2)	0.27	0.27
Elasticity modulus (psi)	100×10^3 [(1)]	100×10^3 [(1)]
Bond stiffness, kbond (psf)	20,885 [(2)]	36,600
Bond friction angle, sfriction (°)	20 [(3)]	25.5
Bond strength, sbond (lbf/ft)	362 [(2)]	560
Tensile yield strength (lbf/ft)	1,920 [(4)]	1,920 [(4)]
Perimeter (ft)	6.5	6.5

References: [(1)] Fakhraldin (2012), [(2)] Prashanth et al. (2016), [(3)] Jiang et al. (2017), [(4)] Tensar (Manufacturer)

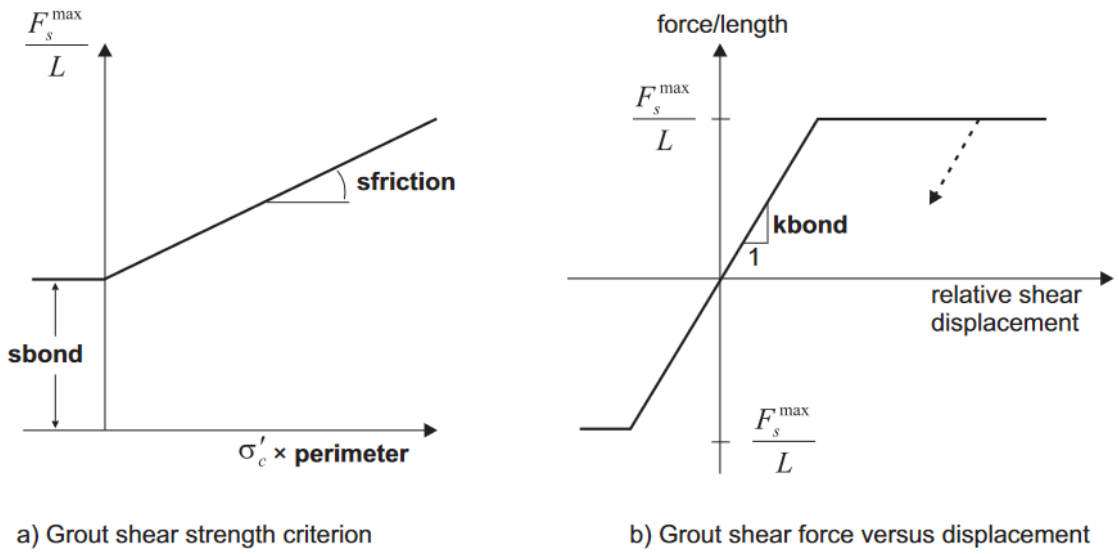

a) Grout shear strength criterion

b) Grout shear force versus displacement

Figure 4.22 The interface behavior of the cable element used in the numerical study (Itasca, 2016).

In order to validate the soil-geosynthetics interaction in the numerical simulation approach by the team, the pullout test was modeled in FLAC, and its results were compared with those from the actual pullout tests in Section 4.1. Readers are referred to Section (2) "Validation of the numerical simulation approach: soil-geosynthetics interaction" in the Appendices for the detail.

For the simulation, four different cases were considered to evaluate the performance of geosynthetics: (1) the individual geosynthetic reinforcement without piles under the grade beam (Case II-1), (2) the extended geosynthetic reinforcement without piles under the grade beam (Case II-2), (3) the individual geosynthetic reinforcement with a sleeper slab (Case II-3), and (4) the individual geosynthetic reinforcement only at the joint between the paving section and roadway (Case II-4).

(1) Investigation of the individual geosynthetic reinforcement (Case II-1)
The effect of individual geosynthetic reinforcement installed under the grade beam without piles on the behavior and performance of the system is investigated for Case II-1. That is, this case examines the effect of geosynthetic with the grade beam only on the system and feasible performance of the geosynthetic reinforcement compared to the current practice. The size of the

grade beam follows the current design as of height of 2.5 ft and width of 3.0 ft. The length of geosynthetic reinforcement was set at 20 ft, and the spacing of the reinforcement was 1.0 ft at both the joint of the approach slab and paving sections. This length was determined after considering the Louisiana DOT guideline and the workability at practice. Three different cases with the number of the geosynthetic layers were conducted to compare the effect of the number of the layers on the behavior and performance of the system (Figure 4.23 and Table 4.5).

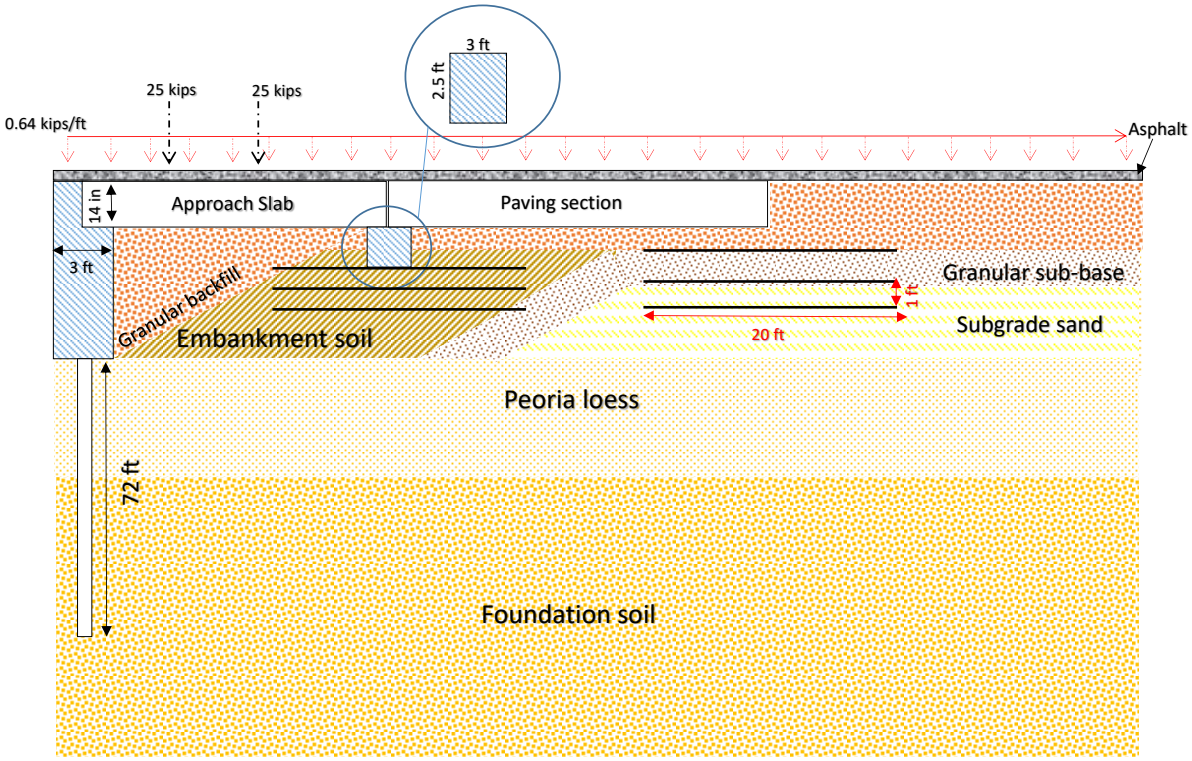

Figure 4.23 The numerical simulation model to investigate the effect of individual geosynthetic reinforcement on both near the end of approach slab and paving sections (not to scale).

Table 4.5 Cases on the individual geosynthetic reinforcement.

Case #	Number of geosynthetic layers
II-1-1	1
II-1-2	2
II-1-3	3

Note: the length of each individual geosynthetic layer is the same at 20 ft.

(2) Investigation of the extended geosynthetic reinforcement (Case II-2)

The effect of extended geosynthetic reinforcement on the behavior and performance of the system is investigated for Case II-2. All other conditions, such as soils, structures, and grade beams, were identical to those of Case II-1. The geosynthetic was installed along with the backfill and foundation soils from the abutment to the roadway. This application can be suitable for new construction or significant reconstructing of the section that connects the approach slab and roadway pavement. The spacing of the reinforcement was set as 1.0 ft. Two different cases with the number of the geosynthetic layers were conducted to compare the effect of the number of the layers on the behavior and performance of the system (Figure 4.24 and Table 4.6).

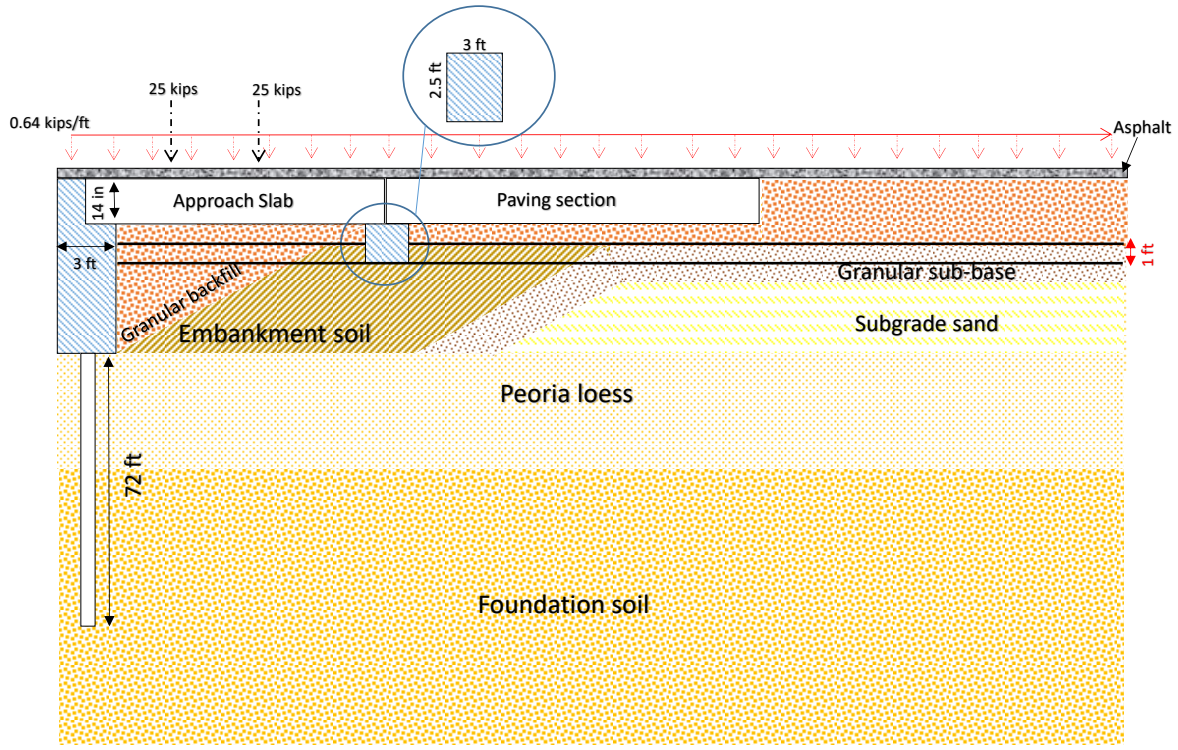

Figure 4.24 The numerical simulation model to investigate the effect of extended geosynthetic reinforcement on both near the end of approach slab and paving sections (not to scale).

Table 4.6 Cases on the extended geosynthetic reinforcement.

Case #	Number of geosynthetic layers
II-2-1	1
II-2-2	2

(3) Investigation of the individual geosynthetic reinforcement + sleeper slab (Case II-3)

The effect of individual geosynthetic reinforcement with a wider sleeper slab on the behavior and performance of the system is investigated for Case II-3. The width of the sleeper slab is 6.0 ft, which is commonly adopted from other state DOTs such as Texas, Kansas, etc. The wider sleeper slab can be more suitable to distribute axial loading from pavement to subgrade evenly and so that the settlement can be reduced. The number and spacing of geosynthetic reinforcement were identical to those of Case II-1. The length of geosynthetic reinforcement was set at 30 ft, and the spacing of the reinforcement was 1.0 ft (Figure 4.25).

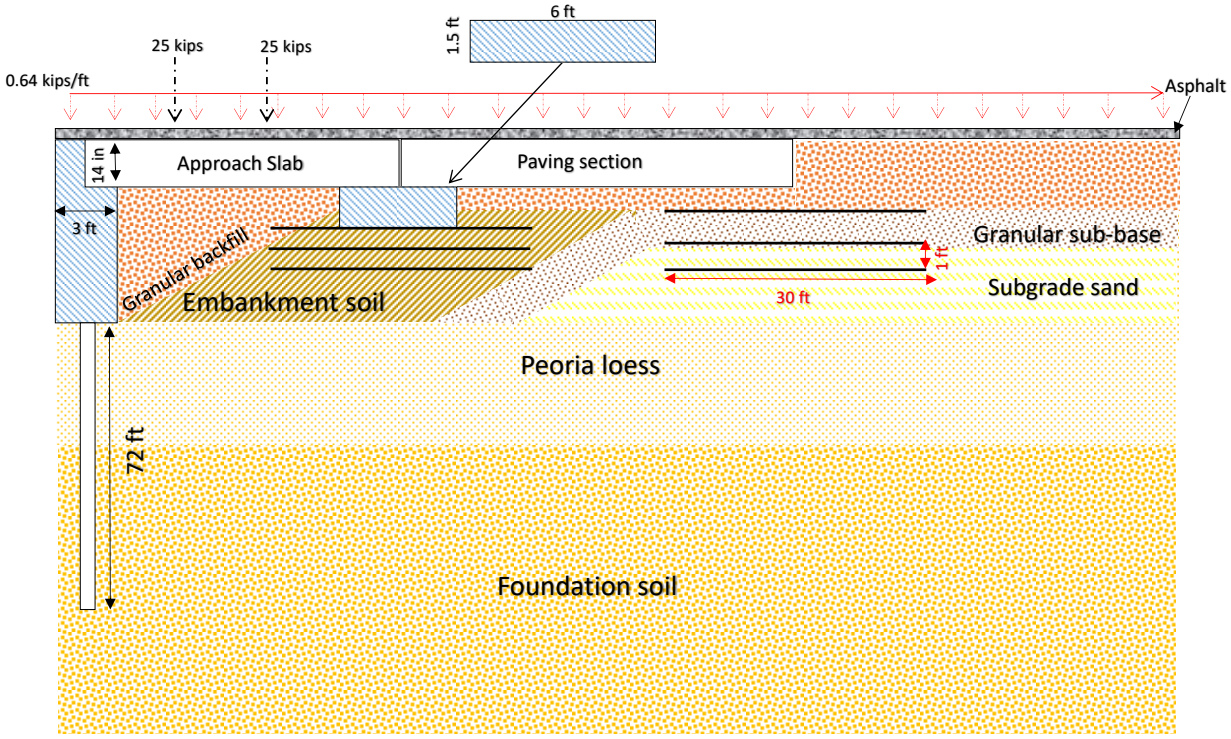

Figure 4.25 The numerical simulation model to investigate the effect of individual geosynthetic reinforcement on both near the end of approach slab and paving sections with wider sleeper slab (not to scale).

(4) Investigation of the individual geosynthetic reinforcement under the paving section only (Case II-4)

The effect of individual geosynthetic reinforcement installed only under the paving section on the behavior and performance of the system is investigated for Case II-4. This case provides promising methods to alleviate the settlement issue at the joint between the paving section and roadway by

installing geosynthetic reinforcement while keeping the current practice that installs a grade beam with bearing piles under the approach slab. The number and spacing of geosynthetic reinforcement at the joint were identical to those of Case II-1. For this case, the number of geosynthetic layers was varied from one to three to evaluate the effect of the geosynthetic reinforcement. The length of geosynthetic reinforcement was set at 30 ft, and the spacing of the reinforcement was 1.0 ft (Figure 4.26 and Table 4.7).

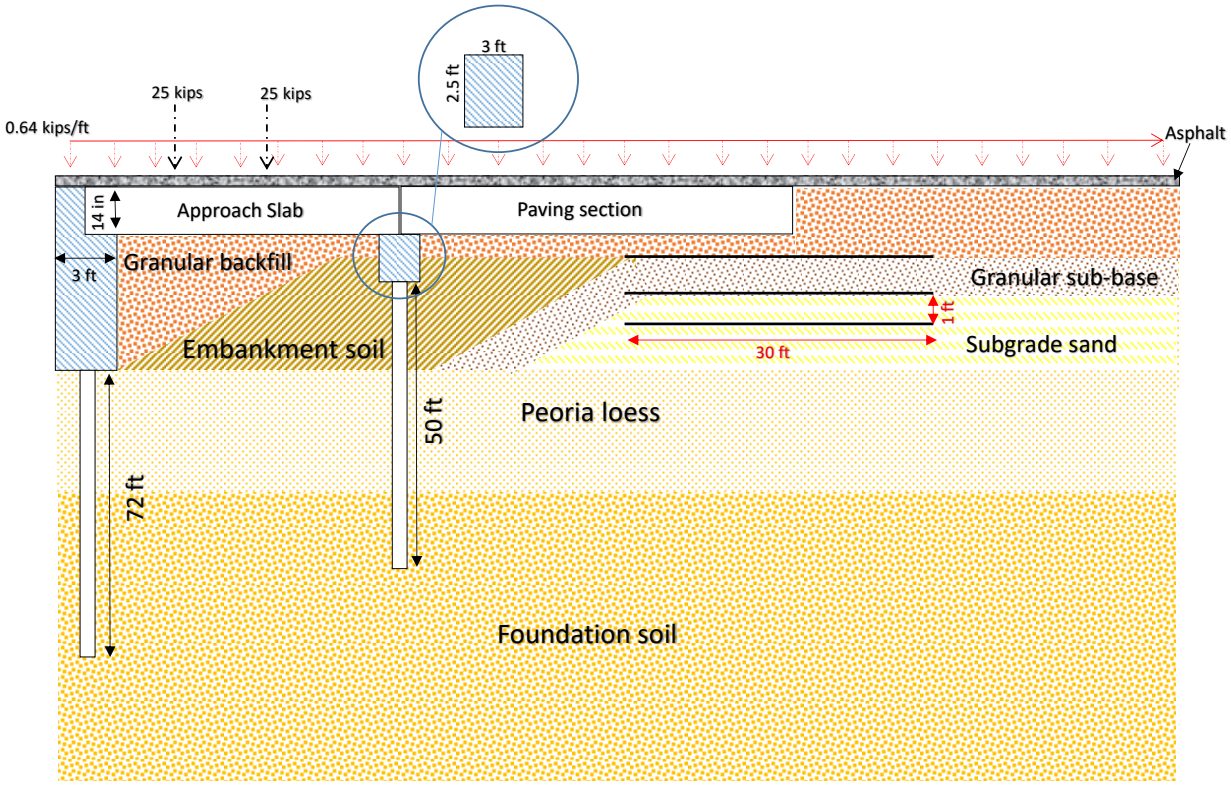

Figure 4.26 The numerical simulation model to investigate the effect of individual geosynthetic reinforcement under the roadway paving section only (not to scale).

Table 4.7 Cases on the individual geosynthetic reinforcement under the paving section.

Case #	Number of geosynthetic layers
II-4-1	1
II-4-2	2
II-4-3	3

Note: the length of each individual geosynthetic layer is the same at 30 ft.

4.3 Results and analyses

This section demonstrates and analyzes the results of four different simulation cases to evaluate the performance of geosynthetic reinforcement: (1) the individual geosynthetic reinforcement without piles under the grade beam (Case II-1), (2) the extended geosynthetic reinforcement without piles under the grade beam (Case II-2), (3) the individual geosynthetic reinforcement with a sleeper slab (Case II-3), and (4) the individual geosynthetic reinforcement only at the joint between the paving section and roadway (Case II-4). Each case presents the axial load and skin friction profiles of the abutment pile with depth, vertical and horizontal stresses, and vertical displacement profiles at different locations. The profiles showed the results obtained from three different locations, including the abutment section next to the pile, the grade beam section, and the paving section.

4.3.1 Investigation of the individual geosynthetic reinforcement

The mechanical response of soil layers, including the base and foundation soils, was examined when the individual geosynthetic reinforcement was installed at the joints between the approach slab and paving section and between the paving section and roadway.

Figure 4.27 shows the axial load profile of the abutment pile transmitted from the deck and approach slab. Applying the geosynthetic reinforcement, instead of the grade beam piles, brings in a remarkable change in the axial load transmitted to the abutment piles. When the geosynthetic reinforcement is installed, the axial load increases approximately by 20% along with the depth. Higher axial load is perceived on the abutment piles as a result of the substitution with geosynthetic layers. However, the number of the geosynthetic layers does not seem to affect the axial load significantly. Figure 4.28 shows the profiles of mobilized skin friction along with the abutment pile. Similar to the case of current design practice, the skin friction shows a negative value above the neutral point of the pile due to the high compressibility of soils at the top layer (Wong et al. 1995, Yao 2012 and Fellenius 2017). And again, the number of the geosynthetic layers does not seem to affect the mobilized skin friction significantly. Overall, applying the geosynthetic reinforcement, instead of the grade beam piles, has a minor impact on the shaft frictional resistance that is mobilized along with the abutment piles.

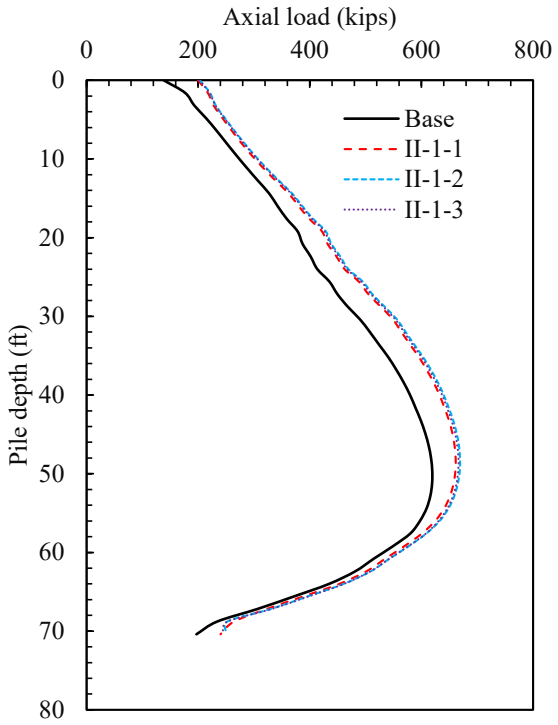

Figure 4.27 The axial load transmitted to the abutment piles for different cases with the individual geosynthetic reinforcement (II-1-1 to II-1-3).

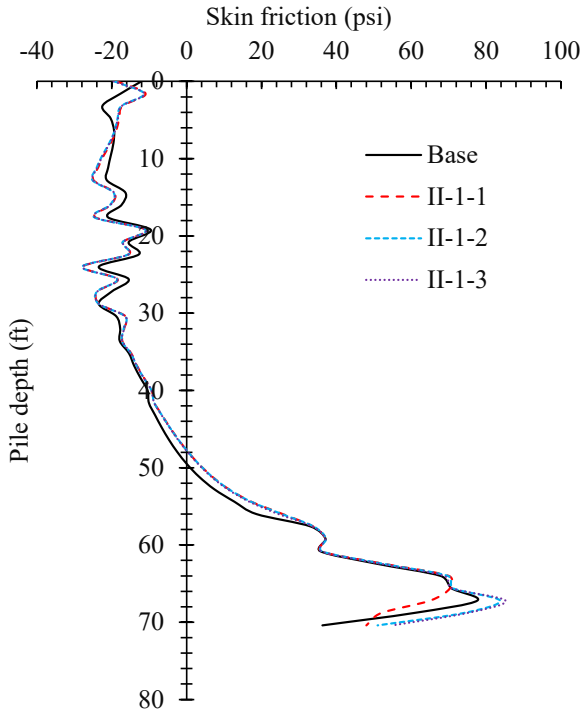

Figure 4.28 The mobilized skin frictional resistance along with the abutment piles for different cases with the individual geosynthetic reinforcement (II-1-1 to II-1-3).

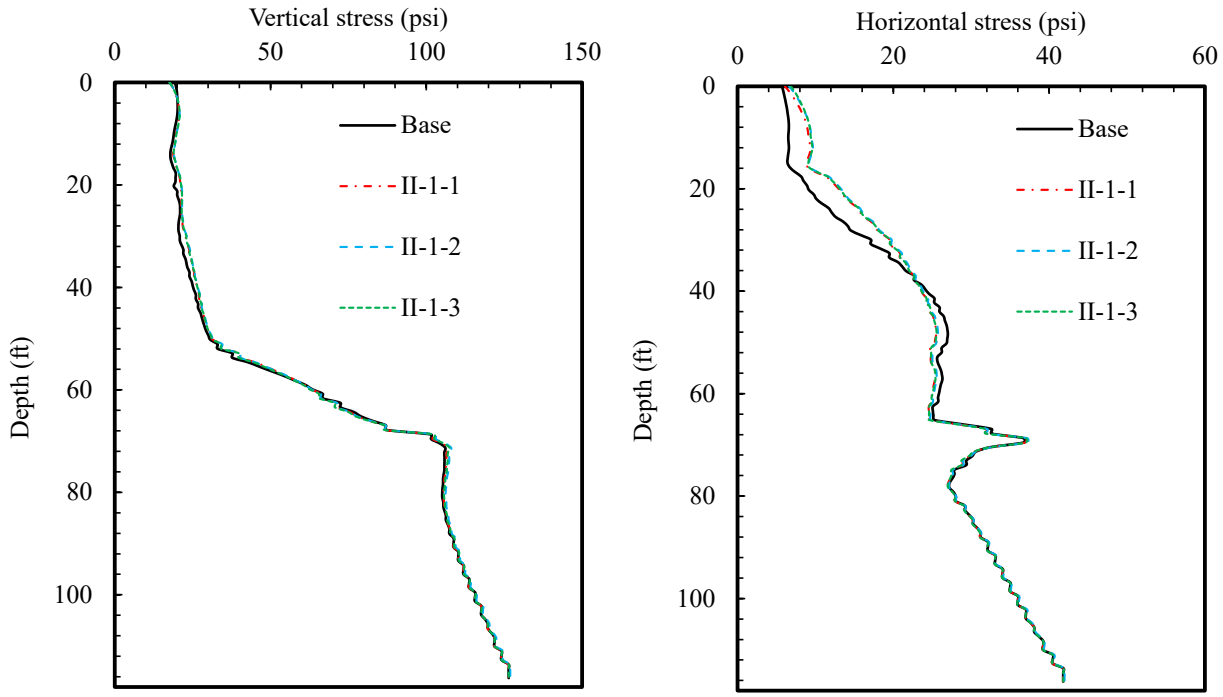

Figure 4.29 The vertical and horizontal stress profiles in the soil in the vicinity of the abutment pile for different numbers of individual geosynthetic reinforcement (II-1-1 to II-1-3).

Figure 4.29 shows the vertical and horizontal stress profiles across the abutment section. Applying the geosynthetic reinforcement, instead of the grade beam piles, has a minor impact on the stress profiles in the surrounding soils across the abutment section. This might be because the geosynthetic location is far from the abutment section, and so the effect of the geosynthetic installation may be negligible.

On the other hand, Figure 4.30 shows the vertical and horizontal stress profiles across the grade beam section. The vertical stress profiles almost coincide with the geostatic stress profile when the geosynthetic reinforcement is applied instead of the grade beam piles.

Figure 4.31 shows the vertical and horizontal stress profiles across the paving section. Again, applying the geosynthetic reinforcement instead of the grade beam piles has a minor impact on the vertical and horizontal stresses that develop in the soil.

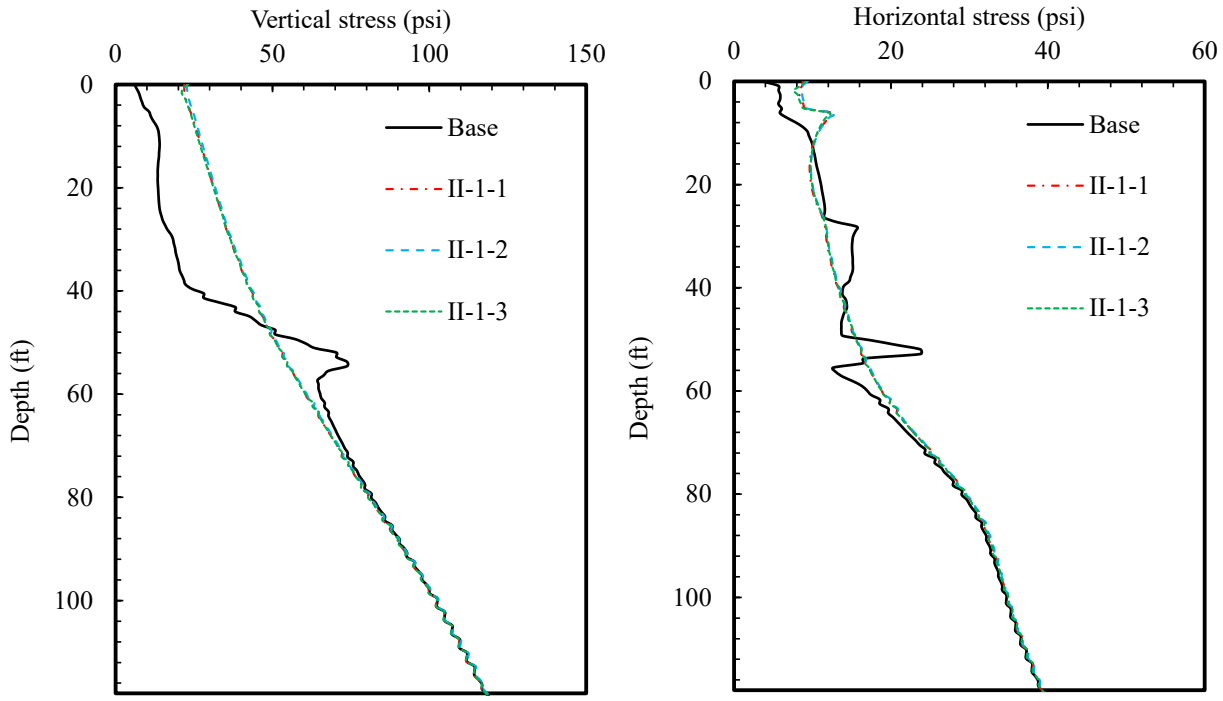

Figure 4.30 The vertical and horizontal stress profiles in the soil in the vicinity of the grade beam section for different numbers of individual geosynthetic reinforcement (II-1-1 to II-1-3).

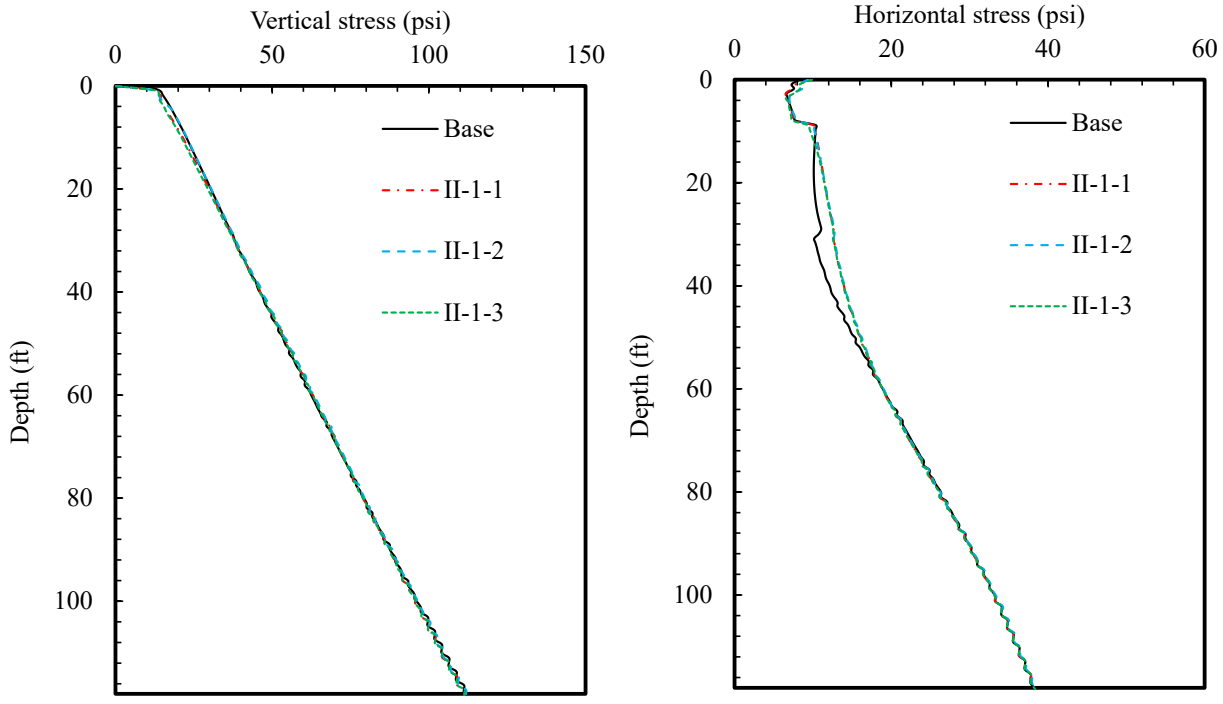

Figure 4.31 The vertical and horizontal stress profiles in the soil in the vicinity of the paving section for different numbers of individual geosynthetic reinforcement (II-1-1 to II-1-3).

Figure 4.32 shows the vertical settlement profile across the abutment section with a various number of geosynthetic layers. The vertical displacement is the largest at the surface of the ground because of the accumulation of the strain along with the depth. Applying the geosynthetic reinforcement, instead of the grade beam piles, has a minor impact on the vertical settlement profiles across the abutment section. Overall, the vertical displacement profiles for all examined cases acceptable, with the maximum value on the surface being less than a quarter inch.

On the other hand, Figure 4.33 shows the vertical settlement profile across the grade beam section with a various number of geosynthetic layers. Applying the geosynthetic reinforcement, instead of the grade beam piles, would result in an increased vertical settlement along the grade beam section. However, its projected maximum settlement is between 0.2 and 0.3 inches for all examined cases, except the single layer reinforcement. The difference between the base and geosynthetics' case is not significant, in particular, when more than two layers of geosynthetic reinforcement are installed.

Lastly, Figure 4.34 shows the vertical settlement profile across the paving section with a various number of geosynthetic layers. Applying the geosynthetic reinforcement brings in a positive impact on the vertical settlement profiles across the paving section. That is, all examined cases result in less vertical settlement compared to the base (original design). In particular, the II-1-3 case (three geosynthetic layers) shows the smallest settlement among all examined cases.

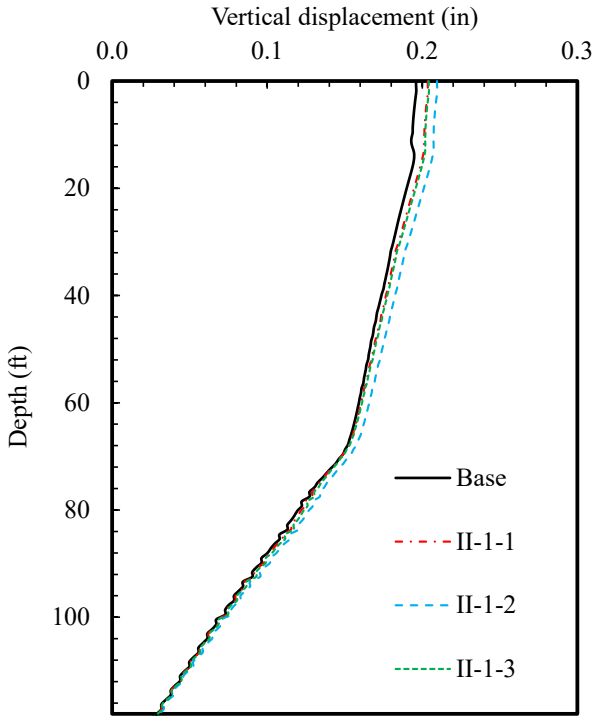

Figure 4.32 The vertical settlement profile across the abutment section for different numbers of individual geosynthetic reinforcement (II-1-1 to II-1-3).

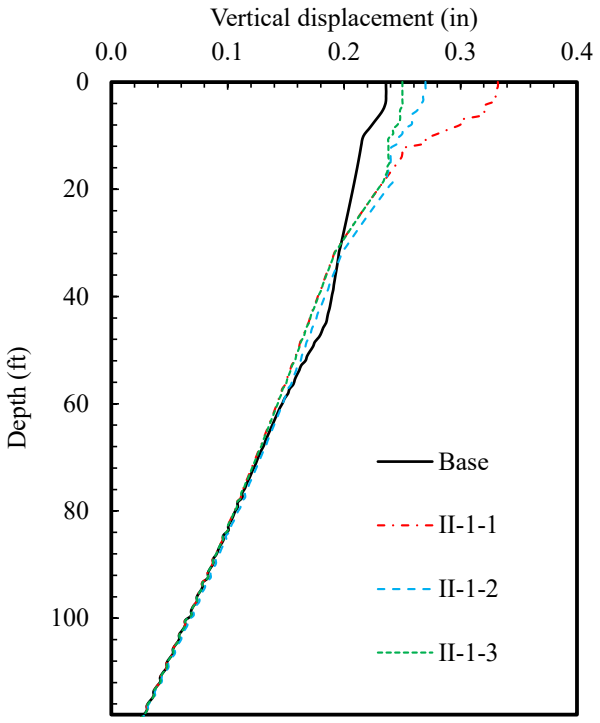

Figure 4.33 The vertical settlement profile across the grade beam section for different numbers of individual geosynthetic reinforcement (II-1-1 to II-1-3).

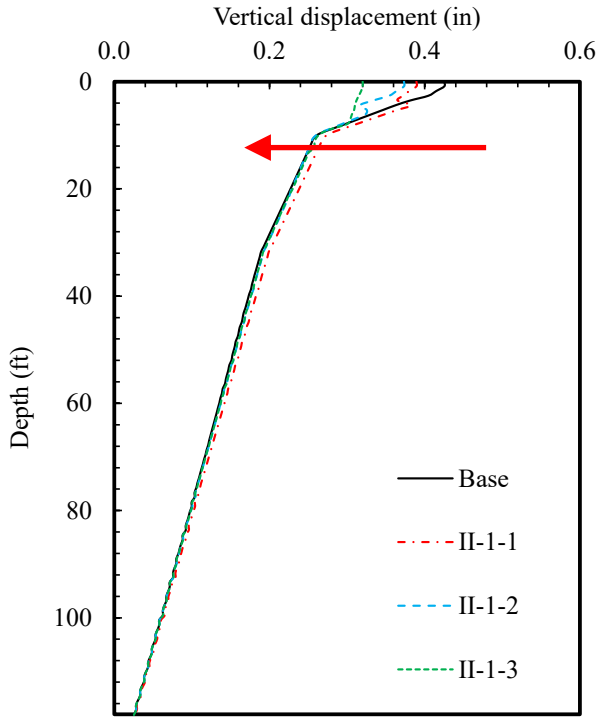

Figure 4.34 The vertical settlement profile across the paving section for different numbers of individual geosynthetic reinforcement (II-1-1 to II-1-3).

Figure 4.35 shows the differential settlement between the abutment and grade beam sections. With increasing the number of geosynthetic layers, less differential settlement is induced. For comparison, a slightly higher value (13%) of the different settlement between the abutment and grade beam sections is obtained as the geosynthetic reinforcement is applied instead of the grade beam piles. However, those differences are trivial (less than 0.02 inches) when more than two layers of the geosynthetic reinforcement are applied in this study.

Figure 4.36 shows the differential settlement between the grade beam and paving sections. Interestingly, this differential settlement could be greatly alleviated when the geosynthetic reinforcement is applied instead of the grade beam piles (i.e., base case). In detail, the differential settlement showed more than a 40% reduction of the settlement compared to the base. This is mainly because the settlement at the joint between the paving section and roadway was reduced as a result of the geosynthetic reinforcement. Thus, the individual geosynthetic reinforcement at both joints could be an effective way to reduce the bump or differential settlements not only near the end of the approach slab but also the end of the paving section.

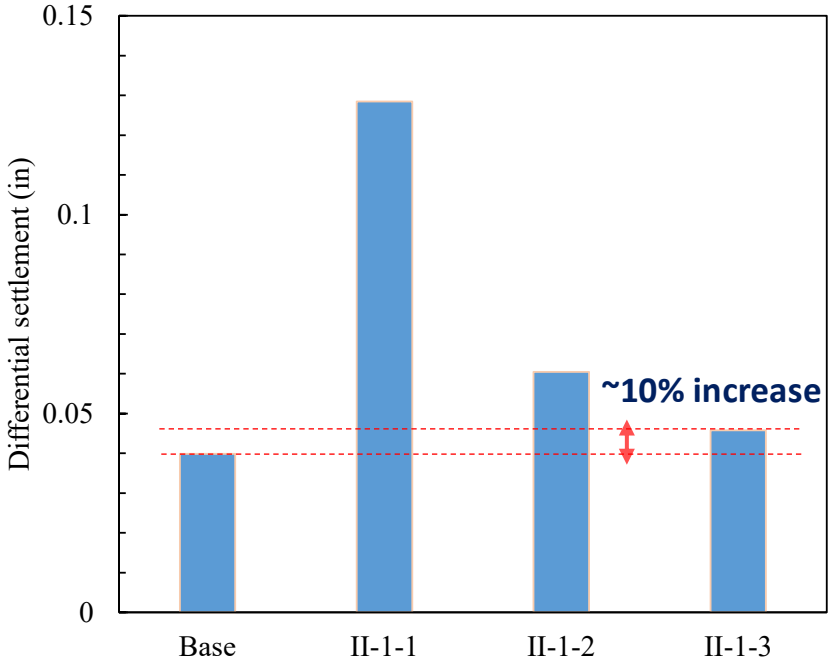

Figure 4.35 Differential settlement between the abutment and grade beam sections for different numbers of individual geosynthetic reinforcement (II-1-1 to II-1-3).

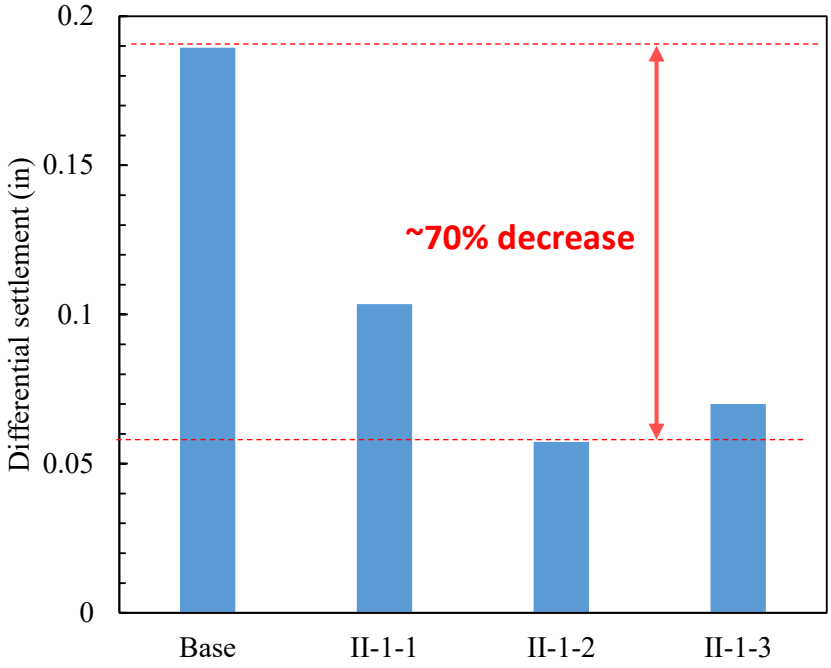

Figure 4.36 Differential settlement between the grade beam and paving sections for different numbers of individual geosynthetic reinforcement (II-1-1 to II-1-3).

4.3.2 Investigation of the extended geosynthetic reinforcement

The mechanical behavior of the soil layer, including base and foundation soils, was examined when the extended geosynthetic reinforcement was installed in this section. The extended geosynthetic reinforcement is expected to increase the resistance and to reduce the settlement in the soil layers more efficiently than individual geosynthetic reinforcement because the extended one has longer reinforcement embedded in the soil layers, and so may generate higher resistance along with soil-geosynthetic interfaces.

First, Figure 4.37 shows the axial load profile of the abutment pile transmitted from the deck and approach slab. Applying the extended geosynthetic reinforcement also brings in a minor change in the axial load transmitted to the abutment piles. When the geosynthetic reinforcement is installed, the axial load increases approximately by 15% - 20% along with the depth. Similar to the individual geosynthetic reinforcement, a slightly higher axial load is perceived on the abutment piles as a result of the substitution with geosynthetic layers.

Figure 4.38 shows the profile of mobilized skin friction along with the abutment pile. Similar to the previous case (II-1), due to the high compressibility of soils at the top layer, the skin friction shows a negative value above the neutral point of the pile. It was observed that applying the extended geosynthetic reinforcement has a minor impact on the shaft frictional resistance that is mobilized along with the abutment piles. Also, the number of geosynthetics does not seem to significantly affect the mobilized skin friction.

Lastly, Figure 4.39 shows the vertical and horizontal stress profiles across the abutment section. Again, applying the geosynthetic reinforcement instead of the grade beam piles has a minor impact on the vertical and horizontal stresses that develop in the surrounding soils. This might be because the geosynthetic location is far from the abutment section, and so the effect of the geosynthetic installation may be negligible.

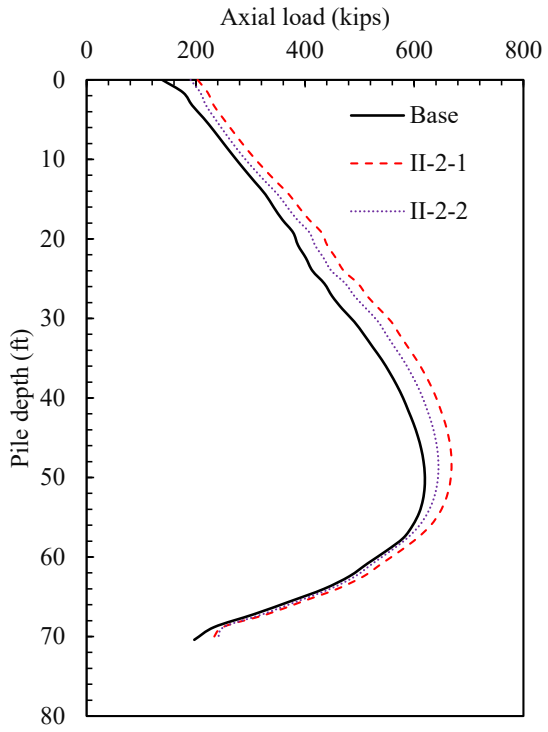

Figure 4.37 The axial load transmitted to the abutment piles for different numbers of extended geosynthetic reinforcement (II-2-1 to II-2-2).

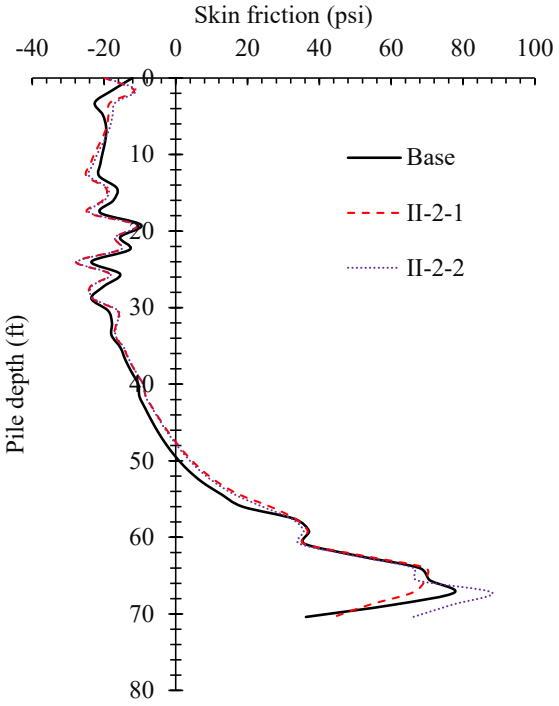

Figure 4.38 The mobilized skin frictional resistance along with the abutment piles for different numbers of extended geosynthetic reinforcement (II-2-1 to II-2-2).

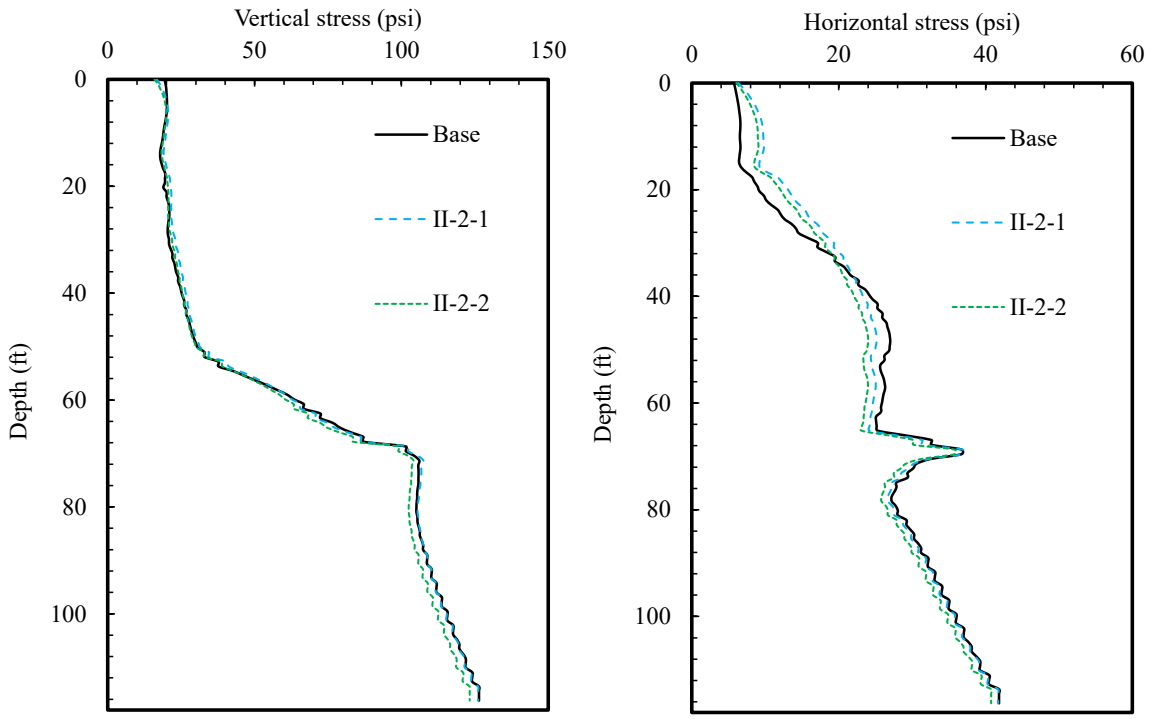

Figure 4.39 The vertical and horizontal stress profiles in the soil in the vicinity of the abutment pile for different numbers of extended geosynthetic reinforcement (II-2-1 to II-2-2).

Figure 4.40 shows the vertical and horizontal stress profiles across the grade beam section. Similar to the case of individual geosynthetic reinforcement, the vertical stress profiles almost coincide with the geostatic stress profile when the geosynthetic reinforcement is applied instead of the grade beam piles. And, the number of geosynthetic layers does not seem to affect such development of vertical and horizontal stress profiles.

Figure 4.41 shows the vertical and horizontal stress profiles across the paving section. Applying the geosynthetic reinforcement, instead of the grade beam piles, has a minor impact on these stress profiles under the paving section.

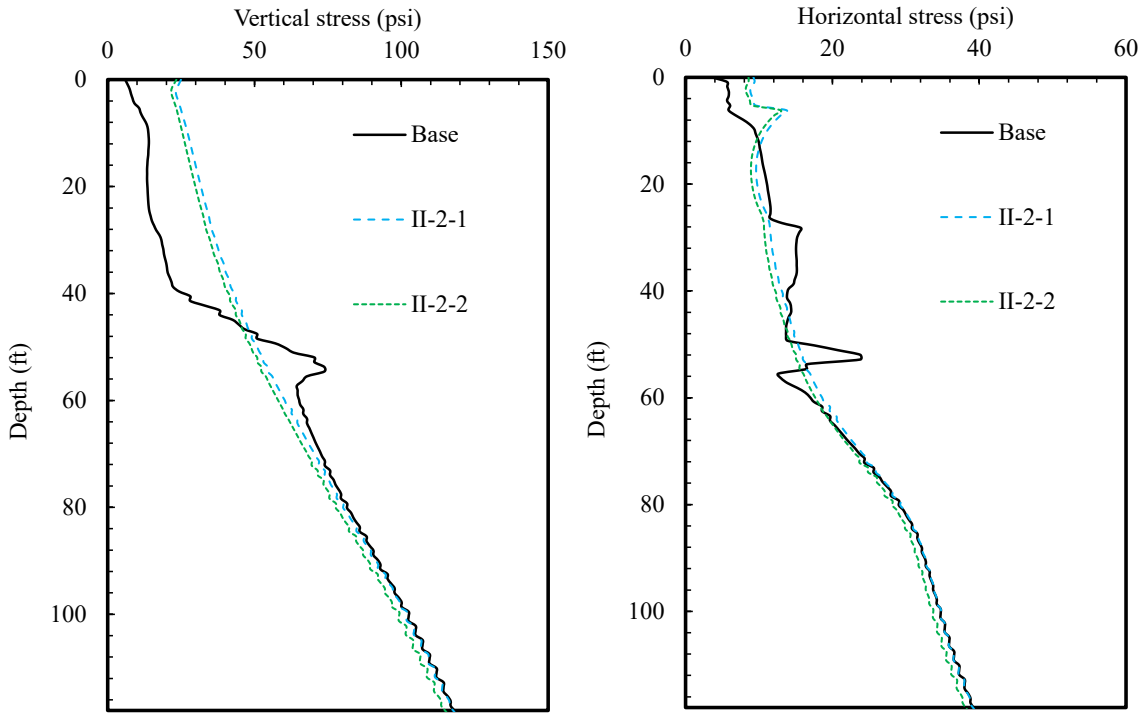

Figure 4.40 The vertical and horizontal stress profiles in the soil in the vicinity of the grade beam section for different numbers of extended geosynthetic reinforcement (II-2-1 to II-2-2).

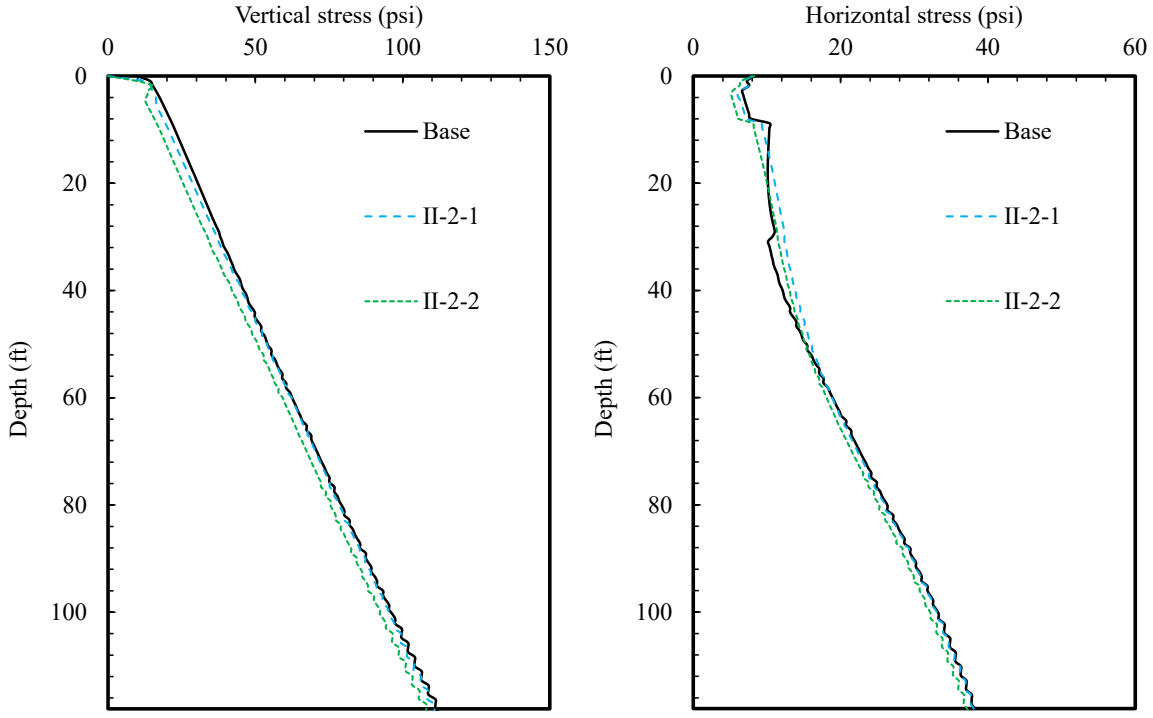

Figure 4.41 The vertical and horizontal stress profiles in the soil in the vicinity of the paving section for different numbers of extended geosynthetic reinforcement (II-2-1 to II-2-2).

Figure 4.42 shows the vertical settlement profile across the abutment section with a various number of extended geosynthetic layers. Applying the extended geosynthetic reinforcement instead of the grade beam piles has a minor impact on the vertical settlement profiles across the abutment section. Interestingly, compared to the original design (base case), a less vertical settlement was resulted when the two layers of extended geosynthetic reinforcement are applied, while the single layer reinforcement resulted in a slightly increased vertical settlement. Overall, the vertical settlement profiles for all examined cases are acceptable, with the maximum value on the surface being less than a quarter inch.

On the other hand, Figure 4.43 shows the vertical settlement profile across the grade beam section with a various number of geosynthetic layers. Overall, the vertical settlement profiles became noticeably different when the extended geosynthetic reinforcement is applied (up to two layers in this simulation). It is clearly observed that applying the extended geosynthetic reinforcement instead of the grade beam piles could result in an increased vertical settlement along the grade beam section. The two layers reinforcement might still be okay, but the single layer reinforcement could be marginal with the maximum settlement value close to 0.4 inches. Those results imply that the extended geosynthetic installation may not effectively alleviate the settlement at the joint between the approach slab and the paving section.

Lastly, Figure 4.44 shows the vertical settlement profile across the paving section. Similar to the previous cases (II-1), applying the extended geosynthetic reinforcement brings in a positive impact on the vertical settlement profiles across the paving section. That is, a less surface settlement is induced as more layers of geosynthetic reinforcement are applied. In particular, its effect is more prominent when two layers of extended geosynthetic reinforcement are applied.

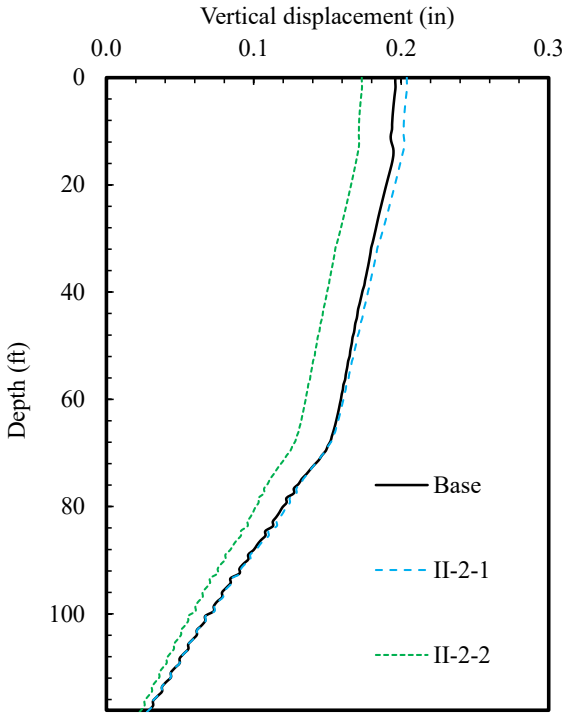

Figure 4.42 The vertical settlement profile across the abutment section for different numbers of extended geosynthetic reinforcement (II-2-1 to II-2-2).

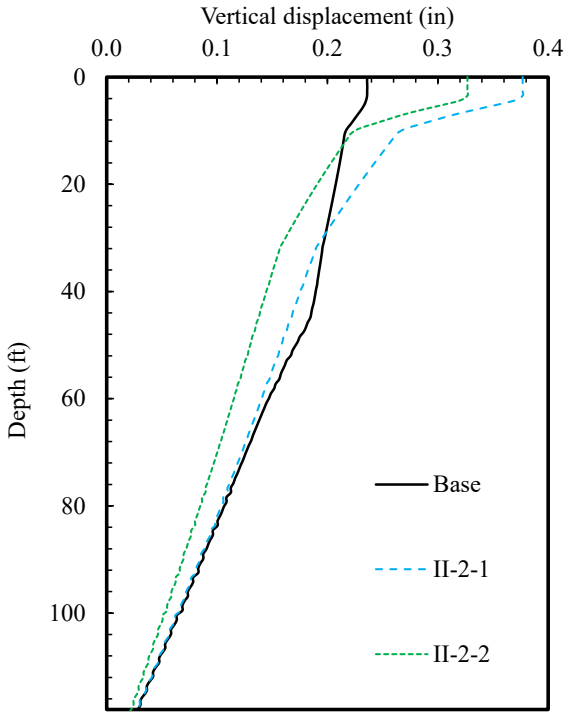

Figure 4.43 The vertical settlement profile across the grade beam section for different numbers of extended geosynthetic reinforcement (II-2-1 to II-2-2).

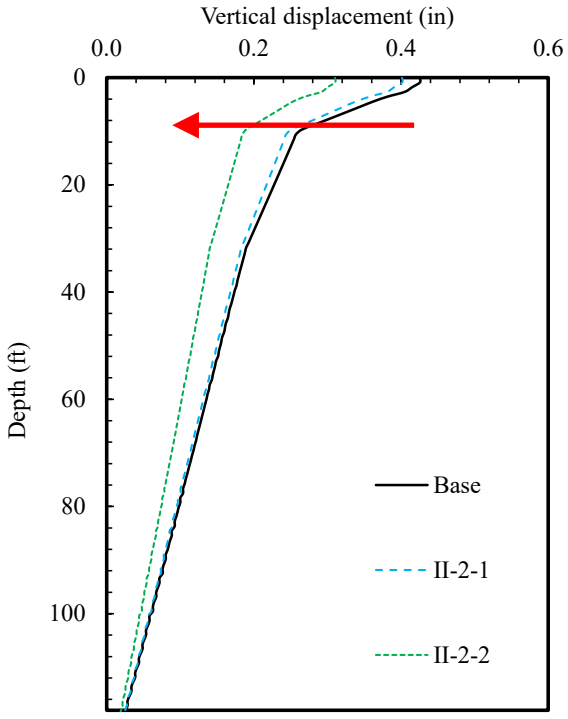

Figure 4.44 The vertical settlement profile across the paving section for different numbers of extended geosynthetic reinforcement (II-2-1 to II-2-2).

Figure 4.45 shows the differential settlement between the abutment and grade beam sections. Compared to the original design (base case), this differential settlement increased more than triple when the extended geosynthetic reinforcement is applied instead of the grade beam piles. The extended geosynthetic reinforcement does not seem as effective as the individual geosynthetic reinforcement in terms of the differential settlement between the abutment and grade beam sections.

On the other hand, Figure 4.46 shows the differential settlement between the grade beam and paving sections. It seems that this differential settlement could be significantly alleviated when the extended geosynthetic reinforcement is applied instead of the grade beam piles. The two layers of reinforcement are obviously more effective than the single-layer reinforcement. That is, the differential settlement showed more than 80% of reduction compared to the base. It is mainly because the settlement at the joint between the paving section and roadway was reduced as a result of the geosynthetic reinforcement. However, the extended geosynthetic reinforcement is not recommended because of the noticeable increase in the vertical settlement across the grade beam section and the differential settlement between the abutment and grade beam sections.

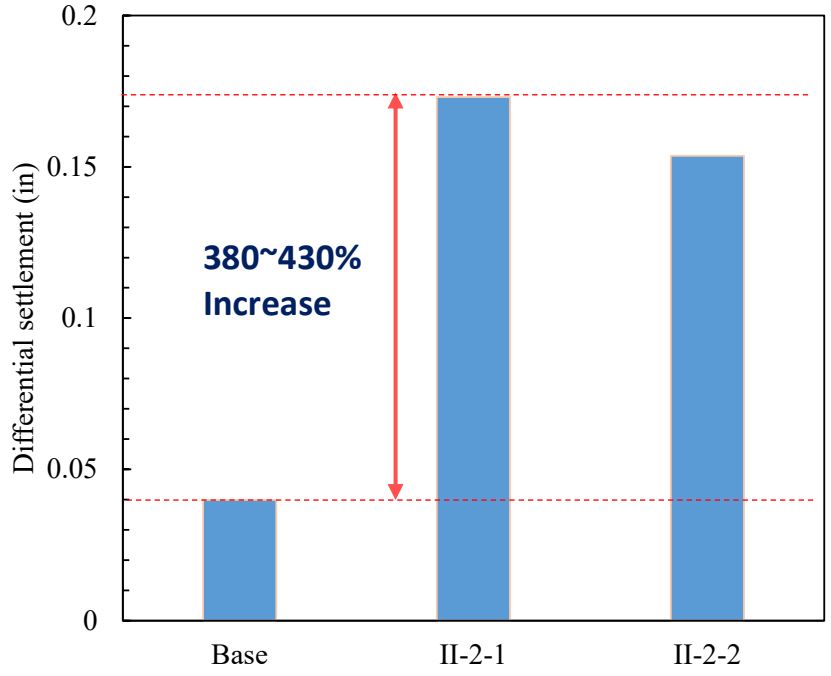

Figure 4.45 Differential settlement between the abutment and grade beam sections for different numbers of extended geosynthetic reinforcement (II-2-1 to II-2-2).

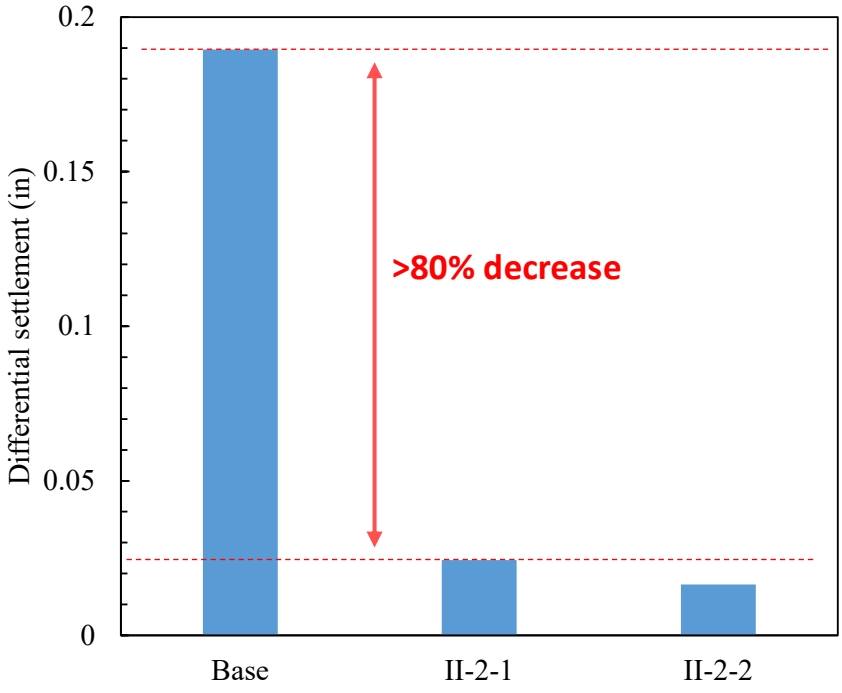

Figure 4.46 Differential settlement between the grade beam and paving sections for different numbers of extended geosynthetic reinforcement (II-2-1 to II-2-2).

4.3.3 Investigation of the individual geosynthetic reinforcement + sleeper slab

The mechanical behavior of the soil layer, including base and foundation soils, is examined when the individual geosynthetic reinforcement with a sleeper slab is installed in this section. Figure 4.47 shows the axial load profile of the abutment pile that is transmitted from the deck and approach slab. Applying the individual geosynthetic reinforcement with the sleeper slab brings in a slight change in the axial load transmitted to the abutment piles. In detail, when the geosynthetic reinforcement is installed, the axial load increases approximately by 10% along with the abutment pile. And then, a further slight increase in the axial load is perceived as a result of the substitution with the wide sleeper slab as it can distribute the axial loading more widely from the grade beam side.

Figure 4.48 shows the profile of mobilized skin frictional resistance along with the abutment pile. Again, due to the high compressibility of soils at the top layer, the mobilized skin friction shows a negative value above the neutral point of the pile and then changed to the positive value. Similar to the previous cases (II-1 and II-2), applying the individual geosynthetic reinforcement with a sleeper slab has a minor impact on the shaft frictional resistance that is mobilized along with the abutment piles.

Lastly, Figure 4.49 shows the vertical and horizontal stress profiles across the abutment section. Applying the geosynthetic reinforcement and a sleeper slab, instead of the grade beam piles, yields a negligible impact on those stress profiles that develop in the surrounding soils.

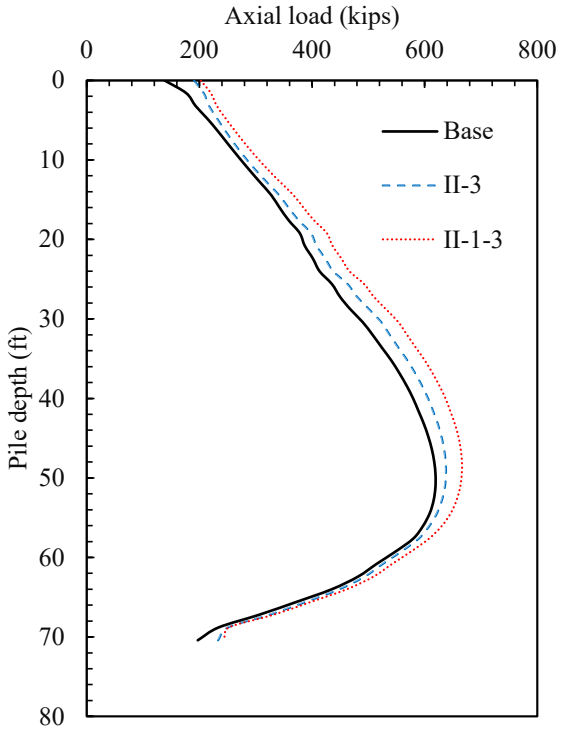

Figure 4.47 The axial load transmitted to the abutment piles for the case of individual geosynthetic reinforcement with three layers + sleeper slab (II-3) *vs*. II-1-3.

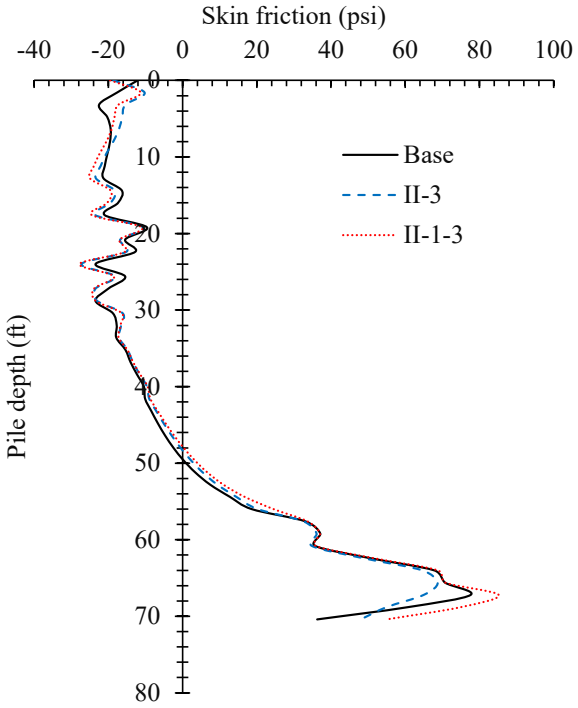

Figure 4.48 The mobilized skin frictional resistance along with the abutment piles for the case of individual geosynthetic reinforcement with three layers + sleeper slab (II-3) *vs*. II-1-3.

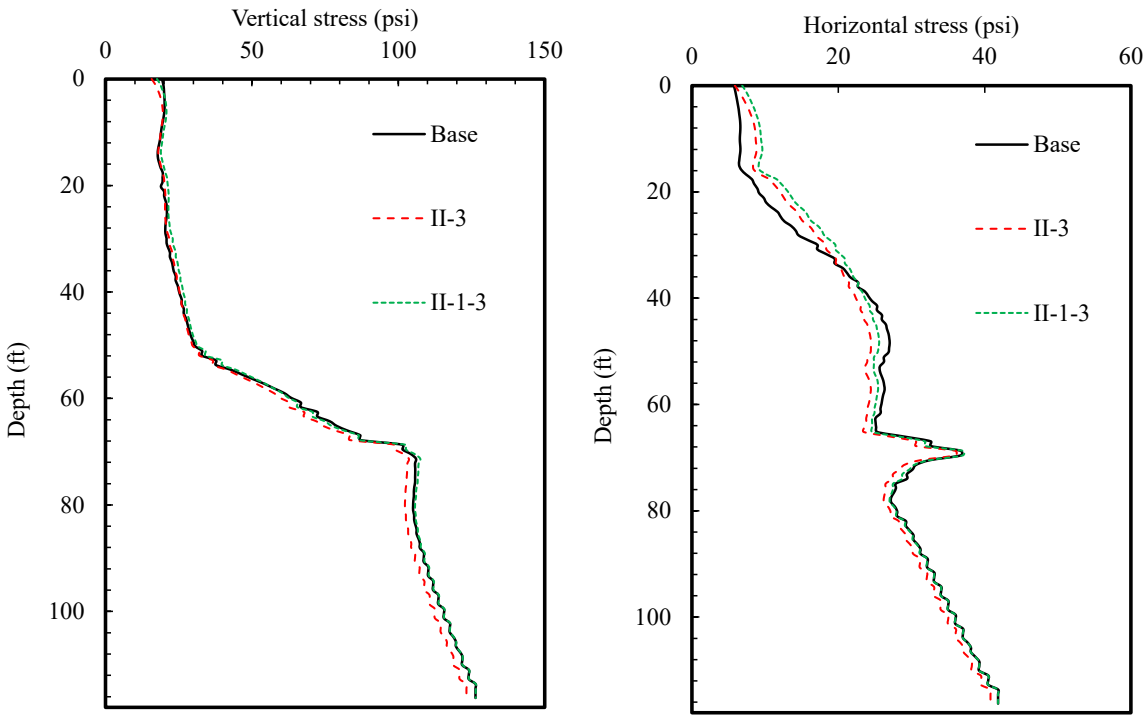

Figure 4.49 The vertical and horizontal stress profiles in the soil in the vicinity of the abutment pile for the case of individual geosynthetic reinforcement with three layers + sleeper slab (II-3) *vs*. II-1-3.

Figure 4.50 shows the vertical and horizontal stress profiles across the sleeper slab section (i.e., equivalent to the grade beam section). Similar to the case of the individual geosynthetic reinforcement, the vertical stress profiles almost coincide with the geostatic stress distribution when the geosynthetic reinforcement is applied instead of the grade beam piles.

Figure 4.51 shows the vertical and horizontal stress profiles across the paving section. Applying the sleeper slab together with the individual geosynthetic reinforcement, instead of the grade beam piles, has a minor impact on those stress profiles that develop in the soils under the paving section. Therefore, it implies that the substitution of the grade beam with a wider sleeper slab does not yield a noticeable change in the stress profiles in the foundation soils.

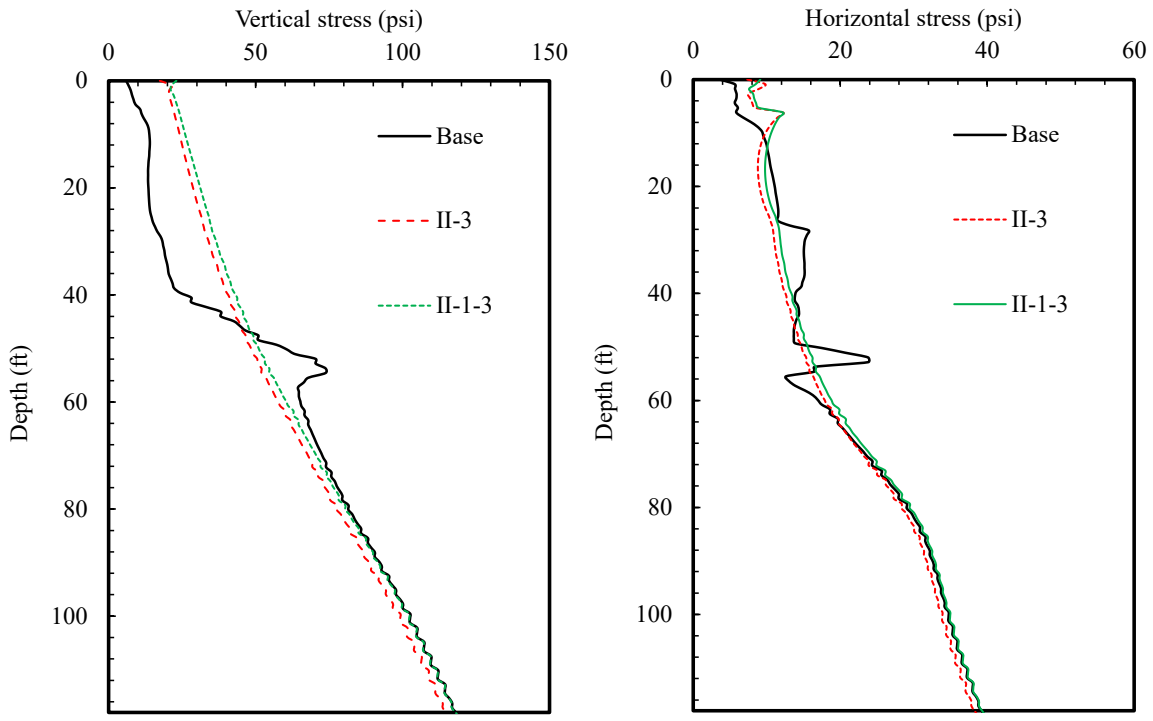

Figure 4.50 The vertical and horizontal stress profiles in soil under the grade beam section for the case of individual geosynthetic reinforcement with three layers + sleeper slab (II-3) *vs*. II-1-3.

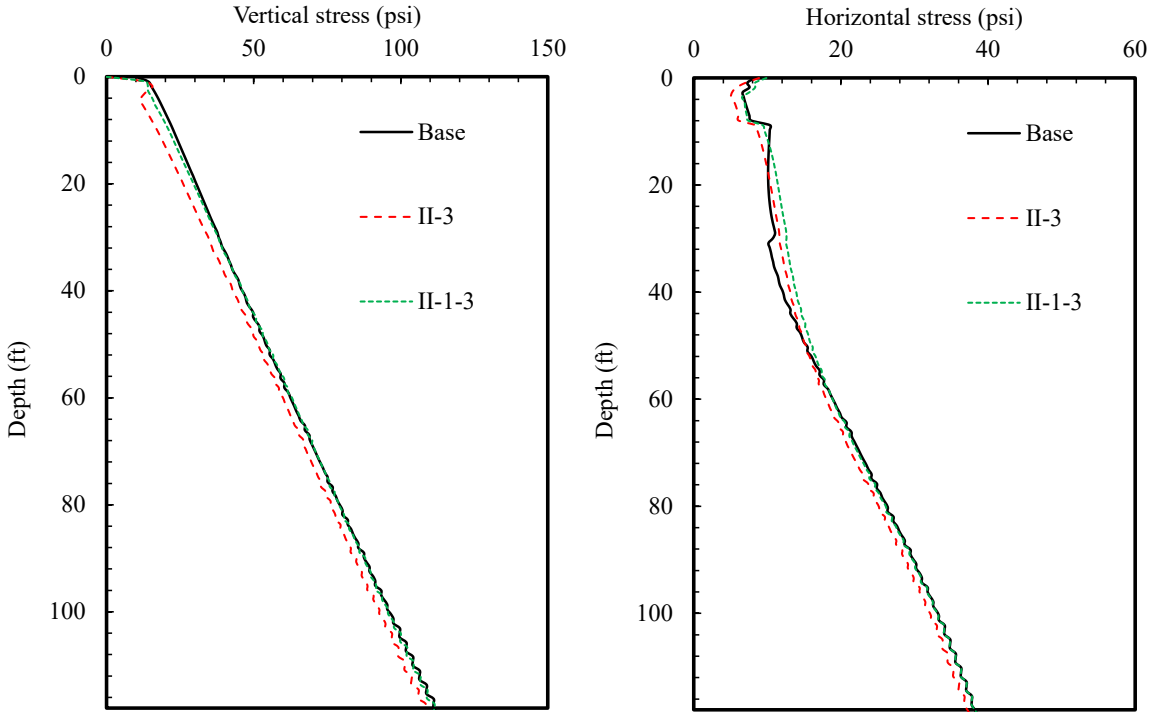

Figure 4.51 The vertical and horizontal stress profiles in soil under the paving section for the case of individual geosynthetic reinforcement with three layers + sleeper slab (II-3) *vs*. II-1-3.

Figure 4.52 shows the vertical settlement profile across the abutment section compared to the base case and the individual geosynthetic reinforcement at three layers under the grade beam (II-1-3). Applying the individual geosynthetic reinforcement with the sleeper slab, instead of the grade beam piles or the grade beam with the geosynthetic reinforcement, presented a noticeable reduction in the vertical settlement across the abutment section. Interestingly, compared to the original design (base case), a less vertical settlement was resulted (by 25%) when the individual geosynthetic reinforcement with the sleeper slab is applied, while the individual geosynthetic reinforcement under the grade beam resulted in a slightly increased vertical settlement. Overall, the vertical settlement profiles for all examined cases are acceptable, with the maximum value on the surface being less than a quarter inch.

Figure 4.53 shows the vertical settlement profile across the grade beam section. Applying the individual geosynthetic reinforcement with the sleeper slab does not seem to meaningfully reduce the vertical settlement compared to the individual geosynthetic reinforcement with the original grade beam design. After all, the sleeper slab and grade beam presented a similar settlement on the surface, even though the vertical settlement in the underlying soils could be alleviated due to the wider distribution of the applied load. Similarly, the adoption of sleep slab does not seem to significantly contribute to reducing the vertical settlement at the paving section compared to the individual geosynthetic reinforcement with the original grade beam design (Figure 4.54). In this regard, the individual geosynthetic reinforcement in conjunction with the sleeper slab may not be particularly effective in decreasing the settlement at the joints between the approach slab and paving sections and between the paving section and roadway, compared to the individual geosynthetic reinforcement under the original grade beam.

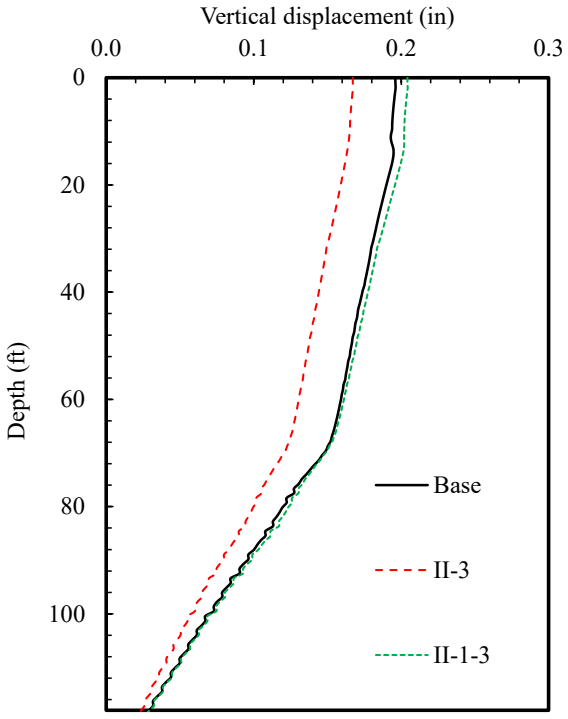

Figure 4.52 The vertical settlement profile across the abutment section for the case of individual geosynthetic reinforcement with three layers + sleeper slab (II-3) *vs*. II-1-3.

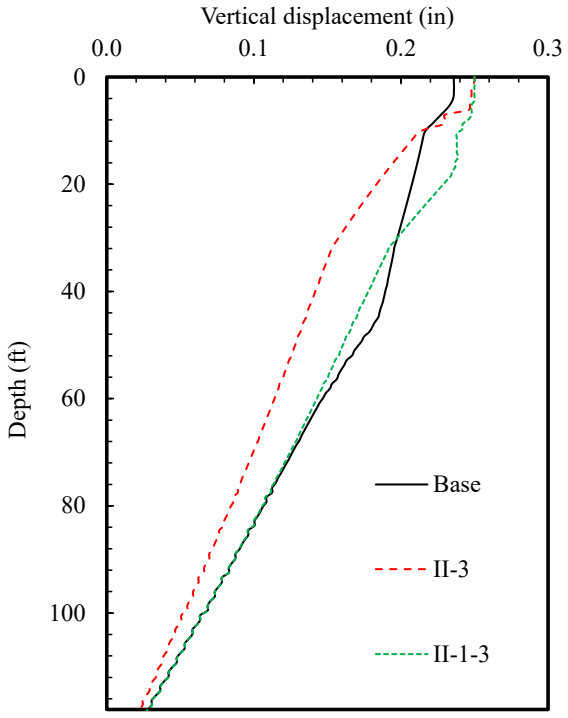

Figure 4.53 The vertical settlement profile across the grade beam section for the case of individual geosynthetic reinforcement with three layers + sleeper slab (II-3) *vs*. II-1-3.

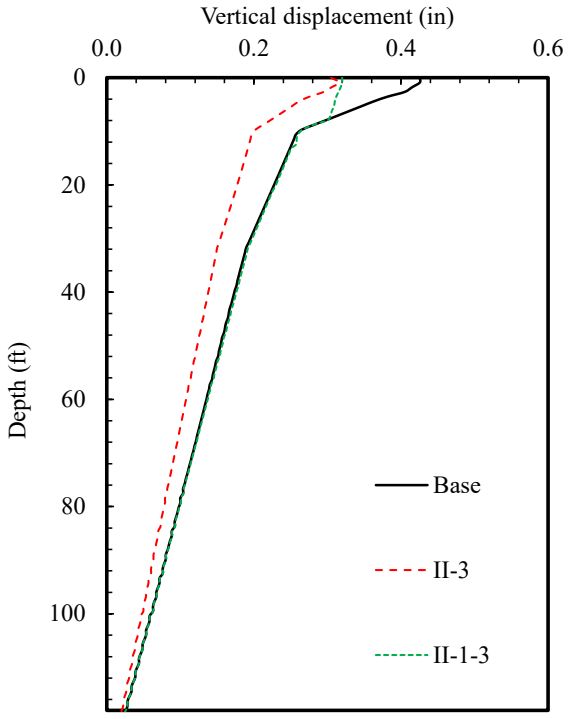

Figure 4.54 The vertical settlement profile across the paving section for the case of individual geosynthetic reinforcement with three layers + sleeper slab (II-3) *vs*. II-1-3.

Figure 4.55 shows the differential settlement between the abutment and grade beam sections. Compared to the original design (base case), this differential settlement increased by approximately 220% when the individual geosynthetic reinforcement with the sleeper slab is applied instead of the grade beam piles. The individual geosynthetic reinforcement with the sleeper slab does not seem as effective as the individual geosynthetic reinforcement with the original grade beam design in this regard. On the other hand, Figure 4.56 shows the differential settlement between the grade beam and paving sections, which is observed to be alleviated further as a result of adopting the wider sleeper slab. A further study is needed on the influence of the wider sleeper slab on reducing vertical settlements, particularly when used together with the geosynthetic reinforcements.

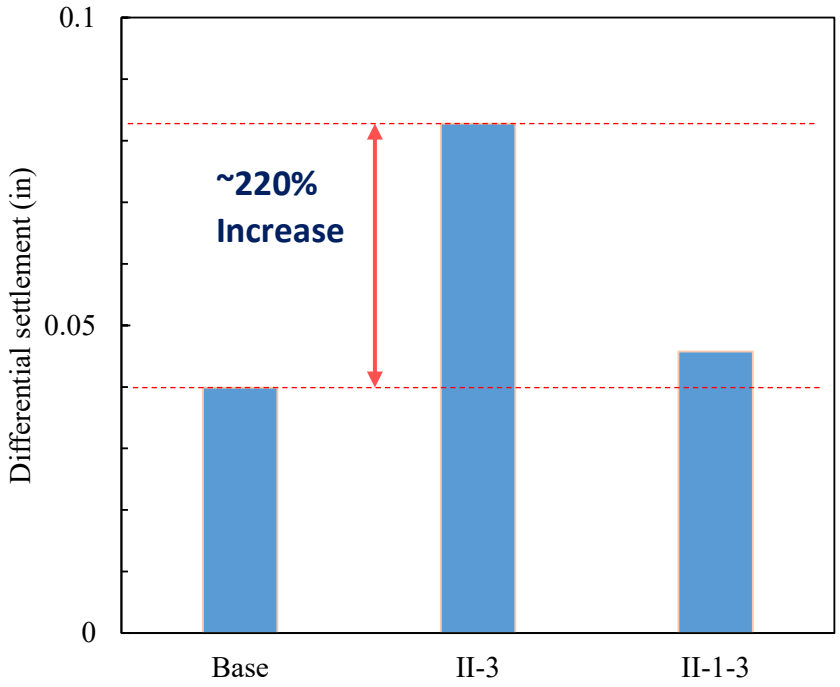

Figure 4.55 Differential settlement between the abutment and grade beam sections for the case of individual geosynthetic reinforcement with three layers + sleeper slab (II-3) *vs*. II-1-3.

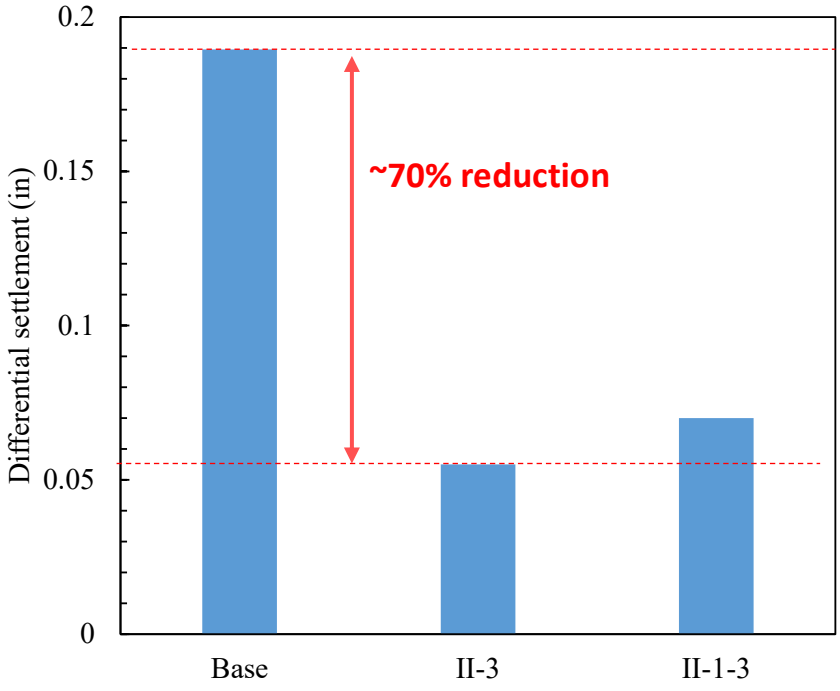

Figure 4.56 Differential settlement between the grade beam and paving sections for the case of individual geosynthetic reinforcement with three layers + sleeper slab (II-3) *vs*. II-1-3.

4.3.4 Investigation of the individual geosynthetic reinforcement under the paving section only

The mechanical behavior of the soil layer, including base and foundation soils, is examined when the individual geosynthetic reinforcement is applied only under the end of the paving section in this section. Figure 4.57 shows the axial load profile of the abutment pile transmitted from the deck and approach slab, and Figure 4.58 shows the profile of mobilized skin frictional resistance along with the abutment pile. Again, due to the high compressibility of soils at the top layer, the mobilized skin friction shows a negative value above the neutral point of the pile and then changed to the positive value. Applying the individual geosynthetic reinforcement under the paving section only brings in a negligible impact on both the axial load and mobilized skin frictional resistance of the abutment piles, which makes sense given that the geosynthetic reinforcement is far from the abutment section.

Similarly, Figure 4.59 shows the axial load profile of the grade beam pile transmitted from the deck and approach slab. Applying the individual geosynthetic reinforcement under the paving section only yields a minor change in the axial load transmitted to the grade beam piles. And the number of the geosynthetic layers does not affect the axial load significantly. Figure 4.60 shows the profile of mobilized skin frictional resistance along with the grade beam pile. Similarly, applying the individual geosynthetic reinforcement under the paving section only has a minor impact on the shaft frictional resistance. Overall, it can be suggested that applying the individual geosynthetic reinforcement only to near the end of the paving section is not likely to meaningfully change the axial load and mobilized skin frictional resistance of the grade beam piles.

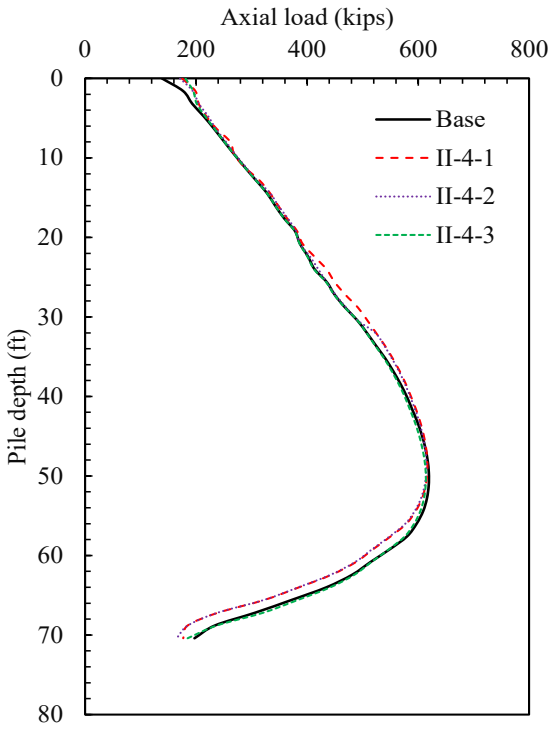

Figure 4.57 The axial load transmitted to the abutment piles for difference cases of individual geosynthetic reinforcement under the paving section only (II-4-1 to II-4-3).

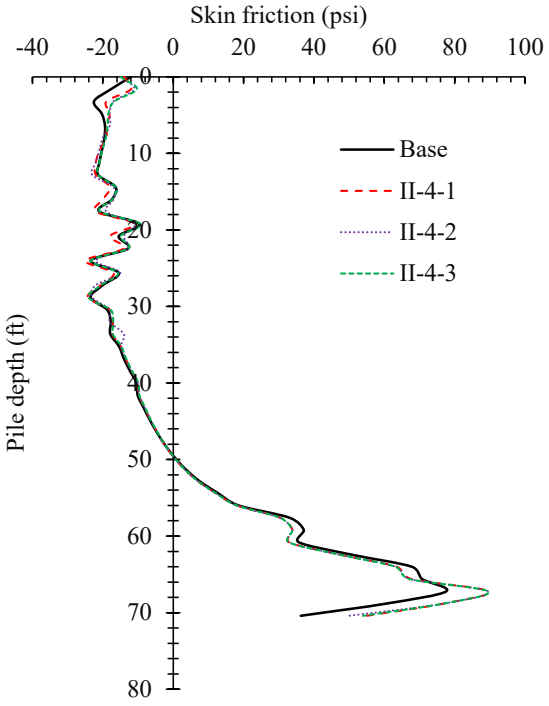

Figure 4.58 The mobilized skin frictional resistance along with the abutment piles for difference cases of individual geosynthetic reinforcement under the paving section only (II-4-1 to II-4-3).

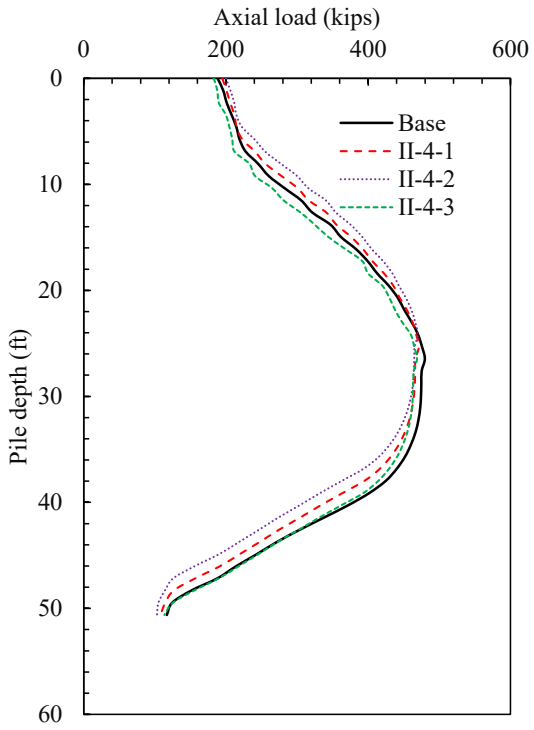

Figure 4.59 The axial load transmitted to the grade beam piles for difference cases of individual geosynthetic reinforcement under the paving section only (II-4-1 to II-4-3).

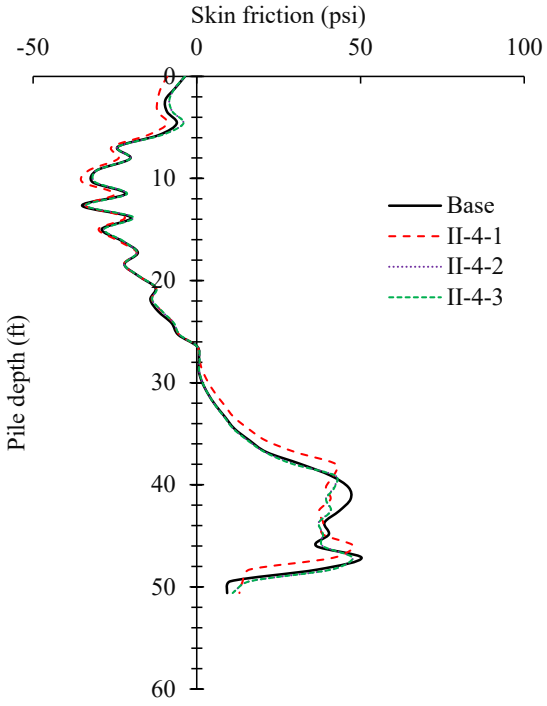

Figure 4.60 The mobilized skin frictional resistance along with grade beam piles for difference cases of individual geosynthetic reinforcement under the paving section only (II-4-1 to II-4-3).

Figure 4.61 shows the vertical and horizontal stress profiles across the abutment section, while Figure 4.62 shows these stress profiles across the grade beam section. Those results confirm that the application of individual geosynthetic reinforcement only to near the end of the paving section is not likely to change the stress profiles that develop in the soil near the abutment and grade beam sections.

On the other hand, Figure 4.63 shows the vertical and horizontal stress profiles across the paving section. The presence of geosynthetic layers helps to reduce the vertical and horizontal stresses in the soil under the paving section to some extent due to the tensile strength of geosynthetics.

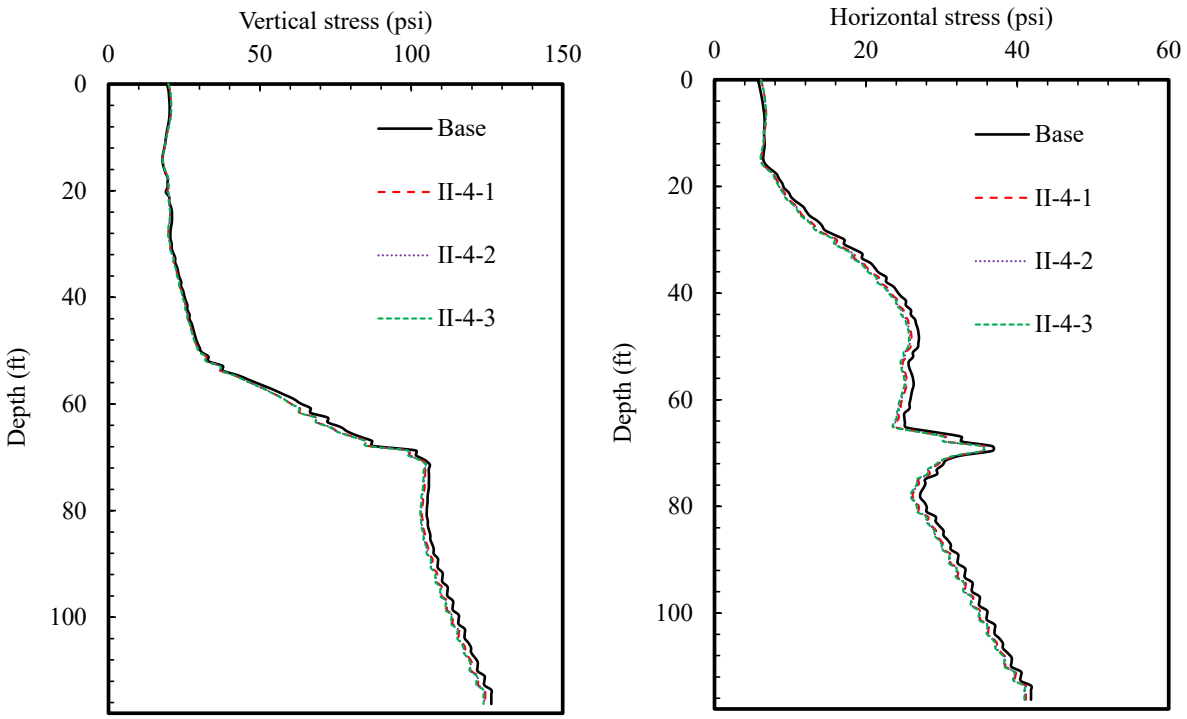

Figure 4.61 The vertical and horizontal stress profiles in the soil in the vicinity of the abutment pile for difference cases of individual geosynthetic reinforcement under the paving section only (II-4-1 to II-4-3).

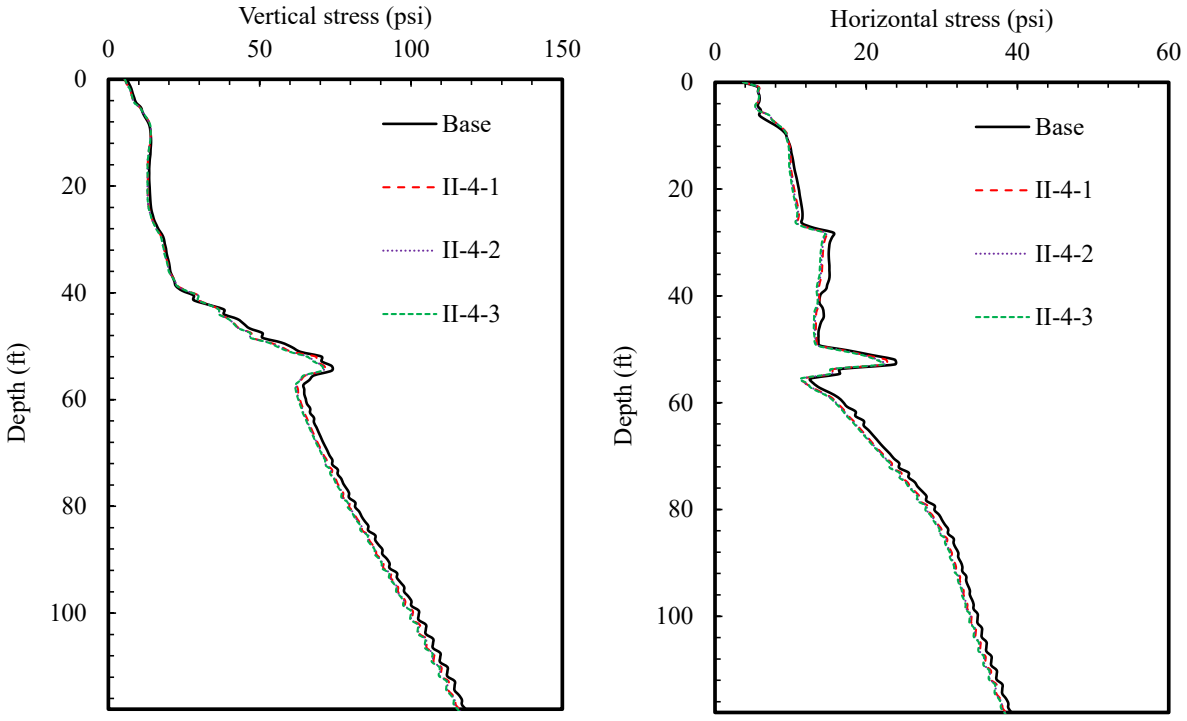

Figure 4.62 The vertical and horizontal stress profiles in the soil in the vicinity of the grade beam pile for difference cases of individual geosynthetic reinforcement under the paving section only (II-4-1 to II-4-3).

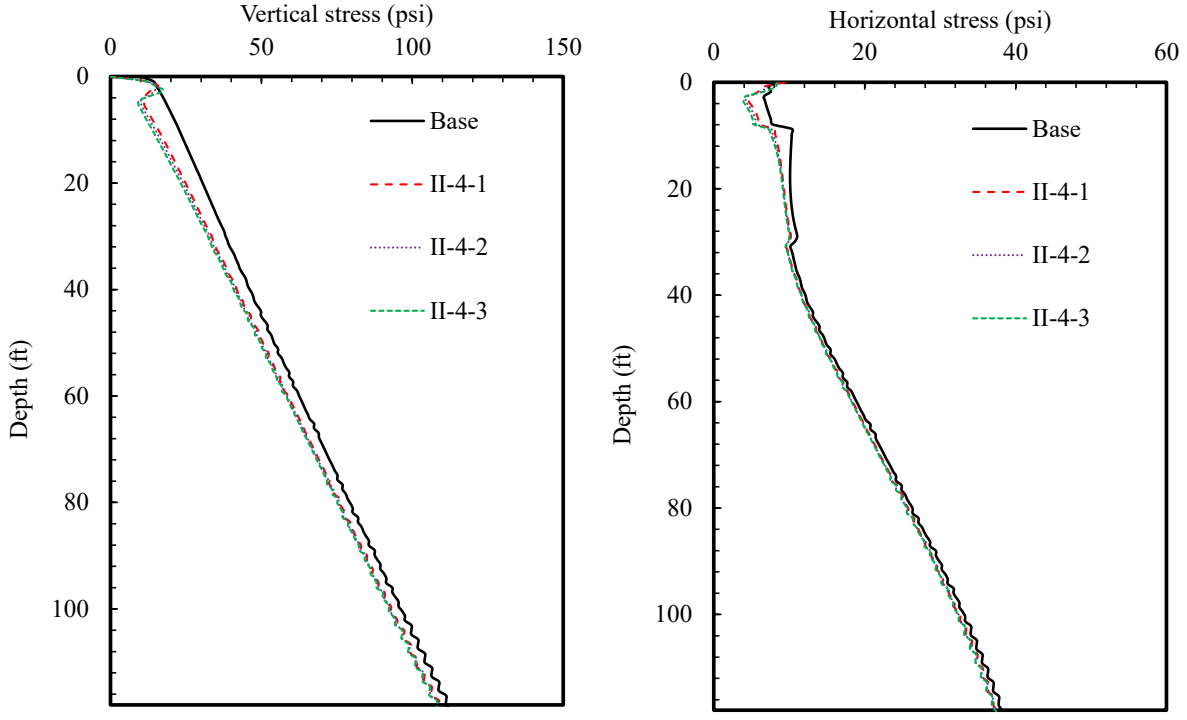

Figure 4.63 The vertical and horizontal stress profiles under the paving section for difference cases of individual geosynthetic reinforcement under the paving section only (II-4-1 to II-4-3).

Figure 4.64 shows the vertical settlement profile across the abutment section with a various number of geosynthetic layers. As expected, applying the individual geosynthetic reinforcement only under the paving section, regardless of the number of geosynthetic layers, has a minor impact on the vertical settlement profiles across the abutment section. Overall, the vertical settlement profiles for all examined cases are acceptable, with the maximum value on the surface being less than a quarter inch.

Figure 4.65 shows the vertical settlement profile across the grade beam section with a various number of geosynthetic layers. The individual geosynthetic reinforcement under the paving section contributes to even reducing the vertical settlement near the grade beam section to some extent. It is partly because that the presence of geosynthetic reinforcement near the end of the paving section helps to distribute the applied load to broader area in the foundation soils.

Lastly, Figure 4.66 shows the vertical settlement profile across the paving section with a various number of geosynthetic layers. Obviously, applying the individual geosynthetic reinforcement under the paving section yields a prominent effect in alleviating the vertical settlement profiles across the paving section. And, more layers of geosynthetic reinforcement results in less settlement across the investigated depth under the paving section. Those simulation results could suggest that placing geosynthetic reinforcement near the end of the paving section could help to greatly alleviate the vertical settlement near the area while the grade beam piles helps to reduce the vertical settlement at the joint between the approach slab and paving sections.

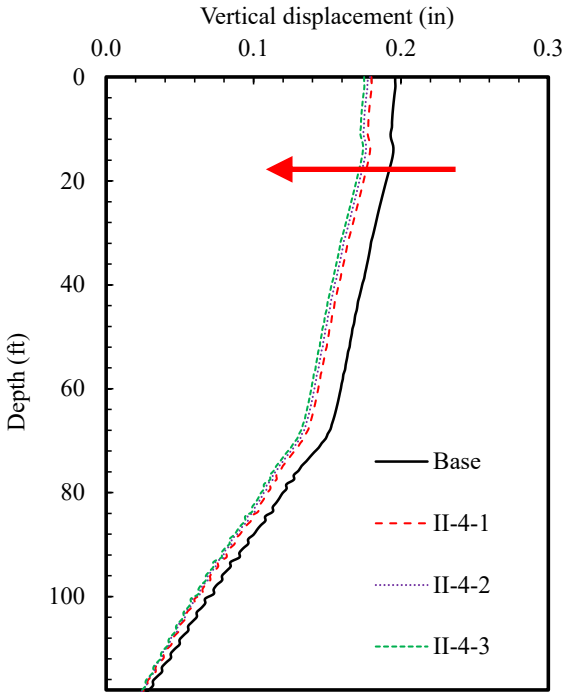

Figure 4.64 The vertical settlement profile across the abutment section for difference cases of individual geosynthetic reinforcement under the paving section only (II-4-1 to II-4-3).

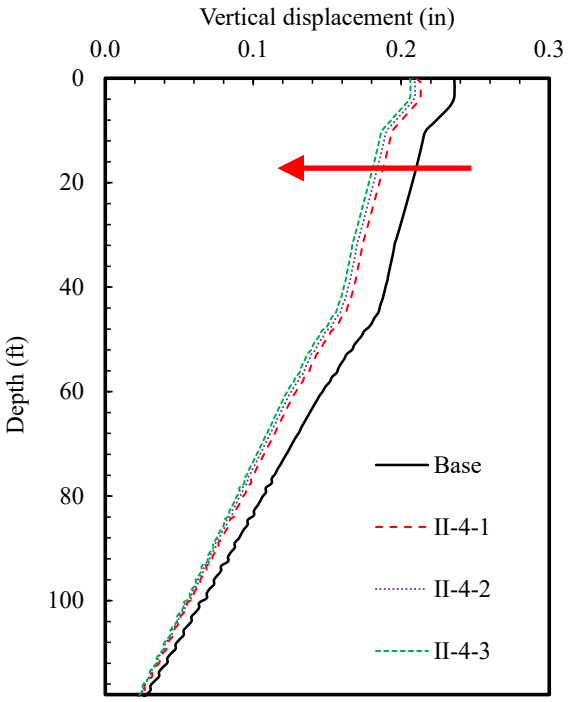

Figure 4.65 The vertical settlement profile across the grade beam section for difference cases of individual geosynthetic reinforcement under the paving section only (II-4-1 to II-4-3).

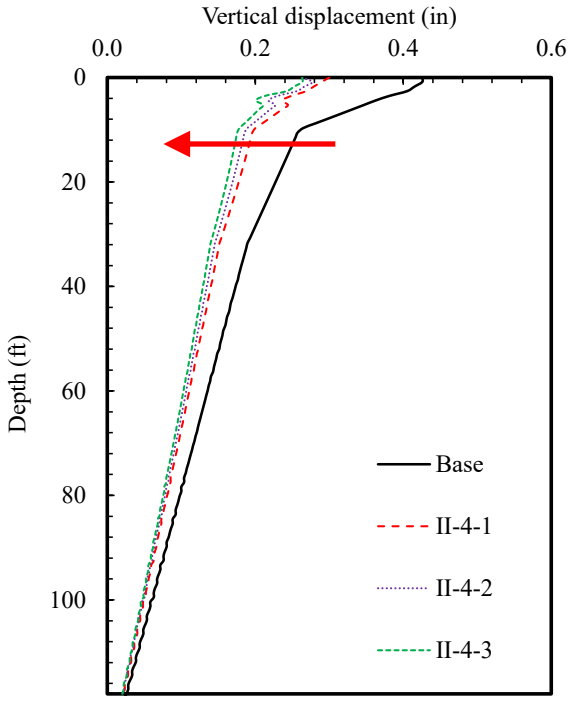

Figure 4.66 The vertical settlement profile across the paving section for difference cases of individual geosynthetic reinforcement under the paving section only (II-4-1 to II-4-3).

Figure 4.67 shows the differential settlement between the abutment and grade beam sections. The differential settlement between the abutment and grade beam sections is slightly reduced (approximately ~25%) compared to the original design (base case) when the individual geosynthetic reinforcement is applied even only under the paving section. Given that the individual geosynthetic reinforcement both near the end of approach slab and paving sections resulted in a minor increase in the differential settlement between the abutment and grade beam sections (i.e., II-1), combining the grade beam piles with the individual geosynthetic reinforcement only under the paving section could be a great option for preventing any undesirable bump issue. Finally, Figure 4.68 shows the differential settlement between the grade beam and paving sections, which is significantly alleviated when the individual geosynthetic reinforcement is applied under the paving section only. At least two layers of reinforcement seems much more effective than the single-layer reinforcement. That is, the differential settlement showed more than 60% of reduction for two or three layers of geosynthetic reinforcement. In this regard, installing the individual geosynthetic layers under the paving

section could be a desirable alternative for repairing existing bridge abutment systems where the grade beam piles were already constructed under the grade beam foundation.

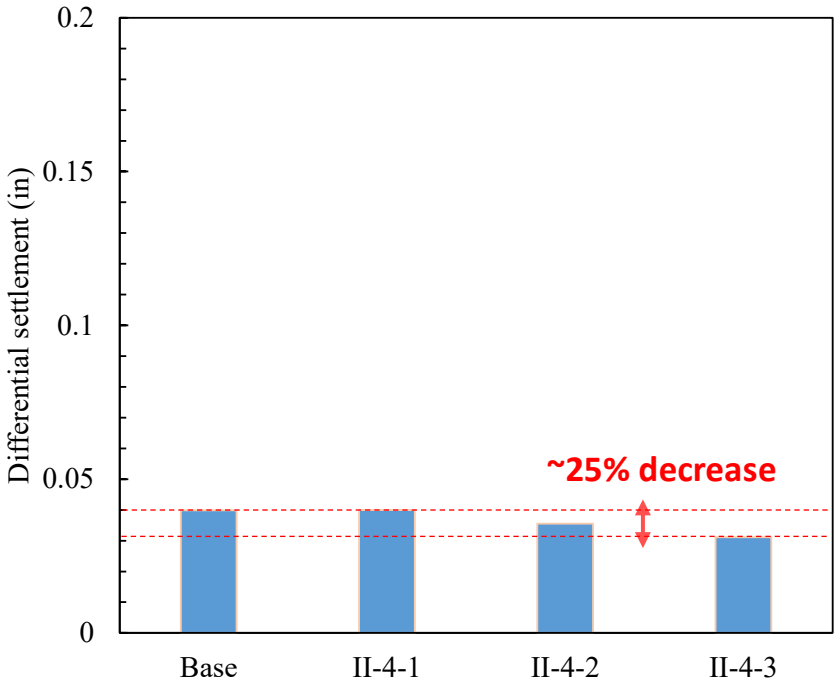

Figure 4.67 Differential settlement between the abutment and grade beam sections for difference cases of individual geosynthetic reinforcement under the paving section only (II-4-1 to II-4-3).

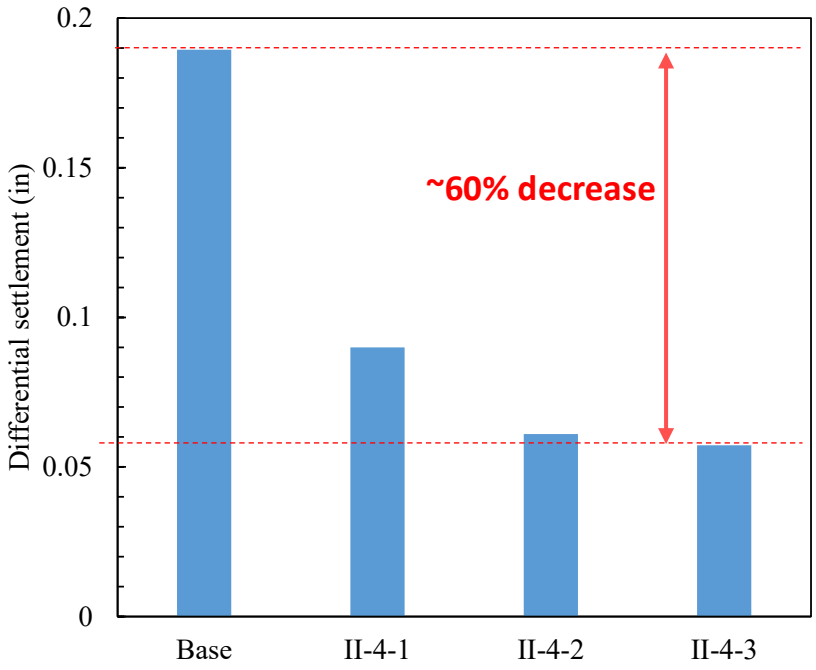

Figure 4.68 Differential settlement between the grade beam and paving sections for difference cases of individual geosynthetic reinforcement under the paving section only (II-4-1 to II-4-3).

5. Discussion and Recommendations

5.1 Cost-effectiveness and constructability analysis

The construction costs between the grade beam pile and geosynthetic reinforcement are compared in this section to analyze the cost-effectiveness and the enhanced performance of the geosynthetic reinforcement as an alternative to the grade beam pile. The unit cost for the installation of the geosynthetic reinforcement, including materials and reasonable transportation, is approximate \$1.0 − 1.5 /ft^2, while those for the grade beam pile installation are \$20 − 60/ft, according to IGS and FHWA's recent report. Note that the unit cost of the grade beam is relatively expensive and uncertain compared to that of the geosynthetic reinforcement. In addition, the constructability of the grade beam pile is highly dependent on the availability of the driving machine and site conditions, which could be regarded as the drawback of the current design practice. If the geosynthetic reinforcement is installed at both the approach slab and paving section, the average area to cover will be about 1,000 ft^2/layer. The numbers of the geosynthetics and grade beam pile are six layers and 22 EA for the studied bridge site, respectively.

Thus, based on the information, the total estimated cost for the geosynthetic reinforcement is ranged between \$6,000 - \$9,000 for the grade beam section alone, and \$12,000 − \$18,000 for both grade beam and paving sections, respectively. Those estimated costs are approximately three to nine times more cost-effective compared to the case of grade beam pile installation. Therefore, geosynthetic reinforcement could be a more cost-effective and economical method compared to the current design practice. Note that those results can be changed depending on the contractor's availability and site conditions.

Table 5.1 Comparison of the estimated cost between the geosynthetic reinforcement and grade beam pile installation.

	Geosynthetic reinforcement (Christopher 2014)	Grade beam pile (FHWA 2016)
Unit cost	\$1.0 − 1.5/ft^2	\$20 − 60/ft
Average amount	1,000 ft^2/layer	40 − 60 ft/EA
Number (for the studied site)	6 layers (12 layers for both grade beam and paving sections)	22 EA
Estimated cost	\$ 6,000 − \$9,000 (\$12,000 − \$18,000)	\$17,600 − \$79,200

5.2 Replacement of granular backfill soils under the paving section

Replacing granular backfill soils under the paving section with in-situ foundation soils could help improve the constructability of a project. In this regard, four representative cases from Study I and II are selected to investigate its influence on the differential settlements as follows:

- Base case (number of grade beam piles = number of abutment piles): Base-1
- The spacing of grade beam piles is widened by 250% of the base case (Study I): I-1-3-1
- Individual geosynthetic reinforcement at three layers (Study II): II-1-3-1
- Grade bean piles + individual geosynthetic reinforcement at three layers under the paving section only (Study II): II-4-3-1

First, the team investigated an alternative case where the granular backfill soils are replaced with in-situ foundation soils for the base case (Base-1; Figure 5.1). Peoria loess is used as the in-situ foundation soil in this analysis. Such a replacement results in a slight increase in the differential settlements between the abutment and grade beam sections (Figure 5.2) and between the grade beam and paving sections (Figure 5.3). Nonetheless, such an increase is less than 0.05 inches, and thus it is not expected to compromise the mechanical performance of the entire backfill area. In addition to the base case, one of the recommendations for the current design modification (I-1-3), in which the spacing of grade beam piles is increased by 250% of the base case, is investigated (I-1-3-1). Similarly, such a replacement of granular backfill soils yields a negligible increase in the differential settlement (less than 0.03 inch) both between the abutment and grade beam sections (Figure 5.4) and between the grade beam and paving sections (Figure 5.5).

On the other hand, an additional measure needs to be in place to help the drainage of infiltrated water for such a replacement. To address this issue, a drainage pipe can be installed next to the grade beam (on the paving section side) to aid the drainage. A conceptual drawing for this count measure is provided in the following section.

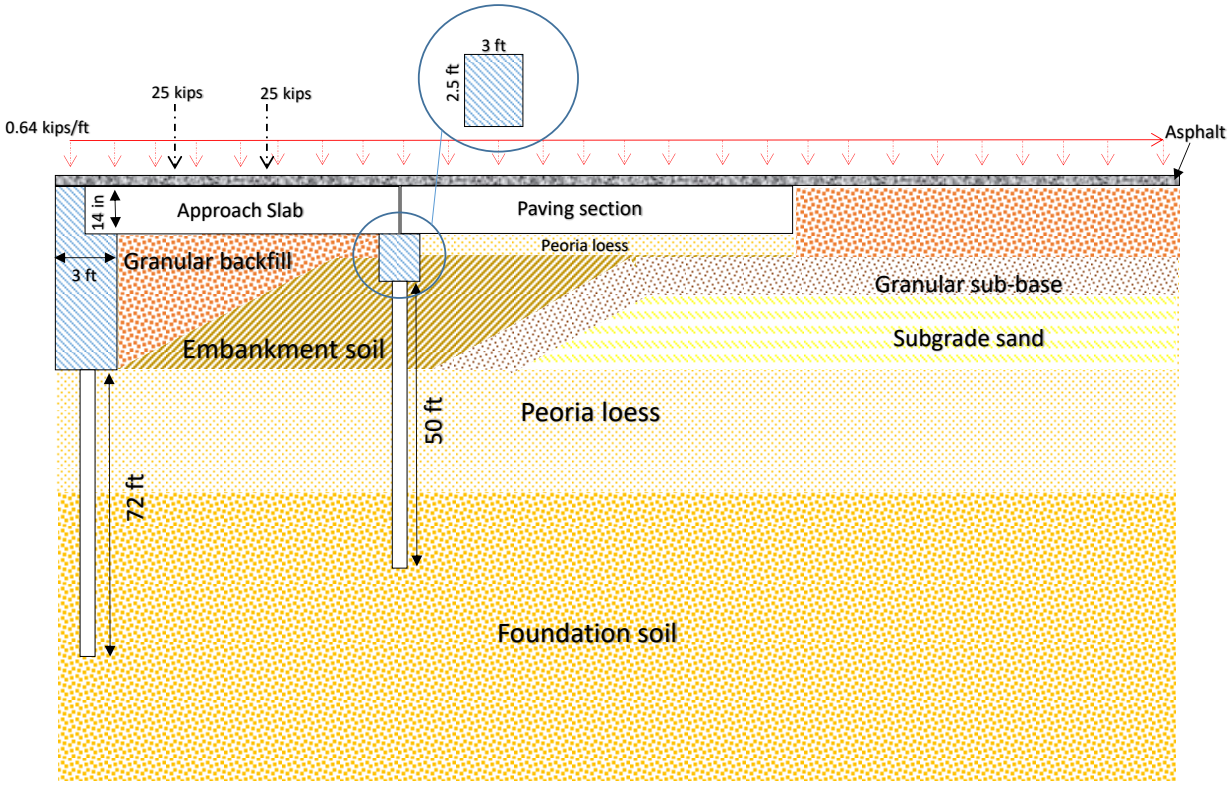

Figure 5.1 The numerical simulation model (Base-1) in which the granular backfill soils under the paving section are replaced with the in-situ foundation soils (Peoria loess in this case) for the base case.

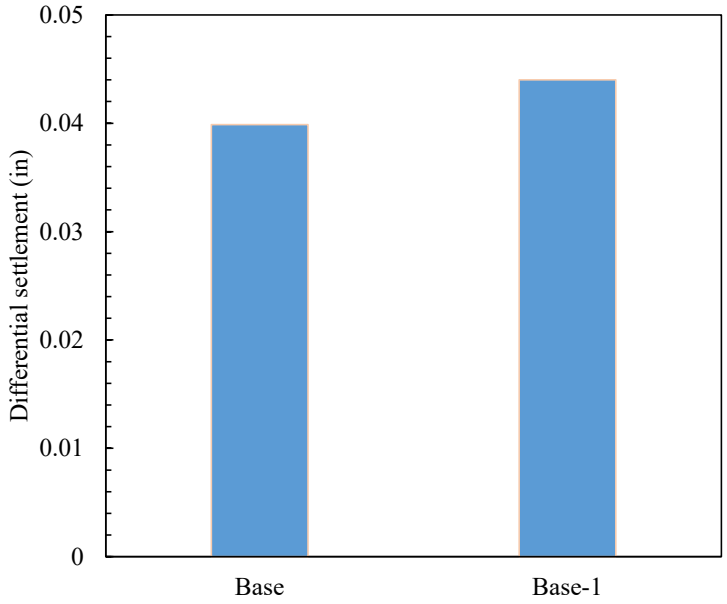

Figure 5.2 A comparison of differential settlement between the abutment and grade beam sections for the base case and base case + replacement of granular backfill soils (Base-1).

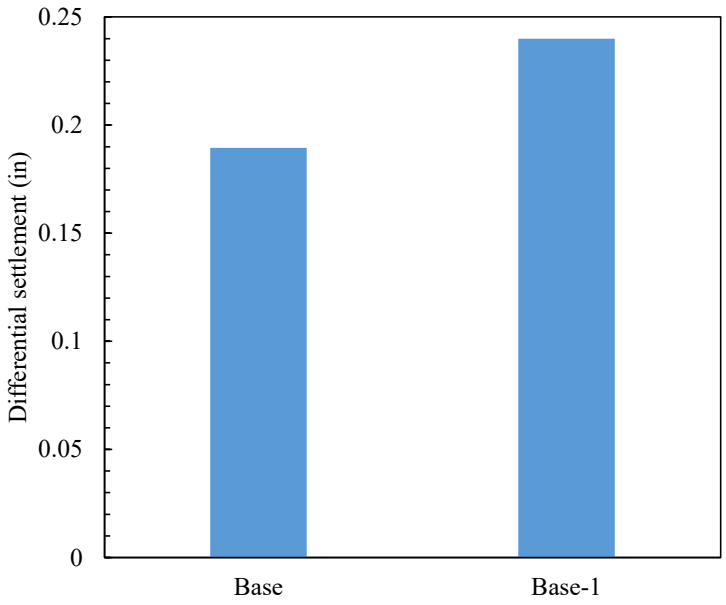

Figure 5.3 A comparison of differential settlement between the grade beam and paving sections for the base case and base case + replacement of granular backfill soils (Base-1).

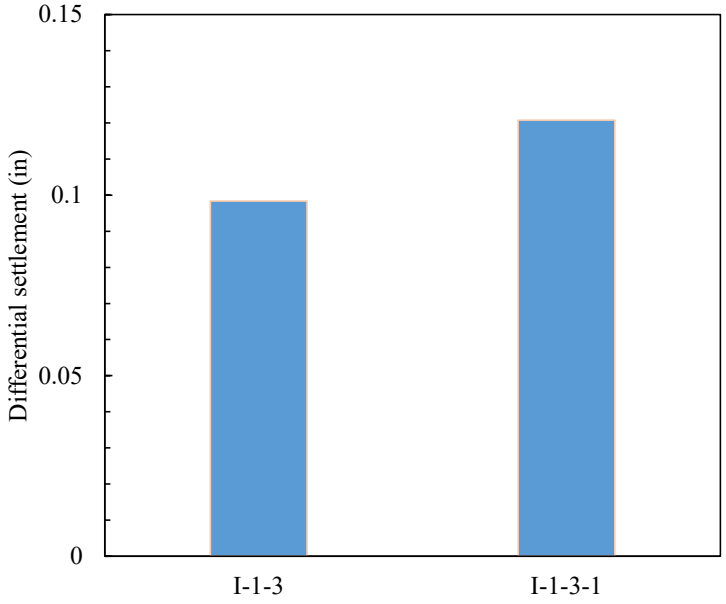

Figure 5.4 A comparison of differential settlement between the abutment and grade beam sections for case I-1-3 and I-1-3 with the replacement of granular backfill soils (I-1-3-1).

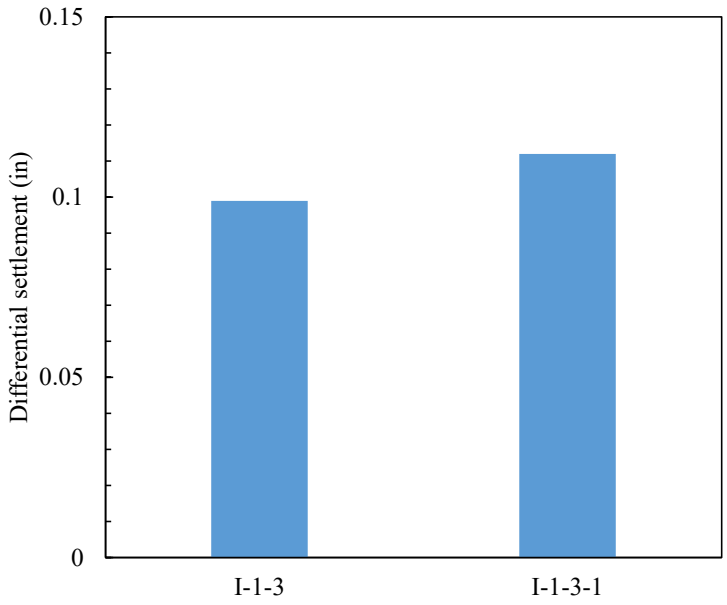

Figure 5.5 A comparison of differential settlement between the grade beam and paving sections for case I-1-3 and I-1-3 with the replacement of granular backfill soils (I-1-3-1).

Next, the case where individual geosynthetic reinforcement at three layers is used instead of grade beam piles is investigated (II-1-3-1; Figure 5.6). Again, replacing the granular backfill soils with in-situ foundation soils yields a negligible increase in the differential settlement (less than 0.02 inch) both between the abutment and grade beam sections (Figure 5.7) and between the grade beam and paving sections (Figure 5.8). Lastly, the case in which individual geosynthetic reinforcement at three layers is only applied near the end of the paving section while grade beam piles are in place is investigated (II-4-3-1; Figure 5.9). Again, an increase in the differential settlement is less than 0.02 inches (Figures 5.10 and 5.11). Therefore, it could be suggested that replacing the granular backfill soils under the paving section with in-situ foundation soils may not influence the differential settlements between the abutment, grade beam, and paving sections for both suggested modifications of current design and a new design with the geosynthetic reinforcement.

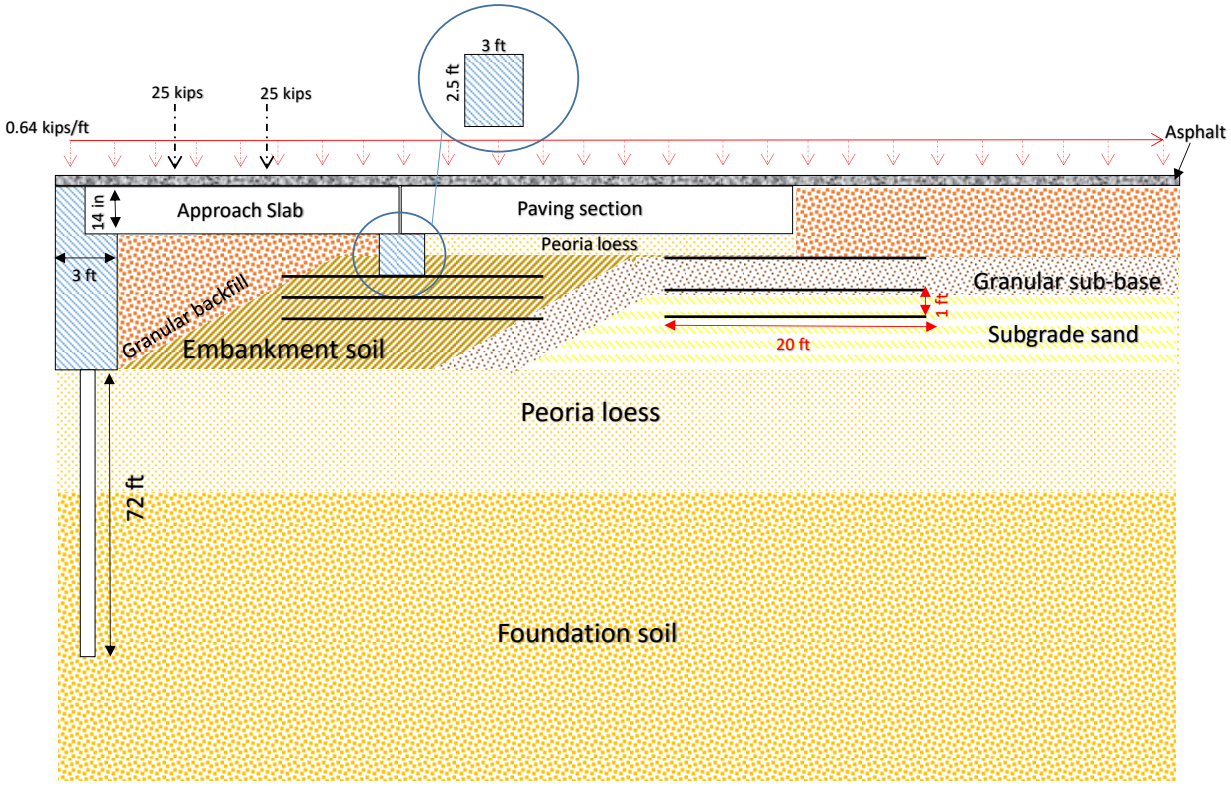

Figure 5.6 The numerical simulation model (II-1-3-1) in which the granular backfill soils under the paving section are replaced with the in-situ foundation soils (Peoria loess in this case) for the case of individual geosynthetic reinforcement with three layers (II-1-3).

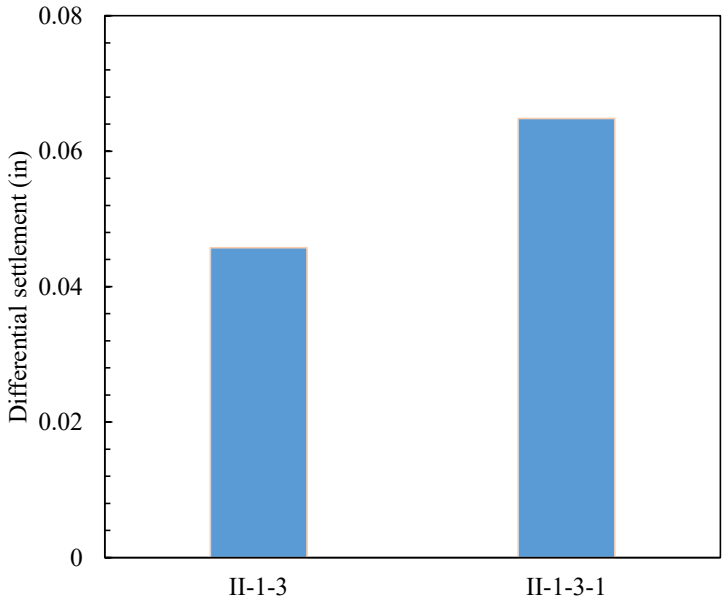

Figure 5.7 A comparison of differential settlement between the abutment and grade beam sections for case II-1-3 and II-1-3 with the replacement of granular backfill soils (II-1-3-1).

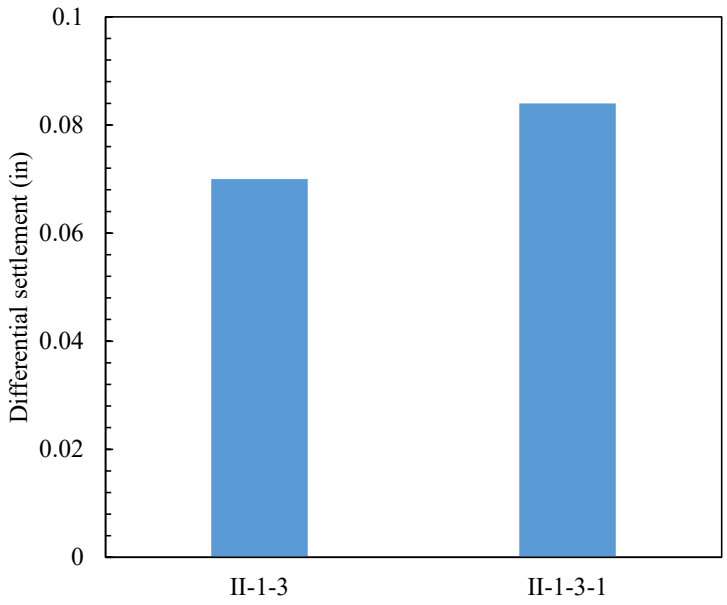

Figure 5.8 A comparison of differential settlement between the grade beam and paving sections for case II-1-3 and II-1-3 with the replacement of granular backfill soils (II-1-3-1).

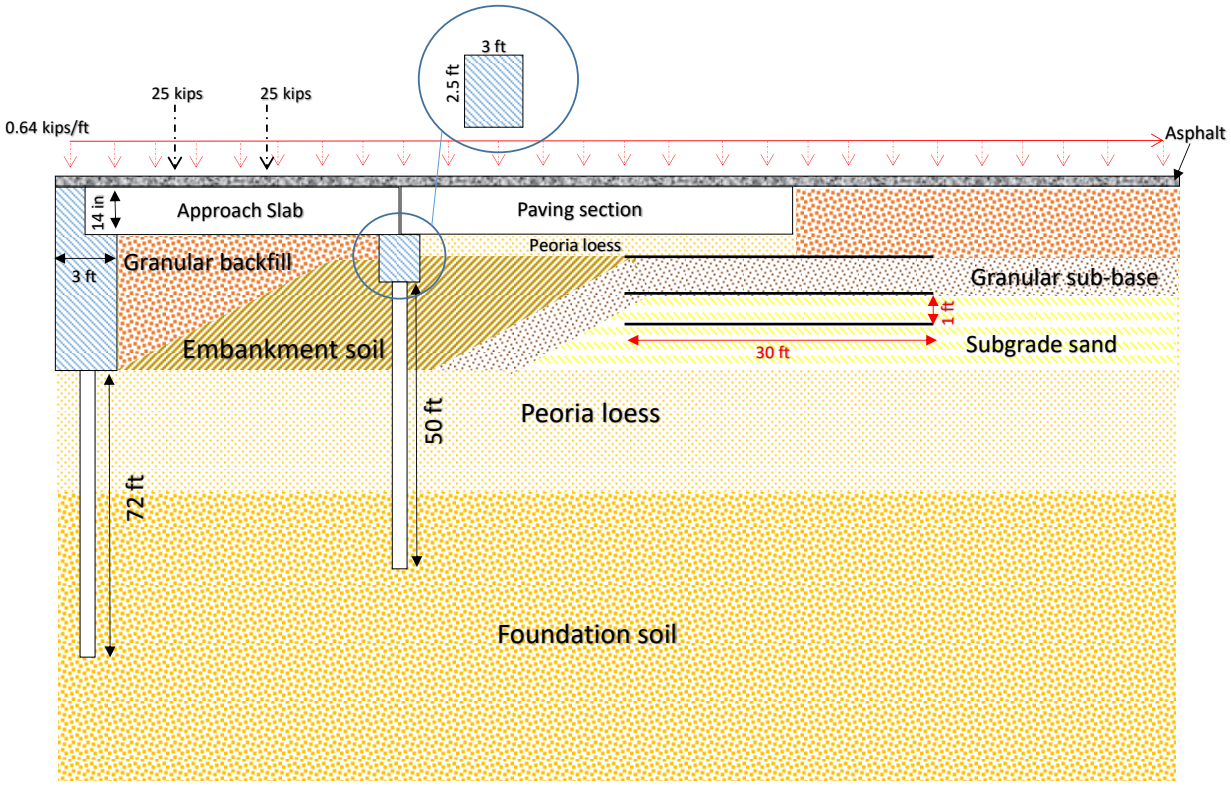

Figure 5.9 The numerical simulation model (II-4-3-1) in which the granular backfill soils under the paving section are replaced with the in-situ foundation soils (Peoria loess in this case) for the case of grade beam piles + individual geosynthetic reinforcement with three layers only under the paving section (II-4-3-1).

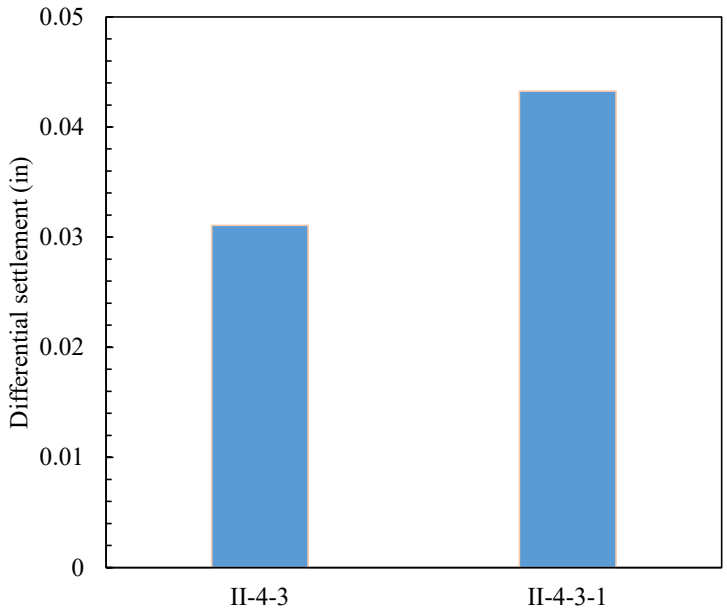

Figure 5.10 A comparison of differential settlement between the abutment and grade beam sections for case II-4-3 and II-4-3 with the replacement of granular backfill soils (II-4-3-1).

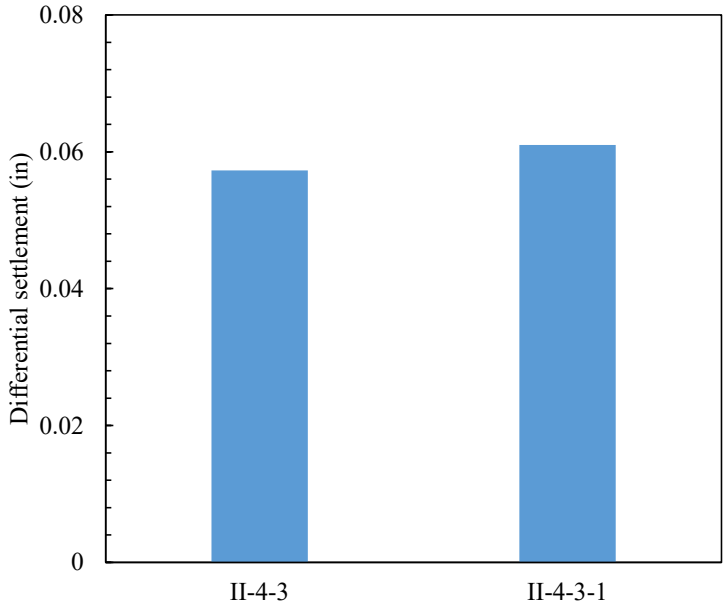

Figure 5.11 A comparison of differential settlement between the grade beam and paving sections for case II-4-3 and II-4-3 with the replacement of granular backfill soils (II-4-3-1).

5.3 Consideration of horizontal movement at the abutment.

It is acceptable to assume that the horizontal displacement at the abutment would be negligible for a traditional bridge structure. In this regard, the roller boundary condition was imposed on the side boundary of the simulation model in this study not to allow any horizontal displacement but a vertical one. On the other hand, there is also a substantial portion of integral abutment bridges in Nebraska in which the abutment may move laterally due to the thermal expansion and contraction of the superstructure. The team conducted an additional set of numerical simulations to examine the effect of such a lateral movement of the abutment on the differential settlements. The magnitude of thermally induced deformation at the abutment, ΔL^{T}, is estimated based on the simple thermal expansion theory as follows:

$$\Delta L^{T} = \alpha_{L} \times \Delta T \times L$$

where α_{L} is the linear coefficient of thermal expansion, ΔT is change in temperature, and L is the length of the superstructure (128.5 ft or 39 m for the bridge in this study). The team considers a cyclic temperature fluctuation of 104 °F (40 °C), and adopts a general value for concrete superstructure $\alpha_{L} = 9\times10^{-6}$/°C (Won, 2005). Then the thermally induced deformation at the top of the abutment could be calculated as follows:

$$\Delta L^{T} = 39\ m \times \left(\frac{9 \times 10^{-6}}{\text{℃}}\right) \times 40\text{℃} = 0.014m = 0.55\ in$$

For comparison, such seasonal temperature fluctuation-induced deformations were presented to be around 1/2 inches (concrete bridges) and 3/4 inches (steel bridge) for a 100 ft span bridge (Berks 1968, as cited in Rynolds 1972). Thus, the calculated horizontal movement of 0.55 inches is in good agreement. Upon it, 4 additional numerical models were considered as follows:

- Base case (number of grade beam piles = number of abutment piles): Base-R (where the abutment moves toward the soil; passive condition).
- Base case (number of grade beam piles = number of abutment piles): Base-L (where the abutment moves away from the soil; active condition).
- Grade beam piles + individual geosynthetic reinforcement at three layers under the paving section only (Study II) + passive condition: II-4-3-R

- Grade beam piles + individual geosynthetic reinforcement at three layers under the paving section only (Study II) + active condition: II-4-3-L

First, the team examined the Base-R case in which the horizontal movement of 0.55 inches is imposed at the top of the abutment towards the backfill soil (Figure 5.12). A slight increase (less than 0.01 inch) in the differential settlement between the abutment and grade beam section is observed as a result of the lateral movement of the abutment in the passive direction (Figure 5.13). On the other hand, such a differential settlement is slightly decreased between the grade beam and paving sections (around 0.02 inch; Figure 5.14).

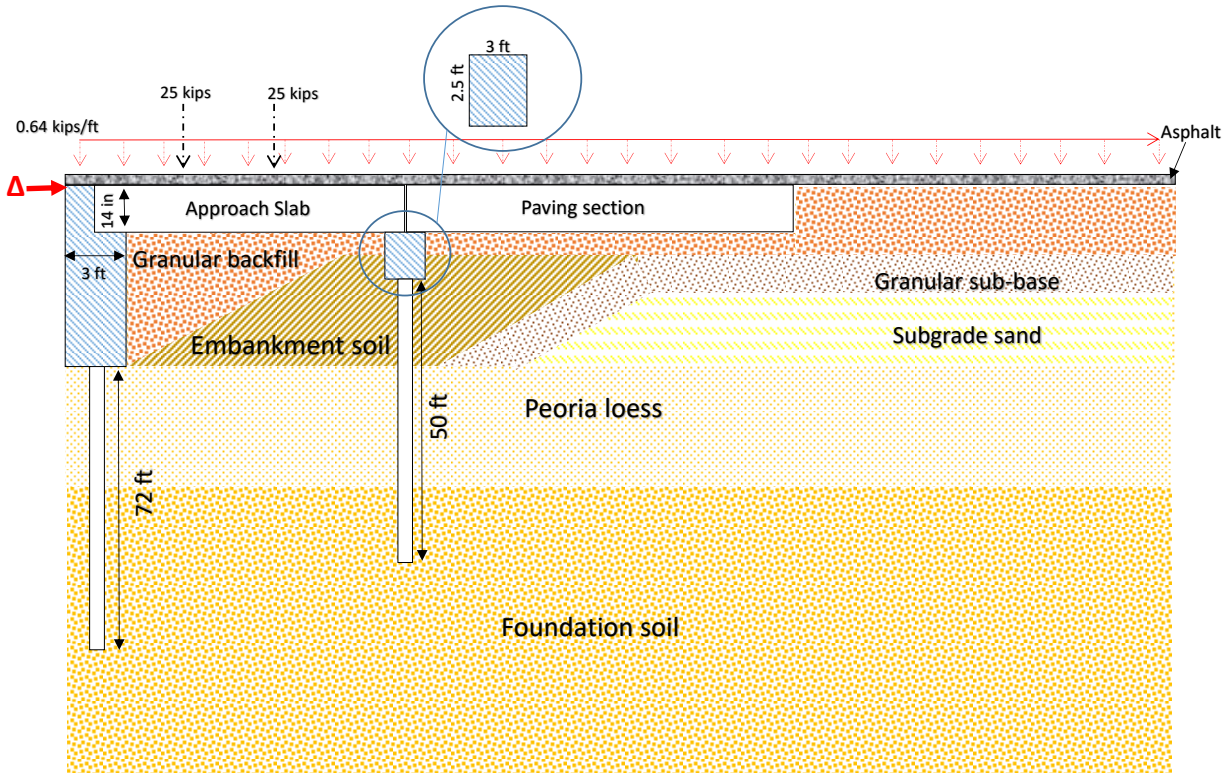

Figure 5.12 The numerical simulation model (Base-R) in which the lateral movement of $\Delta = 0.55$ in. is imposed at the top of the abutment toward the backfill soil (passive).

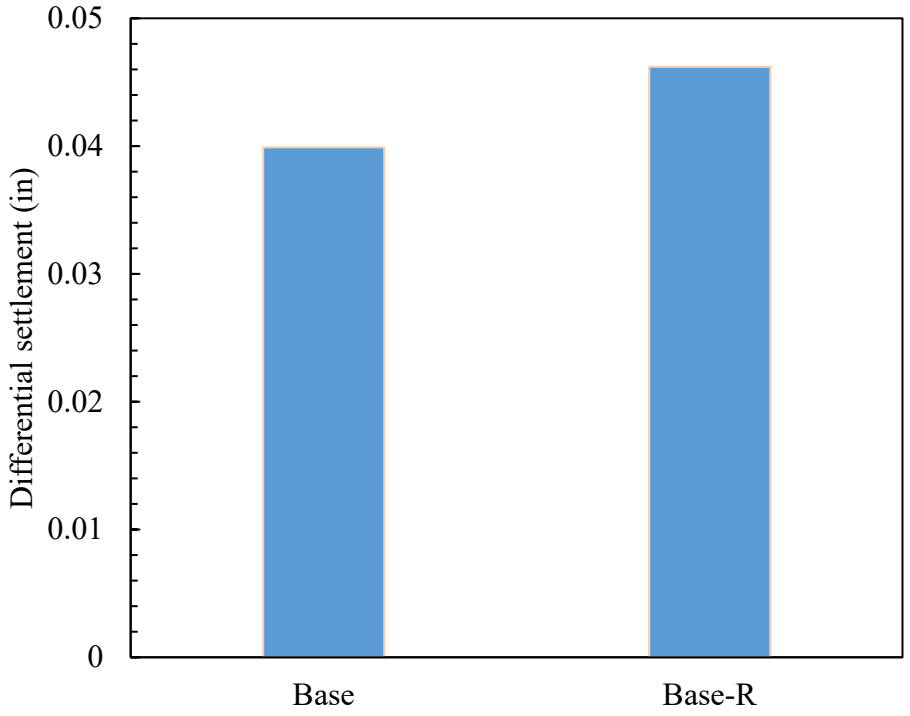

Figure 5.13 A comparison of differential settlement between the abutment and grade beam sections for the base case and base case with lateral movement at abutment (Base-R).

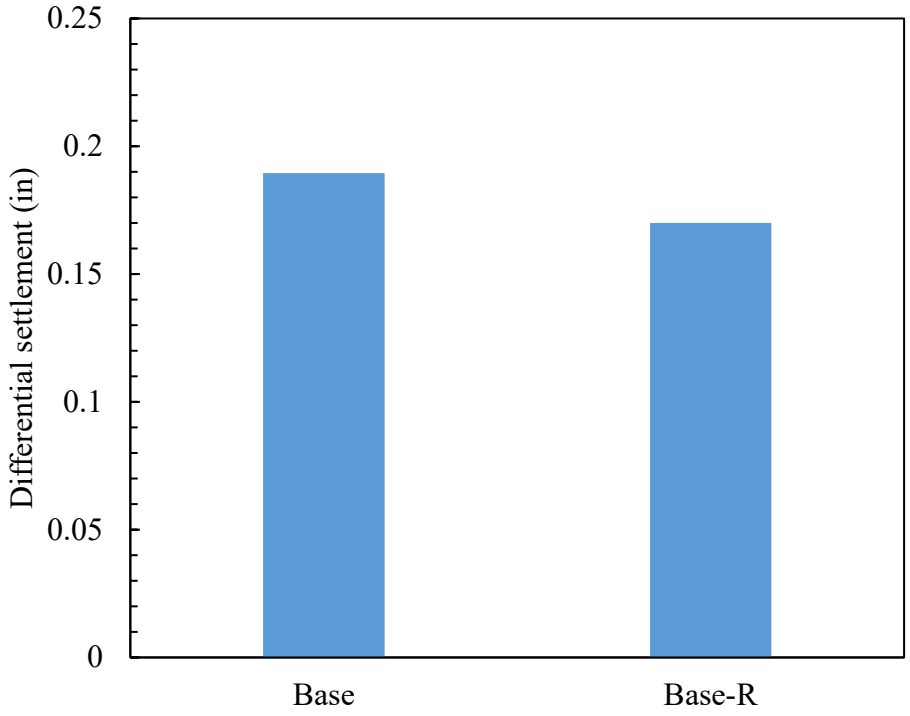

Figure 5.14 A comparison of differential settlement between the grade beam and paving sections for the base case and base case with lateral movement at abutment (Base-R).

Next, the team examined the Base-L case in which the horizontal movement of 0.55 inches is imposed at the top of the abutment to the direction away from the backfill soil (Figure 5.15). Opposite to the Base-R case, a slight decrease and increase in the differential settlement between the abutment and grade beam sections and the grade beam and paving sections, respectively, are observed as a result of the lateral movement of the abutment in the active direction (Figures 5.16 and 5.17). Nonetheless, those changes in the differential settlement are trivial (less than 0.035 inches). Therefore, a similar magnitude of differential settlements could be expected for both traditional and integral abutment bridges with the current design practice.

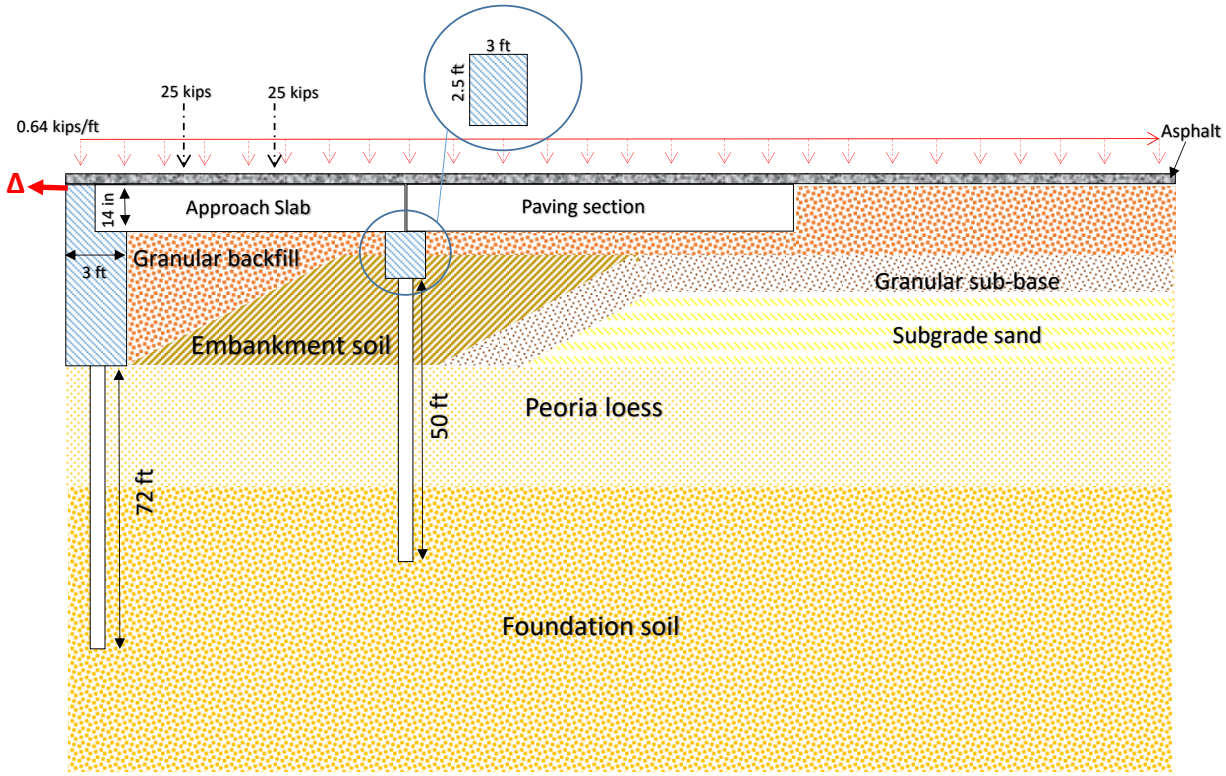

Figure 5.15 The numerical simulation model (Base-L) in which the lateral movement of $\Delta = 0.55$ in. is imposed at the top of the abutment away from the backfill soil (active).

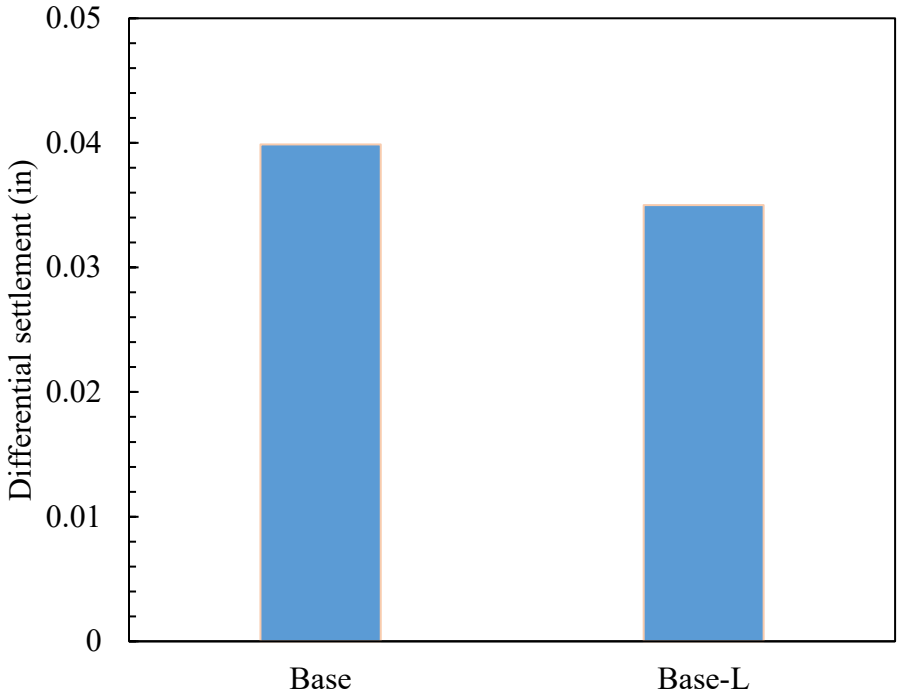

Figure 5.16 A comparison of differential settlement between the abutment and grade beam sections for the base case and base case with lateral movement at abutment (Base-L).

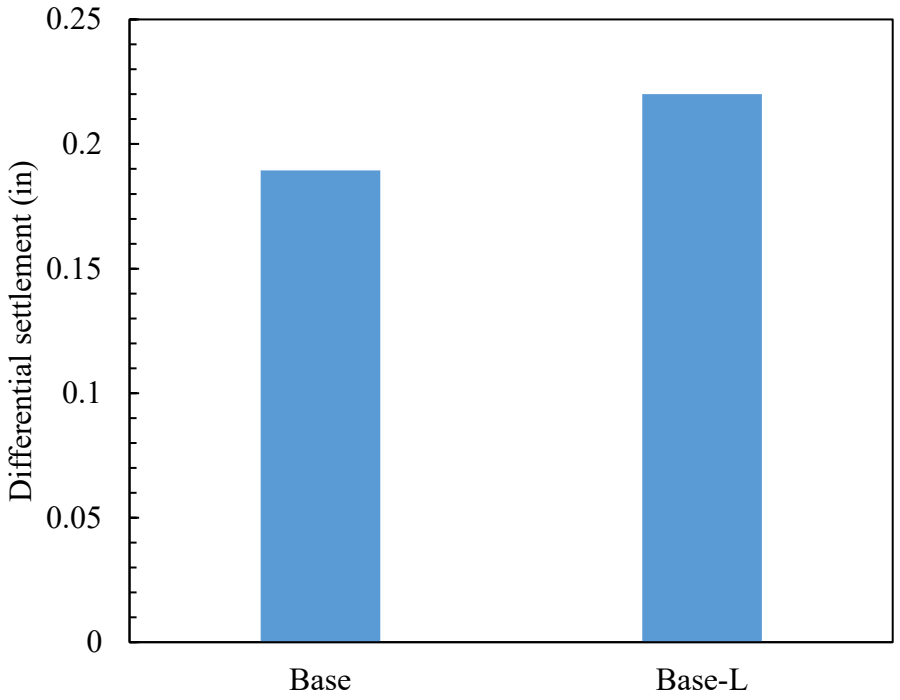

Figure 5.17 A comparison of differential settlement between the grade beam and paving sections for the base case and base case with lateral movement at abutment (Base-L).

In a similar way, the team examines the case in which individual geosynthetic reinforcement at three layers is applied only near the end of the paving section while grade beam piles are in place. Both the lateral movement of the abutment in the passive direction (II-4-3-R; Figure 5.18) and active direction (II-4-3-L; Figure 5.21) are investigated. Again, slight changes in the differential settlement are observed in the same trend as those of Base-R and Base-L. Thus, we can also expect a similar magnitude of differential settlements for both traditional and integral abutment bridges with the suggested design practice with the geosynthetic reinforcement. Note that the cyclic effect of repetitive temperature fluctuations is not considered in the numerical simulation of this study, which may amplify the vertical settlements.

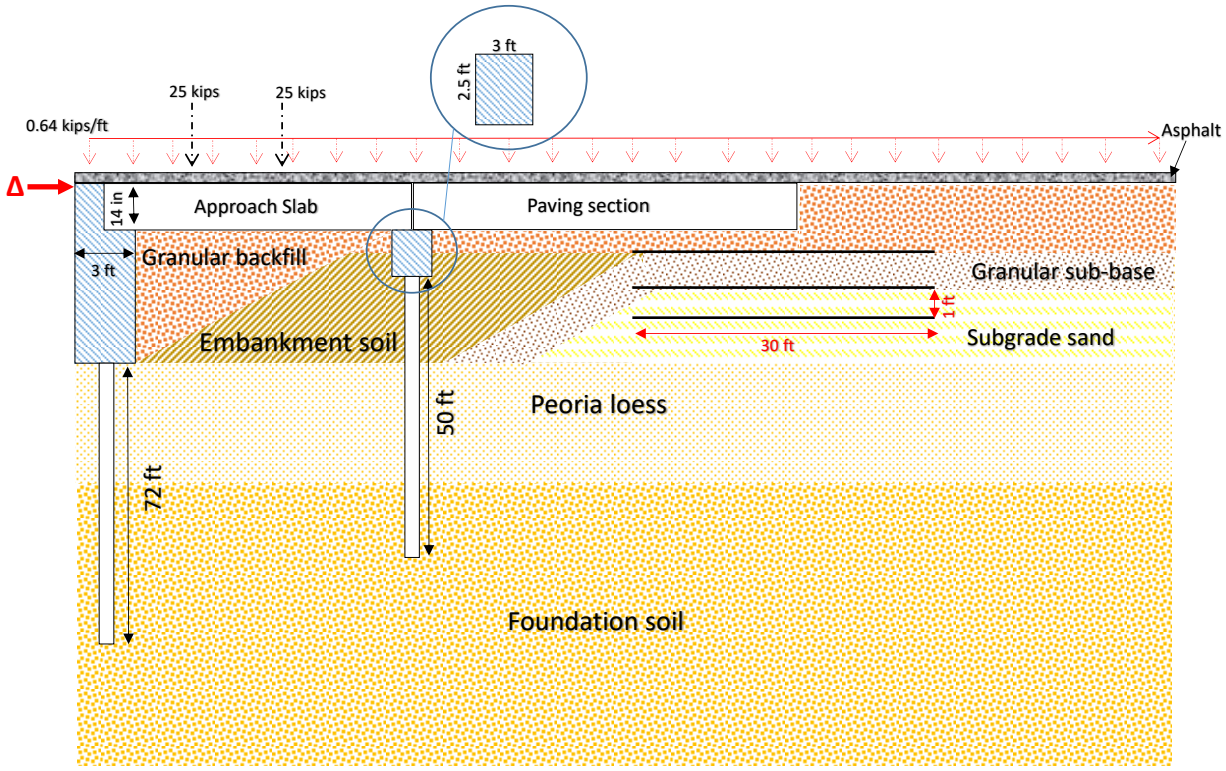

Figure 5.18 The numerical simulation model (II-4-3-R) in which the lateral movement of $\Delta = 0.55$ in. is imposed at the top of the abutment toward the backfill soil (passive).

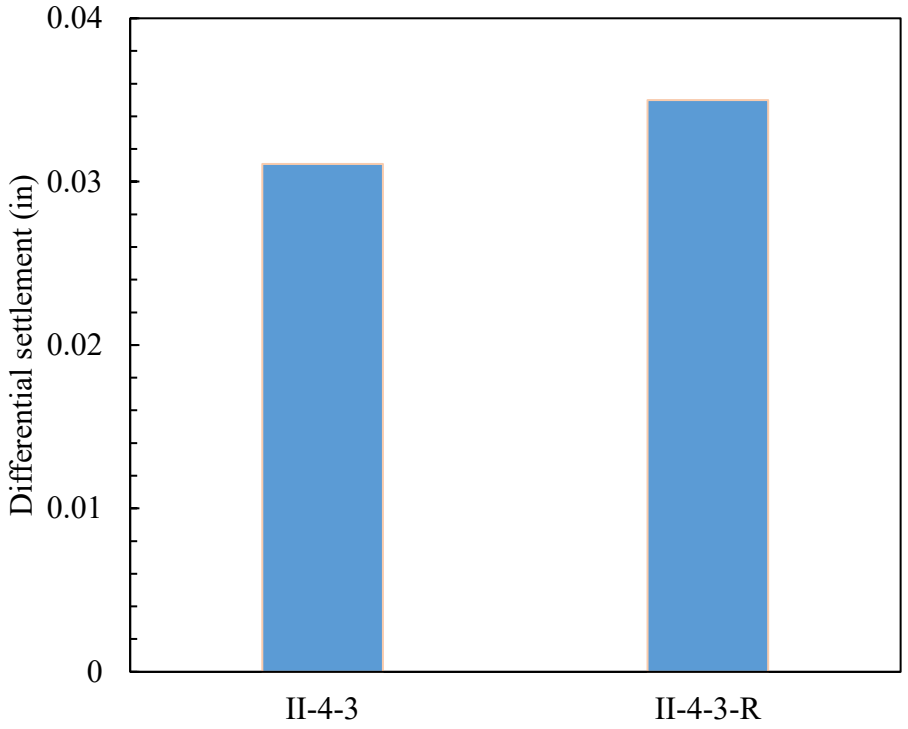

Figure 5.19 A comparison of differential settlement between the abutment and grade beam sections for II-4-3 and II-4-3-R (lateral movement at abutment toward the backfill soil).

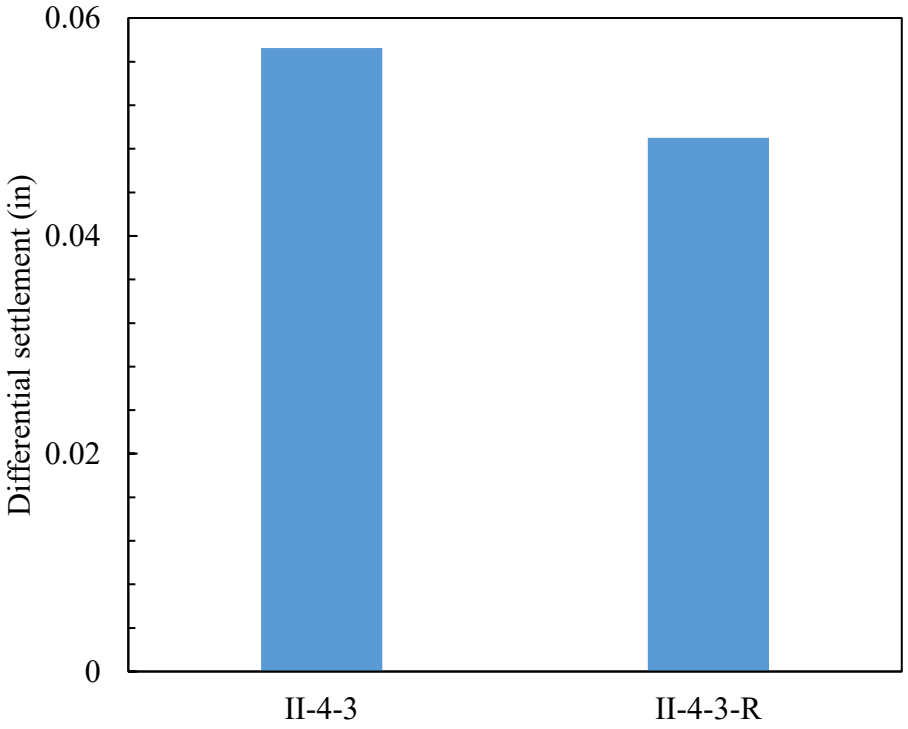

Figure 5.20 A comparison of differential settlement between the grade beam and paving sections for II-4-3 and II-4-3-R (lateral movement at abutment toward the backfill soil).

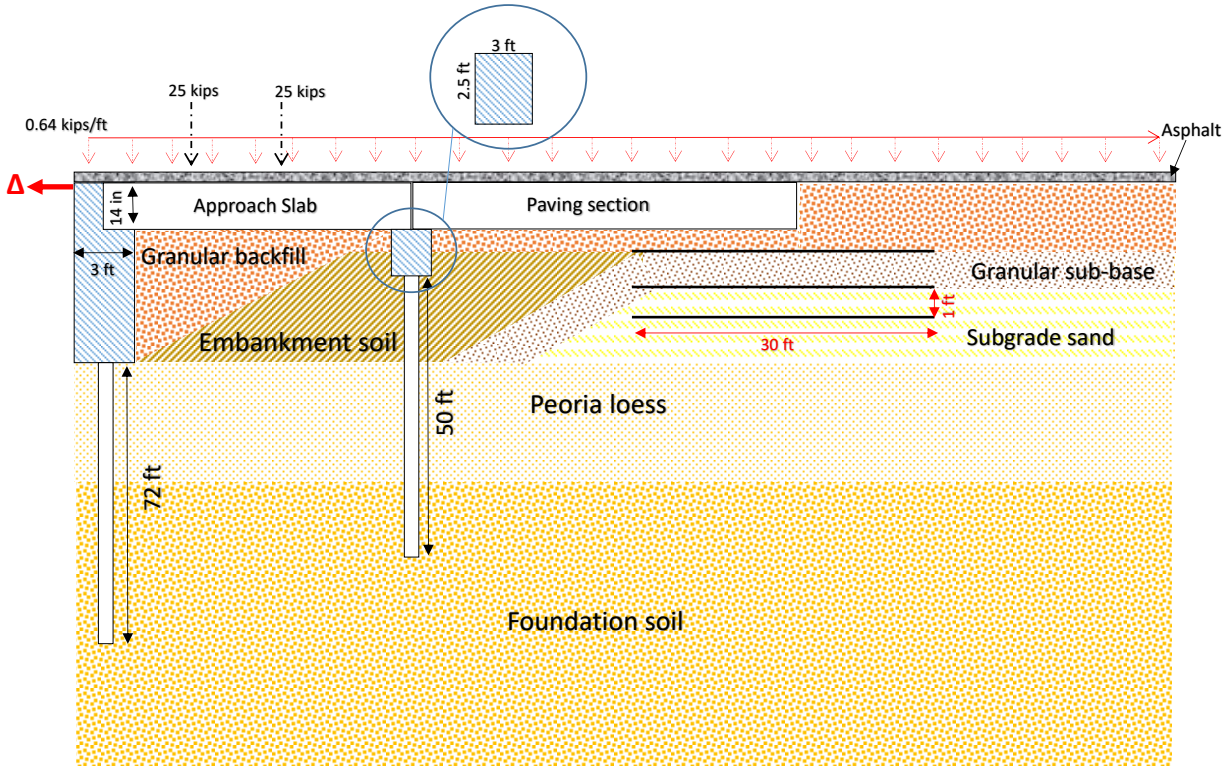

Figure 5.21 The numerical simulation model (II-4-3-L) in which the lateral movement of Δ = 0.55 in. is imposed at the top of the abutment away from the backfill soil (active).

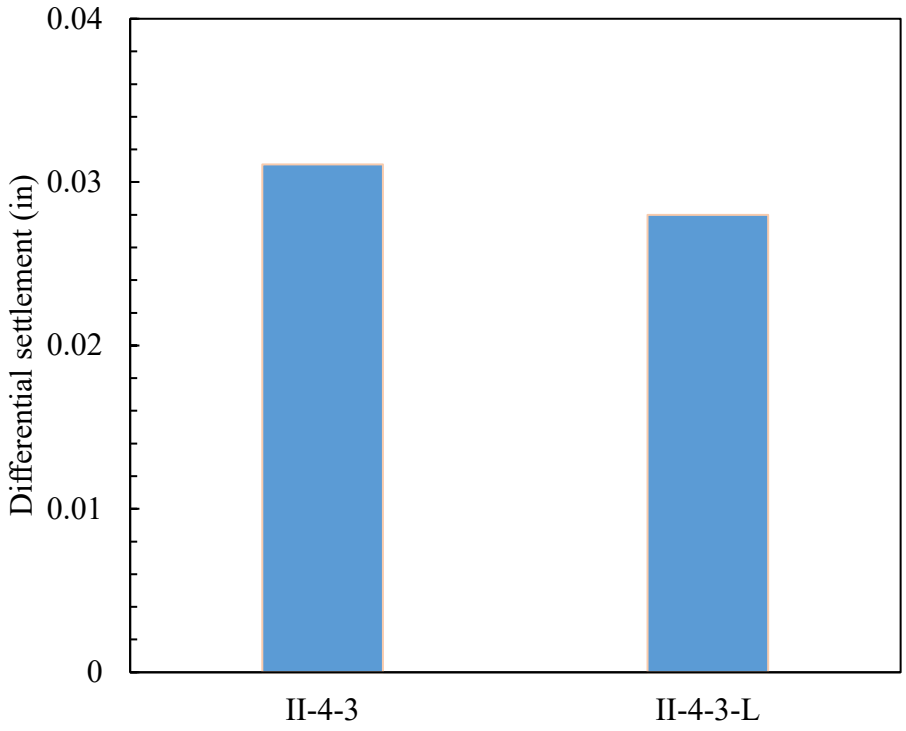

Figure 5.22 A comparison of differential settlement between the abutment and grade beam sections for II-4-3 and II-4-3-L (lateral movement at abutment away from the backfill soil).

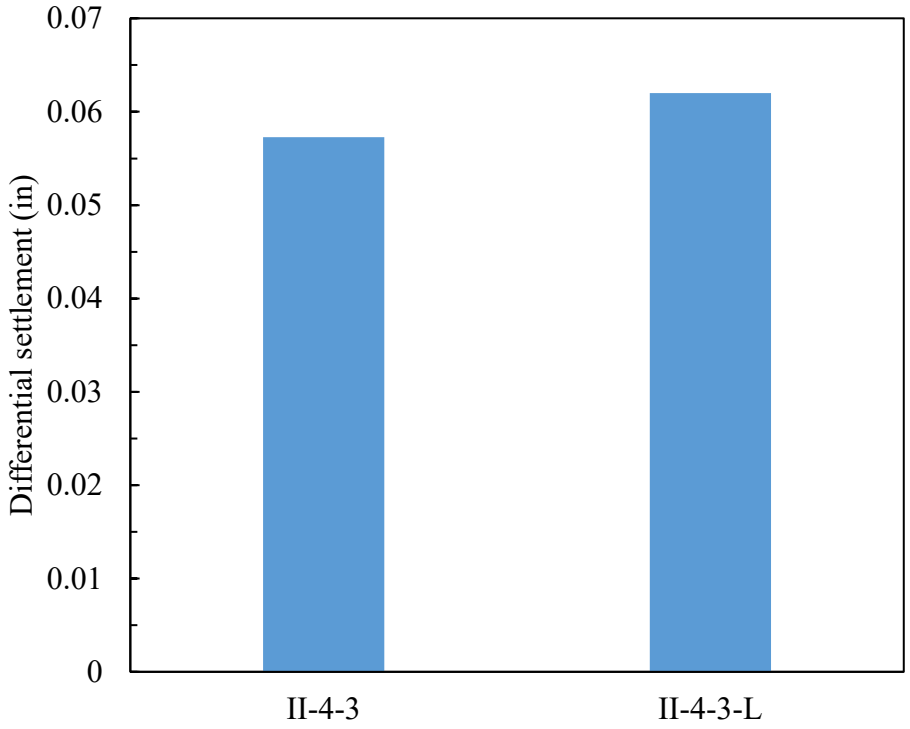

Figure 5.23 A comparison of differential settlement between the grade beam and paving sections for II-4-3 and II-4-3-L (lateral movement at abutment away from the backfill soil).

5.4 Recommendations for the design modification

Based on the study results, the team suggests conceptual drawings for the following two design modifications: (1) grade beam piles (current design practice) + placement of individual geosynthetic reinforcements only under the end of the paving section, and (2) placement of individual geosynthetic reinforcements both at the end of the approach slab (instead of the grade beam piles) and paving sections. Besides, replacement of the granular fill soils with in-situ foundations soils under the paving section is considered in those conceptual drawings, with an addition of the drainage pipe. The team also adopts the placement of a polyethylene sheet between the approach slab and backfill soils that had been suggested to alleviate cracks on the approach slab by another concurrent NDOT project.

(1) Grade beam piles + individual geosynthetic reinforcement only under the paving section

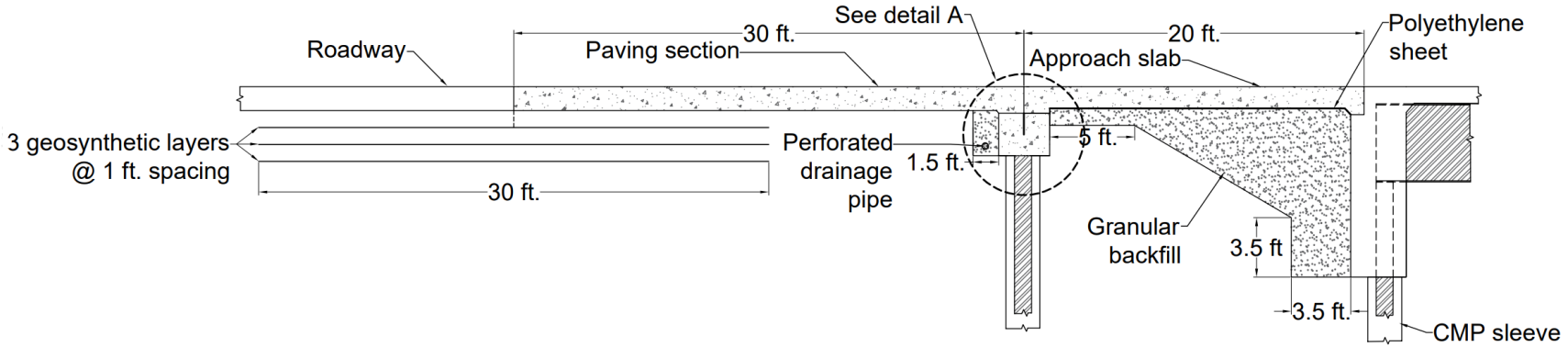

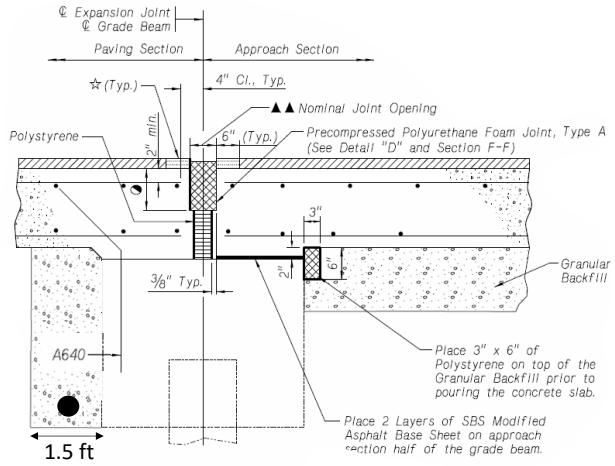

Detail A

Figure 5.24 Conceptual drawing for the design modification (1): grade beam piles + individual geosynthetic reinforcement only under the paving section (Case II-4-3) - cross section.

(2) Individual geosynthetic reinforcement both at the end of the approach slab and paving sections

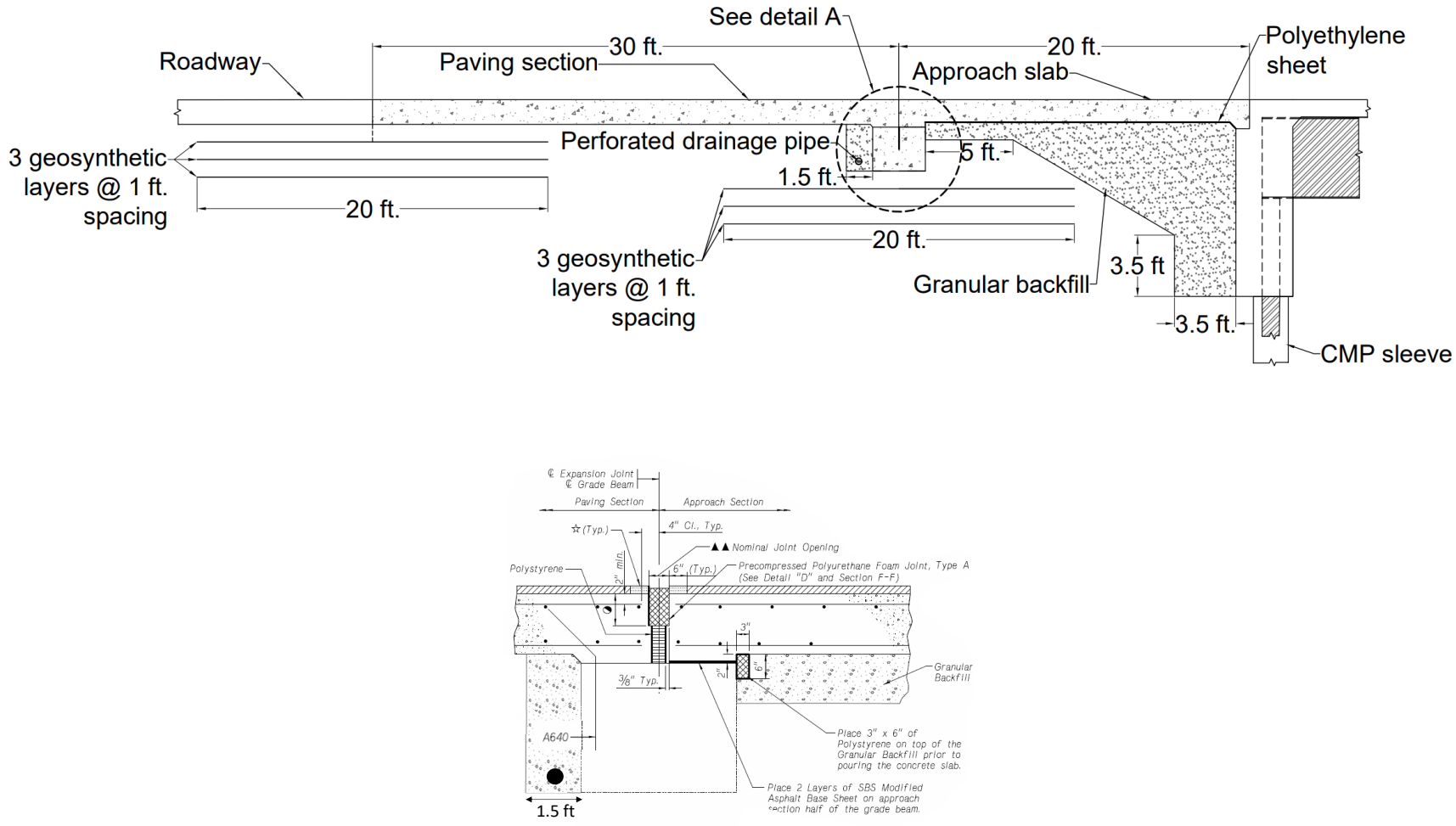

Detail A

Figure 5.25 Conceptual drawing for the design modification (2): individual geosynthetic reinforcement both at the end of the approach slab and paving sections (Case II-1-3) - cross section.

Note for approach slabs and sections

1. Build grade beam without a pile to the full width of the approach slab
2. Three layers of geogrid reinforcement under the grade beam and paving sections are required in a new fill or existing subgrade section.
3. Geosynthetic reinforcement shall consist of a biaxial or triaxial geogrid.
4. Layers of geosynthetic reinforcement (i.e., geogrid) shall either overlap or be sewn to an adjacent roll.
5. Place the geogrid longitudinally in the direction of traffic along the ground without any wrinkles or folds. The geogrid may be cut to conform to curves along the roadway if need be. Damaged geogrid should not be used, or, if salvageable, the damaged area must be covered an additional 24-36 inches in all directions.
6. Do not operate any construction equipment atop the bare geogrid.
7. Four mils-polyethylene sheets shall be installed beneath the approach slab.
8. Before the installation of geosynthetics, the rolls shall be elevated off the ground and stored in a waterproof cover to protect against ultraviolet radiation. The ground should be relatively undisturbed. Rolls shall be covered with a suitable wrapping and stored to protect against moisture and natural elements, such as dirt, mud, or debris.
9. Furnish a certificate of compliance and test data from an approved laboratory that shows the reinforcement meets or exceeds the following strength requirement:
    - Tensile strength @ 2% strain: 550 lb/ft (ASTM D4595)
    - Ultimate tensile strength: 3000 lb/ft (ASTM D 4595)
    - Tensile strength retained after weathering (500 hrs, UVA LAMPS) = 80% (ASTM D7238)
10. Furnish geosynthetic reinforcement in a 25’ long section. Place sections so that reinforcement runs continuously in the direction of the roadway. Install layers of reinforcement flat and taut. And secure layers in place with shoveled piles of fill, pins, or staples.
11. Place and spread layers of fill in the direction of overlaps to prevent peeling or separation of reinforcement layers at the overlaps. Layers of reinforcement must remain flat and taut during and after fill placement.

6. Conclusion

This project conducted an extensive survey and review of the current bridge approach design in Nebraska and practices in other states in the US. Upon the completion of the review, a detailed numerical study was implemented to achieve the two principal goals of (1) improving the current design practice of the approach slab foundation in Nebraska and (2) examining the feasibility of applying geosynthetic reinforcement of soils for preventing the bump issues at the bridge approaches with less cost. A pull-out test was also conducted as a complementary to provide input parameters for the interaction between the regional soil and selected geosynthetics. Finally, cost-effectiveness and constructability were considered to make a recommendation. Recommendations made from the study results of this project are as follows:

Study I: Improvement of the current bridge approach design

- It is recommended that the number of grade beam piles could be about 40-50 % of the total number of abutment piles to prevent "bump" issue not only near the interface of the bridge abutment and the approach but also at the interface of the approach and the roadway pavement.
- And, the dimension and length of the grade beam piles are maintained the same as those of the abutment piles.

Study II: Feasibility of geosynthetic reinforcement of soils

- 2-3 layers of individual geosynthetic reinforcements at both near the interface of the bridge abutment and the approach and the interface of the approach and the roadway pavement could be recommended to prevent the bump issue.
- Unlike individual geosynthetic reinforcement, extended geosynthetic reinforcement is not recommended due to its lower efficacy, constructability issue, and economic reasons.
- A sleeper slab, instead of the current dimension of the grade beam, showed some improvement in further mitigating a potential differential settlement near the paving section. However, its improvement effect near the end of the approach slab is not significant, and further study is needed.
- Alternatively, a combination of grade beam piles (current design practice) and 2-3 layers of individual geosynthetic reinforcements near the interface of the approach and the

roadway pavement could also be recommended to prevent differential settlements at both areas. This approach can also be used for the repair of an existing bridge approach and the roadway pavement.

- The grade beam pile case could be three to nine times more expensive than the geosynthetic reinforcement case. As such, the geosynthetic reinforcement case can be a more cost-effective and economical method compared to the current design practice.

For an additional design modification, in-situ foundation soils may be used instead of granular backfill soils under the roadway paving section. In such a case, drainage pipe, along with surrounding granular soils, is suggested to be placed next to the grade beam on the side of the roadway paving section.

Lastly, the project team recommends conducting a field test program as a follow-up study to demonstrate the performance of the modified design approaches at an actual bridge construction site. Field performances, including deformation and internal stresses in the concrete slabs, stress distribution in the reinforced soils, and strain distributions along the geosynthetics, are recommended to be monitored during the suggested field test program for a minimum of one and half years.

References

Abu-Hejleh, N. M., Hanneman, D., Wang, T., & Ksouri, I. (2008). Evaluation and Recommendations for Flowfill and Mechanically Stabilized Earth Bridge Approaches. Transportation research record, 2045(1), 51-61.

Mishra, D., Jayawickrama, P. W., & Nash, P. T. (2010). Development of Maintenance Strategies to Mitigate Bridge End Damage from Water Intrusion. Transportation research record, 2170(1), 56-63.

Chen, Q. and Abu-Farsakh, M. (2016). Mitigating the bridge end bump problem: A case study of a new approach slab system with geosynthetic reinforced soil foundation. Geotextiles and Geomembranes, 44(1), 39-50.

Lenke, L. R. (2006). Settlement Issues-Bridge Approach Slabs (final Report Phase 1). Report No. NM04MNT-02. Albuquerque, New Mexico. University of New Mexico.

Briaud, J. L., James, R. W., & Hoffman, S. B. (1997). Settlement of Bridge Approaches (The Bump at the End of the Bridge). NCHRP Synthesis of Highway Practice 234. Transportation Research Board, Washington, DC.

Wahls, H. E. (1990). Design and construction of bridge approaches (Vol. 159). NCHRP Synthesis of Highway Practice No. 159, Transportation Research Board, National Research Council, Washington, D.C.

Schaefer, V.R. and Koch, J.C. (1992). Void Development Under Bridge Approaches, ReportSD90-03, SD Dept. of Transportation, Office of Research, November 1992.

Stark, T. D., Olson, S. M., & Long, J. H. (1995). Differential Movement at the Embankment/Structure Interface-Mitigation and Rehabilitation. Final report (No. Project IAB-H1, FY 93).

White, D., Sritharan, S., Suleiman, M. T., & Chetlur, S. (2005). Identification of the best practices for design, construction, and repair of bridge approaches (No. CTRE Project 02-118). Iowa. Dept. of Transportation.

Abu-Hejleh, N., Hanneman, D., White, D. J., Wang, T., & Ksouri, I. (2006). Flowfill and MSE bridge approaches: Performance, cost, and recommendations for improvements. Rep. No. CDOT-DTD-R-2006-2, Final Rep., Colorado Dept. of Transportation, Denver.

White, D. J., Mekkawy, M. M., Sritharan, S., & Suleiman, M. T. (2007). "Underlying" causes for settlement of bridge approach pavement systems. Journal of Performance of Constructed Facilities, 21(4), 273-282.

Tadros, M. K. and Benak, J. V. (1989). Bridge abutment and bridge approach slab settlement, phase I. Final Report, Nebraska Department of Roads.

Nebraska Department of Roads Bridge Division. (2016). Bridge Office Policies and Procedures, BOPP.

Yasrobi, S. Y., Ng, K. W., Edgar, T. V., & Menghini, M. (2016). Investigation of approach slab settlement for highway infrastructure. Transportation Geotechnics, 6, 1-15.

Helwany, S. and Koutnik, T. E. (2007). Evaluation of bridge approach settlement mitigation methods. Wisconsin Highway Research Program.

Abu-Farsakh, M., Chen, Q., & Sharma, R. (2013). An experimental evaluation of the behavior of footings on geosynthetic-reinforced sand. Soils and Foundations, 53(2), 335-348.

Bai, X. H., Huang, X. Z., & Zhang, W. (2013). Bearing capacity of square footing supported by a geobelt-reinforced crushed stone cushion on soft soil. Geotextiles and Geomembranes, 38, 37-42.

Eun, J., Gupta, R., & Zornberg, J. G. (2017). Effect of geogrid geometry on interface resistance in a pullout test. In Geotechnical Frontiers 2017 (pp. 236-246).

Thiagarajan, G., Gopalaratnam, V., Halmen, C., Ajgaonkar, S., Ma, S., Gudimetla, B., & Chamarthi, R. (2010). Bridge approach slabs for Missouri DOT looking at alternative and cost efficient approaches (No. OR 11.009). Missouri. Dept. of Transportation.

Ng, K. W., Yasrobi, S. Y., & Edgar, T. V. (2015). Investigation of approach slab and its settlement for roads and bridges. Report No. FHWA 15/01F. Wyoming Department of Transportation.

Edgar, T. V., Puckett, J. A., and D'Spain, R. B. (1989). Effect of Geotextile on Lateral Pressure and Deformation in Highway Embankments. Geotextiles and Geomembranes, Vol. 8, No. 4, PP 275-306.

Oklahoma Department of Transportation (ODOT), Approach slab and sleeper slab details drawings (2019). State Job No. 28184(04).

Miller, G., Hatami, K., Cerato, A., & Obsorne, C. (2013). Applied Approach Slab Settlement Research Design/Construction (FHWA-OK-13-09 2227).

Texas Department of Transportation (TxDOT). (2019). Bridge Approach slab, Concrete pavement BAS-C drawing. Bridge division standard.

Briaud, J., J. Seo, and H. Ha. (2002). Investigation of Settlement at Bridge Approach Slab Expansion Joint: Numerical Simulation and Model Tests. Texas Transportation Institute.

Jayawickrama, P., Nash, P., Leaverton, M., & Mishra, D. (2005). Water intrusion in base/subgrade materials at bridge ends (No. FHWA/TX-06/0-5096-1).

Puppala, A. J., Archeewa, E., Saride, S., Nazarian, S., & Hoyos, L. (2012). Recommendations for design, construction, and maintenance of bridge approach slabs (No. FHWA/TX-11/0-6022-2). University of Texas at Arlington.

Kansas Department of Transportation (KDOT), Approach slab details drawings (2019). Project Number 31-70 KA-4944-01.

Parsons, R. L., Foster, D. H., & Cross, S. A. (2001). Compaction and Settlement of existing embankments. Report No. KTRAN: KU-00-8, Kansas Department of Transportation, Topeka, 154 pp.

Dupont, B. and Allen, D. L. (2002). Movements and settlements of highway bridge approaches. Report No. KTC-02-18/SPR-220-00-1F, Kentucky Transportation Cabinet, Frankfort, 74 pp.

Ha, H. S., Seo, J., & Briaud, J. L. (2002). Investigation of settlement at bridge approach slab expansion joint: Survey and site investigations. Report No. FHWA/TX-03/4147-1.

Wyoming Department of Transportation (WYDOT), Approach slab details drawings (2018). Standard plans of concrete pavement joints. Plan number 414-2.

Hoppe, E. J. (1999). Guidelines for the use, design, and construction of bridge approach slabs. Report VTRC 00-R4. Virginia Transportation Research Council, 42 pages.

Iowa Department of Transportation (Iowa DOT), Approach slab details drawings (2017). Standard road plan. Section BR-205.

Louisiana Department of Transportation and Development (LDOTD), Approach slab details drawings (2017). Standard plans. Bridge and structural design.

Cai, C. S., Voyiadjis, G. Z., & Shi X. (2005). Determination of Interaction between Bridge Concrete Approach Slab and Embankment Settlement. Report FHWA/LA.05/403. Louisiana Department of Transportation, 150 pages.

Abu-Farsakh, M. Y., & Chen, Q. (2014). Field demonstration of new bridge approach slab designs and performance (No. FHWA/LA. 13/520). Louisiana Transportation Research Center.

Colorado Department of Transportation (CDOT), Approach slab details drawings (2019). Staff Bridge Branch. B-600 series.

Virginia Department of Transportation (VDOT), Approach slab details drawings (2008). Road and bridge standard.

Lu, Q., Li, M., Gunaratne, M., Xin, C., Hoque, M., & Rajalingola, M. (2018). Best practices for construction and repair of bridge approaches and departures. Tallahassee, FL, Report No. BDV25-977-31.

Mississippi Department of Transportation (MDOT), Approach slab details drawings (2017). Roadway design division. Number BE-1.

Tayabji, S. D. (2018). FHWA Project R05 IAP Funded Project Case Study: Florida I-10 Precast Concrete Bridge Approach Slab Demonstration Project (No. FHWA-HIF-18-057). United States. Federal Highway Administration.

Florida Department of Transportation (FDOT). (2016). Approach slab details drawings (2016). FDOT Design standards.

New Mexico Department of Transportation (NMDOT), Approach slab details drawings (2012). New Mexico department of transportation standard drawing No. 514.

Chee, M. M. W. (2018). Assessment of structural concrete approach slab cracking at integral abutment bridges. University of Illinois at Urbana-Champaign.

Missouri Department of Transportation (MoDOT), Approach slab details drawings (2020). Missouri Highway and Transportation commission.

Luna, R. (2004). Evaluation of bridge approach slabs, performance and design (No. RDT 04-010). Missouri. Dept. of Transportation. Research, Development and Technology Division.

Indiana Department of Transportation (INDOT), Approach slab details drawings (2020). Standard drawing No. E503-BATJ-03.

North Carolina Department of Transportation (NCDOT), Approach slab details drawings (2006). Standard drawing No. BAS11SM.

Wisconsin Department of Transportation (WisDOT), Approach slab details drawings (2018). Standard detail drawing No. SDD 13B02.

Nassif, H., Suksawang, N., Shah, N., & Abu-Amra, T. (2007). Field implementation and monitoring of bridge approach slabs (No. FHWA-NJ-2007-012).

New Jersey Department of Transportation (NJDOT), Approach slab details drawings (2005). Standard Drawing Plate 2.9-5.

Bakeer, R. M., Shutt, M. A., Zhong, J., Das, S. C., & Morvant, M. (2005). Performance of pile-supported bridge approach slabs. Journal of Bridge Engineering, 10(2), 228-237.

Hatami, K., & Bathurst, R. J. (2001). Modeling static response of a segmental geosynthetic reinforced soil retaining wall using FLAC. In Proc. 2nd International FLAC Symposium. Numerical Modeling in Geomechanics, Lyon (pp. 223-231).

Lambe, T. W. and Whitman, R. V. (1969). Soil mechanics. Wiley & Sons, New York, NY.

Chung, R. M., Song, C. R., Bahmyari, H., & Bitar, L. (2018). Nebraska specific slope design manual (No. NDOT: SPR-1 (17) M061, NTC: 26-1121-4036-001). Nebraska. Department of Transportation.

Radhakrishna, H. S. and Klym, T. W. (1974). Geotechnical properties of a very dense glacial till. Canadian Geotechnical Journal, 11(3), 396-408.

Iowa DOT office of design. (2015). Engineering Properties of Soil and Rock. Design manual, chapter 200.

Subramanian, N. (2008). Design of steel structures. Oxford University Press.

Zheng, Y., Fox, P. J., & Shing, P. B. (2014). Numerical simulations for response of MSE wall-supported bridge abutments to vertical load. In Ground improvement and geosynthetics (pp. 493-502).

Rajagopal, K., Chandramouli, S., Parayil, A., & Iniyan, K. (2014). Studies on geosynthetic-reinforced road pavement structures. International Journal of Geotechnical Engineering, 8(3), 287-298.

Tan, Y., Sun, Z., Gong, X., Xu, H., Zhang, L., & Bi, Y. (2017). Design parameter of low-temperature performance for asphalt mixtures in cold regions. Construction and Building Materials, 155, 1179-1187.

Owino, A. O., Hossain, Z., & Shiau, J. (2018). Pull-out resistance of single piles and parametric study using the Finite Difference Method (FDM). American Journal of Civil Engineering and Architecture, 6(5), 193-198.

Yao, W., Liu, Y., & Chen, J. (2012). Characteristics of negative skin friction for superlong piles under surcharge loading. International journal of geomechanics, 12(2), 90-97.

Wong, K. S. and Teh, C. I. (1995). Negative skin friction on piles in layered soil deposits. Journal of Geotechnical Engineering, 121(6), 457-465.

Fellenius, B.H. (2017). Basics of foundation design – a textbook. Pile Buck International, Inc., Vero Beach, FL, Electronic Edition, www.fellenius.net.

Ebrahimian, B. (2011). Numerical analysis of strip footing resting on geosynthetic-reinforced sand bed over soft soil. In Deformation Characteristics of Geomaterials (pp. 993-1000). IOS Press.

Zheng, Y. and Fox, P. J. (2017). Numerical investigation of the geosynthetic reinforced soil–integrated bridge system under static loading. Journal of Geotechnical and Geoenvironmental Engineering, 143(6), 04017008.

ASTM D6706-01(2013), Standard Test Method for Measuring Geosynthetic Pullout Resistance in Soil, ASTM International, West Conshohocken, PA, 2013, www.astm.org.

Gupta, R. (2009). A study of geosynthetic reinforced flexible pavement system. Ph.D. Dissertation, submitted to The University of Texas at Austin, Texas, USA.

Roodi, G. H. (2016). Analytical, experimental, and field evaluations of soil-geosynthetic interaction under small displacements. Ph.D. Dissertation, Univ. of Texas, Austin, TX.

Sugimoto, M., Alagiyawanna, A. M. N., & Kadoguchi, K. (2001). Influence of rigid and flexible face on geogrid pullout tests. Geotextiles and Geomembranes, 19(5), 257-277.

Palmeira, E. M. (1987). The study of soil-reinforcement interaction by means of large scale laboratory tests. Ph.D. thesis. Magalen College, University of Oxford, England.

Palmeira, E.M. and Milligan, G.W.E. (1989). Scale and other factors affecting the results of pull-out tests of grid buried in sand. Geotechnique 11 (3), 511-524.

Christopher, B. R. (1986). New tests for determining the in-soil stress-strain properties of geotextiles. In Proc. 3rd Int. Conf. on Geotextiles pp. 683-688.

Raju, D.M. (1995), "Monotonic and cyclic pullout resistance of geosynthetics", PhD. Dissertation, University of British Columbia, Canada.

Ghaaowd, I. and McCartney, J. S. (2020). Pullout of geogrids from tire-derived aggregate having large particle size. Geosynthetics International, 27(6), 671-684.

Roodi, G. H., Zornberg, J. G., Aboelwafa, M. M., Phillips, J. R., Zheng, L., & Martinez, J. (2018). Soil-geosynthetic interaction test to develop specifications for geosynthetic-stabilized roadways (No. FHWA/TX-18/5-4829-03-1). University of Texas at Austin. Center for Transportation Research.

Eun, J., Gupta, R., & Zornberg, J. G. (2017). Effect of geogrid geometry on interface resistance in a pullout test. In Geotechnical Frontiers pp. 236-246.

Bakeer, R. M., Sayed, S. M., Cates, P., & Subramanian, R. (1998). Pullout and shear tests on geogrid reinforced lightweight aggregate. Geotextiles and Geomembranes, 16(2), 119-133.

Koerner, R. M. (2005). Designing with geosynthetics. Fifth edition. Prentice Hall, Englewood Cliffs.

Ingold T. S. (1983). Laboratory pullout testing of grid reinforcements in sand. Geotech Test J 6(3). 101–111.

Ochiai, H., Otani, J., Hayashic, S., & Hirai, T. (1996). The pull-out resistance of geogrids in reinforced soil. Geotextiles and Geomembranes, 14(1), 19-42.

Wang, Z. and Richwien, W. (2002). A study of soil-reinforcement interface friction. Journal of Geotechnical and Geoenvironmental Engineering, 128(1), 92-94.

Prashanth, V., Krishna, A. M., & Dash, S. K. (2016). Pullout tests using modified direct shear test setup for measuring soil–geosynthetic interaction parameters. International Journal of Geosynthetics and Ground Engineering, 2(2), 10.

Holtz, R. D. and Lee, W. F. (1998). Geosynthetic Reinforced Wall Analysis Phase II: Use of In-Soil Geosynthetic Behavior to Predict Deformations, Volume 2: Implementation—Computer Codes and Files (No. WA-RD 452.2).

Vulova, C. and Leshchinsky, D. (2003). Effects of geosynthetic reinforcement spacing on the behavior of mechanically stabilized earth walls (No. FHWA-RD-03-048). United States. Federal Highway Administration. Office of Infrastructure Research and Development.

Fakhraldin, M. K. (2012). Measurement of tensile properties of geogrid. International conference on Geotechnique. Volume: ISBN: 978-4-9905958-1-4.

Jiang, Y., Han, J., Zornberg, J. G., Leshchinsky, D., Christopher, B. R., & Tanyu, B. F. Numerical Evaluation of Boundary Effects on the Interaction between Geosynthetic Reinforcement and Backfill. In Geotechnical Frontiers 2017 (pp. 299-305).

Biaxial geogrid BX1200, Product Specification of Tensar Biaxial Geogrid. Tensar International Corporation. Alpharetta, Georgia. www.tensarcorp.com.

ASTM D4595-17 (2017), Standard Test Method for Tensile Properties of Geotextiles by the Wide-Width Strip Method, ASTM International, West Conshohocken, PA, 2017, www.astm.org.

ASTM D7238-20 (2020), Standard Test Method for Effect of Exposure of Unreinforced Polyolefin Geomembrane Using Fluorescent UV Condensation Apparatus, ASTM International, West Conshohocken, PA, 2020, www.astm.org.

Abdi, M. R. and Zandieh, A. R. (2014). Experimental and numerical analysis of large scale pull out tests conducted on clays reinforced with geogrids encapsulated with coarse material. Geotextiles and Geomembranes, 42(5), 494-504.

Won, M. (2005). Improvements of testing procedures for concrete coefficient of thermal expansion. Transportation Research Record, 1919(1), 23-28.

Reynolds, Joseph Charles, "Thermal stresses and movements in bridges" (1972). Masters Theses. No. 6714, University of Missouri-Rolla.

Christopher, Barry R. (2014). Cost Savings by Using Geosynthetics in the Construction of Civil Works Projects, 10 ICG Berlin, IGS.

NHI Courses No. 132021 and 132022 (2016). Design and Construction of Driven Pile Foundations – Volume I, FHWA-NHI-16-009, FHWA.

Appendices

(1) Validation of the numerical simulation approach: soil-pile interaction

An axisymmetric axially loaded pile is modeled in FLAC to check the vertical stresses in the ground which resulted from the skin friction resistance of the pile and compare the results with the estimated vertical stress approximation using a simple stress approximation. This approximation is based on Flamant solution integration for a point load on an elastic half-plane. The problem analyzed is shown in Figure A.1.

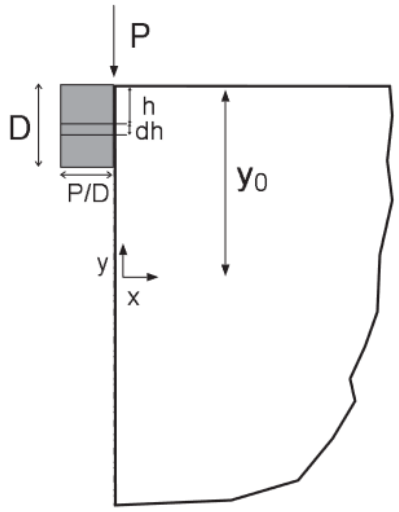

Figure A.1 Axisymmetric axially loaded pile (Itasca 2016).

Where D is the pile depth, P is the axial load applied and y_0 is the pile top elevation. Flamant solution has the following form for $y \geq y_0 - D$:

$$\sigma_{yy} = \frac{P}{\pi D}\left[ln\frac{x^2}{(y_0 - y)^2 + x^2} + \frac{(y_0 - y)^2}{(y_0 - y)^2 + x^2}\right]$$

And for $y \leq y_0 - D$:

$$\sigma_{yy} = \frac{P}{\pi D}\left[ln\frac{(y_0 - D - y)^2 + x^2}{(y_0 - y)^2 + x^2} + \frac{x^2}{(y_0 - D - y)^2 + x^2} - \frac{x^2}{(y_0 - y)^2 + x^2}\right]$$

These two equations were coded in FLAC using FISH language and the vertical stresses obtained from FLAC and the Flamant solution showed a good agreement. The results are shown in Figures A.2 and A.3.

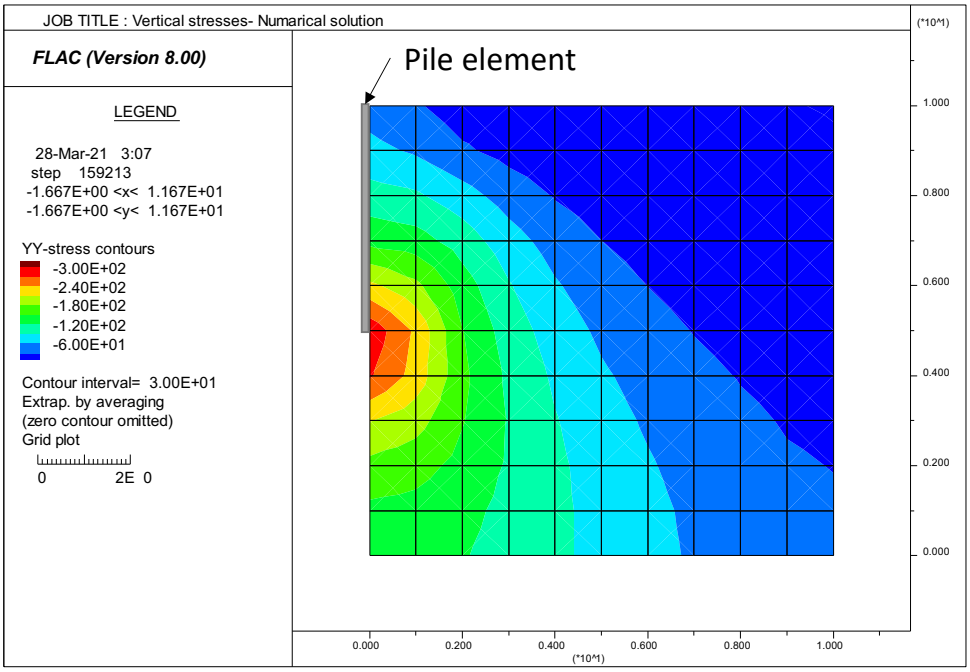

Figure A.2 contours of numerically obtained vertical stresses (FLAC).

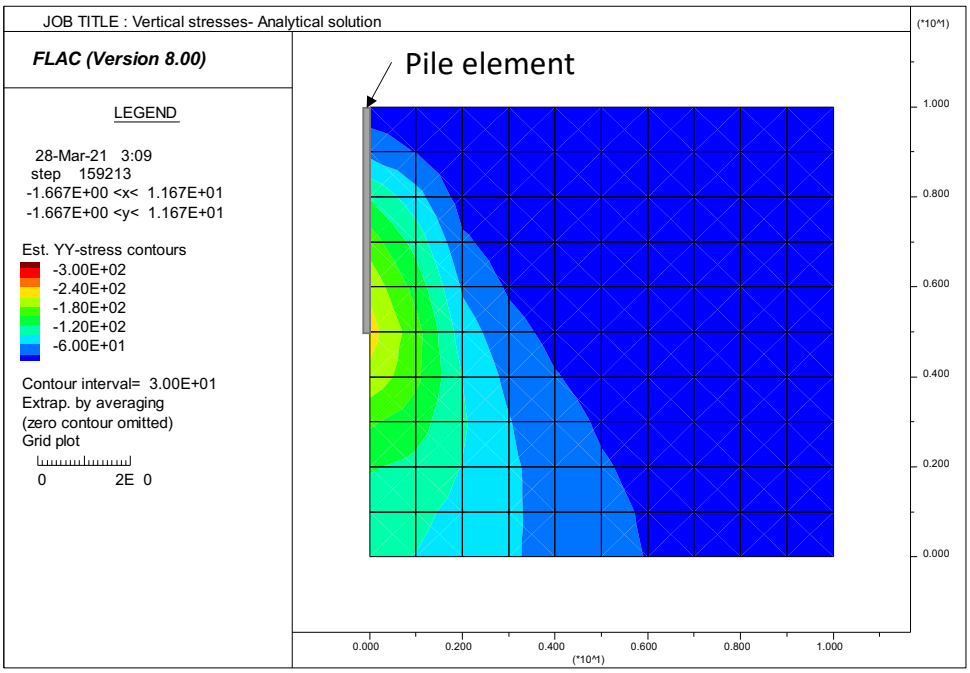

Figure A.3 contours of the estimated vertical stresses (Flamant solution).

(2) Validation of the numerical simulation approach: soil-geosynthetics interaction

A geosynthetic pullout test was conducted to obtain the interface parameters between the soil and the geosynthetic used in the fourth section of this study (Feasibility of Geosynthetics Reinforcement of Soils).

The backfill material was modeled using Mohr-Coulomb failure criteria. This constitutive model was successfully implemented to model the behavior of backfill soil in pullout test by Abdi and Zandieh (2014) and Jiang et al (2017). The geogrid layer was modeled as cable element embedded within a 1-foot soil layer. Cable element in FLAC provides a good representation of geosynthetic materials as shown by Holtz (1998), Vulova and Leshchinsky (2003), Ebrahimian (2010) and Zheng and Fox (2017). The interface properties were included in the cable element properties as well. The numerical simulation model of the pullout test modeled in FLAC is shown in Figure A.4 below. Pullout of the geogrid was conducted by assigning a horizontal velocity of 0.04 in/min (rate of the pullout test) to the first node of the cable element. The axial force at the frontal node (which represents the pullout force) and the horizontal displacement is then obtained and plotted.

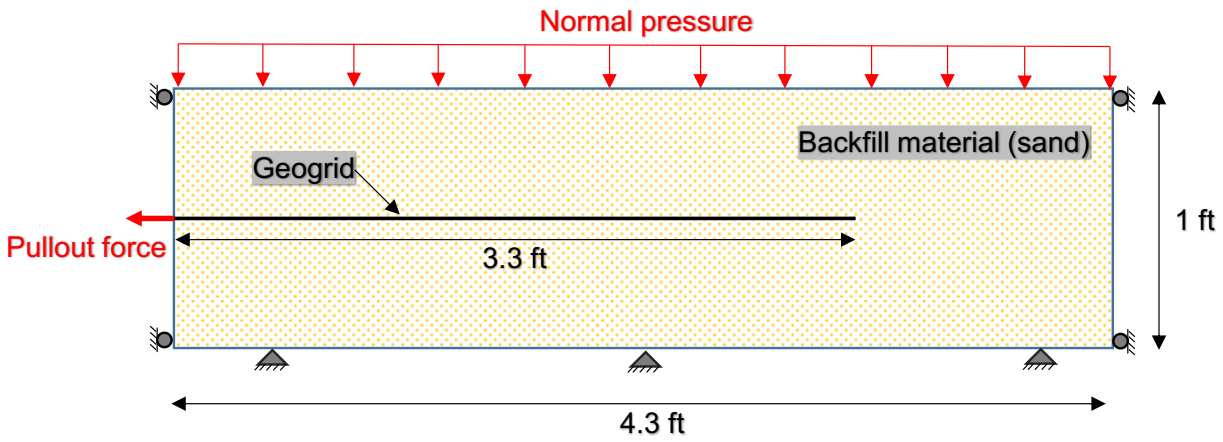

Figure A.4 The numerical simulation model of the pullout test.

The bond stiffness and the bond strength of the interface between the geogrid (cable element) and the used sand were adjusted by the means of matching the pullout test curve obtained from laboratory testing with the simulation calculated results obtained from FLAC under same normal pressure of 1.45 psi.

The numerical model is then verified by comparing the measured results obtained from the pullout test with the calculated results from the numerical model at the other two normal pressures (3.6 psi and 5.8 psi). Those results are shown in Figure A.5.

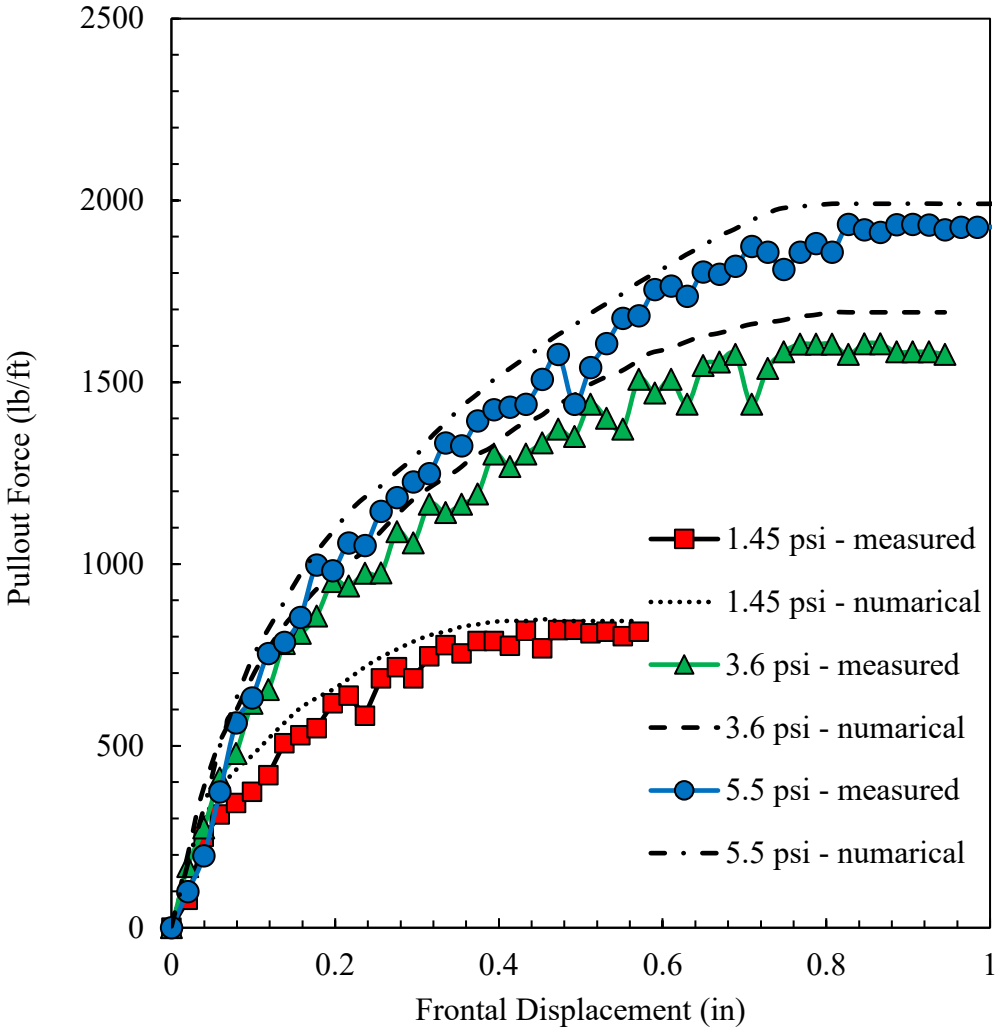

Figure A.5 Comparison between the pullout test measured and simulated results.

The measured resulted shows good agreement with the calculated results from the numerical simulation. The results show how the pullout force increase with a high rate when the geogrid is being pulled. Eventually this rate would decrease until the maximum pullout force becomes constant. This means that the interface between the soil and geosynthetic has yielded. Figure A.6 shows a simulated geosynthetic being pulled from the backfill as part of the numerical model used.

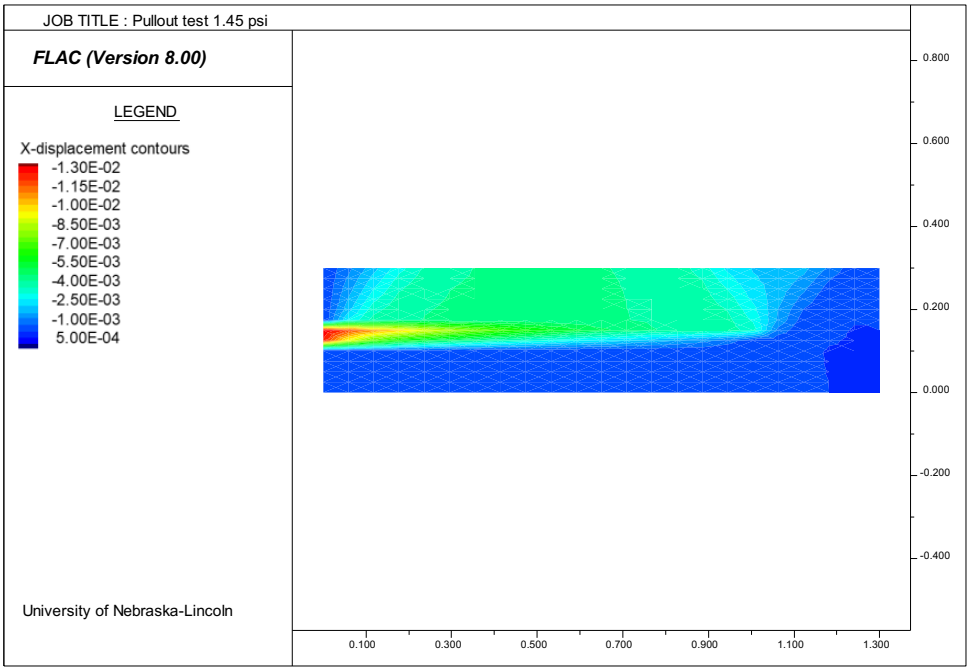

Figure A.6 horizontal displacement contours after conducting the pullout test on the inserted geogrid.